UBFC
UNIVERSITÉ
BOURGOGNE FRANCHE-COMTÉ

icb
Laboratoire Interdisciplinaire
Carnot de Bourgogne

THÈSE DE DOCTORAT DE L'ÉTABLISSEMENT UNIVERSITÉ BOURGOGNE FRANCHE-COMTÉ PRÉPARÉE AU LABORATOIRE INTERDISCIPLINAIRE CARNOT DE BOURGOGNE

École doctorale n°553
École Doctorale Carnot-Pasteur

Doctorat de Physique

Par

M. LAFORGUE Xavier

Robust control for quantum technology and quantum information processing

Thèse présentée et soutenue à Dijon, le 3 Juin 2022

Composition du Jury :

M. LEROY Claude	Professeur, Université Bourgogne Franche-Comté	Président
M. VITANOV Nikolay	Professeur, St Kliment Ohridski University of Sofia, Bulgarie	Rapporteur
M. del CAMPO Adolfo	Professeur, University of Luxembourg	Rapporteur
M. CHEN Xi	Professeur, Shanghai University, Chine; University of the Basque Country, Espagne	Examinateur
Mme. GOGYAN Anahit	Chargée de recherche, Nicolaus Copernicus University, Pologne	Examinatrice
M. JAUSLIN Hans-Rudolph	Professeur, Université Bourgogne Franche-Comté	Examinateur
M. GUÉRIN Stéphane	Professeur, Université Bourgogne Franche-Comté	Directeur de thèse
M. HALFMANN Thomas	Professeur, Technical University of Darmstadt, Allemagne	Codirecteur de thèse

Table of Contents

This Thesis is structured in five Chapters. Chapter 1 presents the principles of the robust inverse optimization (RIO) method. In Chapter 2, we apply RIO on a two-level quantum system. In Chapter 3, we discuss the three-level lambda system, the most relevant resonant case, and various control protocols. In Chapter 4, we use the single-mode Lewis-Riesenfeld method to derive a family of exact population transfers in the three-level lambda resonant system. Finally, in Chapter 5, we demonstrate RIO for the resonant three-level system.

List of Figures

List of Tables

Abstract

We consider the robust inverse geometric optimization of arbitrary population transfers and single-qubit gates in a two-level system. Robustness with respect to pulse inhomogeneities is demonstrated. We show that for time or energy optimization, the pulse amplitude is constant, and we provide the analytic form of the detuning as Jacobi elliptic cosine.

We deal with the task of robust complete population transfer on a 3-level quantum system in lambda configuration. First, we use the Lewis-Riesenfeld method to derive a family of solutions leading to an exact transfer. Among this family, we identify a tracking solution with a single parameter to control simultaneously the fidelity of the transfer, the population of the excited state, and robustness. The ultrahigh-fidelity robustness of the shaped pulses is found superior to that of Gaussian and adiabatically-optimized pulses for moderate pulse areas. Second, we apply robust inverse optimization now to generate a stimulated Raman exact passage (STIREP) considering the loss of the upper state as a characterization parameter. Control fields temporal shapes, robust against pulse inhomogeneities, that are optimal with respect to pulse area, energy, and duration, are found to form a simple sequence with a combination of intuitively (near the beginning and the end) and counter-intuitively ordered pulse pairs. Alternative robust optimal solutions featuring lower losses, larger pulse areas, and fully counter-intuitive pulse sequences are derived.

Résumé

Depuis l'invention du transistor et son utilisation en informatique, les composants électroniques qui composent un ordinateur se miniaturisent en suivant la loi de Moore, une observation empirique remarquablement précise concernant une technologie aux multiples facettes. Cette miniaturisation continue a fait passer les ordinateurs de la taille d'une pièce à celle d'un livre d'une haute complexité technologique que nous utilisons aujourd'hui. Malheureusement, ce schéma atteindra, atteint et a atteint ses limites : comment décrire les transistors et autres composants électroniques classiques lorsqu'ils ont été réduits à quelques atomes ?

L'électronique, application technologique de l'électromagnétisme classique, matérialise l'informatique. Lorsque l'électromagnétisme classique perd de sa validité et que la miniaturisation aboutit à des constructions sans comportement électronique usuel, il nous reste la théorie la plus aboutie pour décrire les phénomènes à l'échelle atomique : la mécanique quantique. Devant d'une part l'impasse apparente de l'électronique et, d'autre part, la difficulté apparemment insurmontable de simuler des systèmes quantiques avec un ordinateur classique, un dispositif basé sur la mécanique quantique pour effectuer la manipulation, le stockage et la transmission de l'information, c'est-à-dire un ordinateur quantique traitant l'information avec les principes quantiques, sera au cœur des prochains développements technologiques.

Le calcul quantique consiste à appliquer des opérations logiques spécifiques sur des informations quantiques afin d'obtenir un résultat dépendant de l'entrée. Ces opérations sont appelées portes quantiques. Concevoir une porte quantique consiste à manipuler avec précision n'importe quel état quantique afin de le transformer en —ou, compte tenu de la dynamique du processus, de le faire évoluer vers— un nouvel état quantique représentant le résultat de l'opération logique souhaitée.

La tâche consistant à contrôler expérimentalement des systèmes quantiques uniques, entreprise depuis les années 1970, comprend le développement des "pièges à atomes" (piégeant des atomes uniques pour permettre le contrôle de l'état de l'électron ou du noyau tout en restant isolé de l'environnement), l'utilisation du microscope à effet tunnel pour déplacer des atomes uniques et les arranger comme on le souhaite, entre autres [1, p. 3]. Des aspects fondamentaux de l'informatique quan-

tique, tels que les algorithmes quantiques simples de quelques qubits, des formes simplifiées de correction d'erreurs quantiques, la simulation quantique et la téléportation quantique, ont été mis en œuvre sur des circuits supraconducteurs, des photons uniques, des spins nucléaires et des ions piégés [1, p. xix].

Bien que de nombreuses avancées aient été réalisées dans le contrôle des systèmes mentionnés, y compris la technologie qui nous permet aujourd'hui de façonner le champ électromagnétique (EM) interagissant avec un atome [2, p. xi], des questions de mécanique quantique très fondamentales nécessitent des investigations spécifiques pour le calcul quantique pratique. Selon DiVincenzo, deux obstacles principaux ont été identifiés : le problème de la correction des erreurs et le problème de la décohérence [3]. La décohérence est un terme souvent utilisé pour désigner plusieurs phénomènes quantiques, dépendant également du système physique utilisé, conduisant à une perte de cohérence due à l'interaction avec l'environnement ; l'isolement imparfait affecte l'évolution du système dans la mesure où il n'est plus unitaire (les portes quantiques doivent être unitaires). D'autre part, la correction d'erreurs traite du fait que de légères imperfections dans la mise en œuvre d'une opération de contrôle (par exemple, une impulsion inexacte, une phase incorrecte, des systèmes ou des contrôles présentant du bruit, etc.) peuvent conduire à l'échec du calcul.

L'objectif central du travail présenté dans ce document est d'approfondir cette forme de correction d'erreur, par la conception de ce que nous appelons des contrôles robustes.

En ce qui concerne le contrôle quantique, nous pouvons différencier les approches selon qu'elles sont adiabatiques ou non. Alors que les schémas adiabatiques tirent parti, en général, de la dynamique approximative des systèmes lorsque les contrôles sont suffisamment forts et/ou lents, satisfaisant ainsi l'objectif du fonctionnement à la limite de l'annulation idéale des termes non-adiabatiques ; l'approche non-adiabatique utilise des prescriptions directes de contrôles plus rapides et plus économiques en énergie.

Les exemples de méthodes adiabatiques sont les passages adiabatiques [4-8] et superadiabatiques [9, 10]. L'exemple classique d'une méthode diabatique (c'est-à-dire non-adiabatique) est l'utilisation des oscillations de Rabi avec ses impulsions π caractéristiques (pour les systèmes à deux niveaux) [11]. L'adiabaticité est intrinsèquement insensible aux déviations des contrôles et, en même temps, elle est très consommatrice de ressources (puisque l'exigence d'adiabaticité correspond strictement à l'utilisation d'énergies infinies). Ces circonstances ont motivé la création de méthodes telles que les raccourcis vers l'adiabaticité, où les conditions formelles d'adiabaticité sont satisfaites en utilisant des champs de contrôle supplémentaires ou en façonnant les contrôles [12]. Diamétralement opposés, les schémas diabatiques

requièrent de faibles énergies mais souffrent d'une grande sensibilité aux conditions non-idéales. De la même manière que des progrès ont été faits pour réduire les exigences énergétiques des processus adiabatiques tout en maintenant leur robustesse, des techniques qui augmentent la robustesse des contrôles diabatiques ont également été développées, comme les impulsions composites [13-18], largement utilisées en résonance magnétique nucléaire (RMN), et les impulsions façonnées à coup unique (SSSP) comme proposition plus récente [19-21]. Alors que les impulsions composites utilisent une succession de contrôles, généralement des champs EM, avec différentes phases à l'origine constantes afin d'annuler les déviations produites par rapport à l'exécution idéale, les SSSP façonnent les champs —et les phases— dynamiquement pour produire le même type de correction d'erreur.

Le SSSP nécessite la paramétrisation du propagateur du système. Pour le système quantique le plus simple et idéalisé, l'atome à deux niveaux, la paramétrisation générale du propagateur est bien connue. Cependant, même pour un système comme l'atome à trois niveaux, le propagateur général n'est pas directement disponible dans la littérature. Une façon de produire des propagateurs paramétrisés menant à des descriptions exactes de la dynamique du système est d'utiliser des invariants dynamiques ; mais nous pouvons aussi utiliser des méthodes de la théorie des groupes pour écrire le propagateur selon leur groupe de symétrie et à partir de ses générateurs différentiels [22].

En paramétrisant le propagateur, par ingénierie inverse des champs de contrôle, ont les décrit par un ensemble de paramètres angulaires. Ces paramètres, qui représentent le degré de mélange entre les niveaux peuplés et les phases relatives dans l'opérateur d'évolution, peuvent être prescrits en leur faisant suivre un chemin respectant les conditions aux limites, où nous pouvons lui permettre une certaine liberté ou, au contraire, en la restreignant.

L'ingénierie inverse, telle que nous l'utilisons, fait référence à la résolution du problème de contrôle "inverse" : à partir d'une certaine dynamique pour le système on obtient des contrôles, par opposition au problème de contrôle "direct" qui résout la dynamique du système pour un certain contrôle.

Le contrôle optimal est une méthode mathématique de plus en plus populaire en particulier dans son application au contrôle quantique. On peut l'utiliser pour optimiser le réglage fin des solutions de suivi ou pour rechercher des dynamiques exactes qui sont optimales par rapport à une certaine condition [2, 23, 24].

Pour le calcul quantique ou, plus généralement, pour la manipulation pratique de l'information quantique, les opérations doivent inéluctablement être effectuées de manière robuste. Malgré de légers écarts par rapport aux conditions non optimales, les opérations doivent être effectuées avec précision et efficacité. Qu'il s'agisse de

modifications indésirables des champs de contrôle qui interagissent avec le système quantique, de la connaissance imparfaite du système à contrôler, de la présence de bruit ou de toute autre condition non idéale des mises en œuvre dans le monde réel, nous devons contrôler le système et obtenir les résultats souhaités de manière résiliente.

Plusieurs approches ont été adoptées à cet égard, dont certaines seront abordées dans les chapitres suivants, notre principal sujet d'intérêt étant les impulsions formées en un seul coup, son extension à l'optimisation inverse robuste et sa comparaison avec des méthodes plus traditionnelles.

Ce document est organisé comme suit : le chapitre 1 aborde les principes de la méthode "robuste inverse optimisée" (RIO). Le chapitre 2 démontre la méthode RIO sur des systèmes à deux niveaux, pour lesquels nous obtenons des expressions analytiques pour la forme des contrôles. Le chapitre 3 aborde les principes fondamentaux du contrôle des systèmes à trois niveaux : schémas adiabatiques et non-adiabatiques. Le chapitre 4 présente le développement d'un équivalent exact et robuste du passage adiabatique Raman stimulé (STIRAP) basé sur les impulsions formées en un seul coup (SSSP) et l'ingénierie inverse via la méthode Lewis-Riesenfeld ; nous l'appelons passage exact Raman stimulé (STIREP). Le chapitre 5 applique la méthode RIO sur le STIREP pour produire la première solution optimale et robuste à notre connaissance pour un transfert Λ. Enfin, les conclusions générales de ce manuscrit sont présentées.

Introduction

Since the invention of the transistor and its use in computation, the size of the electronic components that compose a computer is reduced following Moore's Law, a remarkably accurate empirical observation regarding a multifaceted technological enterprise. The creation of microprocessors and their subsequent continuing miniaturization has driven computers from room-sized constructs to the handheld booklet-sized multi-cored marvels of high technological complexity we use nowadays. Unfortunately, this scheme will reach, is reaching, and has reached its limits: how to speak of transistors and other classical electronic components when they have been reduced to a few atoms?

Electronics, the technological application of classical electromagnetism, is used to materialize the work of computer and information scientists while also providing their toolkit. When classical electromagnetism loses validity and miniaturization arrives to constructs with no clear electronic behavior, we are left with the most successful theory describing the phenomena at atomic scales: quantum mechanics. We can hold in one hand the apparent dead-end of electronics and, in the other, the seemingly insurmountable difficulty at simulating quantum systems with a classical computer, to claim that only a device based purely on quantum mechanics to perform manipulation, storage, and transmission of information, i.e. a quantum computer dealing with quantum information, may eventually open the gates towards next technological developments.

Quantum computation is the action of applying specific logical operations on quantum information in order to obtain an input-dependent result. These operations are called quantum gates. To design a quantum gate is to engineer a control that accurately manipulates any quantum state in order to transform it into —or, considering the dynamics of the process, evolve it to— a new quantum state representing the result of the desired logical operation. Indeed, to produce quantum gates, besides the other numerous applications in multiple fields of physics and chemistry, it is necessary to know how to manipulate accurately any quantum state and produce any other from it.

The task of controlling experimentally single quantum systems, undertaken since

the 1970s, includes the development of: "atom traps" (trapping single atoms to allow the control of the state of electron or nucleus while remaining environmentally isolated), the use of the scanning tunneling microscope to move single atoms and arrange them as desired, among others [1, p. 3]. Fundamental aspects of quantum computation, such as simple quantum algorithms of few qubits, simple forms of quantum error correction, quantum simulation and quantum teleportation, have been implemented on superconducting circuits, single photons, nuclear spins, and trapped ions [1, p. xix].

Although many advances have been made in the control of the mentioned systems, including the technology that allows us nowadays to shape the electromagnetic (EM) field interacting with an atom practically as desired [2, p. xi], very fundamental quantum mechanical issues require extra nuance when practical quantum computation is the end goal. According to DiVincenzo, two principal obstacles have been identified: the error correction problem and the decoherence problem [3]. Decoherence is a term often used to refer to several quantum phenomena, depending also on the physical system in use, leading to loss of coherence due to interaction with the environment; the imperfect isolation affects the system evolution in that it is no longer unitary (quantum gates must be unitary). On the other hand, error correction deals with the fact that slight imperfections in the implementation of a control operation (e.g., inexact pulse area, incorrect phase or chirp, noisy media or controls, etc.) can lead, ultimately, to the failure of the computation.

It is the central goal of the work presented in this document to delve into this form of error correction, by the design of what we refer as robust controls.

Regarding quantum control, we may differentiate approaches with respect to if they are adiabatic or not. While adiabatic schemes take advantage, for general guidelines, of the approximate dynamics of systems when the controls are sufficiently strong and/or slow, thus satisfying the target of the operation at the limit of the ideal nullification of the non-adiabatic terms; the non-adiabatic approach uses direct prescriptions of faster and more energy-economic controls.

Examples of adiabatic methods are the adiabatic passages [4–8] and superadiabatic driving [9, 10]. The classical example of a diabatic (i.e. non-adiabatic) method is the use of Rabi oscillations with its characteristic π pulses (for two-level systems) [11]. Adiabaticity is inherently insensitive to deviations of the controls and, at the same time, it is very resource-consuming (since the adiabaticity requirement may be understood as the use of infinite energies). These circumstances motivated the creation of methods such as shortcuts to adiabaticity, where the formal adiabaticity conditions are satisfied by using additional control fields or by shaping the controls [12]. Diametrically opposed, the diabatic schemes require desirably low energies but

suffer from high sensitivity to non-ideal conditions. In the same manner that efforts were made to lower the energy requirements of adiabatic processes while hoping to maintain their robustness, techniques that increase the robustness of diabatic controls have also been developed, such as composite pulses [13–18], broadly used in nuclear-magnetic resonance (NMR), and single-shot shaped pulses (SSSP), a more recent proposal [19–21]. While composite pulses use controls, usually EM fields, repeated with different constant phases in order to cancel out the produced deviations from the ideal execution; SSSP shape fields —and, often, phases— in time to produce the same type of error correction.

SSSP requires the parametrization of the propagator of the system. For the simplest and idealized quantum system, the two-level atom, the general parametrization of the propagator is well known. However, even for the next simplest system, the three-level atom, the general propagator is not readily provided by the literature. A way to produce parametrized propagators leading to exact descriptions of the system dynamics is to use dynamical invariants; though we may also use methods of group theory to write the propagator according to their symmetry group and from its differential generators [22].

Parametrizing the propagator, inverse-engineering the control fields, we translate the necessity of prescribing the controls into describing a set of angular parameters. These parameters, representing the degree of mixing between populated levels or relative phases in the evolution operator, may be prescribed using tracking (assigning a certain function of time to them in agreement with boundary conditions), where we can allow for some freedom of fine-tuning the dynamics, or by more restrictive means.

Inverse-engineering, as we use it, refers to solving the "inverse" control problem: searching for a certain dynamic for the system and obtaining the controls from it; as opposed to the "direct" control problem that solves the dynamic of the system for a certain control.

Optimal control, as a mathematical method that has gained traction in its application for quantum control, may be used to optimize the fine-tuning of tracking solutions or to search for exact dynamics that are optimal with respect to some condition [2, 23, 24].

For practical quantum computation or, more generally, for the practical manipulation of quantum information, operations must inescapably be made in a robust manner. Slight deviations from non-optimal conditions must be acceptable and the operations must be effectuated precisely and efficiently regardless. Be it undesired changes to the control fields actually interacting with the quantum system, be it the imperfect knowledge of the object to be controlled, or be it the presence of noise

and any other non-ideal conditions of real-world implementations, we must act such that we resiliently produce the desired results.

Several approaches have been taken on this regard, some of which will be discussed in the following chapters, being our main scheme of interest the single-shot shaped pulses, its extension to robust inverse optimization, and their comparison with more traditional methods.

This document is organized as follows: Chapter 1 discusses the principles of the robust inverse optimization (RIO) method; Chapter 2 demonstrates RIO on two-level systems, for which we obtain analytical expressions for the controls; Chapter 3 discusses the fundamentals of the control of three-level systems: adiabatic and non-adiabatic schemes; Chapter 4 presents the development of an exact and robust equivalent of stimulated Raman adiabatic passage (STIRAP) based on single-shot shaped pulses (SSSP) and inverse-engineering via the Lewis-Riesenfeld method, we call this stimulated Raman exact passage (STIREP); Chapter 5 applies the RIO method on STIREP, instead of tracking, to produce the first-to-our-knowledge optimal and robust solution for a Λ transfer; finally global conclusions of this manuscript are presented.

Chapter 1

Principles of robust optimal control by inverse optimization

1.1 Introduction

Quantum mechanics as a branch of science that studies and explains certain natural phenomena was developed between year 1900 and the late 1920s. However, it is in the 1970s and 1980s, after the development of lasers, that a change of mindset began to take root: looking at quantum systems as phenomena to be designed instead of merely observed, take control of the quantum world instead of being satisfied explaining away nature's queer behaviors at this most mysterious scale. It was this new perspective that led to the combination of aspects of physics, mathematics, computer science, and information theory, to give birth to the field of quantum control and quantum information [1, p. xvii].

From the observational point of view, a quantum system is such an object that can be identified by a set of energetic states that may be discrete (levels) or continuous (bands). These energetic states are investigated with electromagnetic (EM) radiation and their characterization makes up the spectroscopic literature. The shift to quantum control occurs when limiting our attention to a few energetic states, considering the application of relevant EM fields, and designing such controls to make the system reach the target configuration (defined by quantum state populations and phases —coherences—). The minimal system that can be examined is that of two levels, widely used to design, test, and analyze strategies of quantum control. It was the consideration of a simple two-level atom that led to the discovery of the Rabi oscillations and from which the π-pulse is born. Being the logical next step, in terms of complexity and usefulness, is the three-level system, when the desired operation may not be reduced to a two-level interaction.

1.2 Quantum control and robustness

We approach the task of robustly controlling a quantum system with the single-shot shaped pulses (SSSP) technique [19–21, 25]. The SSSPs technique is fundamentally defined by two steps: first, the inverse engineering of the desired transfer using an appropriately parametrized quantum state, and second, the study of the robustness of the transfer by applying perturbation theory in the vicinity of the perfect process.

The evolution of an isolated quantum system is described by the Schrödinger equation,

$$i\hbar\partial_t|\psi_\epsilon(t)\rangle = H_\epsilon(t)|\psi_\epsilon(t)\rangle, \tag{1.1}$$

where $i = \sqrt{-1}$ is the imaginary unity, $\hbar$ is Planck's constant divided by 2π, $\partial_t \equiv \partial/\partial t$ is the partial derivative with respect to time t, $|\psi_\epsilon\rangle$ is the quantum state of the system and H_ϵ is its corresponding Hamiltonian. The state and Hamiltonian of the system are taken as time-dependent objects, while the basis on which they are written is taken as time-independent bare states, the $|n\rangle$'s.

The Schrödinger equation can be written in terms of the propagator of the system, defined by $|\psi_\epsilon(t)\rangle = U_\epsilon(t,t_i)|\psi(t_i)\rangle$, and omitting the redundant initial-time statevector $|\psi_i\rangle \equiv |\psi(t_i)\rangle$, as

$$i\hbar\dot{U}_\epsilon = [H(t) + V_\epsilon(t)]U_\epsilon, \tag{1.2}$$

where the Hamiltonian has been split into a term corresponding to the perfect inverse-engineered dynamics, H, and another containing unknown deviations (labeled ϵ) from the ideal desired control fields, V_ϵ. Given that we are interested in the dynamics of the system governed by the deviation term, we write the Schrödinger equation in the interaction picture with the interaction propagator $U_I(t) = U^\dagger(t)U_\epsilon(t)$,

$$i\hbar\dot{U}_I = U^\dagger[(H+V_\epsilon)U - i\hbar\dot{U}]U_I = U^\dagger V_\epsilon U U_I, \tag{1.3}$$

given that H is the inverse-engineered solution producing the desired dynamics in U ($i\hbar\partial_t U = HU$). The superscript dagger denotes complex transpose.

By considering these unknown control deviations ϵ to be only perturbations on the propagator of the system, which contains the effect of the implemented control regardless of the initial condition of the system, we can apply perturbation theory to the interaction propagator with the orders of the perturbative terms given by the

multiplicity of the interaction Hamiltonian in the expression,

$$U_I(t_f,t_i) = \mathbb{1} - \frac{i}{\hbar}\int_{t_i}^{t_f} U^\dagger V_\epsilon U\, dt + \left(-\frac{i}{\hbar}\right)^2 \int_{t_i}^{t_f} U^\dagger V_\epsilon U \int_{t_i}^{t} U'^\dagger V'_\epsilon U'\, dt'\, dt + \widehat{O}(\epsilon^3), \tag{1.4}$$

where the primed objects indicate dependence on the primed time, e.g., $U' \equiv U(t',t_i)$. With the perturbative expression for the interaction propagator we can obtain the state and populations fidelities at the end of the process with respect to the desired final state, the target state $|\psi(t_f)\rangle = U(t_f,t_i)|\psi(t_i)\rangle = |\psi_T\rangle$, i.e.,

$$\langle\psi_T|\psi_f\rangle = 1 - \frac{i}{\hbar}\int_{t_i}^{t_f}\langle\psi|V_\epsilon|\psi\rangle\, dt + \left(-\frac{i}{\hbar}\right)^2\int_{t_i}^{t_f}\int_{t_i}^{t}\langle\psi|V_\epsilon U U'^\dagger V'_\epsilon|\psi'\rangle\, dt'\, dt + \langle\psi_i|\widehat{O}(\epsilon^3)|\psi_i\rangle = 1 - O_1 - O_2 - \cdots, \tag{1.5}$$

$$|\langle\psi_T|\psi_f\rangle|^2 = 1 - \widetilde{O}_1 - \widetilde{O}_2 - \cdots, \tag{1.6}$$

where we have used the identity matrix, explicitly as the initial-time ideal propagator (which is true by the definition of a propagator) for an N-level system,

$$\mathbb{1} = U(t_i,t_i) = \sum_n^N |\psi_n(t_i)\rangle\langle\psi_n(t_i)|, \tag{1.7}$$

with $|\psi_n(t)\rangle$ a dynamical basis, to write the final-state deviation terms, O_n.

1.2.1 Two-level system

For the two-level system, the identity matrix is

$$\mathbb{1} = |\psi_0(t_i)\rangle\langle\psi_0(t_i)| + |\psi_\perp(t_i)\rangle\langle\psi_\perp(t_i)|, \tag{1.8}$$

where $|\psi_0\rangle$ and $|\psi_\perp\rangle$ are an orthonormal basis for the solution of the time-dependent Schrödinger equation (TDSE) for the Hamiltonian H, i.e., $\langle\psi_\perp(t)|\psi_0(t)\rangle = 0$ and the propagator of the unperturbed Hamiltonian is

$$U(t,t_i) = |\psi_0(t)\rangle\langle\psi_0(t_i)| + |\psi_\perp(t)\rangle\langle\psi_\perp(t_i)|. \tag{1.9}$$

The first three deviation terms read

$$O_1 = -(-i)\int_{t_i}^{t_f}\langle\psi_0|V|\psi_0\rangle\, dt \equiv i\int_{t_i}^{t_f} e\, dt \in \mathbb{I}, \quad (e\in\mathbb{R}) \tag{1.10a}$$

$$
\begin{aligned}
O_2 &= -(-i)^2 \int_{t_i}^{t_f}\int_{t_i}^{t} (ee' + f\overline{f}')\, dt'\, dt \\
&= -(-i)^2 \Bigg\{ \frac{1}{2}|O_1|^2 + \frac{1}{2}\left|\int_{t_i}^{t_f} f\, dt\right|^2 \\
&\qquad + i\left[2\int_{t_i}^{t_f}\int_{t_i}^{t} f^I(t) f^R(t')\, dt'\, dt - \int_{t_i}^{t_f} f^R(t)\, dt \int_{t_i}^{t_f} f^I(t)\, dt\right]\Bigg\}, \qquad (1.10b) \\
O_3 &= -(-i)^3 \int_{t_i}^{t_f}\int_{t_i}^{t}\int_{t_i}^{t'} (ee'e'' + ef'\overline{f}'' + f\overline{f}'e'' - fe'\overline{f}'')\, dt''\, dt'\, dt, \\
&= -(-i)^3 \left[\frac{1}{3}\int_{t_i}^{t_f} e\, dt \int_{t_i}^{t_f}\int_{t_i}^{t} ee'\, dt'\, dt + \int_{t_i}^{t_f} e\, dt \int_{t_i}^{t_f}\int_{t_i}^{t} f\overline{f}'\, dt'\, dt \right. \\
&\qquad \left. - 2\int_{t_i}^{t_f}\int_{t_i}^{t}\int_{t_i}^{t'} fe'\overline{f}''\, dt''\, dt'\, dt\right], \qquad (1.10c)
\end{aligned}
$$

with the real and complex variables

$$
\begin{aligned}
e &\equiv \langle\psi_0|V_\epsilon/\hbar|\psi_0\rangle = -\langle\psi_\perp|V_\epsilon/\hbar|\psi_\perp\rangle, \qquad (1.11a) \\
f &\equiv \langle\psi_0|V_\epsilon/\hbar|\psi_\perp\rangle, \qquad (1.11b)
\end{aligned}
$$

respectively. The other terms can be determined from a symbolic diagram [19].

We denote the state and population fidelities at a certain order n

$$
\begin{aligned}
\langle\psi_T|\psi_\epsilon(t_f)\rangle_n &= 1 - O_1 - O_2 - \cdots - O_n, \qquad (1.12a) \\
|\langle\psi_T|\psi_\epsilon(t_f)\rangle|_n^2 &= 1 - \widetilde{O}_1 - \widetilde{O}_2 - \cdots - \widetilde{O}_n. \qquad (1.12b)
\end{aligned}
$$

For population transfer, the relevant figure of merit is the population fidelity, for which the deviation terms are

$$
\begin{aligned}
\widetilde{O}_1 &= O_1 + \overline{O}_1 = 2\,\mathrm{Re}\, O_1 = 0, \qquad (1.13a) \\
\widetilde{O}_2 &= O_2 - O_1\overline{O}_1 + \overline{O}_2 = 2\,\mathrm{Re}\, O_2 - |O_1|^2 = \left(\int_{t_i}^{t_f} e\, dt\right)^2 + \left|\int_{t_i}^{t_f} f\, dt\right|^2, \qquad (1.13b) \\
\widetilde{O}_3 &= O_3 - O_1\overline{O}_2 - \overline{O}_1 O_2 + \overline{O}_3 = 2\,\mathrm{Re}\, O_3 + i2O_1\,\mathrm{Im}\, O_2. \qquad (1.13c)
\end{aligned}
$$

1.2.2 Three-level system

For the three-level system, the identity matrix is

$$
\mathbb{1} = |\psi_0(t_i)\rangle\langle\psi_0(t_i)| + |\psi_+(t_i)\rangle\langle\psi_+(t_i)| + |\psi_-(t_i)\rangle\langle\psi_-(t_i)| \qquad (1.14)
$$

and the first four final-state deviation terms are

$$O_1 = -(-i)\int_{t_i}^{t_f} m\,dt \in \mathbb{I}, \quad (m \in \mathbb{R}) \tag{1.15a}$$

$$\begin{aligned} O_2 &= -(-i)^2 \int_{t_i}^{t_f}\int_{t_i}^{t} (mm' + n\overline{n}' + p\overline{p}')\,dt'\,dt \\ &= \frac{1}{2}\left[|O_1|^2 + \left|\int_{t_i}^{t_f} n\,dt\right|^2 + \left|\int_{t_i}^{t_f} p\,dt\right|^2\right] + i\left[\int_{t_i}^{t_f} n^R\,dt \int_{t_i}^{t_f} n^I\,dt\right. \\ &\quad \left. + \int_{t_i}^{t_f} p^R\,dt \int_{t_i}^{t_f} p^I\,dt - 2\int_{t_i}^{t_f}\int_{t_i}^{t} (n^R n'^I + p^R p'^I)\,dt'\,dt\right], \end{aligned} \tag{1.15b}$$

$$\begin{aligned} O_3 &= -(-i)^3 \int_{t_i}^{t_f}\int_{t_i}^{t}\int_{t_i}^{t'} [m(m'm'' + n'\overline{n}'' + p'\overline{p}'') + n(\overline{n}'m'' + q'\overline{n}'' + r'\overline{p}'') \\ &\quad + p(\overline{p}'m'' + \overline{r}'\overline{n}'' + s'\overline{p}'')]\,dt''\,dt'\,dt, \end{aligned} \tag{1.15c}$$

$$\begin{aligned} &= -(-i)^3\left\{|O_1|O_2 - \frac{1}{3}|O_1|^3 + \int_{t_i}^{t_f} n\,dt \int_{t_i}^{t_f}\int_{t_i}^{t} r\overline{p}'\,dt'\,dt \right. \\ &\quad + \int_{t_i}^{t_f} p\,dt \int_{t_i}^{t_f}\int_{t_i}^{t} \overline{r}\overline{n}'\,dt'\,dt - 2\,\mathrm{Re}\left[\int_{t_i}^{t_f}\left(\int_{t_i}^{t} n'\,dt'\right)\left(\int_{t_i}^{t} \overline{p}'\,dt'\right) r\,dt\right] \\ &\quad \left. + \int_{t_i}^{t_f}\int_{t_i}^{t}\int_{t_i}^{t'} [n(m' + q')\overline{n}'' + p(m' + s')\overline{p}'']\,dt''\,dt'\,dt\right\}, \end{aligned} \tag{1.15d}$$

$$\begin{aligned} O_4 = -(-i)^4 \int_{t_i}^{t_f}\int_{t_i}^{t}\int_{t_i}^{t'}\int_{t_i}^{t''} &\{m[m'(m''m''' + n''\overline{n}''' + p''\overline{p}''') + n'(\overline{n}''m''' + q''\overline{n}''' \\ &+ r''\overline{p}''') + p'(\overline{p}''m''' + \overline{r}''\overline{n}''' + s''\overline{p}''')] + n[\overline{n}'(m''m''' + n''\overline{n}''' + p''\overline{p}''') \\ &+ q'(\overline{n}''m''' + q''\overline{n}''' + r''\overline{p}''') + r'(\overline{p}''m''' + \overline{r}''\overline{n}''' + s''\overline{p}''')] + p[\overline{p}'(m''m''' \\ &+ n''\overline{n}''' + p''\overline{p}''') + \overline{r}'(\overline{n}''m''' + q''\overline{n}''' + r''\overline{p}''') + s'(\overline{p}''m''' + \overline{r}''\overline{n}''' \\ &+ s''\overline{p}''')]\}\,dt'''\,dt''\,dt'\,dt, \end{aligned} \tag{1.15e}$$

where the bar over terms of the expression denotes their complex conjugate, and the superscripts R and I mean real and imaginary parts, respectively. We have used

the properties

$$\int_{t_i}^{t_f}\int_{t_i}^{t}(ab'+ba')\,dt'\,dt = \int_{t_i}^{t_f} a\,dt \int_{t_i}^{t_f} b\,dt, \tag{1.16a}$$

$$\int_{t_i}^{t_f}\int_{t_i}^{t}\int_{t_i}^{t'} ab'c'' = \int_{t_i}^{t_f} a\,dt \int_{t_i}^{t_f}\left(\int_{t_i}^{t} c'\,dt'\right) b\,dt - \int_{t_i}^{t_f}\left(\int_{t_i}^{t} a'\,dt'\right)\left(\int_{t_i}^{t} c'\,dt'\right) b\,dt \tag{1.16b}$$

$$\int_{t_i}^{t_f}\int_{t_i}^{t}\int_{t_i}^{t'}(ab'c''+ba'c''+bc'a'')\,dt''\,dt'\,dt = \int_{t_i}^{t_f} a\,dt \int_{t_i}^{t_f}\int_{t_i}^{t} bc'\,dt'\,dt, \tag{1.16c}$$

$$\int_{t_i}^{t_f}\int_{t_i}^{t}\int_{t_i}^{t'}\sum_{\sigma} a^{(\sigma_1)}b^{(\sigma_2)}c^{(\sigma_3)}\,dt''\,dt'\,dt = \int_{t_i}^{t_f} a\,dt \int_{t_i}^{t_f} b\,dt \int_{t_i}^{t_f} c\,dt, \tag{1.16d}$$

where $\sum_\sigma$ is the summation over all possible permutations of the primed functions, and the last two properties can be generalized for more than three nested integrals, e.g.,

$$\int_{t_i}^{t_f}\int_{t_i}^{t}\int_{t_i}^{t'}\int_{t_i}^{t''}(ab'c''d'''+ba'c''d'''+bc'a''d'''+bc'd''a''')\,dt''\,dt'\,dt = \int_{t_i}^{t_f} a\,dt \int_{t_i}^{t_f}\int_{t_i}^{t}\int_{t_i}^{t'} bc'd''\,dt''\,dt'\,dt. \tag{1.17}$$

The vectors $|\psi_+\rangle$ and $|\psi_-\rangle$ are orthonormal vectors perpendicular to $|\psi_0\rangle$, with which they form a complete basis (thus allowing the previous definition of the identity matrix), and the elements of the interaction Hamiltonian on this basis are

$$m = \langle\psi_0|V_\epsilon/\hbar|\psi_0\rangle, \qquad n = \langle\psi_0|V_\epsilon/\hbar|\psi_+\rangle, \qquad p = \langle\psi_0|V_\epsilon/\hbar|\psi_-\rangle, \tag{1.18a}$$

$$q = \langle\psi_+|V_\epsilon/\hbar|\psi_+\rangle, \qquad r = \langle\psi_+|V_\epsilon/\hbar|\psi_-\rangle, \qquad s = \langle\psi_-|V_\epsilon/\hbar|\psi_-\rangle, \tag{1.18b}$$

where m, q and s, are real quantities since V_ϵ is Hermitian. The final population deviations from the perfect transfer, the $\widetilde{O}_n$'s, are straightforwardly given by

$$\widetilde{O}_1 = O_1 + \overline{O}_1 = 2\,\mathrm{Re}\,O_1 = 0, \tag{1.19a}$$

$$\widetilde{O}_2 = O_2 - O_1\overline{O}_1 + \overline{O}_2 = 2\,\mathrm{Re}\,O_2 - |O_1|^2 = \left|\int_{t_i}^{t_f} n\,dt\right|^2 + \left|\int_{t_i}^{t_f} p\,dt\right|^2, \tag{1.19b}$$

$$\widetilde{O}_3 = O_3 - O_1\overline{O}_2 - \overline{O}_1O_2 + \overline{O}_3 = 2\,\mathrm{Re}\,O_3 + i2O_1\,\mathrm{Im}\,O_2, \tag{1.19c}$$

$$\widetilde{O}_4 = O_4 - O_1\overline{O}_3 - O_2\overline{O}_2 - \overline{O}_1O_3 + \overline{O}_4 = 2\,\mathrm{Re}\,O_4 - |O_2|^2 + i2O_1\,\mathrm{Im}\,O_3. \tag{1.19d}$$

A pictorial representation of the scheme to obtain the O_n's is shown in Fig. 1.1.

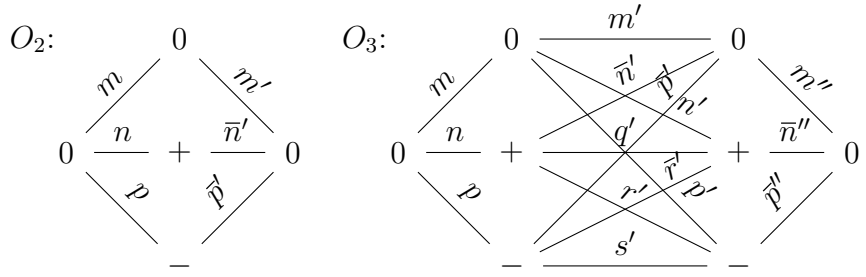

Figure 1.1: Pictorial representation of the obtainment of the O_n's

1.2.3 Procedure to control the robustness of the control

The only requirement for this treatment is that the interaction Hamiltonian V_ϵ needs to represent only a perturbation to the perfect inverse-engineered Hamiltonian H. Satisfied this condition, we can identify the terms that provoke the deviations on the perfect transfer to the target state as the O_n's (or $\widetilde{O}_n$'s if the target fidelity is measured for population). Then, with an appropriately parametrized propagator U, we can obtain the basis vectors $|\psi_n\rangle$ and attempt to improve the robustness of the process by minimizing the deviations.

It is worth noting that the propagator involved in the obtainment of the deviation terms is the one corresponding to the perfect transfer, the system with no perturbations ϵ. This implies that we can treat a complicated system with a simplified propagator if the complications of the system come only from perturbations.

The parametrization necessary for the inverse-engineering procedure is described in the following sections, depending on the symmetry of the system Hamiltonian. Multiple methods of obtaining propagators, with the purpose of providing freedom to choose more convenient parametrizations, are presented before choosing a pair of specially relevant representations, according to their physical interpretation and practicality of their manipulation.

1.2.4 General SU(2) propagator for SSSP on the two-level system

It is easy to show that a general parametrization for a propagator in U(2) (a unitary 2×2 matrix) is

$$U_\phi = e^{i\phi/2} \begin{bmatrix} e^{i(\varphi-\gamma)/2}\cos(\theta/2) & -e^{i(\varphi+\gamma)/2}\sin(\theta/2) \\ e^{-i(\varphi+\gamma)/2}\sin(\theta/2) & e^{-i(\varphi-\gamma)/2}\cos(\theta/2) \end{bmatrix}, \tag{1.20}$$

where ϕ is a global dynamical phase and the necessary initial conditions are $\theta_i = \phi_i = 0$ and $\varphi_i = \gamma_i$. The special unitary group SU(2) is that of matrices in U(2) with determinant equal to 1; in this case, the global phase must be null at all times and the general parametrized propagator is

$$U = \begin{bmatrix} e^{i(\varphi-\gamma)/2}\cos(\theta/2) & -e^{i(\varphi+\gamma)/2}\sin(\theta/2) \\ e^{-i(\varphi+\gamma)/2}\sin(\theta/2) & e^{-i(\varphi-\gamma)/2}\cos(\theta/2) \end{bmatrix}. \tag{1.21}$$

Given that the Schrödinger equation for traceless Hamiltonians demands the propagator to have a constant global phase,

$$i\hbar\,\mathrm{Tr}(\dot{U}_\phi U_\phi^\dagger) = -\hbar\dot{\phi} + i\hbar\cancelto{0}{\mathrm{Tr}(\dot{U}U^\dagger)} = \mathrm{Tr}\,H = 0, \tag{1.22}$$

and that a constant global phase for the propagator is irrelevant,

$$i\hbar\cancel{e^{i\phi/2}}\dot{U} = H\cancel{e^{i\phi/2}}U, \tag{1.23}$$

we can always use a propagator of the form U, in SU(2), to consider the dynamics of traceless Hamiltonian systems.

Similarly, for a Hamiltonian with non-zero trace the global dynamical phase of the propagator in U(2) could be absorbed into the system statevector and we would be again considering an evolution in SU(2).

A well-known way to produce a SU(2) matrix with a general Euler angle parametrization, though with a set of required initial conditions, is with the product of the generators of its algebra, like

$$U = e^{i\sigma_z\varphi/2}e^{-\sigma_y\theta/2}e^{-\sigma_z\gamma/2} = \begin{bmatrix} e^{i(\varphi-\gamma)/2}\cos(\theta/2) & -e^{i(\varphi+\gamma)/2}\sin(\theta/2) \\ e^{-i(\varphi+\gamma)/2}\sin(\theta/2) & e^{-i(\varphi-\gamma)/2}\cos(\theta/2) \end{bmatrix}. \tag{1.24}$$

1.2.5 Lewis-Riesenfeld invariant for SSSP on the two-level system

For a Hamiltonian

$$H = \frac{\hbar}{2}\begin{bmatrix} -\Delta & \Omega \\ \Omega & \Delta \end{bmatrix}, \tag{1.25}$$

with Rabi frequency Ω and detuning Δ, the Lewis-Riesenfeld (L-R) invariant [21, 22, 26, 27] is

$$I = \alpha_1\sigma_x + \alpha_2\sigma_y + \alpha_3\sigma_z, \tag{1.26}$$

where $\sum_{n=1}^{3}\alpha_n^2=\alpha_0^2$, α_0 is a constant (positive by choice) and the generators of the algebra, σ_n, are, as usual, the Pauli matrices

$$\sigma_x=\begin{bmatrix}0&1\\1&0\end{bmatrix},\quad \sigma_y=\begin{bmatrix}0&-i\\i&0\end{bmatrix},\quad \sigma_z=\begin{bmatrix}1&0\\0&-1\end{bmatrix}. \tag{1.27}$$

The eigenvalues of this invariant are $\pm\alpha_0$ and the eigenvectors

$$|\phi_\pm\rangle=\frac{1}{\sqrt{2\alpha_0(\alpha_0\pm\alpha_3)}}\begin{bmatrix}\pm(\alpha_0\pm\alpha_3)\\ \alpha_1+i\alpha_2\end{bmatrix}, \tag{1.28}$$

with their corresponding populations,

$$P_\pm=\begin{bmatrix}|\langle 1|\phi_\pm\rangle|^2\\ |\langle 2|\phi_\pm\rangle|^2\end{bmatrix}=\frac{1}{2\alpha_0}\begin{bmatrix}\alpha_0\pm\alpha_3\\ \alpha_0\mp\alpha_3\end{bmatrix}. \tag{1.29}$$

From the Schrödinger equation for the invariant, $i\hbar\dot{I}=[H,I]$, the Rabi frequency and detuning are

$$\Omega=\frac{\dot{\alpha_3}}{\alpha_2},\quad \Delta=\frac{\dot{\alpha_1}}{\alpha_2}. \tag{1.30}$$

The L-R phases, $\eta_\pm=\int_{t_i}^{t}\langle\phi_\pm|i\hbar\partial_t-H|\phi_\pm\rangle/\hbar$, are given by

$$\dot{\eta}_\pm=\frac{\dot{\alpha}_1}{2\alpha_2}\mp\frac{\alpha_1\dot{\alpha}_3}{2\alpha_2(\alpha_0\pm\alpha_3)} \tag{1.31}$$

The propagator, $U=\begin{bmatrix}U_{|1\rangle} & U_{|2\rangle}\end{bmatrix}/2\alpha_0$, is then

$$U_{|1\rangle}=\begin{bmatrix}e^{i\eta_-}\sqrt{(\alpha_0-\alpha_3)(\alpha_0-\alpha_{3i})}+e^{i\eta_+}\sqrt{(\alpha_0+\alpha_3)(\alpha_0+\alpha_{3i})}\\ e^{i\eta_{12}}\left[-e^{i\eta_-}\sqrt{(\alpha_0+\alpha_3)(\alpha_0-\alpha_{3i})}+e^{i\eta_+}\sqrt{(\alpha_0-\alpha_3)(\alpha_0+\alpha_{3i})}\right]\end{bmatrix}, \tag{1.32a}$$

$$U_{|2\rangle}=e^{-i\eta_{12i}}\begin{bmatrix}-e^{i\eta_-}\sqrt{(\alpha_0-\alpha_3)(\alpha_0+\alpha_{3i})}+e^{i\eta_+}\sqrt{(\alpha_0+\alpha_3)(\alpha_0-\alpha_{3i})}\\ e^{i\eta_{12}}\left[e^{i\eta_-}\sqrt{(\alpha_0+\alpha_3)(\alpha_0+\alpha_{3i})}+e^{i\eta_+}\sqrt{(\alpha_0-\alpha_3)(\alpha_0-\alpha_{3i})}\right]\end{bmatrix}, \tag{1.32b}$$

where $\widetilde{\alpha}_{12}=\alpha_1+i\alpha_2=\alpha_{12}e^{i\eta_{12}}$. $\widetilde{\alpha}_{12}$ is a complex number with modulus α_{12} and phase η_{12}, thus $\alpha_{12}=\sqrt{\alpha_1^2+\alpha_2^2}$ and $e^{i\eta_{12}}=(\alpha_1+i\alpha_2)/\alpha_{12}$.

We can parametrize the α_n's in terms of angular variables as

$$\alpha_1=\alpha_0\cos\varphi\sin\theta,\quad \alpha_2=-\alpha_0\sin\varphi\sin\theta,\quad \alpha_3=\alpha_0\cos\theta, \tag{1.33}$$

thus producing $\widetilde{\alpha}_{12}=\alpha_0e^{-i\varphi}\sin\theta$ and making the states, populations, Rabi fre-

quency, detuning, L-R phases, and propagator be

$$|\phi_+\rangle = \begin{bmatrix} \cos(\theta/2) \\ e^{-i\varphi}\sin(\theta/2) \end{bmatrix}, \quad |\phi_-\rangle = \begin{bmatrix} -\sin(\theta/2) \\ e^{-i\varphi}\cos(\theta/2) \end{bmatrix}, \tag{1.34a}$$

$$P_+ = \begin{bmatrix} \cos^2(\theta/2) \\ \sin^2(\theta/2) \end{bmatrix}, \quad P_- = \begin{bmatrix} \sin^2(\theta/2) \\ \cos^2(\theta/2) \end{bmatrix}, \tag{1.34b}$$

$$\Omega = \frac{\dot{\theta}}{\sin\varphi}, \quad \Delta = \dot{\varphi} - \frac{\dot{\theta}\cos\varphi\cos\theta}{\sin\varphi\sin\theta}, \tag{1.34c}$$

$$\dot{\eta}_\pm = \frac{\dot{\varphi}}{2} \mp \frac{\dot{\theta}\cos\varphi}{2\sin\phi\sin\theta}, \tag{1.34d}$$

$$\frac{U_{|1\rangle}}{2\alpha_0} = \begin{bmatrix} e^{i\eta_-}\sin(\theta/2)\sin(\theta_i/2) + e^{i\eta_+}\cos(\theta/2)\cos(\theta_i/2) \\ e^{-i\varphi}\left[-e^{i\eta_-}\cos(\theta/2)\sin(\theta_i/2) + e^{i\eta_+}\sin(\theta/2)\cos(\theta_i/2)\right] \end{bmatrix}, \tag{1.34e}$$

$$\frac{U_{|2\rangle}}{2\alpha_0} = e^{i\varphi_i}\begin{bmatrix} -e^{i\eta_-}\sin(\theta/2)\cos(\theta_i/2) + e^{i\eta_+}\cos(\theta/2)\sin(\theta_i/2) \\ e^{-i\varphi}\left[e^{i\eta_-}\cos(\theta/2)\cos(\theta_i/2) + e^{i\eta_+}\sin(\theta/2)\sin(\theta_i/2)\right] \end{bmatrix}, \tag{1.34f}$$

respectively. We can rewrite the L-R phases as

$$\eta_\pm = \frac{\varphi - \varphi_i}{2} \mp \frac{\gamma - \gamma_i}{2}, \tag{1.35}$$

by introducing

$$\dot{\gamma} = \frac{\dot{\theta}\cos\varphi}{\sin\varphi\sin\theta}. \tag{1.36}$$

It is worth noting that this propagator is such independently of the initial conditions, unlike the "general" SU(2) parametrization in (1.21). Thus we are free to choose any initial conditions for the parameters in the propagator and obtain the system state afterwards. A choice that simplifies greatly the propagator is $\theta_i = 0$, while $\varphi_i = \gamma_i$ makes it equal to (1.21). Then, the aesthetically simplified but general propagator is

$$U = \begin{bmatrix} e^{i[(\varphi-\varphi_i)-(\gamma-\gamma_i)]/2}\cos(\theta/2) & -e^{i[(\varphi+\varphi_i)+(\gamma-\gamma_i)]/2}\sin(\theta/2) \\ e^{-i[(\varphi+\varphi_i)+(\gamma-\gamma_i)]/2}\sin(\theta/2) & e^{-i[(\varphi-\varphi_i)-(\gamma-\gamma_i)]/2}\cos(\theta/2) \end{bmatrix}. \tag{1.37}$$

For a NOT-type gate $U_{11f} = 0$ and $U_{21f} = 1$, $\theta_f = \pi$, and $\kappa = (\varphi_f + \varphi_i + \gamma_f - \gamma_i)/2$ produce

$$U_{\text{NOT}} = \begin{bmatrix} 0 & -e^{i\kappa} \\ e^{-i\kappa} & 0 \end{bmatrix}. \tag{1.38}$$

A Hadamard-type gate, $U_{11f} = e^{i(\varphi_0-\gamma_0)/2}/\sqrt{2}$ and $U_{21f} = e^{-i(\varphi_0+\gamma_0)/2}/\sqrt{2}$, requires

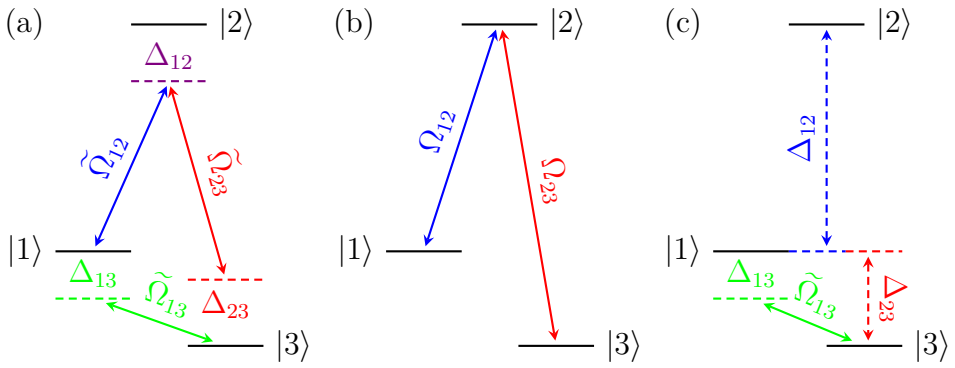

Figure 1.2: From left to right: (a) a general three-level system in lambda (Λ) configuration, (b) a resonant three-level system in Λ configuration with real couplings and no coupling between states $|1\rangle$ and $|3\rangle$, (c) a three-level system in ladder (Ξ) configuration with no couplings between $|2\rangle$ and $|3\rangle$ nor between $|1\rangle$ and $|2\rangle$.

$\theta_f = \pi/2$, $\varphi_f - \varphi_i = \varphi_0$, and $\gamma_f - \gamma_i = \gamma_0$ to produce

$$U_{\mathrm{H}} = \frac{1}{\sqrt{2}} \begin{bmatrix} e^{i(\varphi_0 - \gamma_0)/2} & -e^{i(\varphi_0 + \gamma_0)/2} \\ e^{-i(\varphi_0 + \gamma_0)/2} & e^{-i(\varphi_0 - \gamma_0)/2} \end{bmatrix}. \tag{1.39}$$

We can use it to generate a maximum superposition if the system is initially in either of $|1\rangle$ or $|2\rangle$.

1.2.6 General SU(3) propagator for SSSP on the three-level system

The dynamics of a general three-level system (as the ones in Fig. 1.2), a system comprehending three states, one coupling for each pair of states, and one detuning between coupling and the corresponding transition frequency, as the one with Hamiltonian (1.40), is governed by a propagator belonging to the SU(3) group [when the Hamiltonian is traceless, and U(3) otherwise].

$$\widetilde{H} = \frac{\hbar}{2} \begin{bmatrix} 2(\Delta_{23} - \Delta_{12})/3 & \Omega_{12} & e^{-i(\tilde{\eta}_{12} - \tilde{\eta}_{23})} \widetilde{\Omega}_{13} \\ \Omega_{12} & 2(\Delta_{23} + 2\Delta_{12})/3 & \Omega_{23} \\ e^{i(\tilde{\eta}_{12} - \tilde{\eta}_{23})} \overline{\widetilde{\Omega}}_{13} & \Omega_{23} & -2(\Delta_{12} + 2\Delta_{23})/3 \end{bmatrix}, \tag{1.40}$$

The SU(3) group is characterized by the eight (hermitian and traceless) generators λ_n, commonly known as the Gell-Mann matrices, and obeys the su(3) algebra

described by their commutation relations, i.e.,

$$\lambda_1 = \begin{bmatrix} 0 & 1 & 0 \\ 1 & 0 & 0 \\ 0 & 0 & 0 \end{bmatrix}, \qquad \lambda_2 = \begin{bmatrix} 0 & -i & 0 \\ i & 0 & 0 \\ 0 & 0 & 0 \end{bmatrix}, \qquad \lambda_3 = \begin{bmatrix} 1 & 0 & 0 \\ 0 & -1 & 0 \\ 0 & 0 & 0 \end{bmatrix}, \tag{1.41a}$$

$$\lambda_4 = \begin{bmatrix} 0 & 0 & 1 \\ 0 & 0 & 0 \\ 1 & 0 & 0 \end{bmatrix}, \qquad \lambda_5 = \begin{bmatrix} 0 & 0 & -i \\ 0 & 0 & 0 \\ i & 0 & 0 \end{bmatrix}, \qquad \lambda_8 = \frac{1}{\sqrt{3}} \begin{bmatrix} 1 & 0 & 0 \\ 0 & 1 & 0 \\ 0 & 0 & -2 \end{bmatrix}, \tag{1.41b}$$

$$\lambda_6 = \begin{bmatrix} 0 & 0 & 0 \\ 0 & 0 & 1 \\ 0 & 1 & 0 \end{bmatrix}, \qquad \lambda_7 = \begin{bmatrix} 0 & 0 & 0 \\ 0 & 0 & -i \\ 0 & i & 0 \end{bmatrix}, \qquad [\lambda_i, \lambda_j] = \sum_{k=1}^{8} C_{ij}^k \lambda_k, \tag{1.41c}$$

with $C_{23}^1 = 2i$, $C_{47}^1 = C_{65}^1 = C_{46}^2 = C_{75}^2 = C_{45}^3 = C_{76}^3 = i$, $C_{58}^4 = C_{78}^6 = i\sqrt{3}$, satisfying the properties $C_{ij}^k = -C_{ji}^k$, $C_{ij}^k = C_{jk}^i$ and the normalization condition $\mathrm{Tr}(\lambda_i \lambda_i) = 2\delta_{ij}$, with δ_{ij} the Kronecker Delta.

The su(3) algebra is composed by a few sets of closed algebras, such as the su(2) subalgebras constituted by $\{\lambda_1, \lambda_5, \lambda_6\}$ and $\{\lambda_1, \lambda_2, \lambda_3\}$, or as the extended $\{\lambda_1, \lambda_2, \lambda_3, \lambda_8\}$, with its equivalents $\{\lambda_3, \lambda_6, \lambda_7, \lambda_8\}$ and $\{\lambda_5, \lambda_4, \lambda_3, \lambda_8\}$. Other subalgebras of su(3) exist, but they are redundant in their physical interpretation when considering Hamiltonians written in terms of their generators. Even though the general SU(3) propagator obeying the su(3) algebra is necessary when treating a general Hamiltonian involving a three-state system, some cases significant in their practicality can be described restricting the propagator to the subalgebras of su(3), e.g., the subalgebra constituted by

- $\{\lambda_1, \lambda_5, \lambda_6\}$ is appropriate to treat fully resonant three-level systems with real couplings Ω_{12} and Ω_{23}, and no coupling Ω_{13}, while the one generated by

- $\{\lambda_5, \lambda_4, \lambda_3, \lambda_8\}$ can describe a three-level system with a single coupling, the complex coupling $\widetilde{\Omega}_{13}$, a detuning with respect to the target level $|1\rangle$ and another to the desirably uncoupled level $|2\rangle$. This system reduces to one of two levels, since the third level becomes irrelevant, unless a deviation from this algebra is included in the form of a small coupling with level $|2\rangle$.

The physical systems described by the su(3) algebra and the mentioned subalgebras are pictured in Fig. 1.2. Additional subalgebras may be found, e.g., using equal couplings $\widetilde{\Omega}_{12} = \widetilde{\Omega}_{23} = \widetilde{\Omega}$ and detunings such that $\Delta_{23} = -2\Delta_{12}$, the corresponding generator $\lambda_{16} = \lambda_1 + \lambda_6$ obeys the su(2) algebra with $\lambda_{27} = \lambda_2 + \lambda_7$ and $\lambda_{38} = (\lambda_3 + \sqrt{3}\lambda_8)/2$.

The propagator corresponding to these three-level Hamiltonians is an element of SU(3). In fact, we can write the general Hamiltonian (1.40) in terms of the generators of such algebra as

$$\widetilde{H} = \frac{\hbar}{2}\Big[\Omega_{12}\lambda_1 + \Omega_{23}\lambda_6 - \Delta_{12}\lambda_3 + (\Delta_{12} + 2\Delta_{23})\lambda_8/\sqrt{3}. \\ + \cos(\widetilde{\eta}_{12} - \widetilde{\eta}_{23} - \widetilde{\eta}_{13})\Omega_{13}\lambda_4 + \sin(\widetilde{\eta}_{12} - \widetilde{\eta}_{23} - \widetilde{\eta}_{13})\Omega_{13}\lambda_5\Big]. \tag{1.42}$$

The formula to write a general element belonging to the SU(3) group is known and provided by [28], i.e.,

$$\widetilde{U} = e^{i\lambda_3 x}e^{-i\lambda_2\theta}e^{i\lambda_3 z}e^{i\lambda_5(\phi+\pi/2)}e^{i\lambda_3 a}e^{i\lambda_2(\eta+\pi/2)}e^{i\lambda_3 c}e^{i\lambda_8\sqrt{3}y}, \tag{1.43}$$

where we have taken some liberties when defining the Euler angles. We can reshape, or reparametrize, this propagator by applying unitary transformations using exponential matrices of the same generators (and thus with unity determinant) but with fixed factors, fixed rotations on the abstract eigth-fold parameter space that will only affect the parametrization and not the generality of the group element.

Two versions of this propagator can be highlighted, both general representations of an element of the SU(3) group, but where the Euler angles take different physical interpretations by effect of specified aesthetically-convenient transformations. On one hand, we have a version of the propagator that facilitates the study of population evolution on the bare states when the system is initially in state $|1\rangle$,

$$\widetilde{U}_p = e^{i\lambda_5\pi/2}e^{i\lambda_2\pi/2}e^{i\lambda_5\pi/2}\widetilde{U}e^{i\lambda_5\pi/2} = \left[|\widetilde{\psi}_{p1}\rangle \quad |\widetilde{\psi}_{p2}\rangle \quad |\widetilde{\psi}_{p3}\rangle\right], \tag{1.44}$$

with

$$|\widetilde{\psi}_{p1}\rangle = e^{-2iy}\begin{bmatrix} e^{i(x+z)}\cos\theta\sin\phi \\ -\sin\phi \\ e^{i(-x+z)}\cos\phi\sin\theta \end{bmatrix}, \tag{1.45a}$$

$$|\widetilde{\psi}_{p2}\rangle = e^{i(-c+y)}\begin{bmatrix} e^{i(a+x+z)}\cos\eta\cos\theta\sin\phi - e^{i(-a+x-z)}\sin\eta\sin\theta \\ e^{ia}\cos\eta\cos\phi \\ e^{i(a-x+z)}\cos\eta\sin\theta\sin\phi + e^{i(-a-x-z)}\cos\theta\sin\eta \end{bmatrix}, \tag{1.45b}$$

$$|\widetilde{\psi}_{p3}\rangle = -e^{i(c+y)}\begin{bmatrix} e^{i(a+x+z)}\cos\theta\sin\eta\sin\phi + e^{i(-a+x-z)}\cos\eta\sin\theta \\ e^{ia}\cos\phi\sin\eta \\ e^{i(a-x+z)}\sin\eta\sin\theta\sin\phi - e^{i(-a-x-z)}\cos\eta\cos\theta \end{bmatrix}, \tag{1.45c}$$

where the first column, corresponding to the parametrization of the solution to the

Schrödinger equation if the system satisfies $|\psi_i\rangle = |1\rangle$ has been simplified, thus providing simple physical interpretation to the Euler angles, i.e., as the state of the system is then parametrized as $|\psi\rangle = \widetilde{U}|\psi_i\rangle = |\widetilde{\psi}_{p1}\rangle$ we can see θ as the mixing angle between the states $|1\rangle$ and $|3\rangle$ while ϕ is the mixing angle between them and state $|2\rangle$. The initial conditions of this propagator are given by

$$\phi_i = n_1\pi, \quad \theta_i = n_2\pi, \quad \eta_i = n_3\pi, \tag{1.46a}$$

$$x_i + z_i - 2y_i = (2n_4 + n_1 + n_2)\pi, \quad a_i - c_i + y_i = (2n_5 + n_1 + n_3)\pi, \tag{1.46b}$$

where the n_k's are positive and/or negative integers, i.e., $n_k = 0, \pm1, \pm2, \ldots$

On the other hand, the propagator U_s,

$$\widetilde{U}_s = e^{i\lambda_7\pi/2}\widetilde{U}e^{i\lambda_7\pi/2} = \left[|\widetilde{\psi}_{s1}\rangle \quad |\widetilde{\psi}_{s2}\rangle \quad |\widetilde{\psi}_{s3}\rangle\right], \tag{1.47}$$

with columns

$$|\widetilde{\psi}_{s1}\rangle = e^{i(c+y)} \begin{bmatrix} e^{i(a+x+z)}\cos\theta\sin\eta\sin\phi + e^{i(-a+x-z)}\cos\eta\sin\theta \\ e^{ia}\cos\phi\sin\eta \\ -e^{i(a-x+z)}\sin\eta\sin\theta\sin\phi + e^{i(-a-x-z)}\cos\eta\cos\theta \end{bmatrix}, \tag{1.48a}$$

$$|\widetilde{\psi}_{s2}\rangle = e^{-i2y} \begin{bmatrix} -e^{i(x+z)}\cos\theta\cos\phi \\ \sin\phi \\ e^{i(-x+z)}\cos\phi\sin\theta \end{bmatrix}, \tag{1.48b}$$

$$|\widetilde{\psi}_{s3}\rangle = e^{i(-c+y)} \begin{bmatrix} -e^{i(a+x+z)}\cos\eta\cos\theta\sin\phi + e^{i(-a+x-z)}\sin\eta\sin\theta \\ -e^{ia}\cos\eta\cos\phi \\ e^{i(a-x+z)}\cos\eta\sin\theta\sin\phi + e^{i(-a-x-z)}\cos\theta\sin\eta \end{bmatrix}, \tag{1.48c}$$

exhibits the complementary dynamical behavior for the evolution of the state of the system when it is initially in any given superposition of the ground states, $|\psi_i\rangle = c_1|1\rangle + c_3|3\rangle$. Thus, making it ideal for the design of gates between such states. The initial conditions for U_s include the global and straightforward

$$\phi_i = (2n_1 + 1)\pi/2, \quad y_i = (2n_2 + n_1)\pi/2, \tag{1.49}$$

and two variants:

(1) One where the pair of independent initial values is constituted by one value

from each set $\{\theta_i, \eta_i\}$, $\{a_i, z_i\}$, and $\{c_i, x_i\}$, with

$$\theta_i + (-1)^{n1+n_4}\eta_i = (2n_3+1)\pi/2, \quad a_i + z_i = n_4\pi/2, \tag{1.50a}$$

$$c_i + x_i = (n_4 - n_1)\pi/2 + (n_2 + n_3 + 2n_5)\pi, \tag{1.50b}$$

(2) and one where three initial values taken from the set $\{a_i, z_i, c_i, x_i\}$ are independent, with

$$\eta_i = n_3\pi/2, \quad \theta_i = (n_3 + 2n_4 + 1)\pi/2, \tag{1.51a}$$

$$\widetilde{a}_i - (-1)^{n_3}\widetilde{c}_i = [n_2 + (1+n_1)n_3 + n_4 + 2n_5]\pi + (-1)^{n_3}n_1\pi/2, \tag{1.51b}$$

$$\widetilde{a}_i = a_i + z_i, \quad \widetilde{c}_i = c_i + x_i. \tag{1.51c}$$

The general SU(3) propagators lead to very complicated relations, even the obtainment of their boundary conditions is nontrivial, then making the whole system potentially intractable [29]. Luckily, the subalgebras described by

$$\widetilde{\Omega}_{13} = \Delta_{12} = \Delta_{13} = \Delta_{23} = 0, \tag{1.52a}$$

$$\Omega_{12} = \Omega_{23} = \widetilde{\eta}_{12} = \widetilde{\eta}_{23} = 0, \ \Delta_{23} = \Delta_{13} - \Delta_{12} + \dot{\widetilde{\eta}}_{13}, \ \Delta_{12} = \omega_2 - \omega_1, \tag{1.52b}$$

correspond to the physically realistic, highly relevant and very widely implemented situations depicted by the systems in Figs. 1.2(b) and 1.2(c). Thus, we can focus on obtaining the propagators, boundary conditions and solutions of the Schrödinger equation for particular cases of the three-level system, specifically for the fully resonant Λ system in Fig. 1.2(b) corresponding to a Hamiltonian of the form

$$H = \frac{\hbar}{2}\begin{bmatrix} 0 & \Omega_P & 0 \\ \Omega_P & 0 & \Omega_S \\ 0 & \Omega_S & 0 \end{bmatrix}, \tag{1.53}$$

where Ω_P and Ω_S are the real-valued pulse envelopes of the control fields coupling state $|2\rangle$ with states $|1\rangle$ and $|3\rangle$, respectively; the three-level system is discussed in detail in chapter 3.

These reduced SU(3) propagators U, i.e., the general SU(3) propagators for the subalgebras corresponding to simplified systems, are obtainable by fixing some of the angular variables (or phases) to their initial conditions and restricting the acceptable initial conditions of others, but the minimal set of variables to be fixed in order to obtain the general propagator for the simplified system remains unknown until a direct representation of the subalgebra can be provided.

We will now proceed to demonstrate the direct obtainment of propagators for the subalgebra of SU(3) given by the set of generators $\{\lambda_1, \lambda_5, \lambda_6\}$ using the product of exponential matrices with the generators and angular variables as arguments.

General propagator for the fully resonant system: product of the exponentials of generators

By analogy with the SU(2) algebra, whose elements are produced with the well-known product of exponentials of the Pauli matrices σ_n and Euler angles, i.e., the generators of SU(2) and free angular variables, where a common representation is given by

$$U^{\mathrm{SU}(2)} = e^{i\sigma_z\varphi/2}e^{-i\sigma_y\theta/2}e^{-i\sigma_z\gamma/2} = \begin{bmatrix} e^{i(\varphi-\gamma)/2}\cos(\theta/2) & -e^{i(\varphi+\gamma)/2}\sin(\theta/2) \\ e^{-i(\varphi+\gamma)/2}\sin(\theta/2) & e^{-i(\varphi-\gamma)/2}\cos(\theta/2) \end{bmatrix}, \quad (1.54)$$

we can write a propagator in SU(3), in the su(2) subalgebra formed by the set of generators $\{\lambda_1, \lambda_5, \lambda_6\}$, i.e.,

$$[\lambda_1, \lambda_6] = i\lambda_5, \quad [\lambda_6, \lambda_5] = i\lambda_1, \quad [\lambda_5, \lambda_1] = i\lambda_6, \quad (1.55)$$

with a general parametrization in terms of Euler angles, as a product such as

$$U_p = e^{-i\lambda_5\theta}e^{i\lambda_1\phi}e^{i\lambda_6\eta} = \begin{bmatrix} |\psi_{p1}\rangle & |\psi_{p2}\rangle & |\psi_{p3}\rangle \end{bmatrix}, \quad (1.56)$$

whose columns $|\psi_{pn}\rangle$, corresponding to the tilded versions $|\widetilde{\psi}_{pn}\rangle$ of (1.45) to which the variables x and a have been fixed to their initial conditions x_i and a_i in (1.46) with the additional restrictions

$$n_2 = 2n_6 + n_1, \quad n_3 = 2n_7 + n_1, \quad (1.57a)$$

$$c_i = (4n_8 + 3)\pi/4, \quad y_i = (4n_9 + 1)\pi/4, \quad z_i = (2n_{10} + 1)\pi/2, \quad (1.57b)$$

leading to the initial conditions

$$\phi_i = n_1\pi, \quad \theta_i = (2n_6 + n_1)\pi, \quad \eta_i = (2n_7 + n_1)\pi, \quad (1.58)$$

are explicitly

$$|\psi_{p1}\rangle = \begin{bmatrix} \cos\theta\cos\phi \\ i\sin\phi \\ \cos\phi\sin\theta \end{bmatrix}, \tag{1.59a}$$

$$|\psi_{p2}\rangle = \begin{bmatrix} i(\cos\theta\sin\phi\cos\eta - \sin\theta\sin\eta) \\ \cos\phi\cos\eta \\ i(\sin\theta\sin\phi\cos\eta + \cos\theta\sin\eta) \end{bmatrix}, \tag{1.59b}$$

$$|\psi_{p3}\rangle = \begin{bmatrix} -\sin\theta\cos\eta - \cos\theta\sin\phi\sin\eta \\ i\cos\phi\sin\eta \\ \cos\theta\cos\eta - \sin\theta\sin\phi\sin\eta \end{bmatrix}. \tag{1.59c}$$

The simplified propagator U_p, just like its general form $\widetilde{U}_p$, presents an ideal appearance to represent the dynamics of population transfer, or state evolution, $|1\rangle \to |3\rangle$. Without the phases in $\widetilde{U}_p$, $|\psi_{p1}\rangle$ clearly presents θ and ϕ as mixing angles between the bare states $|n\rangle$, and thus as a measure of the superposition of such states that constitutes the state of the system if this is initially in $|1\rangle$.

The general SU(3) propagator we have deemed most appropriate for logical quantum gates between states $|1\rangle$ and $|3\rangle$, $\widetilde{U}_s$, has also a simplified version obeying the su(2) subalgebra of $\{\lambda_1, \lambda_5, \lambda_6\}$. We can write it by using a different product of exponentials of generators, namely,

$$U_s = e^{i\lambda_5\theta} e^{-i\lambda_1(\phi-\pi/2)} e^{i\lambda_5(\eta-\pi/2)} = \begin{bmatrix} |\psi_{s1}\rangle & |\psi_{s2}\rangle & |\psi_{s3}\rangle \end{bmatrix}, \tag{1.60}$$

with columns

$$|\psi_{s1}\rangle = \begin{bmatrix} \cos\eta\sin\theta + \cos\theta\sin\eta\sin\phi \\ i\cos\phi\sin\eta \\ \cos\eta\cos\theta - \sin\theta\sin\eta\sin\phi \end{bmatrix}, \tag{1.61a}$$

$$|\psi_{s2}\rangle = \begin{bmatrix} i\cos\theta\cos\phi \\ \sin\phi \\ i\sin\theta\cos\phi \end{bmatrix}, \tag{1.61b}$$

$$|\psi_{s3}\rangle = \begin{bmatrix} \sin\eta\sin\theta - \cos\theta\cos\eta\sin\phi \\ -i\cos\phi\cos\eta \\ \sin\eta\cos\theta + \sin\theta\cos\eta\sin\phi \end{bmatrix}. \tag{1.61c}$$

The columns $|\psi_{sn}\rangle$ correspond to the tilded versions $|\widetilde{\psi}_{sn}\rangle$ of (1.48) to which the variables y, a ($\widetilde{a}$), and c ($\widetilde{c}$) were fixed to their initial conditions in (1.50) [or (1.51)]

with the additional restrictions

(1) $n_1 = 2n_6$, $n_3 = 2n_7$, $n_4 = 2n_8$, $x = n_9\pi$, $z = (4n_{10} + 2n_9 + 3)\pi/2$, or

(2) $n_1 = 2n_6$, $n_4 = 2n_{11} + n_3$, $x = n_9\pi$, $z = (4n_{10} + 2n_9 + 3)\pi/2$, $c = n_{12}\pi$.

Leading to the initial conditions

(1) $\phi_i = (4n_6 + 1)\pi/2$, $\theta_i = (4n_7 + 1)\pi/2 - \eta_i$, or

(2) $\phi_i = (4n_6 + 1)\pi/2$, $\eta_i = n_3\pi/2$, $\theta_i = (4n_{11} + 3n_3 + 1)\pi/2$.

1.3 Optimal control: Euler-Lagrange principle

Optimal control deals with the problem of finding the controls that minimize a certain quantity, denominated cost, satisfying certain constraints. In the Lagrange problem, the boundary conditions are fixed, i.e., $x_n(t_f) \equiv x_{nf}$ are known, and the cost functional takes the form [2]

$$J[x_n(t)] = \int_{t_i}^{t_f} \mathcal{L}[x_n(t), \dot{x}_n(t), t]\, dt, \tag{1.62}$$

where $\mathcal{L}$ is the Lagrangian of the system and is a functional dependent of the dynamical variables x_n, their derivative, and time. The first condition of optimality, from the calculus of variations [2, 30], is given by the Euler-Lagrange principle expressed by the satisfaction of the Euler-Lagrange (E-L) equations,

$$\operatorname{grad} \mathcal{L} = \frac{\partial \mathcal{L}}{\partial x_n} - \frac{d}{dt}\frac{\partial \mathcal{L}}{\partial \dot{x}_n} = 0. \tag{1.63}$$

The trajectories or controls that are solutions of the E-L equations are called extremals of the optimization (minimization) problem, candidates to be the global optimal solution.

When the system is subjected to constraints of the form

$$\int_{t_i}^{t_f} f_m[x_n(t), \dot{x}_n(t), t]\, dt = F \tag{1.64}$$

one must consider the modified E-L equation

$$\operatorname{grad} \mathcal{L} + \sum_m \lambda_m \operatorname{grad} f_m = 0, \tag{1.65}$$

often referred to as the E-L equations for the modified Lagrangian $\mathcal{L}_\lambda = \mathcal{L} + \sum_m \lambda_m f_m$, where the λ_m's are constants known as the Lagrange multipliers chosen

to satisfy the constraints. More general dynamical constraints, as those of the form $f_m[x_n(t), \dot{x}_n(t), t] = 0$, require the Lagrange multipliers to be treated as dynamical variables, effectively augmenting the dimensions of the E-L equations.

1.4 Robust inverse optimization: two-level system

1.4.1 The model and the inverse-engineering method

We consider the Hamiltonian $H_\lambda = H_0 + \lambda V$, where

$$H_0 = \frac{\hbar}{2}\begin{bmatrix} -\Delta & \Omega \\ \Omega & \Delta \end{bmatrix} \tag{1.66}$$

represents the qubit $\{|0\rangle, |1\rangle\}$ driven by the controls: the pulsed Rabi frequency $\Omega \equiv \Omega(t)$ (considered real without loss of generality) and the detuning $\Delta \equiv \Delta(t)$. λ gathers unknown real (and time-independent) parameters, which, multiplied by V, represents the errors in the description of the model, as detailed in 1.4.3.

The solution of the time dependent Schrödinger equation (TDSE) $i\hbar\frac{\partial}{\partial t}|\phi_0(t)\rangle = H_0|\phi_0(t)\rangle$ is conveniently parameterized with three angles: the mixing angle $\theta \equiv \theta(t) \in [0, \pi]$, the internal (or relative) phase $\varphi \equiv \varphi(t) \in [-\pi, \pi]$ and a global phase $\gamma \equiv \gamma(t) \in [0, 2\pi]$ as

$$|\phi_0(t)\rangle = \begin{bmatrix} e^{i\varphi/2}\cos(\theta/2) \\ e^{-i\varphi/2}\sin(\theta/2) \end{bmatrix} e^{-i\gamma/2}. \tag{1.67}$$

Inserting it into the TDSE, we obtain

$$\dot{\theta} = \Omega \sin\varphi, \tag{1.68a}$$

$$\dot{\varphi} = \Delta + \Omega\cos\varphi\cot\theta, \tag{1.68b}$$

$$\dot{\gamma} = \Omega\frac{\cos\varphi}{\sin\theta} = \dot{\theta}\frac{\cot\varphi}{\sin\theta}, \tag{1.68c}$$

where the dot represents the derivation with respect to time t.

Adding a static phase η_0 to the control field Ω allows the modification of the internal phase of the state. In this case, we have indeed to consider the Hamiltonian

$$H_{0;\eta_0} = \frac{\hbar}{2}\begin{bmatrix} -\Delta & \Omega e^{-i\eta_0} \\ \Omega e^{i\eta_0} & \Delta \end{bmatrix}, \tag{1.69}$$

associated to the state $|\widetilde{\phi}_0(t)\rangle$. The phase transformation

$$T(\eta_0) = \begin{bmatrix} e^{-i\eta_0/2} & 0 \\ 0 & e^{i\eta_0/2} \end{bmatrix} \tag{1.70}$$

leads to the Hamiltonian originally considered

$$T^\dagger(\eta_0)\widehat{H}_{0,\eta_0}T(\eta_0) = \frac{\hbar}{2}\begin{bmatrix} -\Delta & \Omega \\ \Omega & \Delta \end{bmatrix} \equiv H_0 \tag{1.71}$$

with the state featuring the added internal phase η_0:

$$|\widetilde{\phi}_0(t)\rangle = T(\eta_0)|\phi_0(t)\rangle = \begin{bmatrix} e^{i(\varphi-\eta_0)/2}\cos(\theta/2) \\ e^{-i(\varphi-\eta_0)/2}\sin(\theta/2) \end{bmatrix} e^{-i\gamma/2}. \tag{1.72}$$

The inverse-engineering method consists in determining the Hamiltonian elements from the dynamics by inverting the TDSE: $H_0 = i\hbar[\partial_t U_0(t,t_i)]U_0^\dagger(t,t_i)$ with the propagator $U_0(t,t_i)$ such that $|\phi_0(t)\rangle = U_0(t,t_i)|\phi_0(t_i)\rangle$. From inversion of Eqs. (1.68), one can determine more specifically the detuning and the Rabi frequency as functions of θ, $\dot{\varphi}$ and $\dot{\gamma}$:

$$\Delta = \dot{\varphi} - \dot{\gamma}\cos\theta, \tag{1.73a}$$

$$\Omega = \pm\sqrt{\dot{\theta}^2 + \dot{\gamma}^2\sin^2\theta} = \pm|\dot{\theta}|\sqrt{1 + \left(\frac{d\widetilde{\gamma}}{d\theta}\right)^2\sin^2\theta}, \tag{1.73b}$$

$$= \pm|\dot{\gamma}|\sqrt{\left(\frac{d\widetilde{\theta}}{d\gamma}\right)^2 + \sin^2\widetilde{\theta}}. \tag{1.73c}$$

We will consider $\Omega > 0$.

One can determine from (1.68c), the phase

$$\varphi = \operatorname{atan}\left(\frac{\dot{\theta}}{\dot{\gamma}\sin\theta}\right), \quad \begin{cases} 0 \le \varphi \le \pi, & \text{for } \dot{\theta} \ge 0, \\ -\pi < \varphi < 0, & \text{otherwise.} \end{cases} \tag{1.74}$$

Equation (1.68c) links the three angles: we can thus consider two independent dynamical variables, e.g., $\theta(t)$ and $\gamma(t)$ providing a geometric representation of the problem, and the third dynamical variable $\varphi(t)$ is given by (1.68c), $\cot\varphi = \dot{\gamma}\sin\theta/\dot{\theta}$, from which we obtain

$$\dot{\varphi} = [\ddot{\theta}\dot{\gamma}\sin\theta - \ddot{\gamma}\dot{\theta}\sin\theta - \dot{\gamma}\dot{\theta}^2\cos\theta]/[\dot{\theta}^2 + \dot{\gamma}^2\sin^2\theta]. \tag{1.75}$$

In the right part of Eq. (1.73b), we have assumed that one can write $\gamma(t)$ as a

function of θ: $\widetilde{\gamma}(\theta) \equiv \gamma(t)$. In Eq. (1.73c), we have assumed on the other hand that one can write $\theta(t)$ as a function of γ: $\widetilde{\theta}(\gamma) \equiv \theta(t)$. More generally, we can be led to consider piecewise functions $\widetilde{\gamma}(\theta)$ or $\widetilde{\theta}(\gamma)$. We note that the pulse area from the initial t_i to the final t_f times [denoting $\theta_i \equiv \theta(t_i)$, $\theta_f \equiv \theta(t_f)$ and assuming a monotonic $\theta(t)$, such that $\dot{\theta} > 0$]

$$\int_{t_i}^{t_f} \Omega(t)\, dt = \int_{\theta_i}^{\theta_f} \sqrt{1 + \left(\frac{d\widetilde{\gamma}}{d\theta}\right)^2 \sin^2\theta}\, d\theta \equiv \mathcal{A}(\widetilde{\gamma}) \tag{1.76}$$

does not depend on the time-dependence of $\theta(t)$, but only on the derivative of the expansion $\widetilde{\gamma}(\theta)$. Alternatively, one can write the pulse area [denoting $\gamma_i \equiv \gamma(t_i)$, $\gamma_f \equiv \gamma(t_f)$ and assuming a monotonic $\gamma(t)$ such that $\dot{\gamma} > 0$] as

$$\int_{t_i}^{t_f} \Omega(t)\, dt = \int_{\gamma_i}^{\gamma_f} \sqrt{\left(\frac{d\widetilde{\theta}}{d\gamma}\right)^2 + \sin^2\widetilde{\theta}}\, d\gamma \equiv \mathcal{A}(\widetilde{\theta}), \tag{1.77}$$

which does not depend on the time-dependence of $\gamma(t)$, but only on $\widetilde{\theta}(\gamma)$ and its derivative.

On the other hand, the pulse energy

$$\mathcal{E}(\gamma, \theta) = \int_{t_i}^{t_f} \Omega^2(t)\, dt = \int_{t_i}^{t_f} (\dot{\theta}^2 + \dot{\gamma}^2 \sin^2\theta)\, dt, \tag{1.78}$$

depends on the time-parametrization of the angles $\theta(t)$ and $\gamma(t)$.

We will optimize the cost defined either as the pulse area $\mathcal{A}$, the pulse energy $\mathcal{E}$ (for a fixed duration $t_f - t_i$), or the duration of the process (i.e., time optimization) (for a fixed peak amplitude of the control).

We denote $|\phi_\lambda(t)\rangle$ the state of the complete dynamics, solution of the TDSE $i\hbar\partial_t|\phi_\lambda(t)\rangle = H_\lambda|\phi_\lambda(t)\rangle$.

1.4.2 Complex Hamiltonian

Alternatively, one can consider an equivalent model with a zero detuning and a complex Rabi frequency:

$$\widehat{H}_0(t) = \frac{\hbar}{2}\begin{bmatrix} 0 & \Omega_x(t) - i\Omega_y(t) \\ \Omega_x(t) + i\Omega_y(t) & 0 \end{bmatrix} = \frac{\hbar}{2}[\Omega_x(t)\sigma_x + \Omega_y(t)\sigma_y] \tag{1.79}$$

with $\Omega_c(t) = \Omega(t)e^{-i\eta(t)} = \Omega_x(t) - i\Omega_y(t)$, $\Omega(t) \geq 0$, i.e. with the two controls Ω_x, Ω_y or Ω, η linked as follows:

$$\Omega_x = \Omega \cos\eta, \quad \Omega_y = \Omega \sin\eta, \tag{1.80}$$

and the TDSE $i\hbar\partial_t|\psi_0(t)\rangle = \widehat{H}_0|\psi_0(t)\rangle$. The connection with Hamiltonian (1.66)

$$T^\dagger(t)\widehat{H}_0(t)T(t) - i\hbar T^\dagger(t)\frac{dT}{dt} = \frac{\hbar}{2}\begin{bmatrix} -\Delta & \Omega \\ \Omega & \Delta \end{bmatrix} \equiv H_0 \tag{1.81}$$

is made by the phase transformation

$$T(t) = \begin{bmatrix} e^{-i\eta(t)/2} & 0 \\ 0 & e^{i\eta(t)/2} \end{bmatrix}, \tag{1.82}$$

with the detuning $\Delta = \dot{\eta}$ and the corresponding solution $|\phi_0(t)\rangle = T^\dagger(t)|\psi_0(t)\rangle$, leading to

$$|\psi_0(t)\rangle = \begin{bmatrix} e^{i\chi/2}\cos(\theta/2) \\ e^{-i\chi/2}\sin(\theta/2) \end{bmatrix} e^{-i\gamma/2}, \quad \chi = \varphi - \eta. \tag{1.83}$$

In this case, inserting (1.83) in the TDSE, we get:

$$\dot{\theta} = \Omega_x \sin\chi + \Omega_y \cos\chi = \Omega\sin(\eta + \chi), \tag{1.84a}$$

$$\dot{\chi}\tan\theta = \dot{\gamma}\sin\theta = \Omega_x\cos\chi - \Omega_y\sin\chi = \Omega\cos(\eta+\chi), \tag{1.84b}$$

$$\Delta = \dot{\eta}. \tag{1.84c}$$

This gives for the Rabi frequencies

$$\Omega_x = \dot{\theta}\sin\chi + \dot{\chi}\tan\theta\cos\chi, \tag{1.85a}$$

$$\Omega_y = \dot{\theta}\cos\chi - \dot{\chi}\tan\theta\sin\chi. \tag{1.85b}$$

1.4.3 The single-shot shaped-pulse method for robust process.

From an initial condition at t_i, we assume that the Hamiltonian $H_0(t)$ [or $\widehat{H}_0(t)$) leads to a given target at the end of the process t_f (from which one can require that the field is off, i.e., $\Omega(t_f) = 0$, but this is not obligatory]. The process is robust if a perturbation added to the Hamiltonian leads to a close target at t_f in a way that is defined below.

The perturbed Hamiltonian $H_\lambda = H_0 + \lambda V$ takes the form for the real Hamilto-

nian

$$H_{\alpha,\beta,\delta} = \frac{\hbar}{2}\begin{bmatrix} -\Delta & \Omega \\ \Omega & \Delta \end{bmatrix} + \frac{\hbar}{2}\begin{bmatrix} -\delta & \alpha\Omega+\beta \\ \alpha\Omega+\beta & \delta \end{bmatrix} \tag{1.86}$$

where α, β, γ are real constant coefficients taking into account the inaccuracy of the model, more precisely: α is a coefficient modifying the Rabi field amplitude (pulse inhomogeneities), δ features inhomogeneous broadening or a slow stochastic noise in the energy levels of the qubit (i.e., considered in a quasi-static representation), and β a slow stochastic transverse noise.

We show that the robustness can be formulated with constraint integrals at a certain order. We will consider in this paper pulse inhomogeneities, referred to as α-robustness, i.e., $\delta = \gamma = 0$.

Formulation in terms of state

The SSSP method, detailed in 1.2.1, can be summarized as follows [where $\lambda \equiv (\alpha, \beta, \delta)$]. The perturbative expansion of $|\phi_\lambda(t_f)\rangle$ with respect to α, β, and δ reads

$$\langle\phi_T|\phi_\lambda(t_f)\rangle = 1 - O_1 - O_2 - O_3 - \cdots, \tag{1.87}$$

where O_n denotes the term of total order n: $O_n \equiv O(\lambda^n)$ and $|\phi_T\rangle$ the target state. The first three terms can be found in Eqs. (1.10), for which the relevant variables become, explicitly,

$$\begin{aligned} e &= \langle\phi_0(t)|V(t)|\phi_0(t)\rangle \\ &= -\frac{1}{2}(\delta\cos\theta - \alpha\dot{\gamma}\sin^2\theta - \beta\sin\theta\cos\varphi) \equiv \sum_{\lambda=\alpha,\beta,\gamma}\lambda e_\lambda, \end{aligned} \tag{1.88a}$$

$$\begin{aligned} f = \langle\phi_0|V|\phi_\perp\rangle = \frac{1}{2}\Big[&\delta\sin\theta + \alpha\Big(\frac{1}{2}\dot{\gamma}\sin 2\theta - i\dot{\theta}\Big) \\ &+ \beta(\cos\varphi\cos\theta - i\sin\varphi)\Big]e^{i\gamma} \equiv \sum_{\lambda=\alpha,\beta,\delta}\lambda f_\lambda. \end{aligned} \tag{1.88b}$$

In the expansion (1.12a), since the first-order integral O_1 (1.10a) is imaginary, $\mathrm{Re}\, O_1 = 0$, cancellation of the first order O_1 corresponds thus to

$$\int_{t_i}^{t_f} e(t)\, dt = 0. \tag{1.89}$$

The second-order integral O_2 can be simplified using the properties described in Appendix 1.A:

$$O_2 = \frac{1}{2}\left[\int_{t_i}^{t_f} e(t)\,dt\right]^2 + \int_{t_i}^{t_f}\int_{t_i}^{t} f(t)\bar{f}(t')\,dt'\,dt. \tag{1.90}$$

Defining $f(t) = a(t) + ib(t)$, we calculate the above double integral:

$$\int_{t_i}^{t_f}\int_{t_i}^{t} f(t)\bar{f}(t')\,dt'\,dt = \frac{1}{2}\left|\int_{t_i}^{t_f} f(t)\,dt\right|^2 + i\int_{t_i}^{t_f}\int_{t_i}^{t}[a(t')b(t) - a(t)b(t')]\,dt'\,dt. \tag{1.91}$$

The real part then reads

$$\operatorname{Re} O_2 = \frac{1}{2}\left[\int_{t_i}^{t_f} e(t)\,dt\right]^2 + \frac{1}{2}\left|\int_{t_i}^{t_f} f(t)\,dt\right|^2, \tag{1.92}$$

which is zero when

$$\int_{t_i}^{t_f} e(t)\,dt = 0, \quad \int_{t_i}^{t_f} f(t)\,dt = 0. \tag{1.93}$$

The imaginary part of O_2, given by $\operatorname{Im} O_2 = \operatorname{Im}\left[\int_{t_i}^{t_f}\int_{t_i}^{t} f(t)\bar{f}(t')\,dt'\,dt\right]$, involves higher order corrections that are not considered in the present document.

We now consider the real part of the third order assuming that the first order and the real part of the second order terms are both zero. It is determined in Appendix 1.B, see Eq. (1.126):

$$\operatorname{Re} O_3 = \operatorname{Im} O_2 \int_{t_i}^{t_f} e(t)\,dt. \tag{1.94}$$

It implies that $\operatorname{Re} O_3 = 0$ when the first order is canceled: $O_1 = 0$ (1.89).

Formulation in terms of propagator

We define the propagator associated to the unperturbed Hamiltonian $H_0 \equiv H_{0,0,0}$:

$$U_0(t, t_i) = \begin{bmatrix} a \equiv e^{\frac{i}{2}(\varphi-\gamma)}\cos(\theta/2) & -\bar{b} \\ b \equiv e^{-\frac{i}{2}(\varphi+\gamma)}\sin(\theta/2) & \bar{a} \end{bmatrix} \tag{1.95}$$

with $|a|^2 + |b|^2 = 1$. We define the interaction representation:

$$U_I(t, t_i) = U_0^\dagger(t, t_i)U(t, t_i) \tag{1.96}$$

with $U(t)$ associated to the Hamiltonian $H(t)$ governed by

$$i\hbar \frac{dU_I(t,t_i)}{dt} = \epsilon V_I(t) U_I(t,t_i). \tag{1.97}$$

with

$$\epsilon V_I(t) = \epsilon U_0^\dagger(t,t_i) V(t) U_0(t,t_i). \tag{1.98}$$

The perturbative solution reads:

$$\begin{aligned} U(t_f,t_i) = U_0(t_f,t_i)\Bigg[\mathbb{1} + \frac{\epsilon}{i\hbar}\int_{t_i}^{t_f} V_I(t)\,dt \\ + \Big(\frac{\epsilon}{i\hbar}\Big)^2 \int_{t_i}^{t_t}\int_{t_i}^{t} V_I(t)V_I(t')\,dt'\,dt + \cdots\Bigg], \end{aligned} \tag{1.99}$$

where

$$V_I(t) = \hbar \begin{bmatrix} e(t) & f(t) \\ \overline{f}(t) & -e(t) \end{bmatrix}. \tag{1.100}$$

Canceling the first order of the expansion (1.99) of the propagator corresponds thus to canceling each term of the matrix, which coincides with the conditions (1.93), $\operatorname{Re} O_2 = 0$.

1.4.4 Figures of merit

Population transfer

For the case of a population transfer to a target state $|\phi_T\rangle$ (of given angle θ_0 and internal phase φ_0), the final phase is irrelevant, one can consider the figure of merit

$$\begin{aligned} \mathcal{F}_{\text{pt}} &= |\langle\phi_T|\phi_\lambda(t_f)\rangle|^2 \\ &= (1 - O_1 - O_2 - \cdots)(1 - \overline{O}_1 - \overline{O}_2 - \cdots) \\ &\equiv 1 - \widetilde{O}_2 - \widetilde{O}_3 - \cdots \end{aligned} \tag{1.101}$$

The deviation with respect to one at the second order of $\mathcal{F}_{\text{pt}}$ reduces to a single integral:

$$\widetilde{O}_2 \equiv O_2 - O_1\overline{O}_1 + \overline{O}_2 = \left|\int_{t_i}^{t_f} f(t)\,dt\right|^2. \tag{1.102}$$

The third order is zero:

$$\widetilde{O}_3 \equiv O_3 - O_1\overline{O}_2 - O_2\overline{O}_1 + \overline{O}_3 = 2\operatorname{Re} O_3 - O_1\overline{O}_2 + O_2\overline{O}_1 = 0, \tag{1.103}$$

since $2\,\mathrm{Re}\,O_3$ given in (1.126) cancels out with

$$O_1\overline{O}_2 + O_2\overline{O}_1 = -2\,\mathrm{Im}\,O_2 \int_{t_i}^{t_f} e(t)\,dt. \tag{1.104}$$

Quantum gate

For the case of a quantum gate, a traceless Hamiltonian generates the SU(2) gate, which is taken as the targeted propagator:

$$U_0 = \begin{bmatrix} a & -\bar{b} \\ b & \bar{a} \end{bmatrix} \tag{1.105}$$

with $|a|^2 + |b|^2 = 1$. A figure of merit often adopted to determine the fidelity of a quantum gate is defined as the *trace fidelity*

$$\mathcal{F}_{\mathrm{g}} = \frac{1}{2}\big|\mathrm{Tr}(U_0^{\dagger}U)\big|, \tag{1.106}$$

where

$$U = \begin{bmatrix} c & -\bar{d} \\ d & \bar{c} \end{bmatrix} \tag{1.107}$$

is the actual propagator with $|c|^2 + |d|^2 = 1$. It is based on the fact that, when $U = e^{i\vartheta}U_0$, we have $\mathcal{F}_g = 1$. Here ϑ is a global phase at the level of the propagator, i.e., connected to the choice of the energy reference, which is physically irrelevant. This gives:

$$\mathcal{F}_{\mathrm{g}} = \mathrm{Re}(\bar{a}c + \bar{b}d). \tag{1.108}$$

If we consider the initial condition $\begin{bmatrix} 1 \\ 0 \end{bmatrix}$, we obtain $|\phi_\lambda(t_f)\rangle = \begin{bmatrix} c \\ d \end{bmatrix}$ and $|\phi_T(t_f)\rangle = \begin{bmatrix} a \\ b \end{bmatrix}$, i.e., $\langle\phi_T(t_f)|\phi_\lambda(t_f)\rangle = \bar{a}c + \bar{b}d$, which finally gives

$$\mathcal{F}_{\mathrm{g}} = \mathrm{Re}\langle\phi_T(t_f)|\phi_\lambda(t_f)\rangle = 1 + \mathrm{Re}\,O_2 + \mathrm{Re}\,O_3 + \cdots \tag{1.109}$$

As noticed with (1.94), the cancellation of the error at the third order $\mathrm{Re}\,O_3 = 0$ is satisfied when $\mathrm{Re}\,O_2 = 0$, i.e., when the conditions (1.93) are satisfied.

One notes the remarkable property that, when one considers the robustness with respect to solely α (i.e., $\beta = \delta = 0$), then the integrals O_n do not depend on the particular time-parametrization of $\theta(t)$ [in the case of a monotonic $\theta(t)$, for which

one can define a function $\widetilde{\gamma}(\theta)]$ since

$$\int_{t_i}^{t} e(t)\,dt = \frac{1}{2}\alpha \int_{t_i}^{t} \dot{\gamma}\sin^2\theta\,dt = \frac{1}{2}\alpha \int_{\theta_i}^{\theta} \frac{d\widetilde{\gamma}}{d\theta}\sin^2\theta\,d\theta, \tag{1.110a}$$

$$\int_{t_i}^{t} f(t)\,dt = \frac{1}{2}\alpha \int_{\theta_i}^{\theta} \left(\frac{1}{2}\frac{d\widetilde{\gamma}}{d\theta}\sin 2\theta - i\right) e^{i\widetilde{\gamma}}\,d\theta. \tag{1.110b}$$

We have considered the situation of an increasing $\theta(t)$, i.e., $\dot{\theta}(t) > 0$. The opposite situation [i.e., a decreasing $\theta(t)$, $\dot{\theta}(t) < 0$] would add a minus sign in the right hand sides of Eq. (1.110a) and of Eq. (1.110b).

The nullification of the real part of the second order (1.93) can be further simplified in this case $[\dot{\theta}(t) > 0]$ as

$$\begin{aligned} 0 = \int_{t_i}^{t_f} e(t)\,dt &= \int_{\theta_i}^{\theta_f} \frac{d\widetilde{\gamma}}{d\theta}\sin^2\theta\,d\theta, \\ &= [\widetilde{\gamma}\sin^2\theta]_{\theta_i}^{\theta_f} - 2\int_{\theta_i}^{\theta_f} \widetilde{\gamma}\sin\theta\cos\theta\,d\theta, \end{aligned} \tag{1.111a}$$

$$\begin{aligned} 0 = \int_{t_i}^{t_f} f(t)\,dt &= \int_{\theta_i}^{\theta_f} \left(\frac{1}{2}\frac{d\widetilde{\gamma}}{d\theta}\sin 2\theta - i\right) e^{i\widetilde{\gamma}}\,d\theta, \\ &= \frac{1}{4}[e^{i\widetilde{\gamma}}\sin 2\theta]_{\theta_i}^{\theta_f} + \int_{\theta_i}^{\theta_f} e^{i\widetilde{\gamma}}\sin^2\theta\,d\theta. \end{aligned} \tag{1.111b}$$

Alternatively, in the case of a monotonic $\gamma(t)$, for which one can define a function $\widetilde{\theta}(\gamma)$, when one considers the robustness with respect to solely α (i.e., $\beta = \delta = 0$), then the integrals O_n do not depend on the particular time-parametrization of $\gamma(t)$ since

$$\int_{t_i}^{t} e(t)\,dt = \frac{1}{2}\alpha \int_{t_i}^{t} \dot{\gamma}\sin^2\theta\,dt = \frac{1}{2}\alpha \int_{\gamma_i}^{\gamma} \sin^2\widetilde{\theta}\,d\gamma, \tag{1.112a}$$

$$\begin{aligned} \int_{t_i}^{t} f(t)\,dt &= \frac{1}{2}\alpha \int_{t_i}^{t} \left(\frac{1}{2}\dot{\gamma}\sin 2\theta - i\dot{\theta}\right) e^{i\gamma}\,dt \\ &= \frac{1}{2}\alpha \int_{\gamma_i}^{\gamma} \left(\frac{1}{2}\sin 2\widetilde{\theta} - i\frac{d\widetilde{\theta}}{d\gamma}\right) e^{i\gamma}\,d\gamma. \end{aligned} \tag{1.112b}$$

We have considered the situation of an increasing $\gamma(t)$, i.e., $\dot{\gamma}(t) > 0$. The opposite situation (i.e., a decreasing $\gamma(t)$, $\dot{\gamma}(t) < 0$) would add a minus sign in the right hand sides of Eq. (1.112a) and of Eq. (1.112b).

One can conclude that the design of a trajectory solely robust with respect to α does not depend on a specific time-parametrization.

The nullification of the real part of the second order (1.93) can be expressed in

this case $[\dot{\gamma}(t) > 0]$ as

$$0 = \int_{t_i}^{t_f} e(t)\,dt = \int_{\gamma_i}^{\gamma_f} \sin^2\widetilde{\theta}\,d\gamma, \tag{1.113a}$$

$$\begin{aligned} 0 &= \int_{t_i}^{t_f} f(t)\,dt = \frac{1}{2}\int_{\gamma_i}^{\gamma_f} e^{i\gamma}\sin 2\widetilde{\theta}\,d\gamma - i\int_{\gamma_i}^{\gamma_f}\frac{d\widetilde{\theta}}{d\gamma}e^{i\gamma}\,d\gamma \\ &= \frac{1}{2}\int_{\gamma_i}^{\gamma_f}[e^{i\gamma}(\sin 2\widetilde{\theta} - 2\widetilde{\theta}) - i(\theta_f e^{i\gamma_f} - \theta_i e^{i\gamma_i})]\,d\gamma, \end{aligned} \tag{1.113b}$$

i.e.,

$$\int_{\gamma_i}^{\gamma_f} \sin^2\widetilde{\theta}\,d\gamma = 0, \tag{1.114a}$$

$$\int_{\gamma_i}^{\gamma_f} (\sin 2\widetilde{\theta} - 2\widetilde{\theta})\cos\gamma\,d\gamma = 2(\theta_i\sin\gamma_i - \theta_f\sin\gamma_f), \tag{1.114b}$$

$$\int_{\gamma_i}^{\gamma_f} (\sin 2\widetilde{\theta} - 2\widetilde{\theta})\sin\gamma\,d\gamma = 2(\theta_f\cos\gamma_f - \theta_i\cos\gamma_i). \tag{1.114c}$$

Since the argument of Eq. (1.114a) is positive, the integral cannot be 0 $\theta \neq 0$. Thus, $\gamma(t)$ cannot be monotonic if Eq. (1.114a) has to be satisfied. We have then to consider in this situation a piecewise defined function $\widetilde{\theta}(\gamma)$:

$$\widetilde{\theta}(\gamma) = \begin{cases} \widetilde{\theta}_+(\gamma) & \text{for } \dot{\gamma} \geq 0,\ \gamma = [\gamma_i, \gamma_m] \\ \widetilde{\theta}_-(\gamma) & \text{for } \dot{\gamma} < 0,\ \gamma = [\gamma_f, \gamma_m) \end{cases} \tag{1.115}$$

with $\theta_m = \widetilde{\theta}_+(\gamma_m) = \widetilde{\theta}_-(\gamma_m)$ and the integrals (1.113) to be nullified become:

$$0 = \int_{\gamma_i}^{\gamma_m} \sin^2\widetilde{\theta}_+\,d\gamma - \int_{\gamma_f}^{\gamma_m} \sin^2\widetilde{\theta}_-\,d\gamma, \tag{1.116a}$$

$$\begin{aligned} 0 = \frac{1}{2}\int_{\gamma_i}^{\gamma_m} e^{i\gamma}(\sin 2\widetilde{\theta}_+ - 2\widetilde{\theta}_+)\,d\gamma - i(\theta_f e^{i\gamma_f} - \theta_i e^{i\gamma_i}) \\ - \frac{1}{2}\int_{\gamma_f}^{\gamma_m} e^{i\gamma}(\sin 2\widetilde{\theta}_- - 2\widetilde{\theta}_-)\,d\gamma. \end{aligned} \tag{1.116b}$$

1.5 Conclusions

We have presented a method to measure, quantify, and potentially control the robustness of a quantum process. This, the SSSP scheme, necessitates the inverse-engineering of the dynamics, and this is facilitated by the parametrization of the propagator of the system. The Lewis-Riesenfeld method and the usage of the differential generators of the algebras corresponding to specific Hamiltonians was demonstrated to parametrize the propagators of interest (for two- and three-level systems).

The figure of merit to evaluate the fidelity of quantum processes was also discussed. The basic concept of optimal control via the Euler-Lagrange equation was introduced.

Appendices

1.A Properties of the integrals

The integrals can be simplified using the general property:

$$\int_\tau^T \int_\tau^t [a(t)b(t') + a(t')b(t)]\, dt'\, dt = \int_\tau^T a(t)\, dt \int_\tau^T b(t)\, dt \tag{1.117}$$

from

$$\int_\tau^T v\, du + \int_\tau^T u\, dv = [uv]_\tau^T, \tag{1.118}$$

where

$$u(t) = \int_\tau^t a(t')\, dt', \quad du = a(t)\, dt, \quad v(t) = \int_\tau^t b(t')\, dt', \quad dv = b(t)\, dt. \tag{1.119}$$

For $a = b \equiv e$, (1.117) becomes

$$\int_{t_i}^{t_f} \int_{t_i}^t [e(t)e(t') + e(t')e(t)]\, dt'\, dt = \Big[\int_{t_i}^{t_f} e(t)\, dt\Big]^2. \tag{1.120}$$

For $a \equiv f$ and $b \equiv \bar{f}$, (1.117) becomes

$$\int_{t_i}^{t_f} \int_{t_i}^t [f(t)\bar{f}(t') + f(t')\bar{f}(t)]\, dt' = \Big|\int_{t_i}^{t_f} f(t)\, dt\Big|^2. \tag{1.121}$$

1.B Determination of the Error $\mathrm{Re}(O_3)$

We determine the real part of the third order assuming that the first order and and the real part of the second order terms are both zero:

$$\begin{aligned} \mathrm{Re}\, O_3 &= \int_{t_i}^{t_f} \int_{t_i}^t \int_{t_i}^{t'} \mathrm{Im}[e(t)f(t')\bar{f}(t'') + f(t)\bar{f}(t')e(t'') - f(t)e(t')\bar{f}(t'')]\, dt''\, dt'\, dt \\ &= \int_{t_i}^{t_f} \int_{t_i}^t \int_{t_i}^{t'} \mathrm{Im}[e(t)f(t')\bar{f}(t'') + f(t)\bar{f}(t')e(t'') + \bar{f}(t)e(t')f(t'')]\, dt''\, dt'\, dt, \end{aligned} \tag{1.122}$$

where we have used $\mathrm{Im}[-f(t)e(t')\bar{f}(t'')] = \mathrm{Im}[\overline{f(t)e(t')\bar{f}(t'')}] = \mathrm{Im}[\bar{f}(t)e(t')f(t'')]$ to obtain the latter expression. It can be simplified using the property (1.117) as

follows. The first term of (1.122) gives:

$$\int_{t_i}^{t_f}\int_{t_i}^{t}\int_{t_i}^{t'} e f' \overline{f}''\, dt''\, dt'\, dt = \int_{t_i}^{t_f} e\, dt \int_{t_i}^{t_f}\int_{t_i}^{t} f \overline{f}'\, dt'\, dt - \int_{t_i}^{t_f} f \left(\int_{t_i}^{t} \overline{f}'\, dt'\right)\left(\int_{t_i}^{t} e'\, dt'\right) dt \tag{1.123}$$

where the last term is the complex conjugate of the second term of (1.122):

$$\begin{aligned}\int_{t_i}^{t_f}\int_{t_i}^{t}\int_{t_i}^{t'} f \overline{f}' e''\, dt''\, dt'\, dt &= \int_{t_i}^{t_f} f\, dt \int_{t_i}^{t_f}\int_{t_i}^{t} \overline{f} e'\, dt'\, dt \\ &\quad - \int_{t_i}^{t_f} \overline{f}\left(\int_{t_i}^{t} e'\, dt'\right)\left(\int_{t_i}^{t} f'\, dt'\right) dt \\ &= -\int_{t_i}^{t_f} \overline{f}\left(\int_{t_i}^{t} e'\, dt'\right)\left(\int_{t_i}^{t} f'\, dt'\right) dt, \end{aligned} \tag{1.124}$$

since $\int_{t_i}^{t_f} f\, dt = 0$, and their imaginary parts involved in (1.122) cancel each other out. The last term of (1.122) finally gives

$$\begin{aligned}\int_{t_i}^{t_f}\int_{t_i}^{t}\int_{t_i}^{t'} \overline{f} e' f''\, dt''\, dt'\, dt &= \int_{t_i}^{t_f} \overline{f}\, dt \int_{t_i}^{t_f}\int_{t_i}^{t} e f'\, dt'\, dt \\ &\quad - \int_{t_i}^{t_f} e\left(\int_{t_i}^{t} f'\, dt'\right)\int_{t_i}^{t} \overline{f}'\, dt'\Big) dt \\ &= -\int_{t_i}^{t_f} e \left|\int_{t_i}^{t} f'\, dt'\right|^2 dt, \end{aligned} \tag{1.125}$$

since $\int_{t_i}^{t_f} f\, dt = 0$. The imaginary part of this term gives then 0 since $e(t)$ is real. We finally obtain

$$\mathrm{Re}\, O_3 = \left(\int_{t_i}^{t_f} e\, dt\right) \mathrm{Im}\left(\int_{t_i}^{t_f}\int_{t_i}^{t} f \overline{f}'\, dt'\, dt\right) = \mathrm{Im}\, O_2 \int_{t_i}^{t_f} e\, dt. \tag{1.126}$$

Chapter 2

Optimal robust quantum control against pulse inhomogeneities: Analytical solutions

2.1 Introduction

Engineering time-dependent quantum systems in a controlled way offers various applications in particular in quantum technologies [1]. This requires ultra-high fidelity (typically with relative errors below 10^{-4}) induced by robust and fast controls [24].

Robustness are naturally taken into account using adiabatic, i.e., slow, approximate, and energetic techniques [6, 31]. Robustness can be quantified by considering transfer profile as a function of the deviation of the ideal controls. Cancellation of its derivatives, leading to constraint integrals, can be treated by composite [13–17], combined [32] or shortcut to adiabaticity [12, 19, 21] techniques. However, these methods, while exact, are not optimal and cost unnecessary energy and time.

Optimization with respect to a cost (usually time, pulse area or energy) including the constraint integrals promise very efficient, typically robust time-optimal, control methods. Numerical techniques using time discretization and gradient methods, such as GRAPE [33], have been studied. Alternative techniques involving from a few tens [34] to a few [19, 20] parameters to be optimized, based on specific parametrizations, have been developed, but they do not provide global optimum. Pontryagin's maximum principle (PMP) in an extended Hilbert space has been shown to provide a global optimum [35] for very simple targets, typically complete population transfers.

Geometric approaches [36, 37] have been have been recently proposed. The latter [37] is an optimization procedure treated by Euler-Lagrange equations constrained

by the robustness integrals with boundaries ensuring exact fidelity in the dynamical variable space. The controls are next inversely determined from the time dependent Schrödinger equation and the derived geodesic. It is referred to as robust inverse optimization (RIO).

We explore the method to determine time-optimal geodesics, robust with respect to the pulse area or amplitude, more generally referred to as pulse inhomogeneities (chosen as the cost) at the lowest order, for various partial population transfers and quantum gates. We show that the solutions of all these problems feature a constant pulse and a detuning of Jacobi elliptic cosine form.

2.2 Optimal robust control against field inhomogeneities for arbitrary population transfer

Optimal robust control is developed as an inverse method: we first optimize the trajectory in the parameter space spanned by the dynamical angles γ, θ with respect to a given cost and constrained by the robustness integrals [i.e., at the lowest order, nullification of (1.102) for the case of population transfer, or conditions (1.93) for the case of quantum gate]; we next derive the controls using the geodesic resulting from this constrained optimization and the inverted Schrödinger equation (1.73).

The optimal process for unconstrained (non-robust) complete population transfer is known to lead to the π-pulse transfer [23]. We proceed to rederive this result using the Euler-Lagrange method. This method is then used for the constrained (robust) dynamics.

2.2.1 The (non-robust) unconstrained optimization problem

Let's consider the (non-robust) unconstrained optimization problem. In this case, optimizing with respect to the pulse area, to the energy, or to the duration leads to the same trajectory, as it is shown below.

The problem of minimization of the pulse area

$$\mathcal{A}(\gamma,\theta)=\int_{t_i}^{t_f}\Omega(t)\,dt=\int_{t_i}^{t_f}\sqrt{\dot{\theta}^2+\dot{\gamma}^2\sin^2\theta(t)}\,dt \tag{2.1}$$

leads to a cost which is by definition time-parametrization invariant. The problem can be formulated by the Euler-Lagrange equations

$$\operatorname{grad}\mathcal{A}(\gamma,\theta)=0, \tag{2.2}$$

where the gradient is defined as

$$\operatorname{grad}\mathcal{A}(\gamma,\theta)=\begin{bmatrix}\frac{\partial\mathcal{L}_0}{\partial\gamma}-\frac{d}{dt}\left(\frac{\partial\mathcal{L}_0}{\partial\dot{\gamma}}\right)\\ \frac{\partial\mathcal{L}_0}{\partial\theta}-\frac{d}{dt}\left(\frac{\partial\mathcal{L}_0}{\partial\dot{\theta}}\right)\end{bmatrix} \tag{2.3}$$

with the Lagrangian $\mathcal{L}_0$ defined from the pulse area as the cost:

$$\mathcal{A}(\gamma,\theta)=\int_{t_i}^{t_f}\sqrt{\dot{\theta}^2+\dot{\gamma}^2\sin^2\theta(t)}\,dt\equiv\int_{t_i}^{t_f}\mathcal{L}_0(\dot{\gamma},\theta,\dot{\theta})\,dt, \tag{2.4}$$

i.e.,

$$\frac{\partial\mathcal{L}_0}{\partial\theta}-\frac{d}{dt}\left(\frac{\partial\mathcal{L}_0}{\partial\dot{\theta}}\right)=0,\quad \frac{\partial\mathcal{L}_0}{\partial\gamma}-\frac{d}{dt}\left(\frac{\partial\mathcal{L}_0}{\partial\dot{\gamma}}\right)=0. \tag{2.5}$$

This formulation of optimization problems is well known, see for instance [30].

We remark that the original problem (1.68) features three differential equations (the Schrödinger equation) and three dynamical angles θ,γ,φ, and two controls: Ω and Δ. Minimizing the pulse area by the Euler-equations, as shown above, leads to two constraint equations which will then give a single solution for the three angles and the controls. We notice that this minimization induces a natural parametrization of the problem in terms of the two angles θ and γ, i.e., in terms of the solution of the Schrödinger equation, and the controls are derived from it (inverse procedure). This will also be the case when the robustness constraints are taken into account, as shown below.

On the other hand, the PMP method is expressed directly in terms of the controls [35] (without explicit knowledge of the solution).

The optimal solution, which satisfies the Euler-Lagrange equations, can be found by inspecting the integral (2.1): it is simply achieved for $\dot{\gamma}=0$ for any given $\dot{\theta}$ (note that $\dot{\theta}$ cannot be 0 to accomplish a given transfer), i.e., $\gamma=const.$ This gives $\varphi=\pi/2$ from (1.68c), $\dot{\theta}=\Omega$ from (1.68a), $\Delta=0$ from (1.68b), and $\mathcal{A}_{\min}=\int_{t_i}^{t_f}\Omega(t)\,dt=\int_{t_i}^{t_f}\dot{\theta}\,dt=\int_{\theta_i}^{\theta_f}d\theta=\theta_f-\theta_i$ [assuming a monotonic $\theta(t)$ such that $\dot{\theta}>0$, i.e., $\Omega(t)>0$].

Minimizing the pulse energy

$$\mathcal{E}(\gamma,\theta)=\int_{t_i}^{t_f}\Omega^2(t)\,dt=\int_{t_i}^{t_f}(\dot{\theta}^2+\dot{\gamma}^2\sin^2\theta)\,dt, \tag{2.6}$$

is for the same reason achieved when $\dot{\gamma}=0$, leading to the same trajectory $\gamma=const$ as for the minimization of the pulse area. The function $\theta(t)$ that minimizes the

energy is given by the Euler-Lagrange equation

$$\operatorname{grad}\mathcal{E}(\theta)=0,\quad \mathcal{E}(\theta)=\int_{t_i}^{t_f}\dot{\theta}^2\,dt\equiv\int_{t_i}^{t_f}\mathcal{L}_0(\dot{\theta})\,dt, \tag{2.7}$$

with

$$\operatorname{grad}\mathcal{E}(\theta)=\frac{\partial\mathcal{L}_0}{\partial\theta}-\frac{d}{dt}\left(\frac{\partial\mathcal{L}_0}{\partial\dot{\theta}}\right). \tag{2.8}$$

This leads to $\ddot{\theta}=0$, i.e., to a linear evolution of $\theta(t)$:

$$\theta=(\theta_f-\theta_i)\frac{t-t_i}{t_f-t_i}+\theta_i, \tag{2.9}$$

which gives a constant pulse, $\Omega_0=(\theta_f-\theta_i)/(t_f-t_i)$, and the minimum energy:

$$\mathcal{E}_{\min}=\Omega_0^2(t_f-t_i)=\frac{(\theta_f-\theta_i)^2}{t_f-t_i}. \tag{2.10}$$

This shows that the minimum energy, for given θ_i and θ_f, depends on the duration of the process t_f-t_i: The energy minimization problem has thus to be considered *for a given fixed duration* t_f-t_i.

For the time-minimization problem, we can reparametrize the trajectories by the (normalized) arclength

$$ds=\frac{\Omega(t)}{\Omega_0}\,dt, \tag{2.11}$$

i.e., $s(t)=s_i+\int_{t_i}^{t}[\Omega(t')/\Omega_0]\,dt'$, and the TDSE becomes:

$$i\hbar\frac{\partial}{\partial s}|\widetilde{\phi}_0(s)\rangle=\frac{\hbar}{2}\begin{bmatrix}-\widetilde{\Delta} & \Omega_0\\ \Omega_0 & \widetilde{\Delta}\end{bmatrix}|\widetilde{\phi}_0(s)\rangle,\quad \widetilde{\Delta}=\Delta\Omega_0/\Omega, \tag{2.12}$$

with the cost $\mathcal{A}=\Omega_0\int_{s_i}^{s_f}dt$, which corresponds to a time minimization problem with a bounded control $\widetilde{\Omega}=\Omega_0$, It follows that, for the initial control system, the problem of minimizing the pulse area $\mathcal{A}$ is equivalent to minimizing the time under the constraint on the control $\Omega\leq\Omega_0$, and the minimum time is achieved when the pulse reaches its maximum at all times: $\Omega=\Omega_0$. The minimum time is thus $T\equiv T_{\min}=(\theta_f-\theta_i)/\Omega_0$.

Another formulation of the time-minimization problem uses the Lagrangian $\mathcal{L}_0=1$:

$$T=\int_{t_i=0}^{t_f=T}dt \tag{2.13}$$

with the inequality constraint $|\Omega(t)| = |\dot{\theta}/\sin\varphi| \leq \Omega_0$, leading to the action

$$\mathcal{S} = \int_0^T \left\{ 1 + \lambda(t) \left[\frac{\dot{\theta}}{\sin\varphi} - \Omega_0 \tanh\omega(t) \right] \right\} dt \equiv \int_0^T \mathcal{L}_0(\dot{\theta}, \varphi, \lambda, \omega)\, dt, \tag{2.14}$$

with the slack variable $\omega(t)$ that takes into account the above inequality and the Lagrangian multiplier $\lambda(t)$. The Euler-Lagrange equations read

$$\frac{\partial \mathcal{L}_0}{\partial \varphi} = 0, \quad \frac{d}{dt}\left(\frac{\partial \mathcal{L}_0}{\partial \dot{\theta}} \right) = 0, \quad \frac{\partial \mathcal{L}_0}{\partial \lambda} = 0, \quad \frac{\partial \mathcal{L}_0}{\partial \omega} = 0, \tag{2.15}$$

i.e.,

$$\varphi = \frac{\pi}{2}, \quad \dot{\lambda} = 0, \quad \Omega = \Omega_0 \tanh\omega, \quad \frac{1}{\cosh^2\omega} = 0, \tag{2.16}$$

of solution $\omega = \pm\infty$, $\Omega = \pm\Omega_0$.

For instance for a complete population transfer from $t_i = 0$ to $t_f = T$, requiring $\theta_i = 0$ and $\theta_f = \pi$, we have: $\theta = \pi t/T$, $\Omega = \pi/T$, $\mathcal{A}_{\min} = \pi$ (i.e., the so-called $\pi-$pulse), $\mathcal{E}_{\min} = \pi^2/T$ and $T_{\min} = \pi/\Omega_0$.

2.2.2 Constrained Euler-Lagrange optimization

We consider the optimal robust transfer from the ground state to an arbitrary target state defined by given mixing angle θ_0 and internal phase φ_0 (up to a global phase $\gamma_0/2$ irrelevant for the problem of population transfer):

$$|\phi(t_f)\rangle = |\phi_T\rangle \equiv \begin{bmatrix} e^{i\varphi_0/2}\cos(\theta_0/2) \\ e^{-i\varphi_0/2}\sin(\theta_0/2) \end{bmatrix} e^{-i\gamma_0/2}. \tag{2.17}$$

The internal phase φ_0 is not fixed, but controlled in a robust way. It can be modified via a static phase η_0 added to the control field, see Eqs. (1.69-1.72).

Equation (1.68c) implies $\varphi_i = \pi/2$, $\varphi_f = \pi/2$.

This problem imposes thus the boundaries

$$\theta_i = 0,\ \theta_f = \theta_0,\ \gamma_i = \varphi_i = \pi/2,\ \varphi_f = \varphi_0. \tag{2.18}$$

Nullification of the second order (1.102) reduces to the two (real) conditions (1.111b) for a trajectory $\widetilde{\gamma}(\theta)$:

$$\int_0^{\theta_f} \cos\widetilde{\gamma}\sin^2\theta\, d\theta + \frac{1}{4}\cos\widetilde{\gamma}_f \sin 2\theta_f = 0, \tag{2.19a}$$

$$\int_0^{\theta_f} \sin\widetilde{\gamma}\sin^2\theta\, d\theta + \frac{1}{4}\sin\widetilde{\gamma}_f \sin 2\theta_f = 0, \tag{2.19b}$$

or to the two conditions (1.114b) and (1.114c) for a trajectory $\widetilde{\theta}(\gamma)$:

$$\int_{\pi/2}^{\gamma_f} (\sin 2\widetilde{\theta} - 2\widetilde{\theta}) \cos\gamma \, d\gamma + 2\theta_f \sin\gamma_f = 0, \tag{2.20a}$$

$$\int_{\pi/2}^{\gamma_f} (\sin 2\widetilde{\theta} - 2\widetilde{\theta}) \sin\gamma \, d\gamma - 2\theta_f \cos\gamma_f = 0, \tag{2.20b}$$

which are all time-parametrization invariant.

Pulse-area optimization

We determine the optimal trajectory $\widetilde{\theta}(\gamma)$ considering a monotonic $\gamma(t)$. The determination of the inverse optimal trajectory $\widetilde{\gamma}(\theta)$ is treated in Appendix 2.A. The problem can be formulated as an optimization problem under constraint: finding the trajectory $\widetilde{\theta}(\gamma)$ that minimizes the pulse area (1.77)

$$\mathcal{A}(\widetilde{\theta}) = \int_{\gamma_i}^{\gamma_f} \sqrt{\left(\dot{\widetilde{\theta}}\right)^2 + \sin^2\widetilde{\theta}} \, d\gamma \equiv \int_{\gamma_i}^{\gamma_f} \mathcal{L}_0(\widetilde{\theta}, \dot{\widetilde{\theta}}) \, d\gamma \tag{2.21}$$

with $\dot{\widetilde{\theta}} \equiv \frac{d\widetilde{\theta}}{d\gamma}$, under the two constraints (2.20) rewritten for convenience as

$$\psi_1(\widetilde{\theta}) = -\frac{1}{4}\int_{\gamma_i}^{\gamma_f} (\sin 2\widetilde{\theta} - 2\widetilde{\theta}) \sin\gamma \, d\gamma \equiv \int_{\gamma_i}^{\gamma_f} \varphi_1(\gamma, \widetilde{\theta}) \, d\gamma = -\frac{\pi}{2}\cos\gamma_f, \tag{2.22a}$$

$$\psi_2(\widetilde{\theta}) = \frac{1}{4}\int_{\gamma_i}^{\gamma_f} (\sin 2\widetilde{\theta} - 2\widetilde{\theta}) \cos\gamma \, d\gamma \equiv \int_{\gamma_i}^{\gamma_f} \varphi_2(\gamma, \widetilde{\theta}) \, d\gamma = -\frac{\pi}{2}\sin\gamma_f. \tag{2.22b}$$

Since the final phase is irrelevant for the population transfer problem, the final value γ_f is not fixed, but $\theta_f = \widetilde{\theta}(\gamma_f) = \theta_0$. When the constraints have such integral form, i.e., are defined as functionals of the trajectory, the problem is referred to as isoperimetric [30]. Several generalizations can be found in [30], including functional with multiple integrals (needed if higher order robustness is considered).

This can be solved by the constrained Euler-Lagrange optimization as follows: The trajectory $\widetilde{\theta}(\gamma)$ is solution of

$$\operatorname{grad}\mathcal{A}(\widetilde{\theta}) + \widetilde{\lambda}_1 \operatorname{grad}\psi_1(\widetilde{\theta}) + \widetilde{\lambda}_2 \operatorname{grad}\psi_2(\widetilde{\theta}) = 0, \tag{2.23}$$

with $\widetilde{\lambda}_j$, $j = 1, 2$, the Lagrangian multipliers associated to the constraints, where

$$\operatorname{grad}\mathcal{A}(\widetilde{\theta}) = \frac{\partial\mathcal{L}_0}{\partial\widetilde{\theta}} - \frac{d}{d\gamma}\left(\frac{\partial\mathcal{L}_0}{\partial\dot{\widetilde{\theta}}}\right), \tag{2.24}$$

and $j = 1, 2$

$$\operatorname{grad} \psi_j(\widetilde{\theta}) = \frac{\partial \varphi_j}{\partial \widetilde{\theta}} - \frac{d}{d\gamma}\left(\frac{\partial \varphi_j}{\partial \dot{\widetilde{\theta}}}\right). \tag{2.25}$$

We obtain the differential equation:

$$\ddot{\widetilde{\theta}} = 2\big(\dot{\widetilde{\theta}}\big)^2 \cot \widetilde{\theta} + \sin \widetilde{\theta} \cos \widetilde{\theta} + (\widetilde{\lambda}_1 \sin \gamma - \widetilde{\lambda}_2 \cos \gamma)\big[\big(\dot{\widetilde{\theta}}\big)^2 + \sin^2 \widetilde{\theta}\big]^{3/2}. \tag{2.26}$$

In order to analyze the initial singularity of $\big(\dot{\widetilde{\theta}}\big)^2 \cot \widetilde{\theta}$, with $\dot{\widetilde{\theta}} = 1/\dot{\widetilde{\gamma}} \to \infty$ (see Appendix 2.A.3) and $\widetilde{\theta} \to 0$, we multiply this equation by $\sin \widetilde{\theta}$, and set $\widetilde{\theta} \to 0$ (initial time) with $\gamma = \pi/2$:

$$\ddot{\widetilde{\theta}} \sin \widetilde{\theta} = \big(\dot{\widetilde{\theta}}\big)^2 (2 + \widetilde{\lambda}_1 \dot{\widetilde{\theta}} \sin \widetilde{\theta}). \tag{2.27}$$

This shows that $\ddot{\widetilde{\theta}}$ is initially infinite. This is also symmetrically the case at the final time for the problem of complete population transfer (when $\theta_f = \pi$).

The optimal robust trajectory $\widetilde{\theta}_{\text{opt}}(\gamma)$, solution of (2.26), is obtained for the set of values of $\widetilde{\lambda}_1$ and $\widetilde{\lambda}_2$, which satisfies (2.22) (and we select the trajectory of smallest pulse area in case of more than one solution). We remark that the value of γ_f results from this solution (and that γ_f is not robust in the considered case of population transfer).

Optimization with respect to pulse energy or time

In this case, since the robustness integrals (1.111b) do not depend on the time-parametrization, optimizing with respect to the pulse area, to the energy, or to the duration leads to the same trajectory, as in the unconstrained case. This is precisely shown in Appendix 2.B.

Concerning the time optimization problem, the reparametrization of the trajectory, through the change of variable (2.11), can be applied as in the case of the unconstrained problem. Since the constraints are time-parametrization invariant, the conclusions derived for the unconstrained case still apply: The problem of minimizing the pulse area $\mathcal{A}$ is equivalent to minimizing the time under the constraint on the control $\Omega \leq \Omega_0$, and the minimum time is achieved when the pulse reaches its maximum at all times: $\Omega = \Omega_0$. We obtain from (2.111) for the minimum time

$$T_{\min} = \frac{1}{\Omega_0} \int_{\gamma_i}^{\gamma_f} \sqrt{\big(\dot{\widetilde{\theta}}\big)^2 + \sin^2 \theta}\, d\gamma. \tag{2.28}$$

The optimization with respect to the pulse energy (1.78) uses the same formula but interpreted differently: The minimum (constant) pulse amplitude $\Omega_{0,\min}$ is deter-

mined from a given duration T of the interaction as:

$$\Omega_{0,\min} = \frac{1}{T}\int_{\gamma_i}^{\gamma_f} \sqrt{\left(\dot{\widetilde{\theta}}\right)^2 + \sin^2\theta}\, d\gamma. \tag{2.29}$$

2.2.3 Analytic expression of the detuning for time-optimization

One can express the detuning as a function of the angles θ and γ as follows: The derivation of (1.68c) with (1.68a) leads to

$$\ddot{\gamma}\sin\theta + \dot{\gamma}\dot{\theta}\cos\theta = -\dot{\varphi}\Omega_0\sin\varphi = -\dot{\varphi}\dot{\theta}, \tag{2.30}$$

which allows the substitution of $\dot{\varphi}$ in (1.68b) to give

$$\Delta = -\frac{1}{\dot{\theta}}(\ddot{\gamma}\sin\theta + 2\dot{\gamma}\dot{\theta}\cos\theta). \tag{2.31}$$

From the equations of motions (2.104)

$$\ddot{\gamma} + 2\dot{\gamma}\dot{\theta}\,\cot\,\theta + \dot{\theta}(\lambda_1\sin\gamma - \lambda_2\cos\gamma) = 0, \tag{2.32a}$$

$$\dot{\gamma}^2\sin\theta\cos\theta + \dot{\gamma}\sin^2\theta(\lambda_1\sin\gamma - \lambda_2\cos\gamma) = \ddot{\theta}, \tag{2.32b}$$

where we have redefined $\lambda_1/2 \to \lambda_1$ and $\lambda_2/2 \to \lambda_2$ for convenience, we obtain for the detuning

$$\Delta = \sin\theta(\lambda_1\sin\gamma - \lambda_2\cos\gamma). \tag{2.33}$$

This gives in particular at initial time $\Delta_i = 0$.

We show in Appendix 2.D the general form of the detuning:

$$\Delta = \Delta_0\,\mathrm{cn}\left(\omega t + K(m), m\right), \quad t \in [0, T_{\min}] \tag{2.34}$$

with

$$\Delta_0 = -2\,\mathrm{sgn}(\lambda_1)\,\omega\sqrt{m}, \tag{2.35a}$$

$$|\lambda_1|\Omega_0 = 2\omega^2\sqrt{m}\sqrt{1-m}, \tag{2.35b}$$

$$\lambda_1\Theta_{0x,f} - \lambda_2\Theta_{0y,f} = -\Delta_0\omega\,\mathrm{sn}[\omega T_{\min} + K(m), m] \times \sqrt{1 - m\,\mathrm{sn}^2[\omega T_{\min} + K(m), m]}. \tag{2.35c}$$

From the knowledge of the trajectory $\widetilde{\theta}(\gamma)$, obtained from λ_1 and λ_2, and $T_{\min}$

Table 2.1: Parameters of the RIO process for various transfers.

Parameter				
θ_0 $(\times\pi)$	1	2/3	1/2	1/3
λ_1 $(\times\Omega_0)$	-1.11886	-1.40714	-1.69741	-2.21305
λ_2 $(\times\Omega_0)$	-0.29960	-0.51803	-0.64653	-0.84521
$T_{\min}$ $(/\Omega_0)$	5.84	4.7161	4.05	3.29
$\mathcal{A}$ $(\times\pi)$	1.86	1.50	1.29	1.05
γ_f $(\times\pi)$	5/3	1.50	1.48	1.43
φ_0 $(\times\pi)$	1/2	0.615	1/2	0.335
m	0.235	0.338	0.398	0.465
ω $(\times\Omega_0)$	1.149	1.220	1.317	1.489
Δ_0 $(\times\Omega_0)$	1.114	1.418	1.660	2.032

from (2.28), one can calculate m and ω from the system of equations (2.35b–2.35c), where we substitute Δ_0 from (2.35a). We next obtain Δ_0 from (2.35a), which fully determines the detuning (2.34).

2.2.4 Results

Some results are reported in Table 2.1 for complete population transfer, half transfer, one-quarter $\theta_0 = \pi/3$ (i.e., $\sin^2(\theta_0/2) = 1/4$) and three-quarter $\theta_0 = 2\pi/3$ (i.e., $\sin^2(\theta_0/2) = 3/4$) transfers. In each case, we have numerically determined λ_1 (taking the negative solution), λ_2, the optimal time $T_{\min}$ (giving the pulse area), the final γ_f and φ_0 from the differential equation (2.26). For complete population transfer, we have determined the value $\gamma_f = 5\pi/3$ in Appendix 2.C using the symmetry of the trajectory.

The other parameters are determined according to (2.35).

Equation (2.35c) gives for the duration a complete period of the elliptic cosine:

$$T_{\min} = \frac{4K(m)}{\omega} \tag{2.36}$$

in the case of complete population transfer, and three-quarters of the elliptic cosine period:

$$T_{\min} = \frac{3K(m)}{\omega} \tag{2.37}$$

in the case of half population transfer. The trajectory $\widetilde{\theta}(\gamma)$ and the detuning (for the optimal time) are shown in Figs. 2.1, 2.2, 2.3, and 2.4, [37], for the two cases of complete and half population transfers.

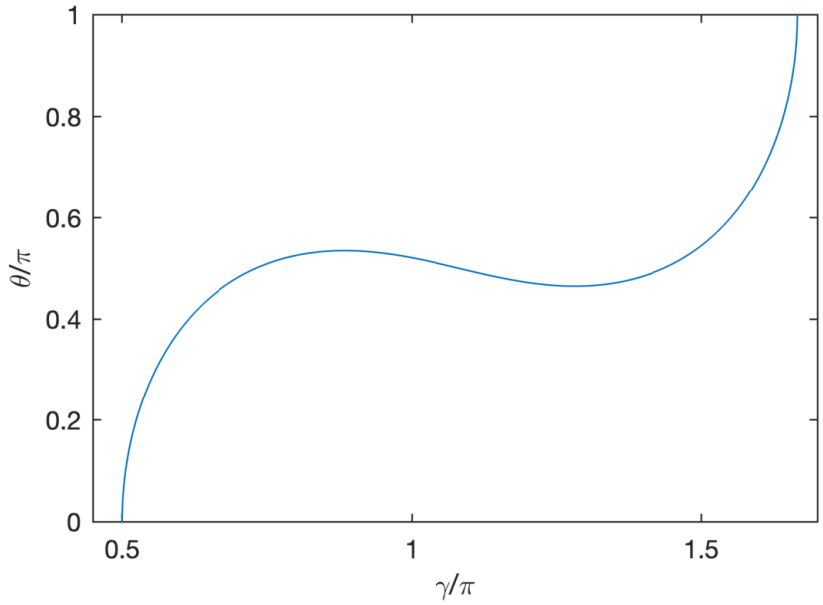

Figure 2.1: Optimal α-robust geodesic $\widetilde{\theta}(\gamma)$ in the dynamical variable space (γ, θ) leading to complete population transfer determined from numerical solution of (2.26) corresponding to $\widetilde{\lambda}_1 \approx -1.11886$, $\widetilde{\lambda}_2 \approx -0.29960$ (with $\gamma_f = 5\pi/3$).

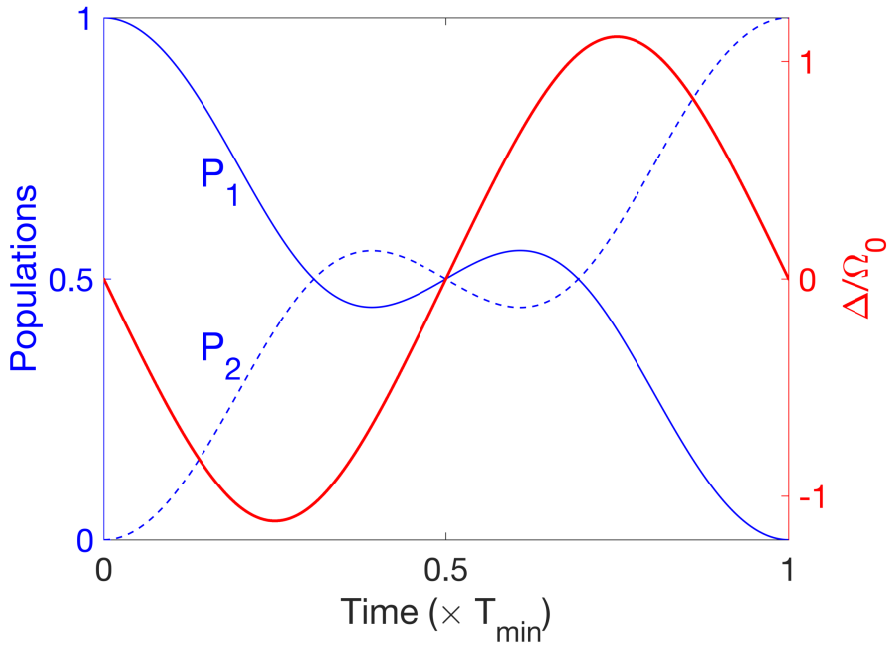

Figure 2.2: Detuning and dynamics of the populations P_j, $j = 1, 2$ resulting from the geodesic $\widetilde{\theta}(\gamma)$ of Fig. 2.1, for robust time-optimal control [obtained for a flat pulse of Rabi frequency Ω_0 according to (2.28)] showing the complete population transfer with the optimal time $T_{\min} \approx 5.842/\Omega_0$.

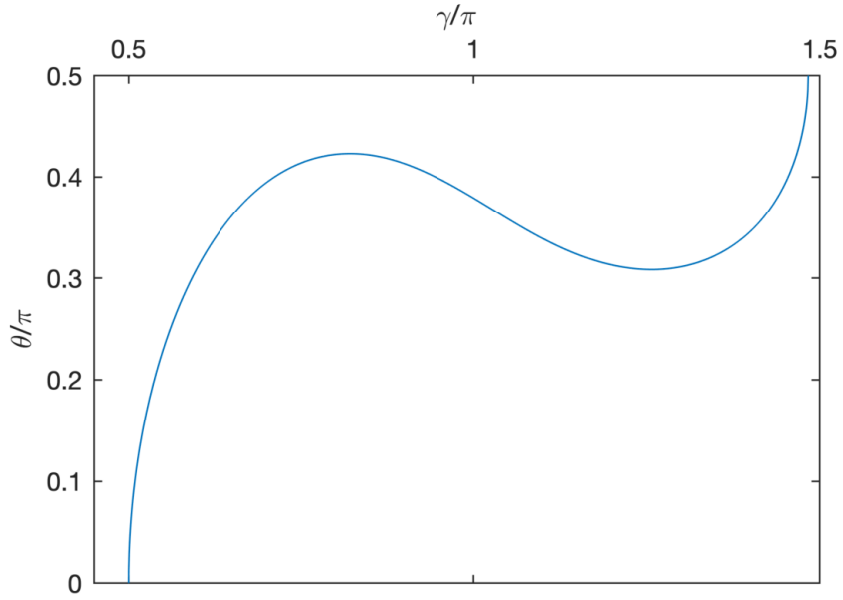

Figure 2.3: Optimal α-robust geodesic $\widetilde{\theta}(\gamma)$ for half population transfer corresponding to $\widetilde{\lambda}_1 \approx -1.69741$, $\widetilde{\lambda}_2 \approx -0.64653$ (leading to $\gamma_f \approx 1.48\pi$ and $\varphi_0 = \pi/2$).

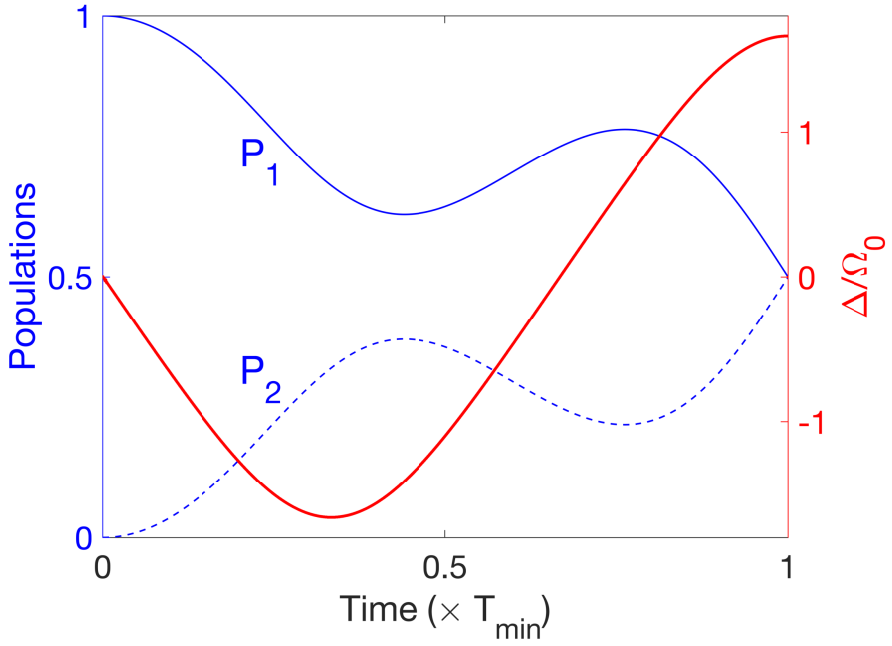

Figure 2.4: Detuning and dynamics of the populations P_j, $j = 1, 2$ resulting from the geodesic $\widetilde{\theta}(\gamma)$ of Fig. 2.3, for robust time-optimal control (for a flat pulse of Rabi frequency Ω_0) showing the half superposition. We obtain the optimal time $T_{\min} \approx 4.05/\Omega_0$.

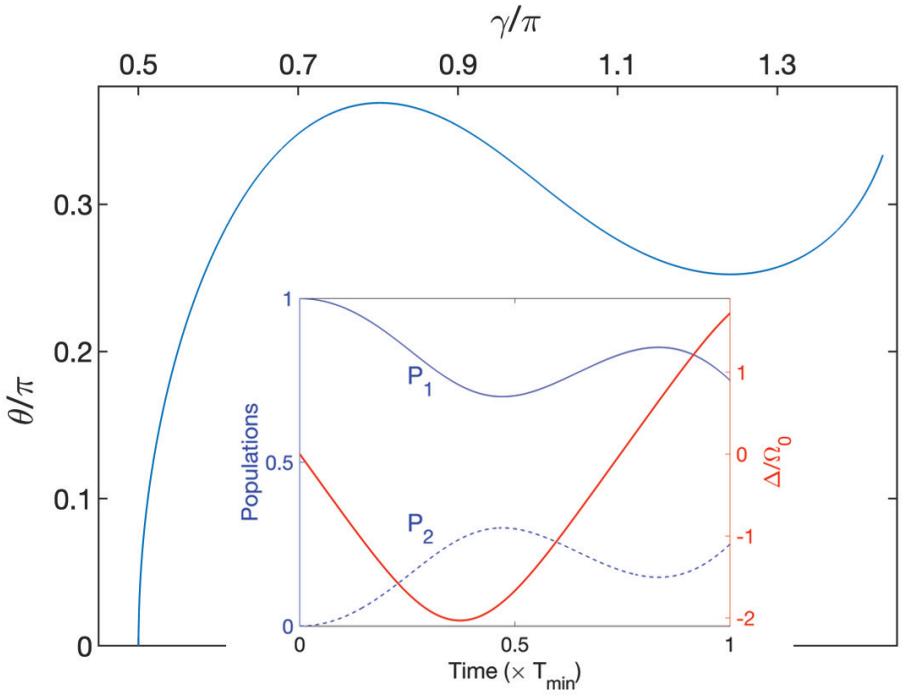

Figure 2.5: Optimal α-robust geodesic $\widetilde{\theta}(\gamma)$ for a quarter population transfer determined from numerical solution of (2.26). Inset: Resulting detuning and dynamics of the populations P_j, $j = 1, 2$, for robust time-optimal control [obtained for a flat pulse of Rabi frequency Ω_0 according to (2.28)].

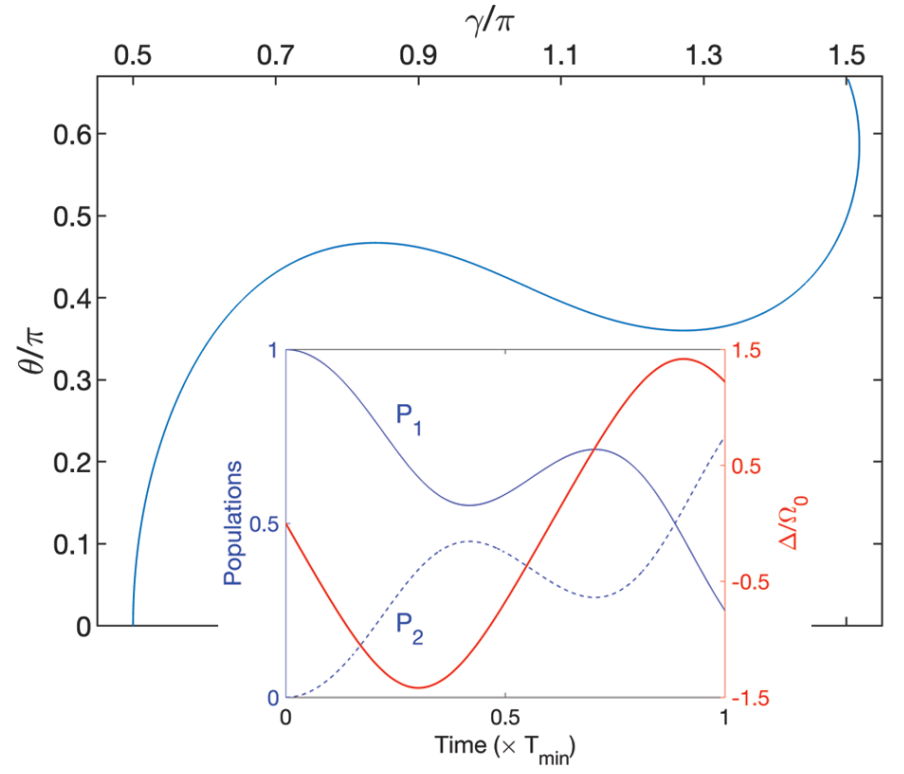

Figure 2.6: Same as Fig. 2.5 for three-quarter population transfer.

The trajectories are shown in Figs. 2.5 and 2.6, respectively. We notice the turning point of the trajectory in Fig. 2.6 near the end, indicating a non-monotonic γ. In fact, in this situation, it is much simpler to solve the problem in the time domain as it is done below for the case of quantum gates, i.e., with Eqs. (2.54) and $\lambda_0 = 0$. Such a feature occurs for a population transfer above 1/2 and different from 1 (i.e., $\pi/4 < \theta_0 < \pi$).

We have considered several other examples of θ_0 transfer. The resulting parameters have been gathered in Fig. 2.7. We notice the discontinuity of the phase φ_0 when one tends to the complete transfer. This is due to the fact that the phase φ_0 becomes not well defined at the complete transfer; what matters is the total phase $\varphi_0 + \gamma_f$. We have checked that the latter is continuous when one tends to the complete transfer.

The transfer profile has been calculated for the case of complete population transfer in Fig. 2.8, compared to the single π-pulse and the optimal composite pulse [featuring three pulses of respective areas, $\pi/2$–π–$\pi/2$ (2.146)], as determined in Appendix 2.E.

Figure 2.9 shows the robustness profile for the half superposition (2.17) with $\varphi_0 = \pi/2$. It is compared to the 2π composite pulses of Ref. [17] (where they have been defined with a figure of merit as the absolute value squared of the amplitude of the superposition, disregarding the internal phase). As anticipated, it shows a lower robustness than RIO when using the complete target state (up to a global phase) as figure of merit (1.101).

As expected, the profile given by the composite pulses is similar to that of RIO since they are of the same order. We notice that the optimal composite pulse technique perform relatively well for the complete population transfer as its total area is 2π, only approximately 10% more than the optimal RIO (1.86π).

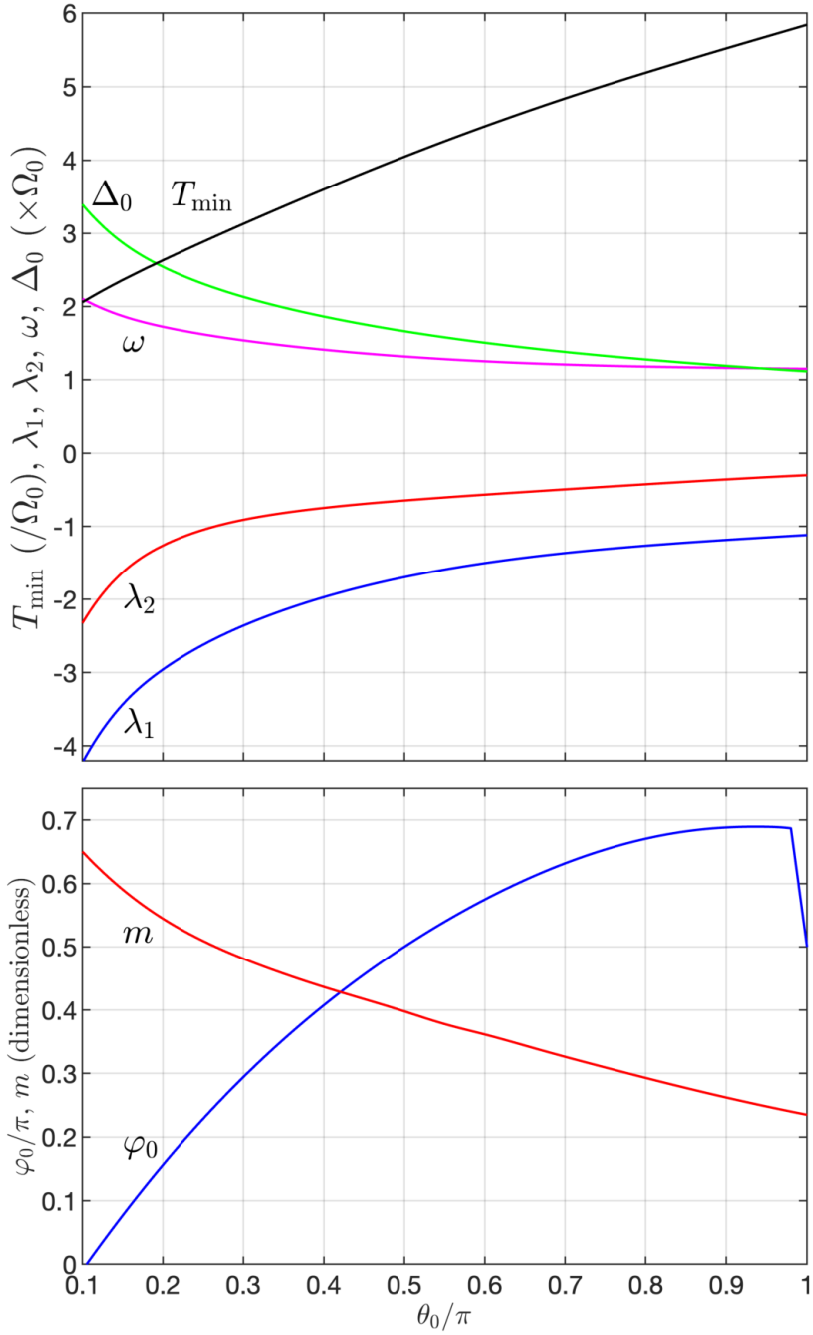

Figure 2.7: Parameters (λ_1, λ_2, φ_0, $T_{\min}$) characterizing the optimal α-robust trajectories $\widetilde{\theta}(\gamma)$ and those (m, ω, Δ_0) of the time- or energy-optimal detunings for arbitrary population transfer given by θ_0.

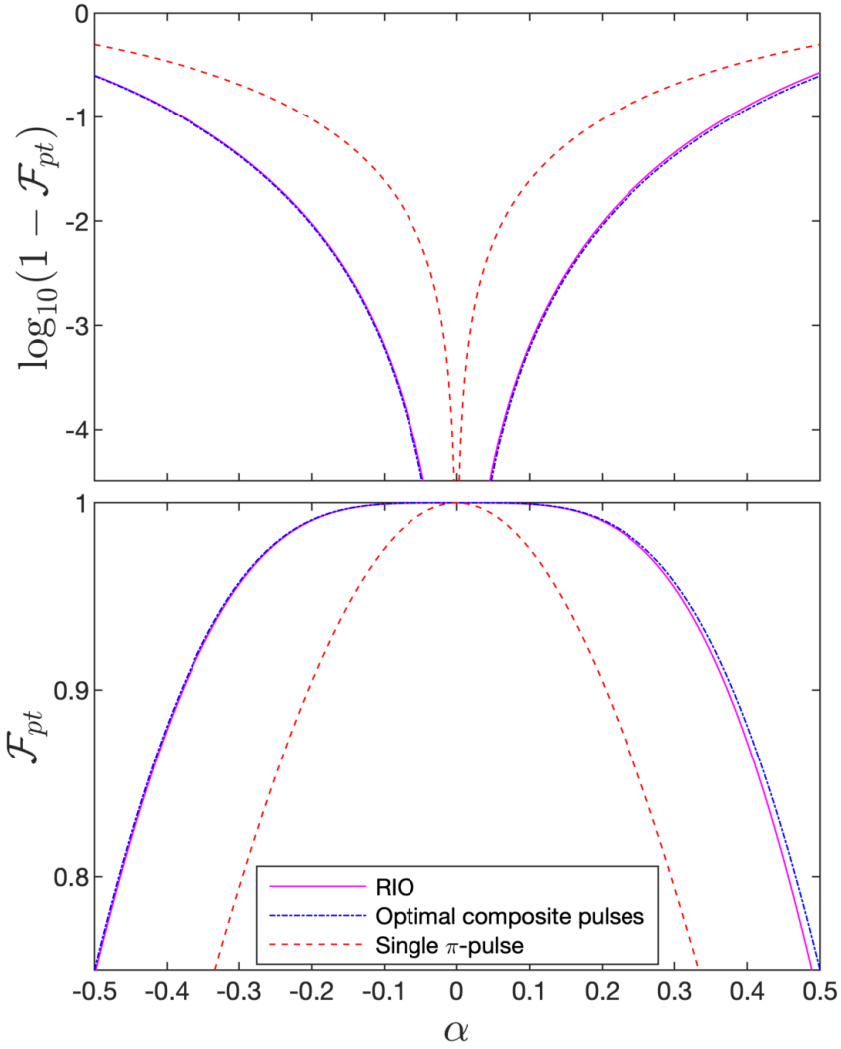

Figure 2.8: Robustness profile for complete population transfer: Fidelity (lower panel) and its deviation with respect to 1 in logarithmic scale (upper panel) as a function of the error α for RIO, for the corresponding optimal three-pulse composite technique, and the single π-pulse.

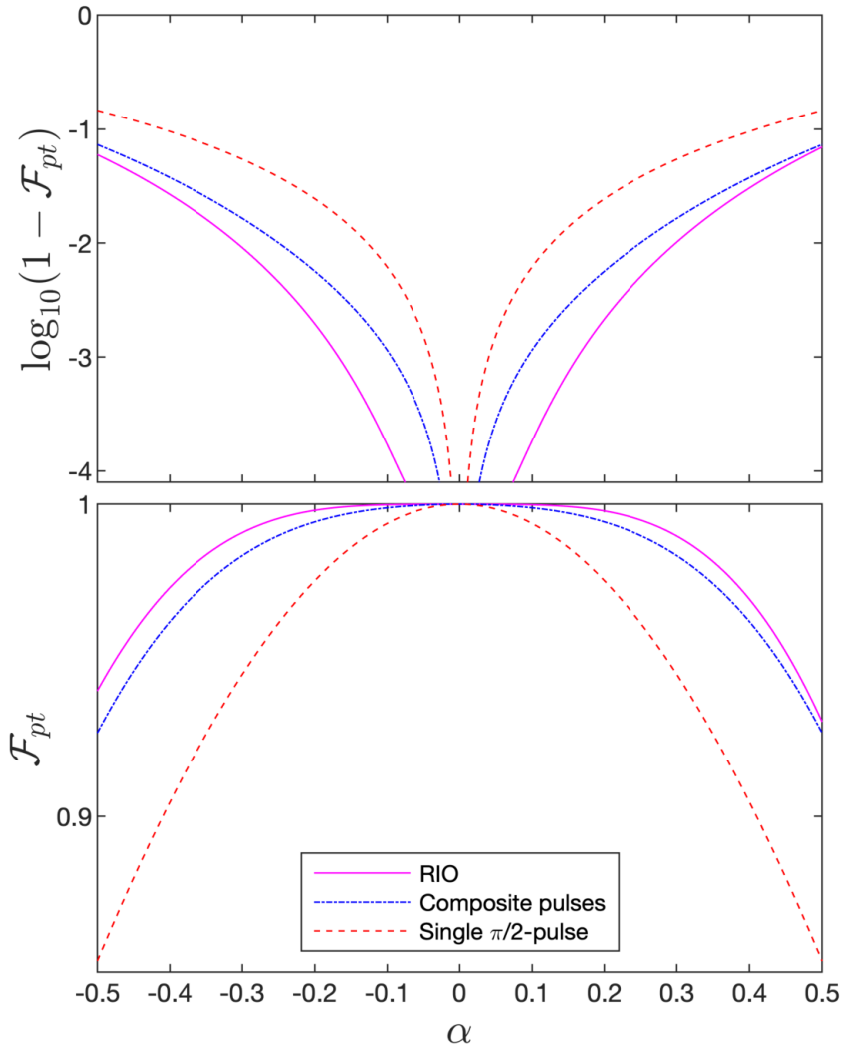

Figure 2.9: Same as Fig. 2.8, but for half population transfer.

2.3 Optimal robust control against field inhomogeneities for quantum gate

2.3.1 General SU(2) gate

An arbitrary SU(2) gate corresponds to (1.105):

$$U(\theta_0,\varphi_0,\gamma_0)=\begin{bmatrix} c\equiv e^{\frac{i}{2}(\varphi_0-\gamma_0)}\cos(\theta_0/2) & -\bar{d} \\ d\equiv e^{-\frac{i}{2}(\varphi_0+\gamma_0)}\sin(\theta_0/2) & \bar{c} \end{bmatrix} \tag{2.38}$$

with the given angle θ_0 and the two phases φ_0, γ_0 to be controlled in a robust way.

We recall that the internal phase of the state can be modified via a static phase η_0 added to the control field, see Eqs. (1.69-1.72). The corresponding propagator reads indeed in this case at the end of the process

$$\widetilde{U}(\theta_0,\varphi_0,\gamma_0,\eta_0)=T(\eta_0)U(\theta_0,\varphi_0,\gamma_0)T^{\dagger}(\eta_0)=\begin{bmatrix} c & -\bar{d}e^{-i\eta_0} \\ de^{i\eta_0} & \bar{c} \end{bmatrix}. \tag{2.39}$$

Application of a preliminary phase gate (of phase κ) (see Sec. 2.3.5 for its implementation)

$$\Phi_\kappa=\begin{bmatrix} e^{-i\kappa/2} & 0 \\ 0 & e^{i\kappa/2} \end{bmatrix} \tag{2.40}$$

allows one to modify the global phase γ_0:

$$\begin{aligned}\widetilde{U}(\theta_0,\varphi_0,\gamma_0,\eta_0)\Phi_\kappa &= \begin{bmatrix} c & -\bar{d}e^{-i\eta_0} \\ de^{i\eta_0} & \bar{c} \end{bmatrix}\begin{bmatrix} e^{-i\kappa/2} & 0 \\ 0 & e^{i\kappa/2} \end{bmatrix} \\ &= \begin{bmatrix} ce^{-i\kappa/2} & -\bar{d}e^{-i\eta_0}e^{i\kappa/2} \\ de^{i\eta_0}e^{-i\kappa/2} & \bar{c}e^{i\kappa/2} \end{bmatrix}.\end{aligned} \tag{2.41}$$

We can thus consider without loss of generality the construction of a robust process driving the ground state $|0\rangle$ to the state

$$|\phi(t_f)\rangle=|\phi_T\rangle\equiv\begin{bmatrix} e^{i\varphi_0/2}\cos(\theta_0/2) \\ e^{-i\varphi_0/2}\sin(\theta_0/2) \end{bmatrix}e^{-i\gamma_0/2} \tag{2.42}$$

with the two phases $\varphi_f=\varphi_0$, $\gamma_f=\gamma_0$, while robust, not fixed *a priori*. They will result from the optimization procedure. This control implies, as in the case of

population transfer, the boundaries

$$\theta_i = 0,\ \theta_f = \theta_0, \gamma_i = \varphi_i = \pi/2. \tag{2.43}$$

From the fidelity (1.109) we aim at nullifying $\mathrm{Re}\, O_2 = 0$ (which automatically nullifies $\mathrm{Re}\, O_3 = 0$).

Optimization with respect to pulse area

Nullification of the second order (1.93) reduces to the three conditions (1.114) for a trajectory $\widetilde{\theta}(\gamma)$ with $\dot{\gamma} > 0$:

$$0 = \int_{\pi/2}^{\gamma_f} \sin^2 \widetilde{\theta}\, d\gamma, \tag{2.44a}$$

$$0 = \int_{\pi/2}^{\gamma_f} (\sin 2\widetilde{\theta} - 2\widetilde{\theta}) \cos\gamma\, d\gamma + 2\pi \sin\gamma_f, \tag{2.44b}$$

$$0 = \int_{\pi/2}^{\gamma_f} (\sin 2\widetilde{\theta} - 2\widetilde{\theta}) \sin\gamma\, d\gamma - 2\pi \cos\gamma_f. \tag{2.44c}$$

We obtain the equation of motion for the trajectory $\widetilde{\theta}(\gamma)$:

$$\begin{aligned}\ddot{\widetilde{\theta}} = {} & 2\big(\dot{\widetilde{\theta}}\big)^2 \cot\widetilde{\theta} + \sin\widetilde{\theta}\cos\widetilde{\theta} + 2\widetilde{\lambda}_0 \cot\theta \big[\sin^2\widetilde{\theta} + \big(\dot{\widetilde{\theta}}\big)^2\big]^{3/2} \\ & + (\lambda_1 \sin\gamma - \lambda_2 \cos\gamma)\big[\sin^2\widetilde{\theta} + \big(\dot{\widetilde{\theta}}\big)^2\big]^{3/2}.\end{aligned} \tag{2.45}$$

It generalizes Eq. (2.26) obtained for the problem of population transfer.

We have seen that $\gamma(t)$ cannot be monotonic when Eq. (1.114a) has to be satisfied. We have then to consider a piecewise defined function $\widetilde{\theta}(\gamma)$:

$$\widetilde{\theta}(\gamma) = \begin{cases} \widetilde{\theta}_+(\gamma) & \text{for } \dot{\gamma} \geq 0,\ \gamma = [\pi/2, \gamma_m], \\ \widetilde{\theta}_-(\gamma) & \text{for } \dot{\gamma} < 0,\ \gamma = [\gamma_f, \gamma_m), \end{cases} \tag{2.46}$$

with $\theta_m = \widetilde{\theta}_+(\gamma_m) = \widetilde{\theta}_-(\gamma_m)$. We use this formulation to determine the trajectory for the NOT gate below.

Optimization with respect to energy and time

We rewrite the constraints (1.93) as functions of time:

$$\psi_0(\gamma,\theta) \equiv \int_{t_i}^{t_f} \dot{\gamma}\sin^2\theta\, dt \equiv \int_{t_i}^{t_f} \varphi_0(\dot{\gamma},\theta)\, dt = 0, \tag{2.47a}$$

$$\psi_f(\gamma,\theta) \equiv \int_{t_i}^{t_f} \dot{\gamma}\sin 2\theta e^{i\gamma}\, dt - 2i\int_{t_i}^{t_f} \dot{\theta}e^{i\gamma}\, dt = 0. \tag{2.47b}$$

The latter equation can be rewritten, after integration by parts, as

$$\int_{t_i}^{t_f} \dot{\gamma}(\sin 2\theta - 2\theta)e^{i\gamma}\, dt - 2i(\theta_f e^{i\gamma_f} - \theta_i e^{i\gamma_i}) = 0, \tag{2.48}$$

giving for the gate:

$$\psi_1(\gamma,\theta) \equiv \int_{t_i}^{t_f} \dot{\gamma}\cos\gamma(\sin 2\theta - 2\theta)\, dt \equiv \int_{t_i}^{t_f} \varphi_1(\gamma,\dot{\gamma},\theta)\, dt = -2\theta_f \sin\gamma_f, \tag{2.49a}$$

$$\psi_2(\gamma,\theta) \equiv \int_{t_i}^{t_f} \dot{\gamma}\sin\gamma(\sin 2\theta - 2\theta)\, dt \equiv \int_{t_i}^{t_f} \varphi_2(\gamma,\dot{\gamma},\theta)\, dt = 2\theta_f \cos\gamma_f. \tag{2.49b}$$

The problem can be formulated by the Euler-Lagrange equations

$$\operatorname{grad}\mathcal{E}(\gamma,\theta) + \sum_j \lambda_j \operatorname{grad}\psi_j(\gamma,\theta) = 0 \tag{2.50}$$

with λ_j, $j = 0, 1, 2$, the Lagrangian multipliers associated to the constraints, where the gradient is defined as

$$\operatorname{grad}\mathcal{E}(\gamma,\theta) = \begin{bmatrix} \frac{\partial\mathcal{L}_0}{\partial\gamma} - \frac{d}{dt}\left(\frac{\partial\mathcal{L}_0}{\partial\dot{\gamma}}\right) \\ \frac{\partial\mathcal{L}_0}{\partial\theta} - \frac{d}{dt}\left(\frac{\partial\mathcal{L}_0}{\partial\dot{\theta}}\right) \end{bmatrix}, \tag{2.51a}$$

$$\operatorname{grad}\psi_j(\gamma,\theta) = \begin{bmatrix} \frac{\partial\varphi_j}{\partial\gamma} - \frac{d}{dt}\left(\frac{\partial\varphi_j}{\partial\dot{\gamma}}\right) \\ \frac{\partial\varphi_j}{\partial\theta} - \frac{d}{dt}\left(\frac{\partial\varphi_j}{\partial\dot{\theta}}\right) \end{bmatrix}, \tag{2.51b}$$

with the Lagrangian $\mathcal{L}_0$ defined from the energy as the cost:

$$\mathcal{E}(\gamma,\theta) = \int_{t_i}^{t_f} (\dot{\theta}^2 + \dot{\gamma}^2\sin^2\theta)\, dt \equiv \int_{t_i}^{t_f} \mathcal{L}_0(\dot{\gamma},\theta,\dot{\theta})\, dt. \tag{2.52}$$

This gives

$$\frac{\partial \mathcal{L}_0}{\partial \gamma} - \frac{d}{dt}\Big(\frac{\partial \mathcal{L}_0}{\partial \dot{\gamma}}\Big) + \lambda_0 \left[\frac{\partial \varphi_0}{\partial \gamma} - \frac{d}{dt}\Big(\frac{\partial \varphi_0}{\partial \dot{\gamma}}\Big)\right] + \lambda_1 \left[\frac{\partial \varphi_1}{\partial \gamma} - \frac{d}{dt}\Big(\frac{\partial \varphi_1}{\partial \dot{\gamma}}\Big)\right] + \lambda_2 \left[\frac{\partial \varphi_2}{\partial \gamma} - \frac{d}{dt}\Big(\frac{\partial \varphi_2}{\partial \dot{\gamma}}\Big)\right] = 0, \tag{2.53a}$$

$$\frac{\partial \mathcal{L}_0}{\partial \theta} - \frac{d}{dt}\Big(\frac{\partial \mathcal{L}_0}{\partial \dot{\theta}}\Big) + \lambda_0 \left[\frac{\partial \varphi_0}{\partial \theta} - \frac{d}{dt}\Big(\frac{\partial \varphi_0}{\partial \dot{\theta}}\Big)\right] + \lambda_1 \left[\frac{\partial \varphi_1}{\partial \theta} - \frac{d}{dt}\Big(\frac{\partial \varphi_1}{\partial \dot{\theta}}\Big)\right] + \lambda_2 \left[\frac{\partial \varphi_2}{\partial \theta} - \frac{d}{dt}\Big(\frac{\partial \varphi_2}{\partial \dot{\theta}}\Big)\right] = 0, \tag{2.53b}$$

i.e.,

$$\ddot{\gamma} + 2\dot{\gamma}\dot{\theta}\cot\theta + \lambda_0\dot{\theta}\cot\theta - 2\dot{\theta}(\lambda_1\cos\gamma + \lambda_2\sin\gamma) = 0, \tag{2.54a}$$

$$\ddot{\theta} - \dot{\gamma}^2\sin\theta\cos\theta - \lambda_0\dot{\gamma}\sin\theta\cos\theta + 2\dot{\gamma}\sin^2\theta(\lambda_1\cos\gamma + \lambda_2\sin\gamma) = 0. \tag{2.54b}$$

We notice that the λ_j's are different from the ones obtained in (2.104) and (2.32) since we have taken the constraints (2.49) written differently from (1.111b).

In order to determine a constant of motion, Eqs. (2.54) are rewritten as

$$\ddot{\gamma}\dot{\gamma}\sin^2\theta + 2\dot{\gamma}^2\dot{\theta}\cos\theta\sin\theta + \dot{\theta}\dot{\gamma}\sin\theta[\lambda_0\cos\theta - 2\sin\theta(\lambda_1\cos\gamma + \lambda_2\sin\gamma)] = 0, \tag{2.55a}$$

$$\ddot{\theta}\dot{\theta} - \dot{\gamma}^2\dot{\theta}\sin\theta\cos\theta - \dot{\gamma}\dot{\theta}\sin\theta[\lambda_0\cos\theta - 2\sin\theta(\lambda_1\cos\gamma + \lambda_2\sin\gamma)] = 0, \tag{2.55b}$$

which give after substitution of the terms containing the Lagrangian multipliers:

$$\ddot{\gamma}\dot{\gamma}\sin^2\theta + \ddot{\theta}\dot{\theta} + \dot{\gamma}^2\dot{\theta}\cos\theta\sin\theta = 0, \tag{2.56}$$

i.e.,

$$0 = \frac{d}{dt}(\dot{\theta}^2 + \dot{\gamma}^2\sin^2\theta). \tag{2.57}$$

The corresponds to a constant of motion corresponding to a constant pulse $\Omega \equiv \Omega_0 = const$:

$$\dot{\theta}^2 + \dot{\gamma}^2\sin^2\theta = \Omega_0^2. \tag{2.58}$$

To determine additional conditions, we make an analysis of the initial condition

on (2.58) considering the limit $\theta \to \theta_i = 0$:

$$\dot{\theta}_i^2 + \dot{\gamma}_i^2 \theta_i^2 = \Omega_0^2. \tag{2.59}$$

If we assume that $|\dot{\gamma}_i| < \infty$, we conclude:

$$|\dot{\theta}_i| = |\Omega_0|. \tag{2.60}$$

The analysis is made on (2.54a) by multiplying it by $\sin\theta$ (and assuming the above condition meaning that $|\dot{\theta}_i| < \infty$):

$$\ddot{\gamma}_i \theta_i + (2\dot{\gamma}_i + \lambda_0)\dot{\theta}_i = 0. \tag{2.61}$$

If we additionally assume that $|\ddot{\gamma}_i| < \infty$, we conclude

$$\dot{\gamma}_i = -\lambda_0/2. \tag{2.62}$$

We do not fix $\gamma_0 = \gamma_f$, neither $\varphi_0 = \varphi_f$. The latter is given by (1.68c):

$$\cos\varphi_f = \dot{\gamma}_f/\Omega_0, \quad \sin\varphi_f = \dot{\theta}_f/\Omega_0. \tag{2.63}$$

The problem is numerically solved with the initial condition $\gamma_i = \pi/2$, $\theta_i = 0$, and $\dot{\gamma}_i = -\lambda_0/2$, $|\dot{\theta}_i| = |\Omega_0|$, such that $\theta_f = \theta_0$ (and both γ_f and φ_f are undefined).

Appendix 2.F shows that optimizing with respect to the pulse area, to the energy, or to the duration leads to the same trajectory, as in the problem of population transfer.

2.3.2 Analytic expression of the detuning for time-optimization

Using (2.54a) in (2.31), the detuning reads

$$\Delta = \lambda_0 \cos\theta - 2\sin\theta(\lambda_1 \cos\gamma + \lambda_2 \sin\gamma). \tag{2.64}$$

This gives in particular at initial and final times

$$\Delta_i = \lambda_0, \tag{2.65a}$$

$$\Delta_f = \lambda_0 \cos\theta_f - 2\sin\theta_f(\lambda_1 \cos\gamma_f + \lambda_2 \sin\gamma_f), \tag{2.65b}$$

respectively.

We show in Appendix (2.G) that the detuning has still the form of the elliptic cosine :

$$\Delta = \Delta_0 \,\mathrm{cn}\,(\omega t + \nu_i, m)\,, \quad t \in [0, T_{\min}], \tag{2.66}$$

but with a modified initial phase ν_i comparing to the case of population transfer:

$$\Delta_0 = -2\,\mathrm{sgn}\,\lambda_1\,\omega\sqrt{m}, \tag{2.67a}$$

$$\lambda_0 = \Delta_0\,\mathrm{cn}\,(\nu_i, m)\,, \tag{2.67b}$$

$$\lambda_1\Omega_0 = -\Delta_0\omega\,\mathrm{sn}\,(\nu_i, m)\,\sqrt{1 - m\,\mathrm{sn}^2\,(\nu_i, m)}, \tag{2.67c}$$

$$\lambda_1\Theta_{0x,f} - \lambda_2\Theta_{0y,f} - \lambda_0\dot{\theta}_f\sin\theta_f = -\Delta_0\omega\,\mathrm{sn}\,(\omega T_{\min} + \nu_i, m) \times \sqrt{1 - m\,\mathrm{sn}^2\,(\omega T_{\min} + \nu_i, m)}, \tag{2.67d}$$

and $\lambda_1 = -2\lambda_2^G$, $\lambda_2 = 2\lambda_1^G$, where we have denoted λ_j^G found for the present gate problem (2.54), (2.64).

We find the parameters ω and m as solutions of the system (2.67c–2.67d) after substituting Δ_0 from (2.67a) and ν_i from (2.67b).

2.3.3 NOT gate

We consider the NOT-type gate:

$$U_{\mathrm{NOT}}(\kappa) = \begin{bmatrix} 0 & -e^{i\kappa} \\ e^{-i\kappa} & 0 \end{bmatrix}, \tag{2.68}$$

corresponding to $|\phi(t_i)\rangle = |0\rangle, |\phi(t_f)\rangle = |\phi_T\rangle \equiv e^{-i\kappa}|1\rangle$, where the phase

$$\kappa = (\varphi_f + \gamma_f)/2 \tag{2.69}$$

is also robust (but not fixed *a priori*).

This control implies, as in the case of population transfer, the boundaries $\theta_i = 0$, $\theta_f = \pi$, $\gamma_i = \varphi_i = \varphi_f = \pi/2$, giving $\kappa = \pi/4 + \gamma_f/2$.

Symmetric trajectory

We consider the symmetric situation :

$$\theta_m = \pi/2, \quad \gamma_f = \gamma_i = \pi/2, \quad \widetilde{\theta}_-(\gamma) = 2\theta_m - \widetilde{\theta}_+(\gamma) \tag{2.70}$$

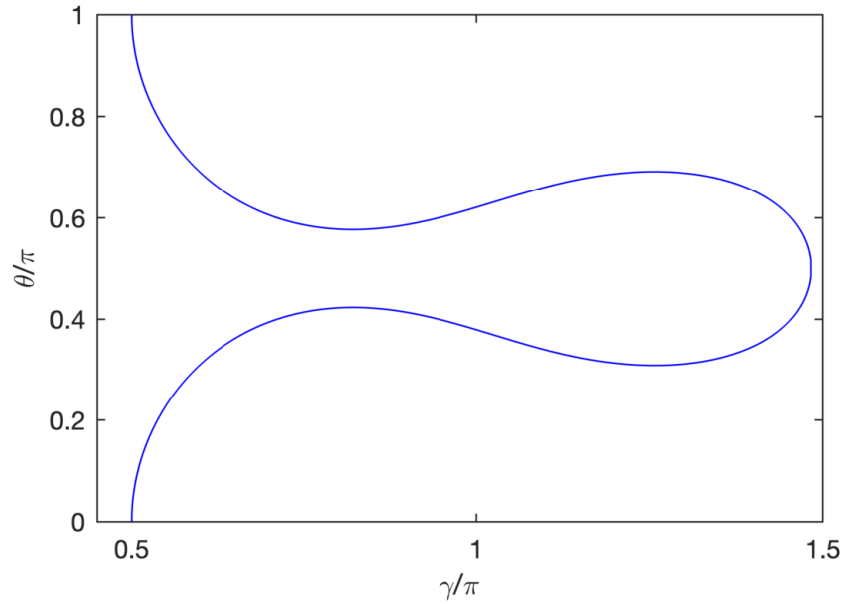

Figure 2.10: Optimal robust geodesic $\widetilde{\theta}(\gamma)$ corresponding to the NOT gate.

giving $\kappa = \pi/2$, $\theta_f = 2\theta_m$, for which the integrals (1.113) to be nullified become [with the use of (1.116)]:

$$0 = \int_{t_i}^{t_f} e(t)\,dt = \int_{\pi/2}^{\gamma_m} \sin^2\widetilde{\theta}_+\,d\gamma - \int_{\pi/2}^{\gamma_m} \sin^2\widetilde{\theta}_+\,d\gamma, \tag{2.71a}$$

$$0 = \int_{t_i}^{t_f} f(t)\,dt = \int_{\pi/2}^{\gamma_m} \cos\gamma(\sin 2\widetilde{\theta}_+ - 2\widetilde{\theta}_+)\,d\gamma + \pi\sin\gamma_m + i\int_{\pi/2}^{\gamma_m} \sin\gamma(\sin 2\widetilde{\theta}_+ - 2\widetilde{\theta}_+)\,d\gamma - i\pi\cos\gamma_m. \tag{2.71b}$$

We see that the nullification of the integral (2.71a) is automatically satisfied, which allows one to avoid considering the additional Lagrange multiplier λ_0. The nullification of the integral (2.71b) with $\widetilde{\theta}_+(\gamma_m) = \pi/2$ leads to Eqs. (2.20) for the half transfer ($\theta_f = \pi/2$) where γ_f is replaced by γ_m. This means that the optimal robust NOT gate is achieved when two consecutive optimal robust half transfers are achieved [37], i.e., $T_{\min} = 8.1/\Omega_0$ giving the pulse area $\mathcal{A}^{\text{opt}}_{\text{NOT}} = \Omega_0 T_{\min} = 2.58\pi$.

The resulting trajectory is shown in Fig. 2.10. This leads to the standard NOT gate, U_{NOT}, up to a global phase

$$U_{\text{NOT}}(\pi/2) = -i\begin{bmatrix} 0 & 1 \\ 1 & 0 \end{bmatrix} \equiv -iU_{\text{NOT}}. \tag{2.72}$$

General formulation for optimization with respect to energy and time.

For the final condition on (2.58) considering the limit $\theta \to \theta_f = \pi$, assuming $|\dot{\gamma}_f| < \infty$, and for (2.54a), assuming $|\dot{\gamma}_f| < \infty$, we have the following symmetric boundaries:

$$|\dot{\theta}_f| = |\Omega_0| = |\dot{\theta}_i|, \quad \dot{\gamma}_f = -\lambda_0/2 = \dot{\gamma}_i. \tag{2.73}$$

We have checked numerically that the optimum is obtained for $\lambda_0 = 0$, validating the above analysis with the symmetric trajectory.

Figure 2.11 shows the robustness profile for the NOT gate. It is compared to the SCROFULOUS composite pulse technique [14] of 3π area (see Appendix 2.E), approximately 20% longer than the RIO NOT gate.

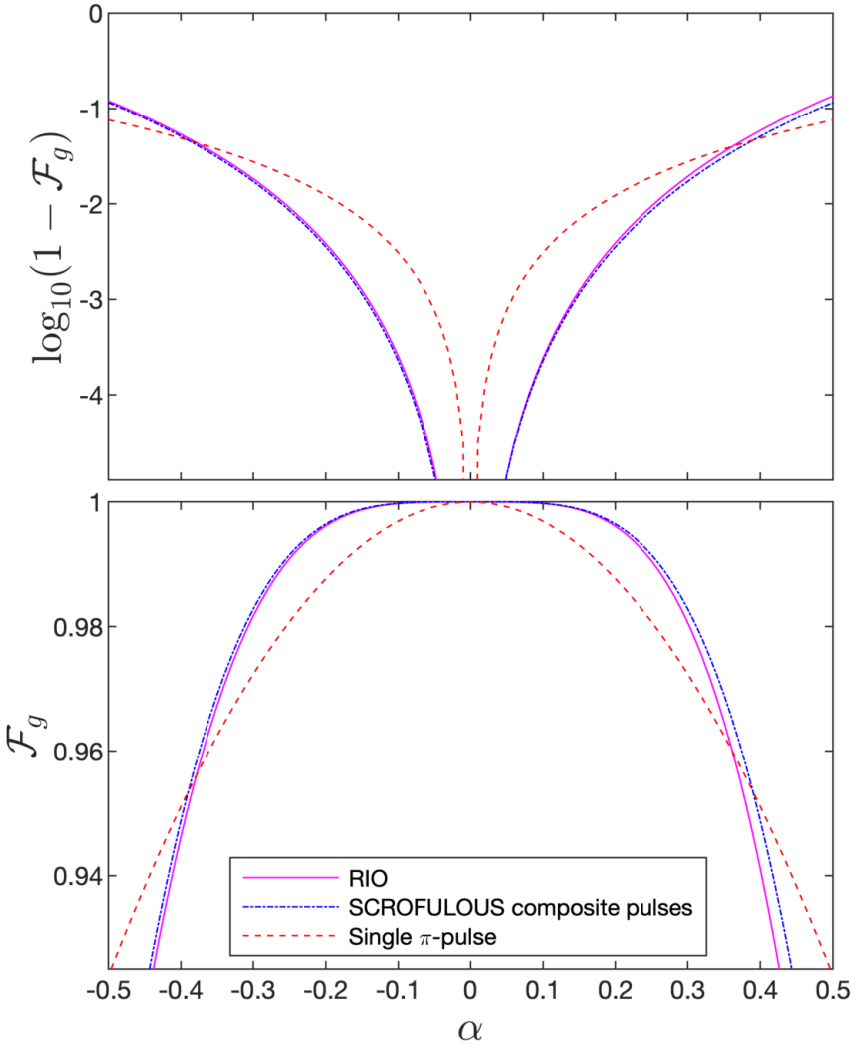

Figure 2.11: Same as Fig. 2.8, but for the NOT gate

2.3.4 Hadamard-type gate

Robust quantum gate of Hadamard-type is defined as

$$U_{\text{H}}(\varphi_0,\gamma_0)=\frac{1}{\sqrt{2}}\begin{bmatrix} e^{\frac{i}{2}(\varphi_0-\gamma_0)} & -e^{\frac{i}{2}(\varphi_0+\gamma_0)} \\ e^{-\frac{i}{2}(\varphi_0+\gamma_0)} & e^{-\frac{i}{2}(\varphi_0-\gamma_0)} \end{bmatrix}. \tag{2.74}$$

We can consider without loss of generality the construction of a robust process driving the ground state $|0\rangle$ to the state (2.42) with $\theta_0=\pi/2$.

We consider optimization with respect to energy and time. The boundaries read:

$$\theta_i=0,\quad \theta_f=\pi/2,\quad \gamma_i=\varphi_i=\pi/2,\quad \gamma_f=\gamma_0,\quad \varphi_f=\varphi_0, \tag{2.75}$$

and

$$|\dot{\theta}_i|=|\Omega_0|,\quad \dot{\gamma}_i=-\lambda_0/2. \tag{2.76}$$

We do not fix $\gamma_0=\gamma_f$, neither $\varphi_0=\varphi_f$.

We determine numerically from the system of differential equations (2.54): $\lambda_0\approx 1.50581/\Omega_0$, $\lambda_1\approx 0.04270/\Omega_0$, $\lambda_2\approx 1.19287/\Omega_0$, $\gamma_0=\varphi_0\approx 0.77135\pi$, and the optimal time $T_{\min}\approx 5.76955/\Omega_0$, i.e., the pulse area $T_{\min}\Omega_0\approx 1.8365\pi$. We obtain from (2.67) $m\approx 0.5091$, $\omega\approx 9.3406/T_{\min}$, $\nu_i\approx 0.9154$, $\Delta_0=2\omega\sqrt{m}\approx 2.3103\Omega_0$.

The trajectory and the dynamics are shown in Fig. 2.12.

Figure 2.13 shows the robustness profile for the Hadamard gate. It is compared to the optimal SCROFULOUS composite pulse technique [14, 17] of 2.28π area, more than 20% longer than the RIO Hadamard gate.

Considering an additional static phase η_0 of the control, we obtain the following gate (since $\gamma_0=\varphi_0$):

$$\begin{aligned} U_{\text{H}}(\varphi_0,\gamma_0=\varphi_0,\eta_0) &\equiv T(\eta_0)U_{\text{H}}(\varphi_0,\gamma_0=\varphi_0)T^{\dagger}(\eta_0) \\ &= \frac{1}{\sqrt{2}}\begin{bmatrix} 1 & -e^{i(\varphi_0-\eta_0)} \\ e^{-i(\varphi_0-\eta_0)} & 1 \end{bmatrix}, \end{aligned} \tag{2.77}$$

which leads to the pseudo-Hadamard gate

$$\widetilde{U}_{\text{pH}}\equiv\widetilde{U}_{\text{H}}(\varphi_0,\varphi_0,\varphi_0)=\frac{1}{\sqrt{2}}\begin{bmatrix} 1 & -1 \\ 1 & 1 \end{bmatrix}, \tag{2.78}$$

when $\eta_0=\varphi_0$.

The standard Hadamard gate $\widetilde{U}_{\text{H}}$ can be obtained (up to a global phase) by

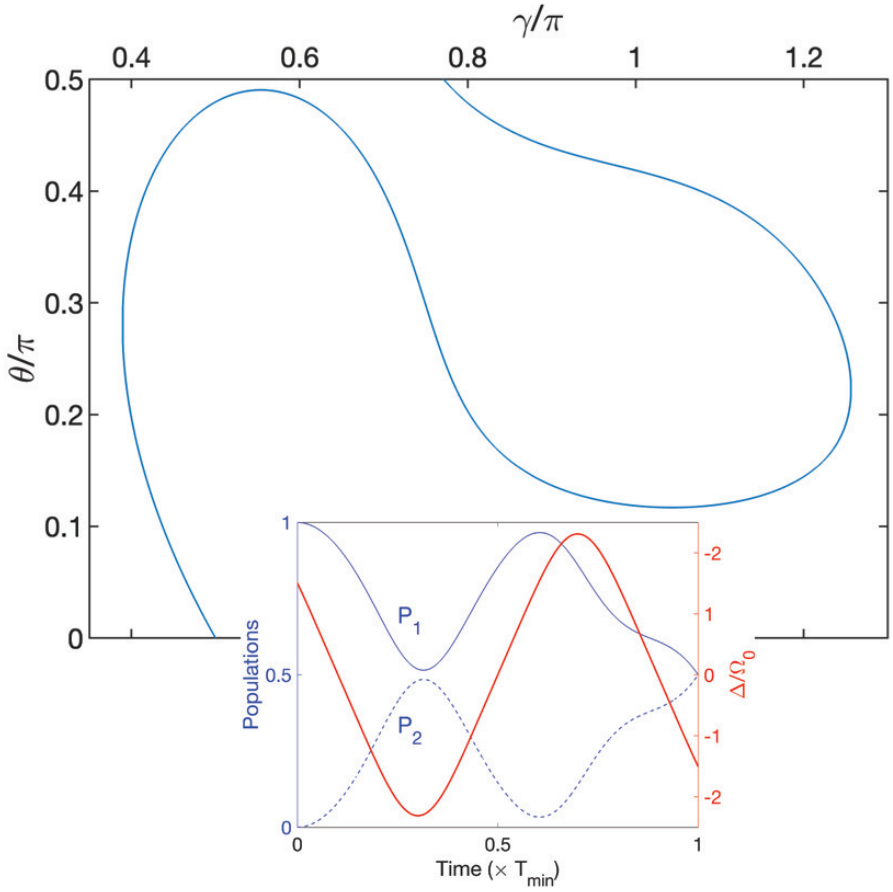

Figure 2.12: Same as Fig. 2.5 for the Hadamard gate from the ground state.

applying a preliminary phase gate of phase π, Φ_π, according to (2.41):

$$\widetilde{U}_{\text{H}} = \widetilde{U}_{\text{pH}}\Phi_\pi = \frac{-i}{\sqrt{2}}\begin{bmatrix} 1 & 1 \\ 1 & -1 \end{bmatrix}. \tag{2.79}$$

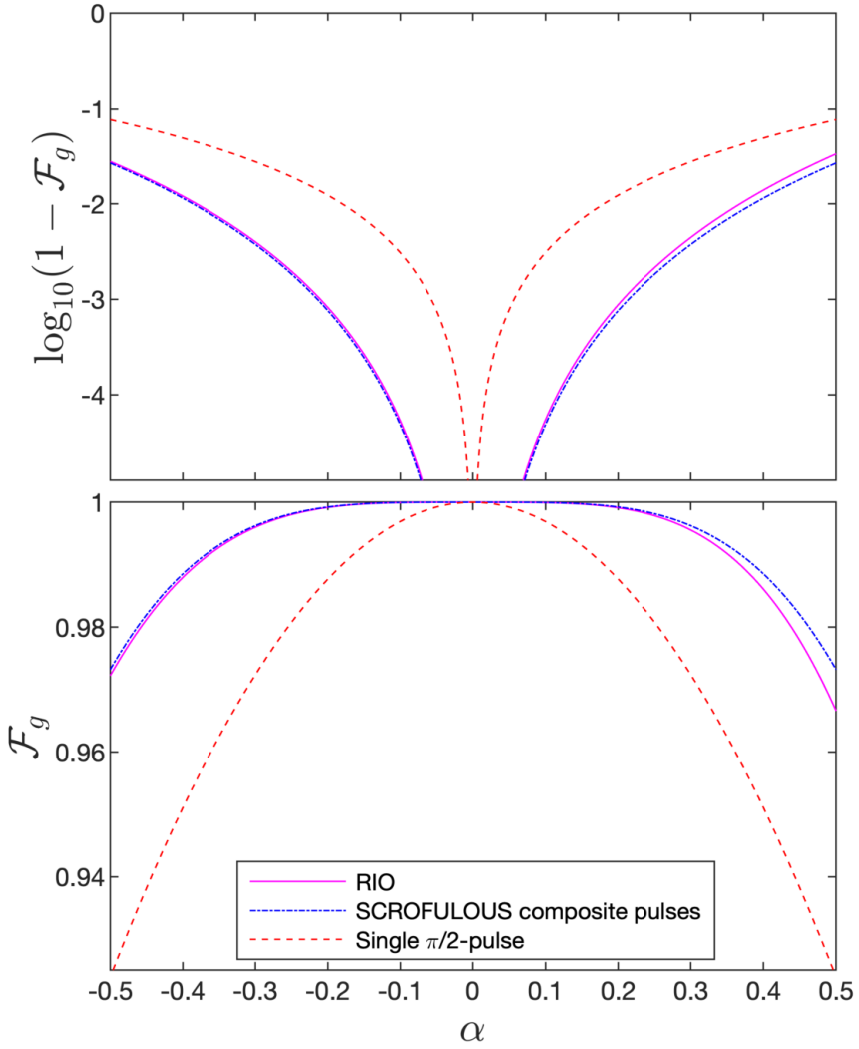

Figure 2.13: Same as Fig. 2.8, but for the Hadamard gate

2.3.5 Phase gate

The phase gate of phase κ (2.40) can be generated (up to a global phase) by applying two successive optimal robust NOT gates, where the second NOT gate is produced by a control of (static) phase $\kappa/2$ [see Eq. (2.39)]:

$$\widetilde{U}_{\text{NOT}}\left(\frac{\pi}{2},\frac{\kappa}{2}\right)U_{\text{NOT}}\left(\frac{\pi}{2}\right)=-\Phi_{\kappa}. \tag{2.80}$$

2.4 Smooth quasi-square pulses

In this section, we analyze a way to smooth the constant (square) pulse amplitude determined by (time) optimization. We use the flexibility of the RIO method in terms of the solutions dynamics. The optimal robust trajectory in Fig. 2.1, leading to

a complete population transfer, offers infinitely many optimal solutions (robust with respect to the pulse area) depending on the time parametrization of $\gamma(t)$. In order to approach the ideal time-optimal robust dynamics, we impose a parametrization given by a smooth quasi-square pulse of same peak amplitude and same area as that of the square pulse. This is modeled by a hyper-Gaussian pulse of high-order even n and width σ:

$$\Omega(t) = \Omega_0 \exp[-(t/\sigma)^n], \tag{2.81}$$

such that $\int_{t_i}^{t_f} \Omega(t)\, dt = 2\Omega_0 \sigma \Gamma(1/n)/n = \Omega_0 T_{\min}$, i.e.,

$$\sigma = \frac{nT_{\min}}{2\Gamma(1/n)}. \tag{2.82}$$

The parametrization of $\gamma(t)$ is more precisely determined from the identity of the partial pulse areas:

$$\Omega_0 \int_{t_i}^{t} \exp[-(t/\sigma)^n]\, dt = \int_{\gamma_i}^{\gamma(t)} \sqrt{\left(\dot{\widetilde{\theta}}\right)^2 + \sin^2\theta}\, d\gamma. \tag{2.83}$$

Figure 2.14 presents the dynamics driven by RIO with a hyper-Gaussian pulse (of high order $n = 14$ and $\sigma \approx 1.095T$, i.e., $\Omega_0 \approx 2.77/T$) replacing the ideal optimal square pulse (of same area 5.84). We may refer to this, in short, as hyper-Gaussian RIO (hG-RIO). As expected the corresponding detunings are very similar. The detuning associated to the hyper-Gaussian pulse also appears smooth (i.e., regularized at the beginning and at the end of the process).

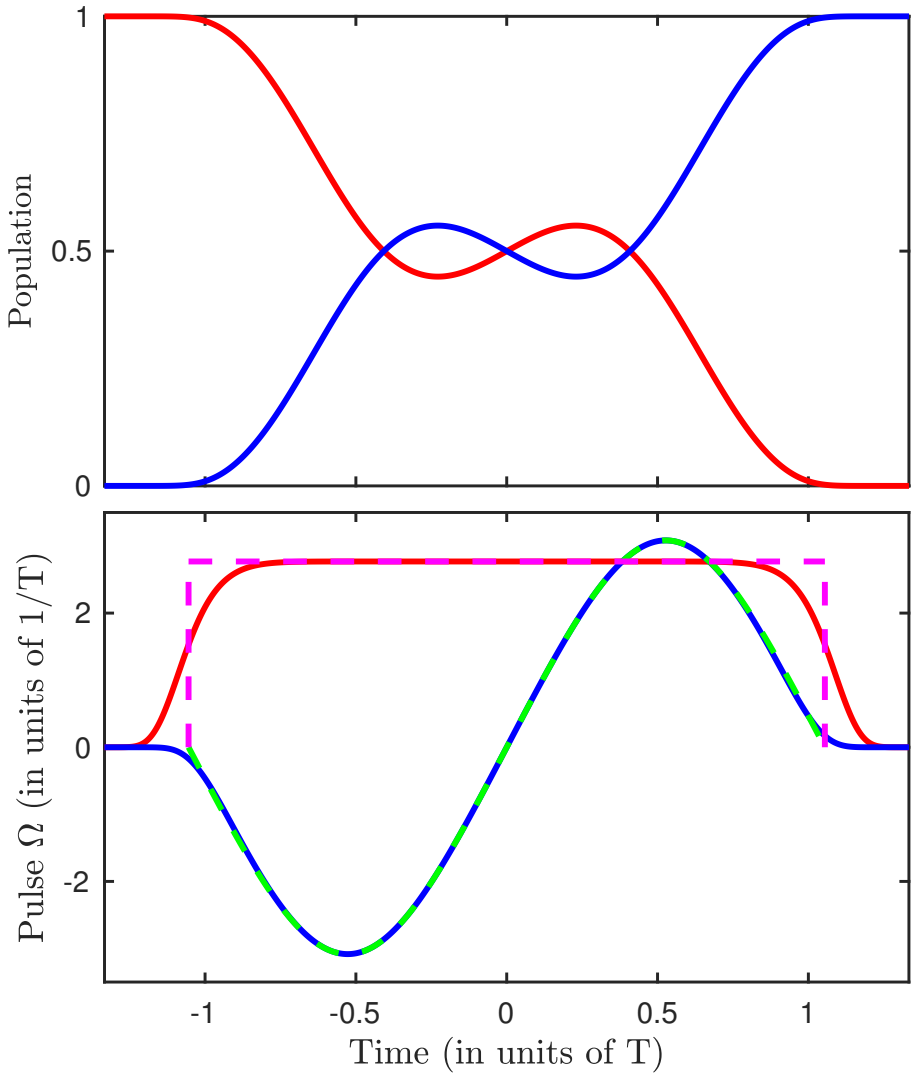

Figure 2.14: Lower frame: Quasi-square hyper-Gaussian pulse (solid lines) and time-optimal ideal square pulse (dashed line) and the corresponding oscillating detunings (almost undistinguishable at the scale of the figure, except at the beginning and at the end). Upper frame: resulting hG-RIO population dynamics showing the full transfer.

2.5 Conclusions

The basis of robust inverse optimization to produce optimal robust complete population transfer, half transfer, and NOT gate has been presented in Ref. [37]. We have completed and extended the work by proposing robust optimal schemes to produce arbitrary population transfers, Hadamard gates, and phase gates. A remarkable result is the analytical solution we have found for all the operations described. The proof uses Ref. [35] as starting point that we could determine the form of all such solutions (as they all obey the same differential equations and differ only in boundary conditions), and generalize them by turning some constants into tunable parame-

ters. Knowing the basic form, we could find the corresponding Lagrange multipliers for each problem and fit the solution to the analytical form.

The generalization of [35] lacks rigorous mathematical proof, but it is supported by numerical evidence.

It should be highlighted that these optimal and robust detuning shapes corresponding to flat Rabi frequencies can be use to determine solutions for any pulse shape: (i) Using a certain detuning and field amplitude (in units of pulse duration), that are area-optimal and robust, we can obtain the corresponding geometric trajectory $\widetilde{\theta}(\gamma)$; (ii) as this trajectory does not depend on the temporal dynamics, we can use the corresponding optimal pulse area and design any pulse shape that satisfies it; (iii) finally, we can recalculate the temporal shape of the detuning that will display the optimal area for the operation, will be robust with respect to pulse inhomogeneities, and will use the desired pulse amplitude shape; obviously, the temporal duration will not be optimal (the interaction will last longer than with a constant control).

Appendices

2.A Determination of the optimal robust trajectory $\widetilde{\gamma}(\theta)$ for a monotonic $\theta(t)$

2.A.1 General case

The problem can be formulated as an optimization problem under constraint : finding the trajectory $\widetilde{\gamma}(\theta)$ that minimizes the pulse area (1.76)

$$\mathcal{A}(\widetilde{\gamma}) = \int_0^\pi \sqrt{1 + \left(\dot{\widetilde{\gamma}}\right)^2 \sin^2\theta}\, d\theta \equiv \int_0^\pi \mathcal{L}_0(\dot{\widetilde{\gamma}}, \theta)\, d\theta \tag{2.84}$$

with $\dot{\widetilde{\gamma}} \equiv \frac{d\widetilde{\gamma}}{d\theta}$, under the two constraints (2.19) rewritten as

$$\psi_1(\widetilde{\gamma}) = \int_0^\pi \cos\widetilde{\gamma} \sin^2\theta\, d\theta \equiv \int_0^\pi \varphi_1(\widetilde{\gamma}, \theta)\, d\theta = 0, \tag{2.85a}$$

$$\psi_2(\widetilde{\gamma}) = \int_0^\pi \sin\widetilde{\gamma} \sin^2\theta\, d\theta \equiv \int_0^\pi \varphi_2(\widetilde{\gamma}, \theta)\, d\theta = 0. \tag{2.85b}$$

Since the final phase is irrelevant for the population transfer problem, the final value $\gamma_f \equiv \widetilde{\gamma}(\theta_f)$ is not fixed. The problem can be solved by the Lagrange multiplier method extended to the function space as follows: The trajectory $\widetilde{\gamma}$ is solution of

$$\operatorname{grad}\mathcal{A}(\widetilde{\gamma}) + \widetilde{\lambda}_1 \operatorname{grad}\psi_1(\widetilde{\gamma}) + \widetilde{\lambda}_2 \operatorname{grad}\psi_2(\widetilde{\gamma}) = 0, \tag{2.86}$$

with $\widetilde{\lambda}_j$, $j = 1, 2$, the Lagrangian multipliers associated to the constraints, where the gradient is defined according to the Euler-Lagrange equation (which is zero without constraint):

$$\operatorname{grad}\mathcal{A}(\widetilde{\gamma}) = \frac{\partial\mathcal{L}_0}{\partial\widetilde{\gamma}} - \frac{d}{d\theta}\left(\frac{\partial\mathcal{L}_0}{\partial\dot{\widetilde{\gamma}}}\right). \tag{2.87}$$

This definition also applies for the constraints, $j = 1, 2$

$$\operatorname{grad}\psi_j(\widetilde{\gamma}) = \frac{\partial\varphi_j}{\partial\widetilde{\gamma}} - \frac{d}{d\theta}\left(\frac{\partial\varphi_j}{\partial\dot{\widetilde{\gamma}}}\right). \tag{2.88}$$

We obtain the differential equation:

$$0 = \ddot{\widetilde{\gamma}} + 2\dot{\widetilde{\gamma}}\cot\theta + (\dot{\widetilde{\gamma}})^3 \cos\theta \sin\theta + (\widetilde{\lambda}_1 \sin\widetilde{\gamma} - \widetilde{\lambda}_2 \cos\widetilde{\gamma})[1 + (\dot{\widetilde{\gamma}})^2 \sin^2\theta]^{3/2}. \tag{2.89}$$

2.A.2 Connection to the trajectory $\widetilde{\theta}(\gamma)$

We notice that one can recover the differential equation (2.26), derived for the trajectory $\widetilde{\theta}(\gamma)$, from (2.89) by inverting the derivatives:

$$\dot{\widetilde{\gamma}} = \frac{d\widetilde{\gamma}}{d\theta} = 1/\left(\frac{d\widetilde{\theta}}{d\gamma}\right) = 1/\dot{\widetilde{\theta}} \tag{2.90a}$$

$$\frac{d}{d\theta}\left(\dot{\widetilde{\gamma}}\dot{\widetilde{\theta}}\right) = 0 = \ddot{\widetilde{\gamma}}\dot{\widetilde{\theta}} + \dot{\widetilde{\gamma}}\frac{d}{d\gamma}\left(\dot{\widetilde{\theta}}\right)\frac{d\widetilde{\gamma}}{d\theta} = \ddot{\widetilde{\gamma}}\dot{\widetilde{\theta}} + \left(\dot{\widetilde{\gamma}}\right)^2\ddot{\widetilde{\theta}}, \tag{2.90b}$$

i.e.,

$$\ddot{\widetilde{\gamma}} = -\ddot{\widetilde{\theta}}/\left(\dot{\widetilde{\theta}}\right)^3. \tag{2.91}$$

We indeed obtain from (2.89):

$$\frac{\ddot{\widetilde{\theta}}}{\left(\dot{\widetilde{\theta}}\right)^3} = \frac{2}{\dot{\widetilde{\theta}}}\cot\widetilde{\theta} + \frac{1}{\left(\dot{\widetilde{\theta}}\right)^3}\cos\widetilde{\theta}\sin\widetilde{\theta} + (\widetilde{\lambda}_1\sin\gamma - \widetilde{\lambda}_2\cos\gamma)\left[1 + \frac{\sin^2\widetilde{\theta}}{\left(\dot{\widetilde{\theta}}\right)^2}\right]^{3/2}. \tag{2.92}$$

which is (2.26) for $\theta \neq 0$.

2.A.3 Treatment of the initial singularity

In order to lift the initial singularity of $\dot{\widetilde{\gamma}}\cot\theta$, we multiplying this equation by $\sin\theta$:

$$0 = \ddot{\widetilde{\gamma}}\sin\theta + 2\dot{\widetilde{\gamma}}\cos\theta + (\dot{\widetilde{\gamma}})^3\cos\theta\sin^2\theta + \sin\theta\frac{\widetilde{\lambda}_1\sin\widetilde{\gamma} - \widetilde{\lambda}_2\cos\widetilde{\gamma}}{[1 + (\dot{\widetilde{\gamma}})^2\sin^2\theta]^{-3/2}}. \tag{2.93}$$

Setting the limit $\theta \to 0$ (initial time) and assuming that $\ddot{\widetilde{\gamma}}(0)$ is finite such that $\ddot{\widetilde{\gamma}}\sin\theta = 0$ for $\theta = 0$, leads to $\dot{\widetilde{\gamma}}_i = 0$.

2.A.4 Particular case of complete population transfer: Symmetric trajectory

We consider the situation of complete population transfer $\theta_f = \pi$. It is useful to consider the backward equation: $\widehat{\gamma}(u) = \widetilde{\gamma}(\theta)$ with $u = \theta_f - \theta$, i.e., satisfying $\widehat{\gamma}(0) = \widetilde{\gamma}(\theta_f)$ and $\widehat{\gamma}(\theta_f) = \widetilde{\gamma}(0)$. This gives $\dot{\widehat{\gamma}} = -\dot{\widetilde{\gamma}}$, $\ddot{\widehat{\gamma}} = \ddot{\widetilde{\gamma}}$, and

$$\begin{aligned} 0 = {} & \ddot{\widehat{\gamma}} - 2\dot{\widehat{\gamma}}\cot(\theta_f - u) - (\dot{\widehat{\gamma}})^3\cos(\theta_f - u)\sin(\theta_f - u) \\ & + (\widetilde{\lambda}_1\sin\widehat{\gamma} - \widetilde{\lambda}_2\cos\widehat{\gamma})[1 + (\dot{\widehat{\gamma}})^2\sin^2(\theta_f - u)]^{3/2}. \end{aligned} \tag{2.94}$$

For the complete population transfer case, the above differential equation becomes

$$0 = \ddot{\widehat{\gamma}} + 2\dot{\widehat{\gamma}} \cot u + (\dot{\widehat{\gamma}})^3 \cos u \sin u + (\widetilde{\lambda}_1 \sin \widehat{\gamma} - \widetilde{\lambda}_2 \cos \widehat{\gamma})[1 + (\dot{\widehat{\gamma}})^2 \sin^2 u]^{3/2}, \quad (2.95)$$

which is of the same form as the original one (2.89): this shows the central symmetry of the trajectory around $\theta = \pi/2$ for the problem of complete population transfer, since $\dot{\widehat{\gamma}} = -\dot{\widetilde{\gamma}}$. By symmetry, we have thus

$$\dot{\widetilde{\gamma}}(0) = \dot{\widetilde{\gamma}}(\pi), \quad \ddot{\widetilde{\gamma}}(0) = -\ddot{\widetilde{\gamma}}(\pi), \quad \widetilde{\gamma}(\pi/2) = \frac{1}{2}[\widetilde{\gamma}(\pi) + \widetilde{\gamma}(0)]. \quad (2.96)$$

The symmetry implies that we can identify the differential equations at early and late times, i.e., in the limit $\theta \to 0$ and $u = \pi - \theta \to \pi$:

$$\begin{aligned} 0 &= \ddot{\widetilde{\gamma}}(\theta) + 2\dot{\widetilde{\gamma}}(\theta) \cot \theta + (\widetilde{\lambda}_1 \sin \widetilde{\gamma}_i - \widetilde{\lambda}_2 \cos \widetilde{\gamma}_i) \\ &= \ddot{\widetilde{\gamma}}(u) + 2\dot{\widetilde{\gamma}}(u) \cot u + (\widetilde{\lambda}_1 \sin \widetilde{\gamma}_f - \widetilde{\lambda}_2 \cos \widetilde{\gamma}_f) \\ &= -\ddot{\widetilde{\gamma}}_i - 2\dot{\widetilde{\gamma}}_i \cot \theta_i + (\widetilde{\lambda}_1 \sin \widetilde{\gamma}_f - \widetilde{\lambda}_2 \cos \widetilde{\gamma}_f), \end{aligned} \quad (2.97)$$

which using $\widetilde{\gamma}_i = \pi/2$, leads to

$$\widetilde{\lambda}_1 = \widetilde{\lambda}_2 \cos \widetilde{\gamma}_f - \widetilde{\lambda}_1 \sin \widetilde{\gamma}_f. \quad (2.98)$$

We remark that this symmetry is not preserved for a partial (incomplete) transfer.

2.B Invariance of the optimal trajectory with the different costs for population transfer

In this section we show that optimizing with respect to the pulse area, to the energy, or to the duration leads to the same trajectory.

We first assume we have determined the optimal trajectory $\widetilde{\gamma}(\theta)$ (possibly piecewise defined), solution of Eq. (2.89), that minimizes the pulse area (1.76) under the robustness constraints (1.111b). We now consider the energy minimization:

$$\mathcal{E}(\gamma, \theta) = \int_{t_i}^{t_f} (\dot{\theta}^2 + \dot{\gamma}^2 \sin^2 \theta)\, dt \equiv \int_{t_i}^{t_f} \mathcal{L}_0(\dot{\gamma}, \theta, \dot{\theta})\, dt, \quad (2.99)$$

and the constraints (1.111b) rewritten in a time representation

$$\psi_1(\gamma,\theta) = \int_{t_i}^{t_t} \varphi_1\, dt = (\cos\gamma_i \sin 2\theta_i - \cos\gamma_f \sin 2\theta_f)/4 \tag{2.100a}$$

$$\psi_2(\gamma,\theta) = \int_{t_i}^{t_t} \varphi_2\, dt = (\sin\gamma_i \sin 2\theta_i - \sin\gamma_f \sin 2\theta_f)/4 \tag{2.100b}$$

with

$$\varphi_1 = \dot{\theta}\cos\gamma\sin^2\theta, \quad \varphi_2 = \dot{\theta}\sin\gamma\sin^2\theta, \tag{2.101}$$

for consistency with the energy minimization representation.

The trajectory $[\gamma(t),\theta(t)]$ solution of the optimal problem can be formulated by the Euler-Lagrange equations:

$$\operatorname{grad}\mathcal{E}(\gamma,\theta) + \lambda_1 \operatorname{grad}\psi_1(\gamma,\theta) + \lambda_2 \operatorname{grad}\psi_2(\gamma,\theta) = 0 \tag{2.102}$$

with λ_j, $j = 1, 2$, the Lagrangian multipliers associated to the constraints, and the gradient

$$\operatorname{grad}\mathcal{E}(\gamma,\theta) = \begin{bmatrix} \frac{\partial\mathcal{L}_0}{\partial\gamma} - \frac{d}{dt}\left(\frac{\partial\mathcal{L}_0}{\partial\dot{\gamma}}\right) \\ \frac{\partial\mathcal{L}_0}{\partial\theta} - \frac{d}{dt}\left(\frac{\partial\mathcal{L}_0}{\partial\dot{\theta}}\right) \end{bmatrix}, \quad \operatorname{grad}\psi_j(\gamma,\theta) = \begin{bmatrix} \frac{\partial\varphi_j}{\partial\gamma} - \frac{d}{dt}\left(\frac{\partial\varphi_j}{\partial\dot{\gamma}}\right) \\ \frac{\partial\varphi_j}{\partial\theta} - \frac{d}{dt}\left(\frac{\partial\varphi_j}{\partial\dot{\theta}}\right) \end{bmatrix}. \tag{2.103}$$

Note that we have changed the notation of the Lagrangian multipliers (without tilde here) to distinguish them from the calculation with the trajectory $\widetilde{\gamma}(\theta)$ or $\widetilde{\theta}(\gamma)$.

The Euler-Lagrange equations lead to the differential equations

$$\begin{aligned} 0 &= \frac{\partial\mathcal{L}_0}{\partial\gamma} - \frac{d}{dt}\left(\frac{\partial\mathcal{L}_0}{\partial\dot{\gamma}}\right) + \sum_{i=1,2}\lambda_i\left[\frac{\partial\varphi_j}{\partial\gamma} - \frac{d}{dt}\left(\frac{\partial\varphi_j}{\partial\dot{\gamma}}\right)\right] \\ &= -2\sin^2\theta[\ddot{\gamma} + 2\dot{\gamma}\dot{\theta}\cot\theta + \dot{\theta}(\lambda_1\sin\gamma - \lambda_2\cos\gamma)/2] \end{aligned} \tag{2.104a}$$

and

$$\begin{aligned} 0 &= \frac{\partial\mathcal{L}_0}{\partial\theta} - \frac{d}{dt}\left(\frac{\partial\mathcal{L}_0}{\partial\dot{\theta}}\right) + \sum_{i=1,2}\lambda_i\left[\frac{\partial\varphi_j}{\partial\theta} - \frac{d}{dt}\left(\frac{\partial\varphi_j}{\partial\dot{\theta}}\right)\right] \\ &= \dot{\gamma}^2\sin 2\theta - 2\ddot{\theta} + \dot{\gamma}\sin^2\theta(\lambda_1\sin\gamma - \lambda_2\cos\gamma). \end{aligned} \tag{2.104b}$$

Equations (2.104a) and (2.104b) can be combined to substitute the term of the Lagrange multipliers:

$$0 = \ddot{\gamma}\dot{\gamma}\sin^2\theta + \dot{\gamma}^2\dot{\theta}\sin\theta\cos\theta + \ddot{\theta}\dot{\theta},$$

i.e.,

$$0 = \frac{d}{dt}(\dot{\theta}^2 + \dot{\gamma}^2 \sin^2\theta). \tag{2.105}$$

The solution gives a constant of motion corresponding to a constant pulse $\Omega \equiv \Omega_0 = const$:

$$\dot{\theta}^2 + \dot{\gamma}^2 \sin^2\theta = \Omega_0^2. \tag{2.106}$$

Using $\ddot{\gamma} = \dot{\theta}^2\ddot{\widetilde{\gamma}} + \ddot{\theta}\dot{\widetilde{\gamma}}$, (2.104a) reads

$$0 = 2(\ddot{\widetilde{\gamma}} + \ddot{\theta}\dot{\widetilde{\gamma}}/\dot{\theta}^2) + 4\dot{\widetilde{\gamma}}\cot\theta + \frac{1}{\dot{\theta}}(\lambda_1 \sin\gamma - \lambda_2 \cos\gamma), \tag{2.107}$$

which becomes, using (2.104b):

$$0 = \ddot{\widetilde{\gamma}} + 2\dot{\widetilde{\gamma}}\cot\theta + \left(\dot{\widetilde{\gamma}}\right)^3 \sin\theta\cos\theta + \frac{1}{2\dot{\theta}}(\lambda_1 \sin\gamma - \lambda_2 \cos\gamma)\left[1 + \left(\dot{\widetilde{\gamma}}\right)^2 \sin^2\theta\right]. \tag{2.108}$$

Using the constant of motion (2.105), rewritten as:

$$\dot{\theta} = \frac{\Omega_0}{\sqrt{1 + \left(\dot{\widetilde{\gamma}}\right)^2 \sin^2\theta}}, \tag{2.109}$$

Eq. (2.108) leads to (2.89) (with the Lagrangian multipliers renormalized by $2\Omega_0$, i.e., $\lambda_j = 2\Omega_0\widetilde{\lambda}_j$).

This means that the two initial equations (2.104) can be equivalently rewritten as (2.89) and (2.109); they produce a particular parametrization $\theta(t)$ [given by (2.109)] of the trajectory $\widetilde{\gamma}(\theta)$ obtained for the problem of minimization of the pulse area $\mathcal{A}$ [given by (2.89)]. The resulting trajectory $\theta(t), \widetilde{\gamma}(\theta(t))$ minimizes thus both the pulse area $\mathcal{A}$ and the energy $\mathcal{E}$.

Equation (2.109) can be rewritten as

$$\int_{\theta_i}^{\theta(t)} \sqrt{1 + \left(\dot{\widetilde{\gamma}}\right)^2 \sin^2\theta}\, d\theta = \Omega_0\,(t - t_i), \tag{2.110}$$

or equivalently for a trajectory $\widetilde{\theta}(\gamma)$

$$\int_{\gamma_i}^{\gamma(t)} \sqrt{\left(\dot{\widetilde{\theta}}\right)^2 + \sin^2\widetilde{\theta}}\, d\gamma = \Omega_0\,(t - t_i), \tag{2.111}$$

where the left-hand side is the partial pulse area [see Eq. (1.76)].

2.C Calculation of γ_f for the complete population transfer

The expression of the detuning (2.33) leads to the exact value of γ_f as follows: Considering the middle time, $t_{1/2} = T_{\min}/2$, for which we have by symmetry $\theta_{1/2} = \pi/2$, $\gamma_{1/2} = (\gamma_f + \gamma_i)/2 = (\gamma_f + \pi/2)/2$, and $\Delta_{1/2} = 0$ (odd function), (2.33) gives $\lambda_1 \sin\gamma_{1/2} - \lambda_2 \cos\gamma_{1/2} = 0$. With the equation (2.98), $\lambda_2 \cos\gamma_f - \lambda_1 \sin\gamma_f = \lambda_1$, they form the system:

$$\lambda_1 \sin\gamma_{1/2} - \lambda_2 \cos\gamma_{1/2} = 0, \quad \lambda_2 \cos\gamma_f - \lambda_1(1 + \sin\gamma_f) = 0, \tag{2.112}$$

which has a solution when the determinant of the system is zero: $-\sin\gamma_{1/2}(1 + \sin\gamma_f) + \cos\gamma_f \cos\gamma_{1/2} = 0$, of exact solution $\gamma_f = 5\pi/3$. As a consequence, we have the relation between the λ_j's:

$$\lambda_2 = \lambda_1 \tan\gamma_{1/2} \approx 0.26795\lambda_1. \tag{2.113}$$

2.D Analytic expression of the detuning for population transfers

In this Appendix, we show that the detuning has the form of a Jacobi elliptic cosine.

From (2.33), we calculate $\dot{\Delta}$ as a function of the two dynamical angles (θ, γ), and redefine it as a function of the two dynamical angles (θ, χ) via two parameters I_1 and I_2 following [35]:

$$\dot{\Delta} = \lambda_1 \Theta_{0x} - \lambda_2 \Theta_{0y} = I_1 \Omega_{0x} - I_2 \Omega_{0y} \tag{2.114}$$

with

$$\Theta_{0x} = \dot{\theta}\cos\theta\sin\gamma + \dot{\gamma}\sin\theta\cos\gamma, \quad \Theta_{0y} = \dot{\theta}\cos\theta\cos\gamma - \dot{\gamma}\sin\theta\sin\gamma, \tag{2.115}$$

and

$$\Omega_{0x} = \dot{\theta}\sin\chi + \dot{\chi}\tan\theta\cos\chi, \quad \Omega_{0y} = \dot{\theta}\cos\chi - \dot{\chi}\tan\theta\sin\chi \tag{2.116}$$

with

$$\dot{\chi} = \dot{\gamma}\cos\theta, \tag{2.117}$$

and χ_i to be defined.

We obtain:

$$\dot{\Omega}_{0x} = \ddot{\theta}\sin\chi + \dot{\theta}\dot{\chi}\cos\chi + \ddot{\gamma}\sin\theta\cos\chi + \dot{\gamma}\dot{\theta}\cos\theta\cos\chi - \dot{\gamma}\dot{\chi}\sin\theta\sin\chi, \tag{2.118a}$$
$$\dot{\Omega}_{0y} = \ddot{\theta}\cos\chi - \dot{\theta}\dot{\chi}\sin\chi - \ddot{\gamma}\sin\theta\sin\chi - \dot{\gamma}\dot{\theta}\cos\theta\sin\chi - \dot{\gamma}\dot{\chi}\sin\theta\cos\chi, \tag{2.118b}$$

i.e., using the equations of motion (2.32) and (2.117):

$$\dot{\Omega}_{0x} = \sin\theta(\dot{\gamma}\sin\theta\sin\chi - \dot{\theta}\cos\chi)(\lambda_1\sin\gamma - \lambda_2\cos\gamma), \tag{2.119a}$$
$$\dot{\Omega}_{0y} = \sin\theta(\dot{\gamma}\sin\theta\cos\chi + \dot{\theta}\sin\chi)(\lambda_1\sin\gamma - \lambda_2\cos\gamma)). \tag{2.119b}$$

This leads to the three equations of motion

$$\dot{\Omega}_{0x} = -\Omega_{0y}\Delta, \quad \dot{\Omega}_{0y} = \Omega_{0x}\Delta, \quad \dot{\Delta} = I_1\Omega_{0x} - I_2\Omega_{0y}. \tag{2.120}$$

The solution of the first two equations allows one to recover the properties of Ω_{0x}, Ω_{0y} (1.80), and Δ (1.84c):

$$\Omega_{0x} = \Omega_0\cos\eta, \quad \Omega_{0y} = \Omega_0\sin\eta, \quad \Omega_0 = const, \quad \Delta = \dot{\eta}. \tag{2.121}$$

From Eq. (2.120), the function η can be determined as [35]:

$$\eta = \pm\left[\frac{\mathrm{sn}(\nu,m)}{|\mathrm{sn}(\nu,m)|}\,\mathrm{acos}\sqrt{1 - m\,\mathrm{sn}^2(\nu,m)} - \mathrm{acos}\sqrt{1-m}\right] \tag{2.122}$$

with the phase

$$\nu = \omega t + \nu_i, \tag{2.123}$$

where the sign + [−] stands for negative [positive] I_1, and the detuning has the form of the elliptic cosine :

$$\Delta = \Delta_0\,\mathrm{cn}\left(\omega t + \nu_i, m\right), \quad t \in [0, T_{\min}] \tag{2.124}$$

with

$$\omega = \sqrt{\Omega_0}(I_1^2 + I_2^2)^{1/4}, \tag{2.125a}$$

$$m = \frac{1}{2} - \frac{\Omega_0}{2\omega^2}(I_2 \cos\eta_i + I_1 \sin\eta_i), \tag{2.125b}$$

$$\Delta_0 = -2 \operatorname{sgn}\lambda_1 \, \omega\sqrt{m}. \tag{2.125c}$$

At the initial time $\theta_i = 0$ ($\gamma_i = \pi/2$, $\dot{\theta}_i = \Omega_0$), we have $\Delta_i = 0$ from (2.33), inducing

$$\nu_i = K(m) \tag{2.126}$$

in (2.124), with $K(m)$ the complete elliptic integral of the first kind. This gives $\eta_i = 0$ from (2.122), i.e., $\chi_i = \pi/2$ (since $\chi = \varphi - \eta$ and $\varphi_i = \pi/2$), and from (2.114):

$$\lambda_1 = I_1, \tag{2.127}$$

i.e., from (2.125b) and (2.125a),

$$m = \frac{1}{2}\left(1 - \sqrt{1 - \lambda_1^2 \frac{\Omega_0^2}{\omega^4}}\right). \tag{2.128}$$

Identifying the initial derivative (2.114) and (2.124) gives

$$|\lambda_1|\Omega_0 = 2\omega^2\sqrt{m}\sqrt{1-m}. \tag{2.129}$$

The last two equations are in fact identical.

Identifying the final derivative (2.114) and (2.124) gives:

$$\lambda_1\Theta_{0x,f} - \lambda_2\Theta_{0y,f} = -\Delta_0\omega \operatorname{sn}\left[\omega T_{\min} + K(m), m\right] \sqrt{1 - m \operatorname{sn}^2\left[\omega T_{\min} + K(m), m\right]} \tag{2.130}$$

with $\Theta_{0x,f} \equiv \Theta_{0x}(t_f)$ and $\Theta_{0y,f} \equiv \Theta_{0y}(t_f)$.

From the knowledge of the trajectory $\widetilde{\theta}(\gamma)$, obtained from λ_1 and λ_2, and $T_{\min}$ from (2.28), one can calculate m and ω from the system of equations (2.129–2.130), where we substitute Δ_0 from (2.125c). We next obtain Δ_0 from (2.125c), which fully determines the detuning (2.124) [also using (2.126)].

2.E Composite pulses technique – Complete population transfer and NOT gate

The technique is based on the composition of resonant pulses [13–17] each corresponding to the propagator:

$$U_{\theta,\varphi} = \begin{bmatrix} \cos(\theta/2) & -i\sin(\theta/2)e^{-i\varphi} \\ -i\sin(\theta/2)e^{i\varphi} & \cos(\theta/2) \end{bmatrix}, \tag{2.131}$$

where θ is the pulse area and φ its (static) phase. We determine in this Appendix the optimal composite pulse technique for some population transfers and gates accurate to third order, considering robustness with respect to field inhomogeneities. This means a systematic error in the pulse area proportional to it: $\theta(1+\alpha) = \theta + \varepsilon$ with $\varepsilon = \alpha\theta$.

A single pulse process, for which the population transfer reads

$$P_{\theta_0}^{(1)} = \sin^2\left[(\theta_0+\varepsilon)/2\right] = \sin^2\left(\theta_0/2\right)\left[1+\varepsilon\cot\theta_0+\cdots\right] \tag{2.132}$$

with θ_0 the targeted mixing angle, shows in general a first order deviation in the error, $O(\varepsilon)$. As a particular case, the complete π-pulse population transfer ($\theta_0 = \pi$) produces a second order deviation in the error:

$$P_{\pi}^{(1)} = \sin^2\left(\theta_0/2\right)\left[1+O(\varepsilon^2)\right]. \tag{2.133}$$

A sequence of two pulses $U_{\theta_1,\varphi_1}U_{\theta_2,\varphi_2=0}$, with the same relative error in the mixing angles $\theta_1(1+\alpha)$, $\theta_2(1+\alpha)$ does not improve the accuracy of the single-pulse complete π-pulse population transfer, but it does for the other transfers when $\theta_1 = \theta_2 = \pi/2$ ($\pi/2$-pulses) with a quadratic improvement [17]:

$$P_{\theta_0}^{(2)} = \sin^2\left(\theta_0/2\right)\left[1+\pi\varepsilon^2/4+\cdots\right]. \tag{2.134}$$

A sequence of three symmetric pulses $U_{\theta_2,0}U_{\theta_1,\varphi_1}U_{\theta_2,\varphi_2=0}$ leads to the propagator, which includes the errors [using the notation $c_1' \equiv \cos(\theta_1'/2)$, $s_1' \equiv \sin(\theta_1'/2)$, $c_2' \equiv \cos\theta_2'$, $s_2' \equiv \sin\theta_2'$]:

$$\begin{aligned} U &= U_{\theta_2',0}U_{\theta_1',\varphi_1}U_{\theta_2',0} \\ &= \begin{bmatrix} c_1'c_2' - s_1's_2'\cos\varphi & -ic_1's_2' - s_1'(ic_2'\cos\varphi+\sin\varphi) \\ -ic_1's_2' - s_1'(ic_2'\cos\varphi-\sin\varphi) & c_1'c_2' - s_1's_2'\cos\varphi \end{bmatrix} \equiv \begin{bmatrix} U_{11} & U_{12} \\ U_{21} & U_{22} \end{bmatrix} \end{aligned} \tag{2.135}$$

We have the same error for the angles: $\theta_1' = \theta_1(1+\alpha) = \theta_1 + \varepsilon_1$ with $\varepsilon_1 = \alpha\theta_1$ and $\theta_2' = \theta_2(1+\alpha) = \theta_2 + \varepsilon_2$ with $\varepsilon_2 = \alpha\theta_2 = \varepsilon_1\theta_2/\theta_1$. For a complete population transfer (population inversion), $|\phi(t_f)\rangle = U[1 \quad 0]^T = [U_{11} \quad U_{21}]^T$, $|U_{11}|^2 + |U_{21}|^2 = 1$, it is sufficient to consider the U_{21} matrix element of the propagator, which has to satisfy $|U_{21}|^2 = 1$ in absence of errors (since the global phase is irrelevant) and to prove $|U_{21}|^2 = 1 + O(\varepsilon^4)$ for a robust transfer at third order.

It reads

$$U_{21} = -i\cos(\theta_1'/2)\sin\theta_2' - \sin(\theta_1'/2)(i\cos\theta_2'\cos\varphi - \sin\varphi) \tag{2.136}$$

with at second order

$$\begin{aligned}
\cos(\theta_1'/2) &= \cos(\theta_1/2)(1-\varepsilon_1^2/8) - \sin(\theta_1/2)\varepsilon_1/2 + O(\varepsilon_1^3)\\
\sin(\theta_1'/2) &= \sin(\theta_1/2)(1-\varepsilon_1^2/8) + \cos(\theta_1/2)\varepsilon_1/2 + O(\varepsilon_1^3)\\
\cos\theta_2' &= \cos\theta_2(1-\varepsilon_2^2/2) - \varepsilon_2\sin\theta_2 + O(\varepsilon_2^3)\\
\sin\theta_2' &= \sin\theta_2(1-\varepsilon_2^2/2) + \varepsilon_2\cos\theta_2 + O(\varepsilon_2^3).
\end{aligned}$$

This leads to

$$\begin{aligned}
U_{21} = -i[&\cos(\theta_1/2)(1-\varepsilon_1^2/8)(\sin\theta_2(1-\varepsilon_2^2/2) + \varepsilon_2\cos\theta_2)\\
&- (\varepsilon_1/2)\sin(\theta_1/2)(\sin\theta_2(1-\varepsilon_2^2/2) + \varepsilon_2\cos\theta_2)]\\
&- [\sin(\theta_1/2)(1-\varepsilon_1^2/8)(i\cos\theta_2'\cos\varphi - \sin\varphi)\\
&+ (\varepsilon_1/2)\cos(\theta_1/2)(i\cos\theta_2'\cos\varphi - \sin\varphi)] + O(\varepsilon_1^3, \varepsilon_2^3).
\end{aligned} \tag{2.137}$$

Analysis of the above expression shows that cancellation of the first order term of $|U_{21}|^2$ implies $\theta_1 = \pi$ (necessary condition). This leads to

$$\begin{aligned}
U_{21} = &\sin\varphi - i\cos\varphi\cos\theta_2 + i(\varepsilon_1/2 + \varepsilon_2\cos\varphi)\sin\theta_2\\
&- (\varepsilon_1^2/8)\sin\varphi + \frac{i}{2}\cos\theta_2[\varepsilon_1\varepsilon_2 + \cos\varphi(\varepsilon_2^2 + \varepsilon_1^2/4)].
\end{aligned} \tag{2.138}$$

When $\varepsilon_1 = \varepsilon_2 = 0$ (no error), we have

$$|U_{21}|^2 = \sin^2\varphi + \cos^2\varphi(1-\sin^2\theta_2) = 1 - \cos^2\varphi\sin^2\theta_2, \tag{2.139}$$

which gives

$$|U_{21}|^2 = 1 \text{ when } \varphi = \pi/2 \text{ or } \theta_2 = \pi. \tag{2.140}$$

We first consider $\theta_2 = \pi$ (for which $\varepsilon_2 = \varepsilon_1 \equiv \varepsilon$):

$$U_{21} = \sin\varphi + i\cos\varphi - \frac{\varepsilon^2}{8}\sin\varphi - \frac{i}{2}\varepsilon^2[1 + (5/4)\cos\varphi] \tag{2.141}$$

i.e.

$$|U_{21}|^2 = 1 - \frac{\varepsilon^2}{2}[\cos\varphi + (5/4)\cos^2\varphi + (1/4)\sin^2\varphi], \tag{2.142}$$

giving $|U_{21}|^2 = 1 + O(\varepsilon^4)$ for $\varphi = \pm 2\pi/3$. Making the expansion further shows in fact that $|U_{21}|^2 = 1 + O(\varepsilon^6)$ featuring a total pulse area of 3π:

$$U_{\pi,0}U_{\pi,2\pi/3}U_{\pi,0}, \qquad |U_{21}|^2 = 1 + O(\varepsilon^6). \tag{2.143}$$

This sequence is known as SCROFULOUS, producing a NOT gate robust at third order [14].

We alternatively consider $\varphi = \pi/2$ to satisfy (2.140):

$$U_{21} = 1 + i\frac{\varepsilon}{2}\sin\theta_2 - \frac{\varepsilon^2}{8} + \frac{i\varepsilon^2}{2}\frac{\theta_2}{\pi}\cos\theta_2, \tag{2.144}$$

i.e.,

$$|U_{21}|^2 = 1 + \frac{\varepsilon^2}{4}(-1 + \sin^2\theta_2), \tag{2.145}$$

giving $|U_{21}|^2 = 1 + O(\varepsilon^4)$ for $\theta_2 = \pi/2$. The latter result shows that the composite sequence

$$U_{\pi/2,0}U_{\pi,\pi/2}U_{\pi/2,0}, \quad |U_{21}|^2 = 1 + O(\varepsilon^4), \tag{2.146}$$

of 2π total pulse area leads to a complete population transfer robust at third order. This represents the optimal composite sequence with respect to pulse area for robust complete population transfer against pulse inhomogeneities.

2.F Invariance of the optimal trajectory with different costs for quantum gates

In this section we show that optimizing with respect to the pulse area, to the energy, or to the duration leads to the same trajectory for the problem of robust quantum gates. To show the equivalence of the trajectory (2.54) with that (2.45) for the pulse

area optimization, we proceed as follows: Using $\ddot{\theta} = \dot{\gamma}^2\dddot{\tilde{\theta}} + \ddot{\gamma}\dot{\tilde{\theta}}$, (2.54b) reads

$$\begin{aligned}\dot{\gamma}^2\dddot{\tilde{\theta}} + \ddot{\gamma}\dot{\tilde{\theta}} - \dot{\gamma}^2 \sin\theta\cos\theta - \lambda_0\dot{\gamma}\sin\theta\cos\theta \\ + 2\dot{\gamma}\sin^2\theta(\lambda_1\cos\gamma + \lambda_2\sin\gamma) = 0,\end{aligned} \tag{2.147}$$

which gives, using (2.54a) and $\dot{\theta} = \dot{\gamma}\dot{\tilde{\theta}}$:

$$\begin{aligned}\dddot{\tilde{\theta}} - [2\cot\theta + \frac{1}{\dot{\gamma}}\lambda_0\cot\theta - \frac{2}{\dot{\gamma}}(\lambda_1\cos\gamma + \lambda_2\sin\gamma)]\big(\dot{\tilde{\theta}}\big)^2 - \sin\theta\cos\theta - \lambda_0\frac{1}{\dot{\gamma}}\sin\theta\cos\theta \\ + \frac{2}{\dot{\gamma}}\sin^2\theta(\lambda_1\cos\gamma + \lambda_2\sin\gamma) = 0,\end{aligned} \tag{2.148}$$

i.e.,

$$\begin{aligned}\dddot{\tilde{\theta}} - [\sin^2\theta + 2\big(\dot{\tilde{\theta}}\big)^2]\cot\theta - \frac{1}{\dot{\gamma}}\lambda_0\cot\theta[\sin^2\theta + \big(\dot{\tilde{\theta}}\big)^2] \\ + \frac{2}{\dot{\gamma}}[\sin^2\theta + \big(\dot{\tilde{\theta}}\big)^2](\lambda_1\cos\gamma + \lambda_2\sin\gamma) = 0.\end{aligned} \tag{2.149}$$

Using the constant of motion (2.58) rewritten as $\Omega_0^2 = \dot{\theta}^2 + \dot{\gamma}^2\sin^2\theta = \dot{\gamma}^2[\sin^2\theta + \big(\dot{\tilde{\theta}}\big)^2]$, we obtain:

$$\begin{aligned}\dddot{\tilde{\theta}} - (\sin^2\theta + 2\big(\dot{\tilde{\theta}}\big)^2)\cot\theta - \frac{\lambda_0}{\Omega_0}\cot\theta[\sin^2\theta + \big(\dot{\tilde{\theta}}\big)^2]^{3/2} \\ + \frac{2}{\Omega_0}(\lambda_1\cos\gamma + \lambda_2\sin\gamma)[\sin^2\theta + \big(\dot{\tilde{\theta}}\big)^2]^{3/2} = 0,\end{aligned} \tag{2.150}$$

i.e.,

$$\begin{aligned}\dddot{\tilde{\theta}} = 2\big(\dot{\tilde{\theta}}\big)^2\cot\widetilde{\theta} + \sin\widetilde{\theta}\cos\widetilde{\theta} + 2\widetilde{\lambda}_0\cot\theta[\sin^2\widetilde{\theta} + \big(\dot{\tilde{\theta}}\big)^2]^{3/2} \\ + (\lambda_1\sin\gamma - \lambda_2\cos\gamma)[\sin^2\widetilde{\theta} + \big(\dot{\tilde{\theta}}\big)^2]^{3/2},\end{aligned} \tag{2.151}$$

where we have redefined the Lagrange multipliers

$$\widetilde{\lambda}_0 = \lambda_0/(2\Omega_0),\ \widetilde{\lambda}_2 = 2\lambda_1/\Omega_0,\ \widetilde{\lambda}_1 = -2\lambda_2/\Omega_0. \tag{2.152}$$

We recover Eq. (2.45) obtained for designing a robust trajectory minimal with respect to the pulse area under the constraints (2.44).

2.G Analytic expression of the detuning for quantum gates

The detuning can be written as in the case of population transfer, (2.114), leading to (2.124) with

$$\Delta_0 = -2 \operatorname{sgn} \lambda_1 \, \omega \sqrt{m}, \tag{2.153}$$

but with a modification of the initial phase of the Jacobi elliptic cosine given by the initial detuning $\Delta_i = \lambda_0$:

$$\lambda_0 = \Delta_0 \operatorname{cn}(\nu_i, m) = -2 \operatorname{sgn} \lambda_1 \, \omega \sqrt{m} \operatorname{cn}(\nu_i, m) \,. \tag{2.154}$$

Identifying the initial derivative (2.114) and (2.124) gives:

$$\lambda_1 \Omega_0 = -\Delta_0 \omega \, \operatorname{sn}(\nu_i, m) \sqrt{1 - m \, \operatorname{sn}^2(\nu_i, m)}, \tag{2.155}$$

and the final derivative:

$$\begin{aligned} \lambda_1 \Theta_{0x,f} - \lambda_2 \Theta_{0y,f} - \lambda_0 \dot{\theta}_f \sin \theta_f = -\Delta_0 \omega \operatorname{sn}(\omega T_{\min} + \nu_i, m) \\ \times \sqrt{1 - m \operatorname{sn}^2(\omega T_{\min} + \nu_i, m)}. \end{aligned} \tag{2.156}$$

We find the parameters ω and m as solutions of the system (2.155–2.156) after substituting Δ_0 from (2.153) and ν_i from (2.154).

One can remark that the above formulation can be reduced to the case of population transfer by considering $\lambda_0 = 0$.

Chapter 3

Control in three-level systems

3.1 Introduction

Having studied extensively the control of a two-level quantum system, we can delve into larger and more complex systems armed with tested techniques; being the next task in complexity, the three-level system. Three-level systems are most relevant when we do not dispose of appropriate controls for a certain two-level system, but we do for a pair that shares one of its levels, or when the control to be used on a two-level system is expected to have a non-negligible interaction with a third level.

Three-level systems are ubiquitous in quantum processes, either with two-field linkages in Lambda (Λ), ladder (Ξ) or Vee (V) configuration; or with three-field linkages in Delta (Δ or loop or triangle) configuration [7]. Their control, be it through diabatic or adiabatic methods, has found many applications, particularly in quantum control. The system configuration transmits at a glance the general situation to consider for the task of control and to discriminate between the available real systems in the laboratory. However, the theoretical models applied for any such configuration may be translated onto another if the physical constraints of the system allow it.

Many applications, particularly in quantum control, are based on our ability of controlling the population transfer in the three-level Λ system [11, 38–41]. Such Λ configurations are most relevant when the two quantum levels of interest, typically two stable ground states, are difficult, impossible, or impractical, to couple while there is a third, more energetic level, accessible from both others. Fine control compatible with quantum information requirements imposes producing robust transfer of population with ultra high fidelity (UH-fidelity), i.e. under the quantum computation infidelity benchmark of $\epsilon < 10^{-4}$ [42], between the two ground states of the system, while maintaining a low transient population on the intermediate (and often

lossy) excited state during the dynamics. We can transfer population between the two ground states, referred in short as Λ transfer, using pump and Stokes controls, both names kept for historical reasons, each connecting the excited state to the initial and target states, respectively, which produce Rabi oscillations when they fully overlap [11, p. 197]. However, this places significant transient population on the excited lossy state, which lead to an incomplete population transfer to the target state. A way to overcome this difficulty was found in the technique known as stimulated Raman adiabatic passage, commonly known as STIRAP [5]; widely used with applications in many physical and chemical problems [5, 6, 11, 38–41]. STIRAP uses adiabaticity in order to avoid populating the intermediate state of a three-level system and to produce a robust transfer, at the expense of the process duration and pulse energy. In STIRAP, the fields coupling the ground states with the excited one must be counter-intuitively ordered (Stokes pulse switched on before pump pulse with both pulses of the same duration) and exhibit high pulse areas and/or long time durations (technically any combination of factors fulfilling the adiabatic condition) in order to produce an adiabatic transfer (following the adiabatic dark state) with small transient population on the excited state. Pulsed fields with increasingly higher areas and a counter-intuitive order, signatures of STIRAP, jointly with an optimized delay between the pulses, improve the adiabaticity and, in consequence, the robustness of the process offered by it, particularly with respect to any specific design of the pulses, while minimizing the unwanted transient population of the excited state.

Even though STIRAP is the 'go-to' standard protocol when to increase the process robustness becomes necessary, it is only at the adiabatic limit that it produces a complete transfer to the desired state and maintains the excited state depopulated. That is to say that the target state $|\psi_T\rangle$ is approached asymptotically by the system state $|\psi(t)\rangle$ while the pulses areas $\mathcal{A}_P = \int_{-\infty}^{\infty} \Omega_P(t)dt$ and $\mathcal{A}_S = \int_{-\infty}^{\infty} \Omega_S(t)dt$ grow without limit. Concretely, the precision of the transfer can be measured with the fidelity $\mathcal{F} = |\langle\psi_T|\psi(t_f)\rangle|^2 = 1-\mathcal{I}$: a quantity equal to 1 when the transfer is perfect (target state achieved exactly by the system state at the process final time t_f) and to 0 when the final state is orthogonal to the target. Thus, in STIRAP, the fidelity tends to unity ($\mathcal{F} \to 1$) as the pulses areas tend to infinity ($\{\mathcal{A}_P, \mathcal{A}_S\} \to \infty$). In this manner, STIRAP provides a robust but inexact way of transferring population between the ground states of a three-level system. Additionally, the use of high area pulses hinders the application of such technique. Be it due to the destructive effects the usage of high intensity fields can produce, like ionization, or to the decoherence and experimental instabilities to which slow processes are susceptible, fields of moderate areas are most desirable for quantum state manipulation, especially for the

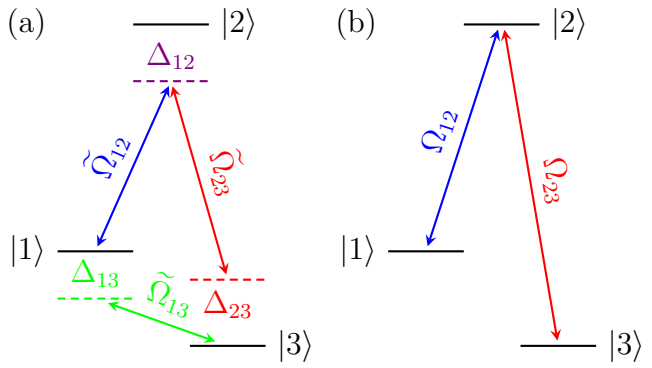

Figure 3.1: From left to right: (a) a general three-level system with all its linkages in Delta (Δ) configuration, (b) a resonant three-level system in Lambda (Λ) configuration with real couplings (the absence of coupling between states $|1\rangle$ and $|3\rangle$, $\Omega_{13} = 0$, makes it a Λ system).

UH-fidelity we aim at.

3.2 General three-level Hamiltonian

The general three-level Hamiltonian, corresponding to the systems in Fig. 3.1, in the bare-states basis and in the rotating wave approximation (RWA) can be written, in terms of the energies of the three bare states ω_n and the three complex couplings

$$\widetilde{\Omega}_{ij}(t) = \Omega_{ij}(t)e^{i\widetilde{\eta}_{ij}(t)} \tag{3.1}$$

with real-valued amplitudes Ω_{ij} and dynamical phases (including central frequency, carrier-envelope phase, and chirp)

$$\widetilde{\eta}_{ij} = \omega_{ij}t + \eta_{ij}(t), \tag{3.2}$$

as

$$\widehat{H} = \frac{\hbar}{2}\begin{bmatrix} 2\omega_1 & \widetilde{\Omega}_{12} & \widetilde{\Omega}_{13} \\ \bar{\widetilde{\Omega}}_{12} & 2\omega_2 & \widetilde{\Omega}_{23} \\ \bar{\widetilde{\Omega}}_{13} & \bar{\widetilde{\Omega}}_{23} & 2\omega_3 \end{bmatrix}. \tag{3.3}$$

This Hamiltonian can be rewritten to show explicitly the detunings between control-fields central frequencies and transition frequencies, either as dynamic quantities

$$\Delta_{13}(t) = \omega_1 - \omega_3 - \dot{\widetilde{\eta}}_{13}, \tag{3.4a}$$
$$\Delta_{12}(t) = \omega_2 - \omega_1 - \dot{\widetilde{\eta}}_{12}, \tag{3.4b}$$
$$\Delta_{23}(t) = \omega_1 - \omega_3 + \dot{\widetilde{\eta}}_{12} - \dot{\widetilde{\eta}}_{23}, \tag{3.4c}$$

by applying a unitary transformation T onto the Schrödinger equation, $i\hbar\partial_t|\widehat{\psi}\rangle = \widehat{H}|\widehat{\psi}\rangle$, with $|\widehat{\psi}\rangle = T|\psi'\rangle$; or as time-independent ones

$$\widetilde{\Delta}_{13} = \omega_1 - \omega_3 - \omega_{13}, \tag{3.5a}$$
$$\widetilde{\Delta}_{12} = \omega_2 - \omega_1 - \omega_{12}, \tag{3.5b}$$
$$\widetilde{\Delta}_{23} = \omega_1 - \omega_3 + \omega_{12} - \omega_{23}, \tag{3.5c}$$

by applying a unitary transformation $|\widehat{\psi}\rangle = \widetilde{T}|\psi''\rangle$. The detunings Δ_{12} ($\widetilde{\Delta}_{12}$) and Δ_{23} ($\widetilde{\Delta}_{23}$) are usually called one- and two-photon detunings, respectively, due to the role they play on the transfer of population between the ground states of the Λ system. The Schrödinger equation for $|\psi'\rangle$ effectively presents, as the system's Hamiltonian,

$$H' = T^\dagger \widehat{H} T - i\hbar T^\dagger \dot{T}, \tag{3.6}$$
$$= \frac{\hbar}{2}\begin{bmatrix} 0 & \Omega_{12} & e^{-i(\widetilde{\eta}_{12}-\widetilde{\eta}_{23}-\widetilde{\eta}_{13})}\Omega_{13} \\ \Omega_{12} & 2\Delta_{12} & \Omega_{23} \\ e^{i(\widetilde{\eta}_{12}-\widetilde{\eta}_{23}-\widetilde{\eta}_{13})}\Omega_{13} & \Omega_{23} & -2\Delta_{23} \end{bmatrix}, \tag{3.7}$$

for a transformation leading to real couplings $|1\rangle \leftrightarrow |2\rangle$ and $|2\rangle \leftrightarrow |3\rangle$ given by

$$\begin{aligned} \zeta_1 &= -\omega_1 t, \\ \zeta_2 &= -\omega_1 t - \widetilde{\eta}_{12}, \\ \zeta_3 &= -\omega_1 t - \widetilde{\eta}_{12} + \widetilde{\eta}_{23}, \end{aligned} \qquad T = \begin{bmatrix} e^{i\zeta_1} & 0 & 0 \\ 0 & e^{i\zeta_2} & 0 \\ 0 & 0 & e^{i\zeta_3} \end{bmatrix}, \tag{3.8}$$

and a Hamiltonian

$$H'' = \widetilde{T}^\dagger \widehat{H} \widetilde{T} - i\hbar \widetilde{T}^\dagger \dot{\widetilde{T}}, \tag{3.9}$$
$$= \frac{\hbar}{2}\begin{bmatrix} 0 & \Omega_{12}e^{i\eta_{12}} & \Omega_{13}e^{i[\widetilde{\eta}_{13}-(\omega_{12}-\omega_{23})t]} \\ \Omega_{12}e^{-i\eta_{12}} & 2\widetilde{\Delta}_{12} & \Omega_{23}e^{-i\eta_{23}} \\ \Omega_{13}e^{-i[\widetilde{\eta}_{13}-(\omega_{12}-\omega_{23})t]} & \Omega_{23}e^{i\eta_{23}} & -2\widetilde{\Delta}_{23} \end{bmatrix}, \tag{3.10}$$

for a transformation like (3.8) but applying the substitution $\widetilde{\eta}_{ij} \to \omega_{ij}t$ in ζ_n to obtain time-independent detunings.

Since we can always factorize the state by an unimportant global phase, Hamiltonians can always be made traceless. It suffices to write the traceless Hamiltonian as $\widetilde{H}^{[\prime]} = H'^{[\prime]} - \frac{\mathbb{1}}{3}\operatorname{Tr}\big(H'^{[\prime]}\big)$ and apply the transformation

$$|\psi'^{[\prime]}\rangle = \exp\left[-\frac{i}{3\hbar}\int \operatorname{Tr}\big(H'^{[\prime]}\big)dt\right]|\psi\rangle. \tag{3.11}$$

Thus, we obtain the following traceless Hamiltonian with real couplings for the general three-level system (left-side diagram in Fig. 3.1):

$$\widetilde{H} = \frac{\hbar}{2}\begin{bmatrix} 2(\Delta_{23}-\Delta_{12})/3 & \Omega_{12} & e^{-i(\widetilde{\eta}_{12}-\widetilde{\eta}_{23})}\widetilde{\Omega}_{13} \\ \Omega_{12} & 2(\Delta_{23}+2\Delta_{12})/3 & \Omega_{23} \\ e^{i(\widetilde{\eta}_{12}-\widetilde{\eta}_{23})}\bar{\widetilde{\Omega}}_{13} & \Omega_{23} & -2(\Delta_{12}+2\Delta_{23})/3 \end{bmatrix}, \tag{3.12}$$

and the following with time-independent detunings:

$$\widetilde{H}' = \frac{\hbar}{2}\begin{bmatrix} 2(\widetilde{\Delta}_{23}-\widetilde{\Delta}_{12})/3 & \Omega_{12}e^{i\eta_{12}} & \widetilde{\Omega}_{13}e^{-i(\omega_{12}-\omega_{23})t} \\ \Omega_{12}e^{-i\eta_{12}} & 2(\widetilde{\Delta}_{23}+2\widetilde{\Delta}_{12})/3 & \Omega_{23}e^{-i\eta_{23}} \\ \bar{\widetilde{\Omega}}_{13}e^{i(\omega_{12}-\omega_{23})t} & \Omega_{23}e^{i\eta_{23}} & -2(\widetilde{\Delta}_{12}+2\widetilde{\Delta}_{23})/3 \end{bmatrix}. \tag{3.13}$$

Naturally, we can also obtain the traceless Hamiltonian (3.12) [(3.13)] by directly applying the transformation T with

$$\zeta_1 = [2\widetilde{\eta}_{12} - \widetilde{\eta}_{23} - (\omega_1+\omega_2+\omega_3)t]/3, \tag{3.14}$$

$$\zeta_2 = -[\widetilde{\eta}_{12} + \widetilde{\eta}_{23} + (\omega_1+\omega_2+\omega_3)t]/3, \tag{3.15}$$

$$\zeta_3 = [2\widetilde{\eta}_{23} - \widetilde{\eta}_{12} - (\omega_1+\omega_2+\omega_3)t]/3, \tag{3.16}$$

on the general RWA three-level Hamiltonian (3.3), [with the substitution $\widetilde{\eta}_{ij} \to \omega_{ij}t$].

The Hamiltonian (3.12) will be from now on the default general one for the three-level systems that will be discussed in this document regarding the special case with broad practical relevance of the fully resonant system shown in Fig. 3.1(b), i.e. with

$$\widetilde{\Omega}_{13} = \Delta_{12} = \Delta_{13} = \Delta_{23} = 0. \tag{3.17}$$

3.3 Fully resonant system

A physically realistic, highly relevant, and very widely implemented configuration is that depicted in the system in Fig. 3.1(b). This system has been studied extensively and the results of such investigations have found many applications even beyond the quantum mechanical system for which they were designed [5, 6, 8]. STIRAP, to take one example, has been at the heart of numerous developments in the 30 years of its existence and many other approaches exist that make this system a cauldron for development of innovative protocols and applications beyond the scope of the two-level system limitations. Thus, in this document, we strive to focus on obtaining the propagators, boundary conditions and solutions of the Schrödinger equation for particular cases of the three-level system, specifically for the fully resonant Λ system

on Fig. 3.1(b) corresponding to a Hamiltonian of the form

$$H = \frac{\hbar}{2}\begin{bmatrix} 0 & \Omega_P & 0 \\ \Omega_P & -i\Gamma & \Omega_S \\ 0 & \Omega_S & 0 \end{bmatrix}, \tag{3.18}$$

where Ω_P and Ω_S are the real-valued pulse envelopes of the control fields coupling state $|2\rangle$ with states $|1\rangle$ and $|3\rangle$, respectively, and Γ is the dissipation rate modeling the excited state's loss. Moreover, we will particularly study optimal processes, which will be achieved in the fully resonant situation.

3.3.1 Fields with phases

Considering that we can apply a transformation $H_\Phi = \Phi^\dagger H \Phi$, with the constant-phase transformation matrix

$$\Phi = \begin{bmatrix} e^{-i\Phi_P} & 0 & 0 \\ 0 & 1 & 0 \\ 0 & 0 & e^{-i\Phi_S} \end{bmatrix}, \tag{3.19}$$

then we may generalize the Hamiltonian (3.18), the lossless (hermitian) part of which is covered by the su(2) algebra (with the general two-level system as its prime member), to

$$H_\Phi = \frac{\hbar}{2}\begin{bmatrix} 0 & e^{i\Phi_P}\Omega_P & 0 \\ e^{-i\Phi_P}\Omega_P & -i\Gamma & e^{-i\Phi_S}\Omega_S \\ 0 & e^{i\Phi_S}\Omega_S & 0 \end{bmatrix}, \tag{3.20}$$

corresponding to a propagator $U_\Phi = \Phi^\dagger U \Phi$,

$$U_\Phi = \begin{bmatrix} U_{11} & e^{i\Phi_P}U_{12} & e^{i(\Phi_P-\Phi_S)}U_{13} \\ e^{-i\Phi_P}U_{21} & U_{22} & e^{-i\Phi_S}U_{23} \\ e^{-i(\Phi_P-\Phi_S)}U_{31} & e^{i\Phi_S}U_{32} & U_{33} \end{bmatrix}, \tag{3.21}$$

non-unitary if $\Gamma \neq 0$.

The effect of these phases is most appreciated with the following examples:

1. A system in state $|1\rangle$ $[|3\rangle]$ under a population inversion propagator would result in the state $e^{-i(\Phi_P-\Phi_S)}|3\rangle$ $[e^{i(\Phi_P-\Phi_S)}|1\rangle]$. These phases are irrelevant in an isolated system, thus their relevance would only be evident if a superposition is produced, i.e.

2. a system in state $|1\rangle$ under a propagator producing a maximal superposition

will evolve into the state $|1\rangle + e^{-i(\Phi_P - \Phi_S)}|3\rangle$, then the dephasing between the fields is the relative phase of the superposition.

3.3.2 Loss model

Loss of population can occur through multiple channels. This is modeled phenomenologically via the dissipation rate, the rate at which coherent population is lost. Using the Schrödinger equations for the statevector elements $c_{n,\Gamma} = \langle n|\psi_\Gamma\rangle$ with $c_n = c_{n,\Gamma=0}$,

$$\dot{c}_{1,\Gamma} = -i\frac{\Omega_P}{2}c_{2,\Gamma}, \tag{3.22}$$

$$\dot{c}_{2,\Gamma} = -i\frac{\Omega_P}{2}c_{1,\Gamma} - \frac{\Gamma}{2}c_{2,\Gamma} - i\frac{\Omega_S}{2}c_{3,\Gamma}, \tag{3.23}$$

$$\dot{c}_{3,\Gamma} = -i\frac{\Omega_S}{2}c_{2,\Gamma}, \tag{3.24}$$

we can find the total-population time-derivative, with $P_{\Gamma,\Sigma} = \sum_{n=1}^{3}|c_{n,\Gamma}|^2$, to be

$$\dot{P}_{\Gamma,\Sigma} = \frac{d}{dt}(|c_{1,\Gamma}|^2 + |c_{2,\Gamma}|^2 + |c_{3,\Gamma}|^2) = -\Gamma|c_{2,\Gamma}|^2, \tag{3.25}$$

implying a transient population $P_{\Gamma,\Sigma}(t) = 1 - \int_{t_i}^{t}\Gamma|c_{2,\Gamma}|^2\,dt$. Eq. (3.25) shows that the total population decreases for any pulse shape of Ω_P and Ω_S (even if Γ were also time-dependent), as $\Gamma \geq 0$.

Dealing with the Hamiltonian (3.18) increases the difficulty of the computations, specially since it is non-hermitian, thus we consider the dissipation rate to produce a small deviation from the lossless evolution and we apply perturbation theory up to first order in Γ for the population loss. It is clear that we need only consider $c_{2,\Gamma} = c_2 + O(\Gamma)$, to attain a first-order–corrected population loss of

$$P_{\text{loss}} = 1 - P_{\Gamma,\Sigma}(t_f) = \Gamma\int_{t_i}^{t_f}|c_2|^2\,dt + O(\Gamma^2) \approx \Gamma\int_{t_i}^{t_f}|c_2|^2\,dt, \tag{3.26}$$

where Γ has been assumed time-independent. This expression allows us to compute the system's dynamics in absence of loss and to estimate the effect of such loss afterwards. Basically, the least we populate the upper state, the better, but we can quantify it via (3.26).

More accurately speaking, it is the ratio of Γ with Ω_P and Ω_S what measures the magnitude of the deviation that the dissipation rate will produce. Eq. (3.26) is then valid when the dissipation rate is much smaller than the peak Rabi frequency, typically at least 10 times smaller.

3.3.3 Consecutive π pulses

We can think of the Λ system as a pair of two-level systems with a common excited state. In this manner, we can apply a π pulse on each branch consecutively to transfer population between the lower levels. The π pulse is the well-known Rabi solution for the two-level system, i.e., for a two-level resonant system with Hamiltonian

$$H = \frac{\hbar\Omega(t)}{2}\begin{bmatrix} 0 & 1 \\ 1 & 0 \end{bmatrix}, \tag{3.27}$$

the corresponding evolution of the system is given by the propagator

$$U_{\Delta=0}^{\mathrm{SU}(2)} = \begin{bmatrix} \cos\frac{\mathcal{A}}{2} & -i\sin\frac{\mathcal{A}}{2} \\ -i\sin\frac{\mathcal{A}}{2} & \cos\frac{\mathcal{A}}{2} \end{bmatrix}, \tag{3.28}$$

where the partial area is $\mathcal{A}(t) = \int_{t_i}^{t} \Omega\, dt$ and population inversion is obviously acquired when $\mathcal{A} = \pi,\, 3\pi, \ldots$

Splitting the transfer $|1\rangle \to |3\rangle$ into two steps: first, in the interval $t_i \le t \le t_i + T/2$, $\Omega_P = \Omega$ while $\Omega_S = 0$ and the propagator $U_{\Delta=0}^{\mathrm{SU}(2)}$ acts on the $|1\rangle \leftrightarrow |2\rangle$ transition with $\mathcal{A} = \mathcal{A}_P \equiv \int_{t_i}^{t_i+T/2} P\, dt$, then, in the interval $t_i + T/2 \le t \le t_f$, $\Omega_S = \Omega$ while $\Omega_P = 0$ and the propagator acts on the $|2\rangle \leftrightarrow |3\rangle$ transition with $\mathcal{A} = \mathcal{A}_S \equiv \int_{t_i+T/2}^{t_f} \Omega_S\, dt$. The loss of population is then, explicitly,

$$P_{\mathrm{loss}} = \Gamma\left[\int_{t_i}^{t_i+T/2} \sin^2\frac{\mathcal{A}_P(t)}{2}\, dt + \int_{t_i+T/2}^{t_f} \cos^2\frac{\mathcal{A}_S(t)}{2}\, dt\right]. \tag{3.29}$$

Assuming a monotonic linear increase in the pulse area $\mathcal{A} = \mathcal{A}_P + \mathcal{A}_S$, that is to say, using constant amplitude Rabi frequencies, e.g., $\Omega_P = 2(2n+1)\pi/T$ and $\Omega_S = 2(2m+1)\pi/T$, the approximate population loss due, using (3.26), to dissipation is

$$\begin{aligned} P_{\mathrm{loss}} = \Gamma\Bigg[&\int_{t_i}^{t_i+T/2} \sin^2\frac{(2n+1)\pi(t-t_i)}{T}\, dt \\ &+ \int_{t_i+T/2}^{t_f} \cos^2\frac{(2m+1)\pi(t-t_i-T/2)}{T}\, dt\Bigg] = \frac{\Gamma T}{2}. \end{aligned} \tag{3.30}$$

This is the lossiest method since it deliberately produces complete population transfer to the lossy excited state.

3.3.4 Rabi method

One can obtain an exact solution for the fully resonant Λ system using the Rabi method just like for the two-level system, i.e. taking fully-overlapping controls (fields having the same time-dependence and equal Rabi frequencies). Thus, taking $\Omega_P(t) = \Omega_S(t) = \Omega(t)$, the Hamiltonian becomes

$$H = \frac{\hbar\Omega}{2}\begin{bmatrix} 0 & 1 & 0 \\ 1 & 0 & 1 \\ 0 & 1 & 0 \end{bmatrix} = \frac{\hbar\Omega}{2}\lambda_{16}, \tag{3.31}$$

where λ_{16} is the linear combination of generators of the SU(3) group: $\lambda_{16} = \lambda_1 + \lambda_6$.

The solution of the Schrödinger equation writes

$$|\psi(t)\rangle = \exp\left[-\frac{i}{2}\lambda_{16}\int_{t_i}^{t}\Omega(t')\,dt'\right]|\psi(t_i)\rangle, \tag{3.32}$$

since the time-dependent term, $\Omega(t)$, factorizes in (3.31), i.e., the Hamiltonian $H(t)$ commutes with itself at different times. This means, for the evolution operator,

$$U_{P=S} = \exp\left[-\frac{i}{2}\lambda_{16}\int_{t_i}^{t}\Omega(t')\,dt'\right] \tag{3.33}$$

$$= \frac{1}{2}\begin{bmatrix} 1+\cos\frac{\mathcal{A}}{2} & -i\sqrt{2}\sin\frac{\mathcal{A}}{2} & \cos\frac{\mathcal{A}}{2}-1 \\ -i\sqrt{2}\sin\frac{\mathcal{A}}{2} & 2\cos\frac{\mathcal{A}}{2} & -i\sqrt{2}\sin\frac{\mathcal{A}}{2} \\ \cos\frac{\mathcal{A}}{2}-1 & -i\sqrt{2}\sin\frac{\mathcal{A}}{2} & 1+\cos\frac{\mathcal{A}}{2} \end{bmatrix}, \tag{3.34}$$

with $\mathcal{A}(t) = \int_{t_i}^{t}\sqrt{\Omega_P^2(t') + \Omega_S^2(t')}\,dt' = \sqrt{2}\int_{t_i}^{t}\Omega(t')\,dt'$.

For a transfer $|1\rangle \to |3\rangle$, the area of each control field is required to rise until it reaches $\mathcal{A} = 2(2n-1)\pi$, with $n = 1, 2\ldots$, which necessitates to populate the intermediate state transiently up to $P_2 = ½$ when the area passes by $\mathcal{A}(t_n) = (2n-1)\pi$; occurring n times. This transfer leads to a loss of

$$P_{\text{loss}} = \frac{\Gamma}{2}\int_{t_i}^{t_f}\sin^2\frac{\mathcal{A}(t)}{2}\,dt, \tag{3.35}$$

which becomes, for rectangular pulses of constant amplitude $\Omega_m = \sqrt{2}(2n-1)\pi/T$,

$$P_{\text{loss}} = \frac{\Gamma}{2}\int_{t_i}^{t_f}\sin^2\frac{(2n-1)\pi(t-t_i)}{T}\,dt = \frac{\Gamma T}{4}, \tag{3.36}$$

i.e. half of the loss resulting of using consecutive π pulses.

3.4 STIRAP

In STIRAP, the state of the system is written in terms of the eigenstates of the Hamiltonian and these are parameterized with trigonometric functions of angular variables, or a single one of these for the resonant Hamiltonian (3.18). The so-called mixing angle $\vartheta(t)$, is given by

$$\sin\vartheta = \Omega_P/\sqrt{\Omega_P^2+\Omega_S^2}, \qquad \cos\vartheta = \Omega_S/\sqrt{\Omega_P^2+\Omega_S^2}, \tag{3.37}$$

and serves as an indicator of the distribution of population between states $|1\rangle$ and $|3\rangle$, the states among which we want to transfer population, as it is clear from the expressions of the Hamiltonian eigenstates,

$$|\Phi_0\rangle = \begin{bmatrix} \cos\vartheta \\ 0 \\ -\sin\vartheta \end{bmatrix}, \quad |\Phi_\pm\rangle = \frac{1}{\sqrt{2}}\begin{bmatrix} \sin\vartheta \\ \pm 1 \\ \cos\vartheta \end{bmatrix}, \tag{3.38}$$

where both eigenstates present an invariable excited state population while P_1 and P_3 are, consequently, complementary to each other. The eigenvectors $|\Phi_0\rangle$ and $|\Phi_\pm\rangle$ correspond to the eigenvalues

$$\epsilon_0(t) = 0, \quad \epsilon_\pm(t) = \pm\frac{\hbar}{2}\sqrt{\Omega_P^2+\Omega_S^2}. \tag{3.39}$$

Our goal is to follow a parametrized state that would allow us to control the transfer of population between the ground states with a controlled transient population in the excited state (imposed low in general to minimize the loss) by providing a suitable tracking solution to the parameters, which would translate, in turn, into shapes or conditions for the pulses Ω_P and Ω_S. For this purpose, STIRAP attempts to follow the Hamiltonian eigenstate $|\Phi_0\rangle$ whose projection on the excited state is always null, called dark state. However, writing the Schrödinger equation in the basis of the Hamiltonian eigenstates $|\Phi_n\rangle$ shows that these states are coupled by the derivatives of the mixing angle, i.e. applying the transformation

$$T_{\text{ad}}(t) = \sum_n |\Phi_n\rangle\langle n| = \frac{1}{\sqrt{2}}\begin{bmatrix} \sin\vartheta & \sqrt{2}\cos\vartheta & \sin\vartheta \\ -1 & 0 & 1 \\ \cos\vartheta & -\sqrt{2}\sin\vartheta & \cos\vartheta \end{bmatrix}, \tag{3.40}$$

that takes the state of the system from the adiabatic states basis to the bare states basis, we obtain the adiabatic Hamiltonian (the effective Hamiltonian in the adia-

batic basis) and non-adiabatic coupling:

$$H^{\mathrm{ad}}(t) = T_{\mathrm{ad}}^{\dagger} H T_{\mathrm{ad}} - i\hbar T_{\mathrm{ad}}^{\dagger} \dot{T}_{\mathrm{ad}} = \begin{bmatrix} \epsilon_- & 0 & 0 \\ 0 & 0 & 0 \\ 0 & 0 & \epsilon_+ \end{bmatrix} - i\frac{\hbar\dot{\vartheta}}{\sqrt{2}} \begin{bmatrix} 0 & -1 & 0 \\ 1 & 0 & 1 \\ 0 & -1 & 0 \end{bmatrix}, \tag{3.41a}$$

$$\dot{\vartheta}(t) = \frac{\dot{\Omega}_P \Omega_S - \Omega_P \dot{\Omega}_S}{\Omega_P^2 + \Omega_S^2}. \tag{3.41b}$$

The non-adiabatic correction is given at the lowest order by the strength of this non-adiabatic coupling between the adiabatic states $|\Phi_n\rangle$ with respect to the energy gap between them, i.e.,

$$\frac{\hbar|\dot{\vartheta}|/\sqrt{2}}{|\epsilon_\pm|} = \sqrt{2}\frac{|\dot{\Omega}_P\Omega_S - \Omega_P\dot{\Omega}_S|}{(\Omega_P^2+\Omega_S^2)^{3/2}} \sim \frac{(\Omega_0^2/T)}{\Omega_0^3}\frac{|f_S\partial_s f_P - f_P\partial_s f_S|}{(f_P^2+f_S^2)^{3/2}} = \frac{f(s)}{\Omega_0 T}, \tag{3.42}$$

where T is the pulse duration, Ω_0 the maximum amplitude of each pulse (assumed to be equal for both pulses), $f_{P,S}(s)$ are the time-shapes of the Ω_P and Ω_S fields, respectively, $s = t/T$ is a unitless normalized time, and $f(s)$ is a function of time provided by the pulse shapes. This shows that the non-adiabatic connection is smaller for larger pulse areas.

This non-adiabatic term implies that even if we prepare our pulses to follow the $|\Phi_0\rangle$ state (naturally, also preparing the system such that $|\psi(t_i)\rangle = |\Phi_0(t_i)\rangle$ at the beginning of the process), the population would be transferred to the other states, i.e. the system would not follow exactly the prescribed dynamics of the $|\Phi_0\rangle$ state. The derivative of the mixing angle, the speed of population change between the ground states, is a measure of the departure from adiabaticity the process suffers and is due to this that it is referred as the non-adiabatic coupling. A fast process, a swift population evolution, means a strong coupling between the eigenstates of the Hamiltonian. In contrast, an infinitely slow process means an infinitesimally weak coupling.

The eigenstates of the Hamiltonian, the so-called adiabatic states, are the keystones of STIRAP and can then be followed exactly by the system only at the adiabatic limit (when the diabatic coupling tends to zero, i.e. $\dot{\vartheta} \to 0$). Under this

condition, the propagator is then

$$\begin{aligned}
\lim_{\dot\vartheta\to 0} U(t) &= \lim_{\dot\vartheta\to 0} T_{\mathrm{ad}}(t) U^{\mathrm{ad}}(t) T_{\mathrm{ad}}^{\dagger}(t_i) \\
&= T_{\mathrm{ad}}(t) \exp\left[-\frac{i}{\hbar}\int_{t_i}^{t} \lim_{\dot\vartheta\to 0} H^{\mathrm{ad}}(t')\,dt'\right] T_{\mathrm{ad}}^{\dagger}(t_i), \\
&= \sum_{n=1}^{3} \exp\left[-\frac{i}{\hbar}\int_{t_i}^{t} \epsilon_n(t')\,dt'\right] |\Phi_n\rangle\langle\Phi_n(t_i)|, \qquad (3.43a) \\
&= \begin{bmatrix} |\Psi_-\rangle & |\Psi_0\rangle & |\Psi_+\rangle \end{bmatrix}, \qquad (3.43b)
\end{aligned}$$

where the column vectors, with $\hbar\xi \equiv \int_{t_i}^{t} \epsilon_+(t')\,dt$, are

$$\begin{aligned}
|\Psi_-\rangle &= \begin{bmatrix} \cos\vartheta_i\cos\vartheta + \sin\vartheta_i\sin\vartheta\cos\xi \\ -i\sin\vartheta_i\sin\xi \\ -\cos\vartheta_i\sin\vartheta + \sin\vartheta_i\cos\vartheta\cos\xi \end{bmatrix}, \\
&= \cos\vartheta_i|\Phi_0\rangle + \frac{\sin\vartheta_i}{\sqrt{2}}\big(e^{i\xi}|\Phi_-\rangle + e^{-i\xi}|\Phi_+\rangle\big), \qquad (3.44a) \\
|\Psi_0\rangle &= \begin{bmatrix} -i\sin\vartheta\sin\xi \\ \cos\xi \\ -i\cos\vartheta\sin\xi \end{bmatrix} = \frac{1}{\sqrt{2}}\big(e^{-i\xi}|\Phi_+\rangle - e^{i\xi}|\Phi_-\rangle\big), \qquad (3.44b) \\
|\Psi_+\rangle &= \begin{bmatrix} -\sin\vartheta_i\cos\vartheta + \cos\vartheta_i\sin\vartheta\cos\xi \\ -i\cos\vartheta_i\sin\xi \\ \sin\vartheta_i\sin\vartheta + \cos\vartheta_i\cos\vartheta\cos\xi \end{bmatrix}, \\
&= -\sin\vartheta_i|\Phi_0\rangle + \frac{\cos\vartheta_i}{\sqrt{2}}\big(e^{i\xi}|\Phi_-\rangle + e^{-i\xi}|\Phi_+\rangle\big). \qquad (3.44c)
\end{aligned}$$

Equation (3.43a) means that the system will remain in whatever superposition of adiabatic states it was initially found to be and only the relative phase between them will change along the evolution. The accumulated relative phases being given by the integral of the eigenenergies $\epsilon_\pm$.

Three initial conditions are most notable: $\vartheta_i = n\pi$, $\vartheta_i = (2n+1)\pi/2$, and $\vartheta_i = (2n+1)\pi/4$. In the first case, achieved for a Stokes–pump sequence of pulses, a system initially in state $|1\rangle$ would evolve along the dark state $|\Phi_0\rangle$, thus never populating the excited state (in the adiabatic limit). This is not the case if, instead, the system is prepared to be in any other state —or a superposition of, or with, them—. In the second case, achieved for a pump–Stokes sequence, the situation is inverted and only a system initially in $|3\rangle$ would evolve along $|\Phi_0\rangle$ while any other initial state would lead to populating the excited state along the dynamics. Although we may produce a NOT gate of sorts between the ground states, i.e. a propagator

$U^{\text{NOT}} = e^{in\pi}\begin{bmatrix}0 & \pm 1\\ 1 & 0\end{bmatrix}$, by using $\vartheta = m\pi$ and $\vartheta = (2l+1)\pi/2$ as initial and final conditions, respectively and *viceversa*, while enforcing $\xi_f = p\pi$ (a generalized pulse area multiple of 2π), the excited state will be populated "asymmetrically" depending on the initial distribution of populations. The third and last case is meant as the middle point between the other two when the goal is to produce a NOT gate: the excited state is populated up to $P_2 = ½$ irrespective of the initial superposition, compared to the transiently complete population in the excited state for the asymmetric NOT gate. For a population transfer $|1\rangle \to |3\rangle$, the first and second cases correspond to counter-intuitively– and intuitively–ordered control fields, while the third case correspond to equal couplings $|\Omega_P| = |\Omega_S|$. As a side note, $\vartheta_i = \pi/4$ leads to a NOT gate with $U_{13}^{\text{NOT}} = |U_{31}^{\text{NOT}}|$ when $\xi_f = (2n+1)\pi$ and $\vartheta_f = (4n+1)\pi/4$, and $U_{13}^{\text{NOT}} = -|U_{31}^{\text{NOT}}|$ when $\xi_f = 2n\pi$ and $\vartheta_f = (4n+3)\pi/4$.

The idea with STIRAP is to follow the dark state, whose desired dynamics prescribes the signature counterintuitive ordering of Ω_P and Ω_S, by minimizing the diabatic coupling as to make negligible the deviations to other adiabatic states. Meanwhile, utilizing intuitively-ordered fields is referred to as bright STIRAP since it leads to larger transient populations on the excited state. Adiabaticity is then the condition in which the coupling between the adiabatic states, or at least between the dark state (the one where the excited state remains unpopulated) and the brights (those who allow population in the excited state), are negligible. Naturally, very slow-evolving pulses would minimize the derivative of the mixing angle and practically uncouple the adiabatic states in consequence. Nevertheless, the adiabatic states can never be followed exactly in real-world implementations.

3.4.1 Loss in STIRAP

Using perturbation theory we may estimate the loss due to imperfect adiabaticity incurred during the application of STIRAP. Considering the adiabatic coupling to be a small deviation to the Hamiltonian in the adiabatic basis (3.41a), i.e., $H^{\text{ad}} = H_0 + \epsilon V$, where $H_0 = \lim_{\dot\vartheta\to 0} H^{\text{ad}} = T_{\text{ad}}^\dagger H T_{\text{ad}}$, $V = -i\hbar T_{\text{ad}}^\dagger \dot T_{\text{ad}}$, and ϵ only labels the perturbation term, we can write the Schrödinger equation in the interaction representation with the interaction propagator $U_I = U_0^{\text{ad}\dagger} U^{\text{ad}}$ and interaction Hamiltonian $H_I = \epsilon V_I = \epsilon U_0^{\text{ad}\dagger} V U_0^{\text{ad}}$, $i\hbar \dot U_I = \epsilon V_I U_I$, where $U_0^{\text{ad}} = \lim_{\dot\vartheta\to 0} U^{\text{ad}} = \sum_{n=1}^{3} e^{-i\int_{t_i}^{t}\epsilon_n(t')\,dt'/\hbar}|n\rangle\langle n|$ is the propagator solution of the Schrödinger equation for H_0 shown in (3.43b) with (3.44). The factor ϵ takes into account the non-adiabatic strength with respect to the gap between the considered adiabatic energies.

The interaction propagator can be obtained perturbatively as

$$U_I = \mathbb{1} - \frac{i\epsilon}{\hbar}\int_{t_i}^{t} V_I(t')\,dt' - \frac{\epsilon^2}{\hbar^2}\int_{t_i}^{t}\int_{t_i}^{t'} V_I(t')V_I(t'')\,dt''dt' - O(\epsilon^3). \tag{3.45}$$

Here, ϵ allows one to keep track of the perturbation order and will be set to 1 at the end of the calculation. The system propagator in the bare states basis is then $U = U_0 + U_1 + U_2 + \widetilde{O}(\epsilon^3)$, with

$$\begin{aligned}
U_0 &= T_{\rm ad}U_0^{\rm ad}T_{\rm ad}^{\dagger}(t_i),\\
&= e^{i\xi}|\Phi_-\rangle\langle\Phi_-(t_i)| + |\Phi_0\rangle\langle\Phi_0(t_i)| + e^{-i\xi}|\Phi_+\rangle\langle\Phi_+(t_i)|, &\text{(3.46a)}\\
U_1 &= -\frac{i\epsilon}{\hbar}T_{\rm ad}U_0^{\rm ad}\int_{t_i}^{t} V_I'\,dt'\; T_{\rm ad}^{\dagger}(t_i),\\
&= \frac{\epsilon}{\sqrt{2}}\Bigg[e^{i\xi}|\Phi_-\rangle\langle\Phi_0(t_i)|\int_{t_i}^{t}\dot\vartheta' e^{-i\xi'}\,dt' + e^{-i\xi}|\Phi_+\rangle\langle\Phi_0(t_i)|\int_{t_i}^{t}\dot\vartheta' e^{i\xi'}\,dt'\\
&\qquad - |\Phi_0\rangle\langle\Phi_-(t_i)|\int_{t_i}^{t}\dot\vartheta' e^{i\xi'}\,dt' - |\Phi_0\rangle\langle\Phi_+(t_i)|\int_{t_i}^{t}\dot\vartheta' e^{-i\xi'}\,dt'\Bigg], &\text{(3.46b)}\\
U_2 &= -\frac{\epsilon^2}{\hbar^2}T_{\rm ad}U_0^{\rm ad}\int_{t_i}^{t}\int_{t_i}^{t'} V_I'V_I''\,dt''dt'\; T_{\rm ad}^{\dagger}(t_i),\\
&= -\frac{\epsilon^2}{2}\Bigg[e^{i\xi}|\Phi_-\rangle\langle\Phi_-(t_i)|\int_{t_i}^{t}\int_{t_i}^{t'}\dot\vartheta'\dot\vartheta'' e^{-i(\xi'-\xi'')}\,dt''dt'\\
&\qquad + e^{i\xi}|\Phi_-\rangle\langle\Phi_+(t_i)|\int_{t_i}^{t}\int_{t_i}^{t'}\dot\vartheta'\dot\vartheta'' e^{-i(\xi'+\xi'')}\,dt''dt'\\
&\qquad + e^{-i\xi}|\Phi_+\rangle\langle\Phi_-(t_i)|\int_{t_i}^{t}\int_{t_i}^{t'}\dot\vartheta'\dot\vartheta'' e^{i(\xi'+\xi'')}\,dt''dt'\\
&\qquad + e^{-i\xi}|\Phi_+\rangle\langle\Phi_+(t_i)|\int_{t_i}^{t}\int_{t_i}^{t'}\dot\vartheta'\dot\vartheta'' e^{i(\xi'-\xi'')}\,dt''dt'\\
&\qquad + 2|\Phi_0\rangle\langle\Phi_0(t_i)|\int_{t_i}^{t}\int_{t_i}^{t'}\dot\vartheta'\dot\vartheta''\cos(\xi'-\xi'')\,dt''dt'\Bigg]. &\text{(3.46c)}
\end{aligned}$$

and

$$V_I(t) = -i\frac{\hbar v\dot\vartheta(t)}{\sqrt{2}}\begin{bmatrix} 0 & -e^{-i\xi(t)} & 0\\ e^{i\xi(t)} & 0 & e^{-i\xi(t)}\\ 0 & -e^{i\xi(t)} & 0\end{bmatrix}. \tag{3.47}$$

The dynamics of the excited state for a system initially in $|1\rangle$ would be, perturba-

tively,

$$\begin{aligned} c_2(t) &= c_2^{(0)} + \epsilon c_2^{(1)} + \epsilon^2 c_2^{(2)} + \cdots = \sum_n \langle 2|U_n(\epsilon^n)|1\rangle, \\ &= -i \sin\vartheta_i \sin\xi - i\epsilon \cos\vartheta_i \operatorname{Im}\left(e^{i\xi} \int_{t_i}^{t} \dot{\vartheta}' e^{-i\xi'}\, dt' \right) \\ &\quad + i\epsilon^2 \sin\vartheta_i \operatorname{Im}\left(e^{i\xi} \int_{t_i}^{t} \dot{\vartheta}' e^{-i\xi'} \int_{t_i}^{t'} \dot{\vartheta}'' \cos\xi''\, dt'' dt' \right) + O(\epsilon^3), \end{aligned} \tag{3.48}$$

with its corresponding population

$$|c_2|^2 = \left|c_2^{(0)}\right|^2 + 2\epsilon \operatorname{Re}\left[\bar{c}_2^{(0)} c_2^{(1)}\right] + \epsilon^2 \left\{ \left|c_2^{(1)}\right|^2 + 2\operatorname{Re}\left[\bar{c}_2^{(0)} c_2^{(2)}\right] \right\} + O(\epsilon^3). \tag{3.49}$$

We can illustrate the loss of each method by prescribing a simple analytical model for the coupling fields. For the population transfer $|1\rangle \to |3\rangle$ we may consider the three dynamics mentioned before for ϑ: $0 \to \pi/2$, $\pi/2 \to 0$, and $\pi/4 \to \pi/4$ (since a sign-change of the fields is undesirable). A simple model for the evolution $\pi/4 \to \pi/4$ with $\xi_f = 2\mathcal{A} = (2n+1)\pi$ to achieve the transfer, which has already been discussed to be a `NOT` gate between the ground states, is that of fields with equal and constant amplitudes (corresponding to the model we used for the Rabi method). In the case of equal couplings the dynamics corresponds exactly with the Rabi model since the non-adiabatic coupling $\dot{\vartheta}$ is null.

A very relevant and analytically solvable model for the other two cases, traditional (dark) and bright STIRAP, is that of cosine–sine pulses: using the sine and cosine functions, truncated to a quarter of their period, as the fields which are also taken to have the same maximum amplitude Ω_0. For STIRAP we would use the sine function for the pump and the cosine for the Stokes, we invert this association for bright STIRAP. Then

$$\xi = \frac{\Omega_0}{2}(t - t_i), \quad \dot{\vartheta} = \frac{\dot{\Omega}_P \Omega_S - \dot{\Omega}_S \Omega_P}{\Omega_P^2 + \Omega_S^2} = (\delta_d - \delta_b)\frac{\pi}{2T}, \quad \mathcal{A} = \Omega_0 T, \tag{3.50}$$

where δ_d and δ_b are equal to 1 for dark and bright STIRAP, respectively, and zero otherwise, and

$$c_2^{(0)} = -i\delta_b \sin\left[\frac{\Omega_0}{2}(t - t_i)\right], \tag{3.51a}$$

$$c_2^{(1)} = -i\frac{2\delta_d(\delta_d - \delta_b)\pi}{\Omega_0 T} \sin^2\left[\frac{\Omega_0}{4}(t - t_i)\right], \tag{3.51b}$$

$$c_2^{(2)} = i\frac{\delta_b \pi^2}{4\Omega_0^2 T^2} \left\{ 2\sin\left[\frac{\Omega_0}{2}(t - t_i)\right] - \Omega_0 (t - t_i) \cos\left[\frac{\Omega_0}{2}(t - t_i)\right] \right\}. \tag{3.51c}$$

$$\int_{t_i}^{t_f} \left|c_2^{(0)}\right|^2 dt = \delta_b \frac{T}{2}\left(1 - \frac{\sin\mathcal{A}}{\mathcal{A}}\right), \tag{3.52a}$$

$$\int_{t_i}^{t_f} \bar{c}_2^{(0)} c_2^{(1)}\, dt = 0, \tag{3.52b}$$

$$\int_{t_i}^{t_f} \left|c_2^{(1)}\right|^2 dt = \delta_d \frac{\pi^2 T}{2\mathcal{A}^2}\left[3 - \frac{8\sin(\mathcal{A}/2) - \sin\mathcal{A}}{\mathcal{A}}\right], \tag{3.52c}$$

$$\int_{t_i}^{t_f} \bar{c}_2^{(0)} c_2^{(2)}\, dt = -\delta_b \frac{\pi^2 T}{8\mathcal{A}^2}\left(2 + \cos\mathcal{A} - \frac{3\sin\mathcal{A}}{\mathcal{A}}\right). \tag{3.52d}$$

Thus, the losses up to second order of the non-adiabatic coupling with cosine–sine fields, are

$$P_{\text{loss}}^d = \frac{\Gamma T}{2(\mathcal{A}/\pi)^2}\left[3 - \frac{8\sin(\mathcal{A}/2) - \sin\mathcal{A}}{\mathcal{A}}\right] \xrightarrow[\mathcal{A}\gg 1]{} \frac{3\Gamma T}{2(\mathcal{A}/\pi)^2}, \tag{3.53a}$$

$$P_{\text{loss}}^b = \frac{\Gamma T}{2}\left[1 - \frac{\sin\mathcal{A}}{\mathcal{A}} - \frac{1}{2(\mathcal{A}/\pi)^2}\left(2 + \cos\mathcal{A} - \frac{3\sin\mathcal{A}}{\mathcal{A}}\right)\right] \xrightarrow[\mathcal{A}\gg 1]{} \frac{\Gamma T}{2}, \tag{3.53b}$$

for dark and bright STIRAP, respectively. We notice that the loss of bright STIRAP does not decrease for better adiabaticity (i.e. larger pulse area), contrarily to the dark STIRAP.

The fidelity of the transfer

$$\begin{aligned}
|c_3(t_f)|^2 &= \left|\sum_n \langle 3|U_n(t_f,t_i)|1\rangle\right|^2, \\
&= \left|c_3^{(0)}(t_f)\right|^2 + 2\epsilon\,\mathrm{Re}\left[\bar{c}_3^{(0)}(t_f)c_3^{(1)}(t_f)\right] \\
&\quad + \epsilon^2\left\{\left|c_3^{(1)}(t_f)\right|^2 + 2\,\mathrm{Re}\left[\bar{c}_3^{(0)}(t_f)c_3^{(2)}(t_f)\right]\right\} + O(\epsilon^3) \\
&= \delta_b \cos\frac{\mathcal{A}}{2}\left(\cos\frac{\mathcal{A}}{2} - \epsilon^2\frac{\pi^2}{2\mathcal{A}}\sin\frac{\mathcal{A}}{2}\right) \\
&\quad + \delta_d\left(1 - \epsilon^2\frac{4\pi^2}{\mathcal{A}^2}\sin^2\frac{\mathcal{A}}{4}\right) + O(\epsilon^3).
\end{aligned} \tag{3.54}$$

With a target state population of, up to the second order of non-adiabatic deviation,

$$P_{3f} = 1 - \frac{4\pi^2}{\mathcal{A}^2}\sin^2\frac{\mathcal{A}}{4}, \tag{3.55}$$

for dark STIRAP. Considering up to the second order non-adiabatic correction, we visualize the first message of STIRAP: for a large enough area, the system will evolve towards the target state and reach it asymptotically ($\lim_{\mathcal{A}\to\infty} P_{3f} = 1$). According to this expression, $\mathcal{A} = 4\pi$ is the minimum pulse area to produce complete population

transfer. Up to this order, the transfer is exact ($P_{3f} = 1$) for $\mathcal{A} = 4n\pi$, with respect to which the first nonzero order of deviation on the area would be

$$\Delta P_{3f}(\mathcal{A} \to 4n\pi) = P_{3f}(4n\pi + \Delta\mathcal{A}) - P_{3f}(4n\pi) = -\frac{\Delta\mathcal{A}^2}{4(\mathcal{A}/\pi)^2}. \tag{3.56}$$

From this, we extract the second message of STIRAP: transfer sensitivity decreases as we increase the pulse area. While the Rabi transfer displays a squared robustness profile on the area deviations, $\Delta P_{3f} \propto -(\Delta\mathcal{A})^2$, negative signifying the target-state–population reduction caused by any area deviation, STIRAP diminishes this relation by making it inversely proportional to the magnitude of used area, $\Delta P_{3f} \propto \mathcal{A}^{-2}$.

Regarding the loss of population due to dissipation during STIRAP,

$$P_{\text{loss}} \approx \frac{3\Gamma T}{2(\mathcal{A}/\pi)^2}, \tag{3.57}$$

the third and last main message of STIRAP is exhibited: the loss is inversely proportional to the pulse area, thus, in the ideal adiabatic evolution, there is no loss of population, $\lim_{\mathcal{A}\to\infty} P_{\text{loss}} = 0$, as the excited state is not at all populated in the adiabatic limit. For the "exact" transfers of this model, with $\mathcal{A} = 4n\pi$, Eq. (3.57) is valid exactly.

In the case of bright STIRAP with intuitively-ordered sine–cosine pulses, the final population on the target state up to second order of non-adiabatic perturbation,

$$P_{3f} = \cos^2\frac{\mathcal{A}}{2} - \frac{\pi^2}{4}\frac{\sin\mathcal{A}}{\mathcal{A}}, \tag{3.58}$$

tends to Rabi oscillations between complete and zero population transfers for large areas, i.e. $\lim_{\mathcal{A}\to\infty} P_{3f} = \cos^2(\mathcal{A}/2)$, with the exact (up to second order) transfer condition being $\mathcal{A} = 2n\pi$. The population deviation around these points up to second order,

$$\begin{aligned}\Delta P_{3f}(\mathcal{A} \to 2n\pi) &= P_{3f}(2n\pi + \Delta\mathcal{A}) - P_{3f}(2n\pi) \\ &= -\frac{\pi^2}{16}\frac{\Delta\mathcal{A}}{\mathcal{A}} - \frac{1}{4}\left(1 - \frac{\pi^2}{\mathcal{A}^2}\right)\Delta\mathcal{A}^2 \xrightarrow[\mathcal{A}\to\infty]{} -\frac{\Delta\mathcal{A}^2}{4},\end{aligned} \tag{3.59}$$

is linearly dependent on the area deviations for small areas and quadratic for large areas. However, the sensitivity is not further reduced by an increase of the area, as with traditional counter–intuitive STIRAP. With respect to the loss up to second

order and about the pseudo-exact transfers of $\mathcal{A} = 2n\pi$,

$$P_{\text{loss}} \approx \frac{\Gamma T}{2}\left(1 - \frac{\Delta\mathcal{A}}{\mathcal{A}} - \frac{3\pi^2}{2\mathcal{A}^2}\right), \tag{3.60}$$

it finds its minimum at the lowest transfer-producing area for this model, $\mathcal{A} = 2\pi$, while remaining still larger than the Rabi-method result, and tends to the consecutive π-pulses result for large areas, i.e.

$$P_{\text{loss}} \xrightarrow[\mathcal{A}=2\pi]{} P_{\text{loss}}^{\min} \approx \frac{5\Gamma T}{16}, \quad P_{\text{loss}} \xrightarrow[\mathcal{A}\gg 1]{} P_{\text{loss}}^{\max} = \frac{\Gamma T}{2}. \tag{3.61}$$

3.5 Counter-diabatic driving via superadiabaticity

3.5.1 Superadiabatic transformation

The adiabatic technique means that the dynamics follows approximately one (or more) instantaneous eigenstate(s) of the Hamiltonian. A transfer is achieved when one eigenstate is initially connected to the initial state and finally connected to the target state.

The adiabatic transfer from the initial ground state (connected to the pump coupling) to the target ground state (connected to the Stokes coupling) is ensured when $\vartheta(t_i) = 0$ and $\vartheta(t_f) = \pi/2$ (with t_i and t_f the initial and final times, respectively), since, in this case, the adiabatic dark state connects the initial state initially and the target state finally, Eqs. (3.44) and (3.38). This is achieved by a counterintuitive Stokes–pump sequence.

In order to improve the approximation (3.43a), one can iterate the procedure of diagonalizing the Hamiltonian and deriving their superadiabatic iterations, e.g., we provide, by diagonalizing H^{ad}, the second iteration (to which we refer as second order):

$$H_2^{\text{sa}} \equiv T_2^\dagger H^{\text{ad}} T_2 - i\hbar T_2^\dagger \dot{T}_2 = (T_{\text{ad}}T_2)^\dagger H T_{\text{ad}} T_2 - i\hbar (T_{\text{ad}}T_2)^\dagger \frac{d}{dt}(T_{\text{ad}}T_2). \tag{3.62}$$

We obtain, for $H^{\text{ad}}|\chi_n\rangle = \zeta_n|\chi_n\rangle$,

$$T_2 = \sum_n |\chi_n\rangle\langle n| = \begin{bmatrix} \cos^2(\vartheta_2/2) & i\sin(\vartheta_2)/\sqrt{2} & \sin^2(\vartheta_2/2) \\ i\sin(\vartheta_2)/\sqrt{2} & \cos\vartheta_2 & -i\sin(\vartheta_2)/\sqrt{2} \\ \sin^2(\vartheta_2/2) & -i\sin(\vartheta_2)/\sqrt{2} & \cos^2(\vartheta_2/2) \end{bmatrix}, \tag{3.63}$$

where

$$\sin\vartheta_2 \equiv 2\dot{\vartheta}/\Omega_1, \qquad \cos\vartheta_2 \equiv \Omega_0/\Omega_1, \tag{3.64a}$$

$$\Omega_0 \equiv \sqrt{\Omega_P^2+\Omega_S^2}, \qquad \Omega_1 \equiv \sqrt{\Omega_0^2+4\dot{\vartheta}^2}. \tag{3.64b}$$

This corresponds to the effective superadiabatic Hamiltonian

$$H_2^{\mathrm{sa}} = \begin{bmatrix} \zeta_- & 0 & 0 \\ 0 & 0 & 0 \\ 0 & 0 & \zeta_+ \end{bmatrix} + \frac{\hbar\dot{\vartheta}_2}{\sqrt{2}} \begin{bmatrix} 0 & 1 & 0 \\ 1 & 0 & -1 \\ 0 & -1 & 0 \end{bmatrix}, \quad \zeta_\pm = \pm\frac{\hbar\Omega_1}{2}, \tag{3.65}$$

and the second-order non-adiabatic coupling (deviation)

$$\dot{\vartheta}_2 = \frac{2}{1+4(\dot{\vartheta}/\Omega_0)^2}\frac{\partial}{\partial t}\left(\frac{\dot{\vartheta}}{\Omega_0}\right) = 2\frac{\ddot{\vartheta}\Omega_0 - \dot{\vartheta}\dot{\Omega}_0}{\Omega_0^2+4\dot{\vartheta}^2}. \tag{3.66}$$

The superadiabatic correction is

$$\frac{\hbar|\dot{\vartheta}_2|/\sqrt{2}}{|\zeta_\pm|} = \frac{2\sqrt{2}|\partial_t(\dot{\vartheta}/\Omega_0)|}{\Omega_0\left[1+4(\dot{\vartheta}/\Omega_0)^2\right]^{3/2}} \sim \frac{|\partial_s f|/\sqrt{f_P^2+f_S^2}}{\Omega_m^2T^2\left[1+4f^2/(\Omega_m^2T^2)\right]^{3/2}}, \tag{3.67}$$

where $s = t/T$ is a unitless normalized time, $f(s)$ and $f_{P,S}(s)$ are shape functions [see Eq. (3.42)], both fields have the same maximum amplitude Ω_m, and T is the pulse duration. The superadiabatic limit, under which the superadiabatic correction is neglected and the superadiabatic Hamiltonian is diagonal, is equivalent to the adiabatic limit in that it requires large areas to be negligible; moreover, it corresponds to a smaller (higher-order) correction.

The superadiabatic propagator at the superadiabatic limit,

$$U_0^{\mathrm{sa}} = \lim_{\dot{\vartheta}_2\to 0} U^{\mathrm{sa}} = \sum_n e^{-i\int_{t_i}^t \zeta_n(t')/\hbar\, dt'}|n\rangle\langle n|, \tag{3.68}$$

leads us to the zeroth order of the expansion of the propagator of the system, with $\hbar\kappa \equiv \int_{t_i}^t \zeta_+(t')\,dt'$,

$$\begin{aligned} U_0 &= T_{\mathrm{ad}}T_2U_0^{\mathrm{sa}}T_2^\dagger(t_i)T_{\mathrm{ad}}^\dagger(t_i), \\ &= \sum_{nml} e^{-i\int_{t_i}^t \zeta_m(t')/\hbar\, dt'}\langle n|\chi_m\rangle\langle\chi_m(t_i)|l\rangle|\Phi_n\rangle\langle\Phi_l(t_i)|. \end{aligned} \tag{3.69}$$

The first column of the propagator,

$$\begin{aligned} U_0|1\rangle = \frac{1}{\sqrt{2}}\sin\vartheta_i\Big\{ & i2\sin\kappa\Big[\cos^2(\vartheta_2/2)\Big(|\Phi_-\rangle - |\Phi_+\rangle\Big) \\ & + \frac{i}{\sqrt{2}}\sin\vartheta_2|\Phi_0\rangle\Big] + e^{i\kappa}|\Phi_+\rangle + e^{-i\kappa}|\Phi_-\rangle\Big\} \\ & + \cos\vartheta_i\Bigg\{\cos\vartheta_{2i}\Big[\frac{i}{\sqrt{2}}\sin\vartheta_2\Big(|\Phi_-\rangle - |\Phi_+\rangle\Big) + \cos\vartheta_2|\Phi_0\rangle\Big] \\ & - \frac{i}{\sqrt{2}}\sin\vartheta_{2i}\Bigg\{2\cos\kappa\Bigg[\Big(|\Phi_-\rangle - |\Phi_+\rangle\Big)\cos^2\frac{\vartheta_2}{2} \\ & + \frac{i}{\sqrt{2}}\sin\vartheta_2|\Phi_0\rangle\Bigg] + e^{i\kappa}|\Phi_+\rangle - e^{-i\kappa}|\Phi_-\rangle\Bigg\}\Bigg\}, \end{aligned} \tag{3.70}$$

is of particular importance since its parametrization can be used as that of the system state when $|\psi_i\rangle = |1\rangle$. Although no initial value of ϑ_n is invalid for the propagator nor for the system initial condition, some values facilitate the understanding of the corresponding dynamics; three conditions are most relevant:

1. $\vartheta_i = 0$, $\vartheta_{2i} = 0$, i.e.

$$\begin{aligned} U_0|1\rangle &= \cos\vartheta_2|\Phi_0\rangle + \frac{i}{\sqrt{2}}\sin\vartheta_2\Big(|\Phi_-\rangle - |\Phi_+\rangle\Big), \\ &= \begin{bmatrix} \cos\vartheta_2\cos\vartheta \\ -i\sin\vartheta_2 \\ -\cos\vartheta_2\sin\vartheta \end{bmatrix}, \end{aligned} \tag{3.71}$$

   which corresponds to equalizing the superadiabatic basis of second order to the dark state of the adiabatic basis (superadiabatic basis of first order) at initial time. To reach the target state $|\psi_f\rangle = \pm|3\rangle$ in the most direct way demands the terminal value $\vartheta_f = \pm\pi/2$ and, trying to avoid populating the excited state, $\vartheta_{2f} = 0$.

   Under these conditions, we may describe (super)adiabatic following of the dark state with a deviation, given by the second order mixing angle ϑ_2, that accounts for the more realistic condition of allowing to transiently populate the excited state. As with STIRAP, the conditions $\vartheta_i = 0$, $\vartheta_f = \pm\pi/2$ correspond to counter-intuitively ordered pump–Stokes pulses; while $\vartheta_{2i,2f} = 0$ correspond to the nullification of the first order non-adiabatic coupling at the beginning and end of the process, i.e. $\dot{\vartheta}_{i,f} = 0$. This model does not require, though, a null non-adiabatic coupling along the dynamics (as in STIRAP); now, only its second order counterpart, $\dot{\vartheta}_2$, needs to be negligible such that the system

dynamics obeys (3.71). The minimization of $\dot{\vartheta}_2$ does imply also a small $\dot{\vartheta}$, but, as the deviation is of higher order, the requirement of large areas is less strict (lower areas should be sufficient to achieve the same degree of correction).

2. $\vartheta_i = 0$, $\vartheta_{2i} = \pi/2$, i.e.

$$\begin{aligned} U_0|1\rangle &= -\frac{i}{\sqrt{2}}\Big\{2\cos\kappa\Big[\cos^2(\vartheta_2/2)\Big(|\Phi_-\rangle - |\Phi_+\rangle\Big) \\ &\quad + \frac{i}{\sqrt{2}}\sin\vartheta_2|\Phi_0\rangle\Big] + e^{i\kappa}|\Phi_+\rangle - e^{-i\kappa}|\Phi_-\rangle\Big\}, \\ &= \begin{bmatrix} \sin\vartheta_2\cos\vartheta\cos\kappa + \sin\vartheta\sin\kappa \\ i\cos\vartheta_2\cos\kappa \\ -\sin\vartheta_2\sin\vartheta\cos\kappa + \cos\vartheta\sin\kappa \end{bmatrix}, \end{aligned} \tag{3.72}$$

which, as in the previous case, corresponds to the adiabatic dark state at the initial time. However, unlike it, this propagator contains the monotonically growing κ term (the area separating the eigenvalues of the adiabatic Hamiltonian), implying the appearance of an oscillatory evolution. To reach the target state $|\psi_f\rangle = \pm|3\rangle$, directly and while hoping to maintain a low transient population on the excited state, the conditions $\vartheta_f = \pm\pi/2$, $\vartheta_{2f} = \pi/2$, and $\kappa_f = n\pi$ must be satisfied.

The requirement $\kappa_f = n\pi$, given that κ is related to the area of the pulses, is reminiscent of the bright STIRAP in that the final state population oscillates between the ground states as a function of pulse area. It differentiates from it, though, by maintaining a low population on the excited state.

These conditions are not physically feasible exactly since $\vartheta_{2i,2f} = \pi/2$ require both pulses to be off while $\dot{\vartheta}$ isn't. Nevertheless, they may be approximated by fast growing pulses still counter-intuitively ordered since $\vartheta_i = 0$ and $\vartheta_i = \pm\pi/2$.

3. $\vartheta_i = \pi/2$, i.e.

$$\begin{aligned} U_0|1\rangle &= \frac{1}{\sqrt{2}}\Big\{i2\sin\kappa\Big[\cos^2(\vartheta_2/2)\Big(|\Phi_-\rangle - |\Phi_+\rangle\Big) \\ &\quad + \frac{i}{\sqrt{2}}\sin\vartheta_2|\Phi_0\rangle\Big] + e^{i\kappa}|\Phi_+\rangle + e^{-i\kappa}|\Phi_-\rangle\Big\}, \\ &= \begin{bmatrix} \sin\vartheta\cos\kappa - \sin\vartheta_2\cos\vartheta\sin\kappa \\ -i\cos\vartheta_2\sin\kappa \\ \cos\vartheta\cos\kappa + \sin\vartheta_2\sin\vartheta\sin\kappa \end{bmatrix}, \end{aligned} \tag{3.73}$$

for which the transient excited state population may be limited by $\vartheta_{2i} = \vartheta_{2f}$, and, for both $\vartheta_{2i} = \vartheta_{2f} = 0$ and $\pi/2$, $\vartheta_f = 0$ (or π) and $\kappa_f = n\pi$ $(n > 1)$.

The most convenient conditions are clearly the ones that reproduce a kind of dark state in the superadiabatic basis, which is not exactly a dark state but a slightly changed dark state from the adiabatic basis (first order). Thus, if the pulses are such that $\vartheta_i = 0$ and $\vartheta_f = \pi/2$ (counter-intuitively ordered), and $\vartheta_{2i} = 0$ and $\vartheta_{2f} = 0$, which is equivalent to $\dot{\vartheta}_i = \dot{\vartheta}_f = 0$ (zero derivative of the nonzero field at the boundary), then $T_2(t_i) = T_2(t_f) = \mathbb{1}$. This means that the transformation T_2, Eq. (3.63), would not change the adiabatic connection with the initial and target states.

Since $T_2(t_f) = \mathbb{1}$ (as it is the case for all the transformations $T_n(t_f) = \mathbb{1}$), the superadiabatic basis does not modify the transfer at the end of the process, i.e. it does not improve the transfer efficiency of the adiabatic following in STIRAP. It rather corresponds to a basis closer to the actual dynamics, as we have evidenced that it allows for a limited transient population in the excited state. Thus, we do not expect a convergence $\dot{\vartheta} \xrightarrow[n\to\infty]{} 0$.

In practice, the superadiabatic basis which describes best the dynamics is given by the order n for which $\dot{\vartheta}_n$ is minimum [9, 10, 43]. In this case, we expect a projection of the non-adiabatic dynamics in this basis evolving monotonically (typically via a smooth error function).

3.5.2 Loss in superadiabatic passage

The evolution of $\langle 2|\psi\rangle$ for $|\psi_i\rangle = |1\rangle$ is, at the zeroth order of the deviation caused by the non-adiabatic coupling of second order,

$$\begin{aligned}\langle 2|U_0|1\rangle = &-i\cos\vartheta_i\Big(\cos\vartheta_{2i}\sin\vartheta_2 - \sin\vartheta_{2i}\cos\vartheta_2\cos\kappa\Big)\\ &- i\sin\vartheta_i\cos\vartheta_2\sin\kappa.\end{aligned} \tag{3.74}$$

We can see now how the superadiabatic basis is closer to the actual dynamics of the system, as from the superadiabatic propagator the loss for STIRAP becomes visible already at the zeroth order of the non-adiabatic coupling of second order. It is worth noting that this result generalizes and reduces to (3.48) at the adiabatic limit ($\dot{\vartheta} \to 0$).

The sine–cosine pulse sequence we have used to illustrate STIRAP is not appropriate to do the same for the second order iteration. Since, recalling (3.50), the non-adiabatic coupling of second order, the rate of change of the mixing angle between the adiabatic states $|\Phi_n\rangle$, is exactly zero, i.e. $\dot{\vartheta}_2 = 0$, the superadiabatic

transformation of second order offers only a superposition of adiabatic states with static coefficients, making the transformation redundant. ϑ_2 is only zero for infinite pulse areas, the first order non-adiabatic coupling is only nil for infinite pulse duration, meaning that only strictly at the adiabatic limit the superadiabatic states match the adiabatic ones. The benefit of changing the basis is to picture the system in such a dynamic combination of states that new paths of system evolution may be devised (additional controls become available); a constant ϑ_2 adds nothing to the representation of the system, nothing that wasn't already obvious using the (first-order super)adiabatic basis. For this very reason, at its most fundamental level, the non-adiabatic coupling can never be made exactly zero but taken only to be sufficiently small.

A simple model we may use instead is a since–cosine pulse sequence with common maximum amplitudes Ω_m, area $\mathcal{A} \equiv \Omega_m T$, and a nonlinear time-dependent argument for the trigonometric functions, $\eta(t)$, satisfying $\eta_i = 0$ and $\eta_f = \pi/2$, e.g.,

$$\Omega_P = \Omega_m \sin\eta, \quad \Omega_S = \Omega_m \cos\eta, \quad \eta = \frac{\pi}{4}\left\{1 - \cos\left[\frac{\pi}{T}(t - t_i)\right]\right\}. \tag{3.75}$$

This corresponds to a counterintuitive pulse ordering ($\vartheta_i = 0$ and $\vartheta_f = \pi/2$), the intuitive version is obtained by swapping the sine and cosine functions ($\vartheta_i = \pi/2$ and $\vartheta_f = 0$). The modified sine–cosine model leads to

$$\vartheta = (\delta_d - \delta_b)\eta + \delta_b\frac{\pi}{2}, \tag{3.76a}$$

$$\dot{\vartheta} = (\delta_d - \delta_b)\dot{\eta} = (\delta_d - \delta_b)\frac{\pi^2}{4T}\sin\left[\frac{\pi}{T}(t - t_i)\right], \tag{3.76b}$$

$$\kappa = \frac{\mathcal{A}}{2}\int_0^s \left[1 + \frac{\pi^4}{8\mathcal{A}^2}\sin^2(\pi s') - O\left(\frac{1}{\mathcal{A}^4}\right)\right] ds' \xrightarrow[\mathcal{A}\gg 1]{} \frac{\Omega_m(t - t_i)}{2}, \tag{3.76c}$$

$$\cos^2\vartheta_2 \approx 1 - \frac{\pi^4}{4\mathcal{A}^2}\sin^2\left[\frac{\pi}{T}(t - t_i)\right] + O\left(\frac{1}{\mathcal{A}^4}\right) \xrightarrow[\mathcal{A}\gg 1]{} 1, \tag{3.76d}$$

$$\sin^2\vartheta_2 = \frac{\pi^4\sin^2(\pi s)}{4\mathcal{A}^2 + \pi^4\sin^2(\pi s)}, \tag{3.76e}$$

considering the necessity of large areas, to neglect the non-superadiabatic deviation, for the κ term that is given exactly by an elliptic integral of second order. The loss $P_{\text{loss}} = \Gamma\int_{t_i}^{t_f}|\langle 2|U_0|1\rangle|^2\,dt$,

$$P_{\text{loss}}^{b} = \Gamma\int_{t_i}^{t_f}\cos^2\vartheta_2\sin^2\kappa\,dt \xrightarrow[\mathcal{A}\gg 1]{} \frac{\Gamma T}{2}, \tag{3.77a}$$

$$P_{\text{loss}}^{d(\vartheta_{2i}=0)} = \Gamma\int_{t_i}^{t_f}\sin^2\vartheta_2\,dt \xrightarrow[\mathcal{A}\gg 1]{} \frac{\pi^2}{4}\frac{\Gamma T}{2(\mathcal{A}/\pi)^2}, \tag{3.77b}$$

which reproduce the dependence on the area of the first nonzero terms in (3.53), thus the discussion is the same.

Similar results for P_{3f} and ΔP_{3f} may be obtained as for STIRAP, identical if we were to use the same pulse shapes, with exactly the same area-dependence, i.e. $P_{3f} = 1 - |\langle 3|U_1(t_f)|1\rangle|^2 - O(\mathcal{A}^{-3})$ with $|\langle 3|U_1(t_f)|1\rangle|^2 \propto \mathcal{A}^{-2}$. Although truncated expressions for the final state population may present exact results for specific areas, there is no exact transfer possible short of reaching exactly the adiabatic limit, which is not realistically feasible, i.e., the transfer is never exact for finite areas ($\mathcal{A} < \infty$).

3.5.3 Shortcut to Adiabaticity (STA): counter-diabatic driving

Shortcut to superadiabaticity consists in compensating the non-adiabatic coupling by an additional term, named counter-diabatic Hamiltonian: $H^{\rm cd}$, i.e., at the first adiabatic iteration,

$$T_{\rm ad}^\dagger (H + H_1^{\rm cd}) T_{\rm ad} - i\hbar T_{\rm ad}^\dagger \dot{T}_{\rm ad} = D_0' \tag{3.78}$$

with the counter-diabatic–modified Hamiltonian:

$$\widetilde{H}_1 = H + H_1^{\rm cd}. \tag{3.79}$$

D_0' is a diagonal Hamiltonian, which can be exactly $D_0 = T_{\rm ad}^\dagger H T_{\rm ad}$ or a modification of it. We can derive

$$H_1^{\rm cd} = T_{\rm ad}(D_0' + i\hbar T_{\rm ad}^\dagger \dot{T}_{\rm ad}) T_{\rm ad}^\dagger - H. \tag{3.80}$$

If we choose D_0' to be a general traceless diagonal matrix,

$$D_0' = \hbar \begin{bmatrix} a & 0 & 0 \\ 0 & b-a & 0 \\ 0 & 0 & -b \end{bmatrix}, \tag{3.81}$$

we obtain, with $a^+ = a + b$ and $a^- = a - b$,

$$T_{\rm ad} D_0' T_{\rm ad}^\dagger = \frac{\hbar}{4} \begin{bmatrix} -a^-(1+3\cos 2\vartheta) & -2a^+ \sin\vartheta & 3a^- \sin 2\vartheta \\ -2a^+ \sin\vartheta & 2a^- & -2a^+ \cos\vartheta \\ 3a^- \sin 2\vartheta & -2a^+ \cos\vartheta & -a^-(1-3\cos 2\vartheta) \end{bmatrix}, \tag{3.82}$$

leading to the counter-diabatic Hamiltonian

$$H_1^{\mathrm{cd}} = T_{\mathrm{ad}} D_0' T_{\mathrm{ad}}^\dagger + i\hbar\dot{\vartheta} \begin{bmatrix} 0 & 0 & 1 \\ 0 & 0 & 0 \\ -1 & 0 & 0 \end{bmatrix} - \frac{\hbar}{2} \begin{bmatrix} 0 & P & 0 \\ P & 0 & S \\ 0 & S & 0 \end{bmatrix}, \tag{3.83}$$

which utilizes, in general, modified pump and Stokes fields but, most importantly, adds a non-desirable (and unavoidable) direct coupling between the two ground states. Particularly, if we choose $D_0' = D_0$, i.e. $b = -a = \Omega_0/2$, the counterdiabatic Hamiltonian

$$H_1^{\mathrm{cd}} = i\hbar\dot{T}_{\mathrm{ad}} T_{\mathrm{ad}}^\dagger = i\hbar\dot{\vartheta} \begin{bmatrix} 0 & 0 & 1 \\ 0 & 0 & 0 \\ -1 & 0 & 0 \end{bmatrix} \tag{3.84}$$

is exactly the coupling between the two ground states, producing the "corrected" Hamiltonian

$$\widetilde{H}_1 = \frac{\hbar}{2} \begin{bmatrix} 0 & \Omega_P & i2\dot{\vartheta} \\ \Omega_P & 0 & \Omega_S \\ -i2\dot{\vartheta} & \Omega_S & 0 \end{bmatrix}. \tag{3.85}$$

We determine $\mathcal{A}_1^{\mathrm{cd}} = 2\int_{t_i}^{t_f} \dot{\vartheta}\, dt = 2\int_0^{\pi/2} d\vartheta = \pi$, which corresponds to a π pulse between the two ground states. This is also true in the limit $\max_t(\Omega_P, \Omega_S) \to 0$, which ensures a complete transfer by a π-pulse. This is the straightforward solution, making the three-level model unnecessary.

The second adiabatic iteration corresponds to

$$T_2^\dagger \left[T_{\mathrm{ad}}^\dagger (H + H_2^{\mathrm{cd}}) T_{\mathrm{ad}} - i\hbar T_{\mathrm{ad}}^\dagger \dot{T}_{\mathrm{ad}}\right] T_2 - i\hbar T_2^\dagger \dot{T}_2 = D_1', \tag{3.86}$$

giving, for $D_1' = D_1 \equiv T_2^\dagger (T_{\mathrm{ad}}^\dagger H T_{\mathrm{ad}}) T_2 - i\hbar T_2^\dagger T_{\mathrm{ad}}^\dagger \dot{T}_{\mathrm{ad}} T_2$,

$$H_2^{\mathrm{cd}} = i\hbar T_{\mathrm{ad}} \dot{T}_2 T_2^\dagger T_{\mathrm{ad}}^\dagger = \hbar\dot{\vartheta}_2 \begin{bmatrix} 0 & \cos\vartheta & 0 \\ \cos\vartheta & 0 & -\sin\vartheta \\ 0 & -\sin\vartheta & 0 \end{bmatrix}, \tag{3.87}$$

with the counter-diabatic modified Hamiltonian:

$$\widetilde{H}_2 = H + H_2^{\mathrm{cd}} = \frac{\hbar}{2} \begin{bmatrix} 0 & \Omega_P + 2\dot{\vartheta}_2 \cos\vartheta & 0 \\ \Omega_P + 2\dot{\vartheta}_2 \cos\vartheta & 0 & \Omega_S - 2\dot{\vartheta}_2 \sin\vartheta \\ 0 & \Omega_S - 2\dot{\vartheta}_2 \sin\vartheta & 0 \end{bmatrix}. \tag{3.88}$$

This corresponds to a modification of the original pump and Stokes fields, with no undesirable coupling between the ground states.

The associated propagator $\widetilde{U} = T_{\mathrm{ad}} T_2 \widetilde{U}^{\mathrm{sa}} T_2^{\dagger}(t_i) T_{\mathrm{ad}}^{\dagger}(t_i) = U_0$, from (3.68), produces

$$c_{3f} = -\delta_d\big(\cos\vartheta_{2f}\cos\vartheta_{2i} + \cos\kappa_f \sin\vartheta_{2f}\sin\vartheta_{2i}\big) + \delta_b\cos\kappa_f, \tag{3.89}$$

for dark and bright STIRAP. The boundary conditions are as presented in Sec. 3.5.1, however, the result is not identical: $|c_{3f}|^2$ is the exact final state population in the target state, not the zeroth order as in Eqs. (3.71)–(3.73), and it does not assume the validity of neglecting the non-(super)adiabatic coupling; instead, it is valid if the boundary conditions are satisfied. The dark transfer with $\vartheta_{2i} = 0$ is then achieved for any pulse area as long as $\vartheta_{2f} = 0$. The other two alternatives produce a successful transfer only at specific areas given by $\kappa_f = n\pi$.

It is clear from the expressions of the corrected fields that, for a standard counterintuitive sequence, the correction corresponds to the addition of an intuitive component to the fields, and viceversa.

Recalling (3.75) and (3.76), let's use the modified sine–cosine model to observe the effect of the counter-diabatic correction:

$$\dot\vartheta_2 = 2\frac{(\delta_d-\delta_b)\ddot\eta\Omega_m}{\Omega_m^2+4\dot\eta^2}, \qquad \ddot\eta = \frac{\pi^3}{4T^2}\cos\left[\frac{\pi}{T}(t-t_i)\right] = \frac{\pi^2}{T^2}\left(\frac{\pi}{4}-\eta\right), \tag{3.90a}$$

$$\dot\eta^2 = \frac{\pi^4}{16T^2}\sin^2\left[\frac{\pi}{T}(t-t_i)\right] = \frac{\pi^2}{T^2}\eta\left(\frac{\pi}{2}-\eta\right), \tag{3.90b}$$

$$\begin{aligned}\widetilde\Omega_P &= \Omega_P + 2\dot\vartheta_2\cos\vartheta = \Omega_0\sin\vartheta + 2\dot\vartheta_2\cos\vartheta \\ &= \delta_d\Omega_m\left[\sin\eta + \frac{(\frac{\pi}{4}-\eta)\cos\eta}{(\frac{\mathcal{A}}{2\pi})^2+\eta(\frac{\pi}{2}-\eta)}\right] \\ &\quad + \delta_b\Omega_m\left[\cos\eta - \frac{(\frac{\pi}{4}-\eta)\sin\eta}{(\frac{\mathcal{A}}{2\pi})^2+\eta(\frac{\pi}{2}-\eta)}\right],\end{aligned} \tag{3.90c}$$

$$\begin{aligned}\widetilde\Omega_S &= \Omega_S - 2\dot\vartheta_2\sin\vartheta = \Omega_0\cos\vartheta - 2\dot\vartheta_2\sin\vartheta \\ &= \delta_d\Omega_m\left[\cos\eta - \frac{(\frac{\pi}{4}-\eta)\sin\eta}{(\frac{\mathcal{A}}{2\pi})^2+\eta(\frac{\pi}{2}-\eta)}\right] \\ &\quad + \delta_b\Omega_m\left[\sin\eta + \frac{(\frac{\pi}{4}-\eta)\cos\eta}{(\frac{\mathcal{A}}{2\pi})^2+\eta(\frac{\pi}{2}-\eta)}\right],\end{aligned} \tag{3.90d}$$

$$\widetilde\Omega_0^2 = \widetilde\Omega_P^2 + \widetilde\Omega_S^2 = \Omega_m^2 + 4(\dot\vartheta_2)^2. \tag{3.90e}$$

Then, following the dark state involves a corrected pump that is unchanged at the final time ($\widetilde\Omega_{Pf} = \Omega_{Pf} = \Omega_m$) but nonzero initially, $\widetilde\Omega_{Pi} = 2\dot\vartheta_2$, and a corrected Stokes that is unchanged at the initial time ($\widetilde\Omega_S = \Omega_S = \Omega_m$) but nonzero finally, $\widetilde\Omega_{Sf} = -2\dot\vartheta_2$, with $2\dot\vartheta_2 = \pi^3/(\Omega_m T^2)$ for the modified sine–cosine model. The magnitude of the correction depends on the area of the original fields, i.e., larger the area

smaller the correction, with the largest modification occurring at the boundaries.

3.6 Conclusions

We have summarized in this chapter the main protocols of control regarding a three-level system in Λ configuration, implying we take into account the population loss via dissipation that populating the intermediate state causes. Offering robustness and control of the losses, the main exponent is STIRAP and its associated shortcuts. Using them as inspiration new techniques may be devised and using these as benchmarks novel approaches can be evaluated.

The presented simple diabatic methods, consecutive π pulses and the Rabi method, exhibit the highest losses, lowest robustness (highest propensity to deviations), and no way to improve these measures. Adiabatic passage, in the form of STIRAP, brings forward control of the robustness and loses in exchange for as approximated (design of the) dynamics and an energy-costly accuracy. The dynamics can be modeled more closely using a superadiabatic basis, opening adiabatic paths with higher order approximations though unchanging the expensive accuracy.

With counter-diabatic driving we attain both an exact dynamics and accuracy by reshaping the control fields with the superadiabatic-correction–dependent term. The drawback being that we are left blind searching for pulse shapes satisfying certain boundary conditions and, even though the specific shapes control the nonadiabatic aspects of robustness, we do not dispose of any means to control it.

Chapter 4

Robust stimulated Raman exact passage by single-shot shaped pulses

4.1 Introduction

In this chapter, we propose a scheme for robust UH-fidelity transfers similar to STIRAP, but exact and with moderate areas, to which we refer as stimulated Raman exact passage (STIREP) [23, 27, 44]. Exact, in this context, refers to schemes that provide the dynamics of the system "exactly", i.e. approaches that prescribe a mathematical description of the complete dynamics of the system (the control fields and, consequently, the state are known for all instances of time).

We do not consider loss in this chapter, i.e., $\Gamma = 0$. Loss will be considered in the next when optimization (while satisfying robustness) becomes the goal.

Improvements of STIRAP have been proposed by optimizing single properties: nonresonant fast STIRAP [31] but with large transient population in the excited state and robust but slow STIRAP [45]. However, there are exact methods available that take different approaches on their search to compete with STIRAP's well-stablished robustness, such as single-shot shaped pulses (SSSP) [19, 20] and composite pulses [16, 32, 46–50], among others. Techniques as SSSP and composite pulses deal with error reduction directly, while methods as shortcuts to adiabaticity [26, 27, 31, 45, 51–59] rely on optimizing the adiabaticity of the process as their source of robustness. In a way, the first ones are bottom-up techniques, starting with energy economic strategies and remolding them to gain robustness; while the latter are top-down technologies, starting with the adiabatic and infinitely energetically costly paradigm and working their way down towards faster and cheaper processes.

Physically speaking, exact methods are all those that offer detailed mathematical solutions for the desired task, i.e. a description of the process with which to obtain the goal at a finite time. Meanwhile, adiabatic methods rely on the asymptotic behavior of the system under the adiabatic condition. To use an exact technique instead of an adiabatic one means to sacrifice the freedom that adiabaticity affords on field shapes for the rigidity of prescribed pulses and state dynamics. These prescriptions, provided by means of inverse engineering, are applied in order to gain the advantage of reaching the desired target state with finite pulse areas in a finite time.

SSSP is a technique that takes exact transfer inverse-engineering as a first step, and error resistance through the transfer perturbative expansion as a second step. Firstly, SSSP applies inverse-engineering from the desired process onto the control fields by means of the prescription of a tracking solution for a certain parametrization of the quantum state of the system. Then, it uses perturbation theory to gradually diminish the susceptibility of the transfer fidelity to deviations from the optimal experimental conditions. Perturbation theory is applied in terms of deviations from the ideal conditions, taking into consideration realistic experimental complications, and is analyzed through the Schrödinger equation. The minimization of the deviation terms, representing the result of non-optimal conditions, is expected to have the systematic decimation of the dynamics sensitivity to perturbations as a consequence, i.e. improving the robustness. In order to manipulate the deviation terms, the tracking expression of the reverse-engineered dynamics must contain a suitable parameterization, meaning that the desired system evolution is prescribed with expressions containing free parameters to be chosen afterwards regarding they nullify or at least reduce the terms of the perturbative expansion.

In this chapter, we introduce SSSP for the robust UH-fidelity transfer of population between the ground states of a three-level Λ-system. We show a scheme similar to STIRAP but exact (thus not actually adiabatic) and highly robust using the Lewis-Riesenfeld (L-R) method driving a single dynamical mode [22, 26]. The second section contains the parameterization of the propagator and Hamiltonian in terms of Euler angles. Section 4.3 shows the application of perturbation theory on the Hamiltonian, a working tracking solution (based on [23, 27, 44]) and an analysis of the origin of robustness for this chosen tracking solution. We propose the direct study of the robustness of any given process for a range of pulse areas through the usage of a measurement of robustness based on the minimum UH-fidelity confidence range around the unperturbed ideal system. Additionally, definitions of STIRAP, considering Gaussian-shaped fields, and the adiabatically-optimized pulses with which we compare our SSSP are described. Section 4.4 presents the discussion

and conclusions.

4.2 The Hamiltonian and its state angular parameterization

Let's consider a three-level system driven by two resonant fields, $\Omega_P(t)$ and $\Omega_S(t)$, for which the Hamiltonian, on the bare states basis $\{|1\rangle, |2\rangle, |3\rangle\}$ and under the rotating wave approximation, is

$$H(t) = \frac{\hbar}{2}\begin{bmatrix} 0 & \Omega_P & 0 \\ \Omega_P & 0 & \Omega_S \\ 0 & \Omega_S & 0 \end{bmatrix}. \tag{4.1}$$

In STIRAP, the state of the system is written in terms of the eigenstates of the Hamiltonian,

$$\Phi_0 = \begin{bmatrix} \cos\vartheta \\ 0 \\ -\sin\vartheta \end{bmatrix}, \quad \Phi_\pm = \frac{1}{\sqrt{2}}\begin{bmatrix} \sin\vartheta \\ \pm 1 \\ \cos\vartheta \end{bmatrix}, \tag{4.2}$$

where $\vartheta(t)$ is the so-called mixing angle, given by

$$\sin\vartheta = \Omega_P/\sqrt{\Omega_P^2 + \Omega_S^2}, \quad \cos\vartheta = \Omega_S/\sqrt{\Omega_P^2 + \Omega_S^2}. \tag{4.3}$$

The idea is to follow the dark state, the Hamiltonian eigenstate $|\Phi_0\rangle$, whose projection on the excited state is always null. This state allows for control of population transfer between the ground states without populating the intermediate state, the desired dynamics, which prescribes the signature counter-intuitive ordering of Ω_P and Ω_S. However, the derivatives of the mixing angle, the non-adiabatic coupling, couple the $|\Phi_n\rangle$'s, the adiabatic states, preventing their exact following (since population would be uncontrollably exchanged via it). Then, adiabaticity, the condition in which the non-adiabatic coupling is negligible (with $\dot{\vartheta} \to 0$ being the adiabatic limit), is paramount to minimize the deviations of the dynamics from the dark state and produce the desired transfer. Naturally, very slow-evolving pulses would minimize the non-adiabatic coupling and practically uncouple the adiabatic states in consequence. Nevertheless, the adiabatic states can never be followed exactly in real-world implementations.

4.2.1 Lewis-Riesenfeld invariant

A method that has taken notoriety in recent years is the use of dynamical invariants, also referred to as Lewis-Riesenfeld (L-R) invariants [22, 26, 27, 60, 61]. The L-R invariant $I(t)$ is defined by having a time-invariant expectation value, i.e., a constant $\langle\psi(t)|I|\psi(t)\rangle$, where $|\psi\rangle$ is the state of the system. This condition is equivalent to $i\hbar\dot{I} = [H, I]$ when considering the evolution of such system as described by the Schrödinger equation $i\hbar|\dot{\psi}(t)\rangle = H|\psi(t)\rangle$, where the dotted function denotes its partial derivative with respect to time.

We can use the eigenstates of this invariant, $|\varphi_n(t)\rangle$, to write the state of our system with the advantage that, unlike with the adiabatic states, the coupling between these is always null under any condition. This can be shown by applying the transformation operator $T_{\mathrm{LR}}(t) = \sum_n |\varphi_n\rangle\langle n|$, that writes the system into the basis of the L-R eigenstates, onto the Schödinger equation and demonstrating the effective Hamiltonian on the new basis, $H^{\mathrm{LR}}(t) = T_{\mathrm{LR}}HT_{\mathrm{LR}}^{\dagger} - i\hbar T_{\mathrm{LR}}\dot{T}_{\mathrm{LR}}^{\dagger}$, to have only the diagonal elements $H_n^{\mathrm{LR}} = \langle\varphi_n|H|\varphi_n\rangle$. Thus, we can describe the complete dynamics of our system by a fixed combination of the L-R eigenstates and, with a suitable parameterization and tracking solution, we can follow exactly the system evolution and, consequently, reach exactly the desired target state.

A simple picture of the difference between the use of adiabatic states (key of STIRAP) and of the eigenvectors of the dynamical invariant (L-R method) is: while the adiabatic states represent the dynamics of the system under the adiabatic condition, the L-R eigenvectors contain the whole dynamics of the system; the firsts are a particular case of the seconds, as we will show at the end of this section.

In order to write the solution of the Schrödinger equation in terms of the eigenvectors of the L-R invariant we first need to write the latter explicitly in terms of practical parameters. For this purpose, we can exploit the property that establishes that, for an invariant that is member of the Lie algebra with (Hermitian) generators Q_n, i.e. $I = \sum_n^N \alpha_n(t)Q_n$, these coefficients must obey the relation $\sum_n^N \alpha_n^2 = \alpha_0^2$, where the α_n's are real quantities, α_0 is a constant and N is the number of generators of the algebra.

Considering that the propagator of the Hamiltonian (4.1) belongs to the SU(3) symmetry group, we can write said Hamiltonian as a linear combination of the well-known Gell-Mann matrices λ_n of the group [27, 62, 63] [generators of the Lie algebra of SU(3) as the Pauli matrices are the generators of the algebra of SU(2)],

i.e., $H = (\hbar/2)(\Omega_P\lambda_1 + \Omega_S\lambda_6)$, with

$$\lambda_1 = \begin{bmatrix} 0 & 1 & 0 \\ 1 & 0 & 0 \\ 0 & 0 & 0 \end{bmatrix}, \ \lambda_5 = \begin{bmatrix} 0 & 0 & -i \\ 0 & 0 & 0 \\ i & 0 & 0 \end{bmatrix}, \ \lambda_6 = \begin{bmatrix} 0 & 0 & 0 \\ 0 & 0 & 1 \\ 0 & 1 & 0 \end{bmatrix}. \tag{4.4}$$

Moreover, given that the matrices λ_1, λ_5 and λ_6 form a closed algebra, fulfilling the Lie algebra of SU(2), i.e. their commutation relations require no other generator ($[\lambda_i, \lambda_j] = C_{ij}^k\lambda_k$ for i, j, and k taking any combination of values 1, 5 and 6 without repetitions, $C_{ij}^k = -C_{ji}^k = C_{jk}^i = C_{ki}^j$ and $C_{16}^5 = i$), we can now write the L-R invariant in terms of only these three matrices and three α_n's:

$$I(t) = \alpha_1\lambda_1 + \alpha_2\lambda_6 + \alpha_3\lambda_5. \tag{4.5}$$

This is a much simpler case than that of a general member of the SU(3) algebra that contains up to 8 α_n's (7 of which are independent). With this simple expression for our dynamical invariant we can solve the eigenvalue equation.

Using the eigenvectors $|\varphi_n(t)\rangle$ of this invariant to write the state of the system solution to the Schrödinger equation:

$$|\psi(t)\rangle = \sum_{n=1}^{3} C_n \, \mathrm{e}^{i\eta_n(t)} \, |\varphi_n(t)\rangle, \tag{4.6}$$

with the Lewis-Riesenfeld phase

$$\eta_n(t) = \frac{1}{\hbar}\int_{t_i}^{t} \left\langle \varphi_n(t') \left| i\hbar\frac{\partial}{\partial t'} - H(t') \right| \varphi_n(t') \right\rangle dt', \tag{4.7}$$

we can also write the evolution operator $U(t, t_i)$, to which we refer as the propagator of the system, in terms of the α_n's through $U = \sum_{n=1}^{3} \exp[i\eta_n(t)]|\varphi_n(t)\rangle\langle\varphi_n(t_i)|$. The Lewis-Riesenfeld phase corresponding to the null eigenvalue, e.g., η_1, is a constant we set to 0. Considering we intend to prescribe the time evolution of the α_n's, we facilitate the search for the boundary conditions by imposing a single-mode driving, i.e. a dynamics along a single eigenvector of the invariant, setting $C_1 = 1$ and $C_2 = C_3 = 0$, which makes $|\psi\rangle = |\varphi_1\rangle$. This dynamics can be seen as a generalization of adiabatic passage, occurring along a single eigenstate, to an exact passage.

Given the relation between the α_n's, we can propose the following representation

in terms of time-dependent Euler angles:

$$\alpha_1 = \alpha_0 \cos\phi \sin\theta, \quad \alpha_2 = -\alpha_0 \cos\phi \cos\theta, \quad \alpha_3 = \alpha_0 \sin\phi, \tag{4.8}$$

which consequently makes the other two L-R phases

$$\eta \equiv \eta_2 = -\eta_3 = -\int_{t_i}^{t} \dot{\theta}(t')/\sin[\phi(t')]\, dt'. \tag{4.9}$$

Defining the desired transfer to be $|\psi(t_i)\rangle = |1\rangle \rightarrow |\psi_T\rangle = |3\rangle$, we can now say that, for a Hamiltonian fulfilling the closed algebra of λ_1, λ_5 and λ_6, with no coupling $|1\rangle$–$|3\rangle$, the propagator of the system can be written as

$$U = \left[|\varphi_1\rangle \quad |\psi_+\rangle \quad |\psi_-\rangle\right], \tag{4.10}$$

with the composing column vectors described by

$$|\varphi_1\rangle = \begin{bmatrix} \cos\phi\cos\theta \\ i\sin\phi \\ \cos\phi\sin\theta \end{bmatrix}, \tag{4.11a}$$

$$|\psi_+\rangle = \begin{bmatrix} i\cos\eta\sin\phi\cos\theta - i\sin\eta\sin\theta \\ \cos\eta\cos\phi \\ i\cos\eta\sin\phi\sin\theta + i\sin\eta\cos\theta \end{bmatrix}, \tag{4.11b}$$

$$|\psi_-\rangle = \begin{bmatrix} -\sin\eta\sin\phi\cos\theta - \cos\eta\sin\theta \\ i\sin\eta\cos\phi \\ -\sin\eta\sin\phi\sin\theta + \cos\eta\cos\theta \end{bmatrix}, \tag{4.11c}$$

where the first column of the propagator corresponds to a parameterization in Euler angles of the solution of the Schrödinger equation. With the representation in (4.8), the control fields can also be expressed in terms of these so-called Euler angles as

$$\Omega_P/2 = -\dot{\theta}\cot\phi\sin\theta - \dot{\phi}\cos\theta, \tag{4.12a}$$

$$\Omega_S/2 = \dot{\theta}\cot\phi\cos\theta - \dot{\phi}\sin\theta, \tag{4.12b}$$

which provide the remaining boundary conditions when demanding the pulses to have finite area, i.e. $0 \leftarrow \Omega_P \rightarrow 0$ and $0 \leftarrow \Omega_S \rightarrow 0$, thus

$$0 \leftarrow \{\phi, \dot{\phi}, \dot{\theta}, \dot{\eta}\} \rightarrow 0, \text{ and } 0 \leftarrow \theta \rightarrow \pi/2, \tag{4.13}$$

where the arrows to the right and left represent the limits when $t \rightarrow t_f$ and $t \rightarrow t_i$,

respectively. It can be noted that the transient population of the excited state in this representation is given exactly by

$$P_2(t) = |\langle 2|\psi(t)\rangle|^2 = \sin^2\phi(t). \tag{4.14}$$

We can interpret the invariant's eigenstate $|\varphi_1\rangle$ as equivalent to the dark state of STIRAP, $|\Phi_0\rangle$, where the latter has been allowed to exhibit a non-zero transient excited state population in order to make the dynamics exact. In fact, the particular case of single-mode driving corresponding to adiabatic following is given by $|\Phi_0\rangle = |\varphi_1(\theta = -\vartheta, \phi = 0)\rangle$; for which the excited state population (4.14) remains exactly null, the fields (4.12) are infinite and, thus, the adiabatic condition is fulfilled.

Equations (4.12) and (4.13) define a family of exact transfer solutions. Consequently, if such tracking solutions satisfying the previous conditions can be engineered, then we are able to control at will, in principle, the population on the middle state and we would be exposing an exact method for realizing stimulated Raman passage.

4.3 Perturbed Hamiltonian, exact tracking and the measure of robustness

Having set the requirements the angles must fulfill to describe the desired process, we proceed to deal with its robustness. Firstly, we add an unknown deviation $V(\epsilon)$ to the Hamiltonian (4.1), introducing the possibility of a non-optimal implementation of the control strategy that contains an error ϵ in the area of the pulses interacting with the system, i.e., $H_\epsilon = H + V(\epsilon)$, where $V = \epsilon H$; thus,

$$H_\epsilon = \frac{\hbar}{2}\begin{bmatrix} 0 & (1+\epsilon)\Omega_P & 0 \\ (1+\epsilon)\Omega_P & 0 & (1+\epsilon)\Omega_S \\ 0 & (1+\epsilon)\Omega_S & 0 \end{bmatrix}. \tag{4.15}$$

Secondly, we apply standard perturbation theory at the transfer profile regarding the perfect realization, or

$$\langle\psi_T|\psi_\epsilon(t_f)\rangle = 1 - O_1 - O_2 - \cdots, \tag{4.16a}$$

$$|\langle\psi_T|\psi_\epsilon(t_f)\rangle|^2 = 1 - \widetilde{O}_1 - \widetilde{O}_2 - \cdots = \mathcal{F}. \tag{4.16b}$$

The deviation terms $O_n \equiv O(\epsilon^n)$ are integral expressions whose level of complexity increases accordingly to the corresponding perturbation orders. Given that the

evolution of the state of our system coincides with that of $|\varphi_1\rangle$, and that conjointly with $|\psi_+\rangle$ and $|\psi_-\rangle$ these form a complete basis, the deviation terms are, explicitly,

$$O_1 = 0, \tag{4.17a}$$

$$O_2 = -(-i)^2 \int_{t_i}^{t_f}\int_{t_i}^{t} [nn' - pp']\, dt'\, dt \in \mathbb{R}, \tag{4.17b}$$

$$O_3 = -(-i)^3 \int_{t_i}^{t_f}\int_{t_i}^{t}\int_{t_i}^{t'} [pr'n'' - nr'p'']\, dt''\, dt'\, dt \in \mathbb{I}, \tag{4.17c}$$

$$\begin{aligned} O_4 = -(-i)^4 \int_{t_i}^{t_f}\int_{t_i}^{t}\int_{t_i}^{t'}\int_{t_i}^{t''} & [nn'n''n''' - nn'p''p''' + nr'r''n''' - pp'pn''n''' \\ & + pp'p''p''' - pr'r''p'''] \in \mathbb{R}, \end{aligned} \tag{4.17d}$$

and so on, where the non-null elements of the Hamiltonian deviation, for an unknown pulse area scaling error ϵ, on the basis of the vectors in (4.11), are identified as $n = \langle\varphi_1|V/\hbar|\psi_+\rangle$, $p = \langle\varphi_1|V/\hbar|\psi_-\rangle$ and $r = \langle\psi_+|V/\hbar|\psi_-\rangle$, with the primed function representing the function with its argument primed, e.g., $n' = \langle\varphi_1(t')|V(t')/\hbar|\psi_+(t')\rangle$.

To consistently increase the robustness of the process via the nullification of the first orders of infidelity, $\widetilde{O}_n \equiv \widetilde{O}(\epsilon^n)$, is the goal of our strategy. These terms are, from (4.16), given by $\widetilde{O}_1 = O_1 + \overline{O}_1$, $\widetilde{O}_2 = O_2 - O_1\overline{O}_1 + \overline{O}_2$ and so on, where the odd orders are automatically null. However, the prescription of adequate tracking solutions with free parameters is the actual core of our recipe and also its sole non-systematic step.

Finally, we propose a tracking solution where the maximum transient population on the excited state, $P_2^{\max} = \max\left[|\langle 2|\psi(t)\rangle|^2\right]$, is the control parameter.

4.3.1 Population cap parameterization

The first found successful parameterization contains a unique free coefficient fixing a cap for the transient population on the excited state. The mixing angle of the levels $|1\rangle$ and $|3\rangle$ with $|2\rangle$, identified as $\phi(t)$, is written in terms of the other one, $\theta(t)$, which describes the state evolution from $|1\rangle$ to $|3\rangle$, and, in this manner, we propose the following suitable (fulfilling the requirements on (4.13)) and convenient tracking solutions (based on [23, 27, 44]):

$$\theta(t) = (\pi/4)\left\{\tanh[(t - t_i - T/2)/v_0] + 1\right\}, \tag{4.18a}$$

$$\widetilde{\phi}(\theta) = (4\phi_0/\pi)\sqrt{\theta(\pi/2 - \theta)}, \tag{4.18b}$$

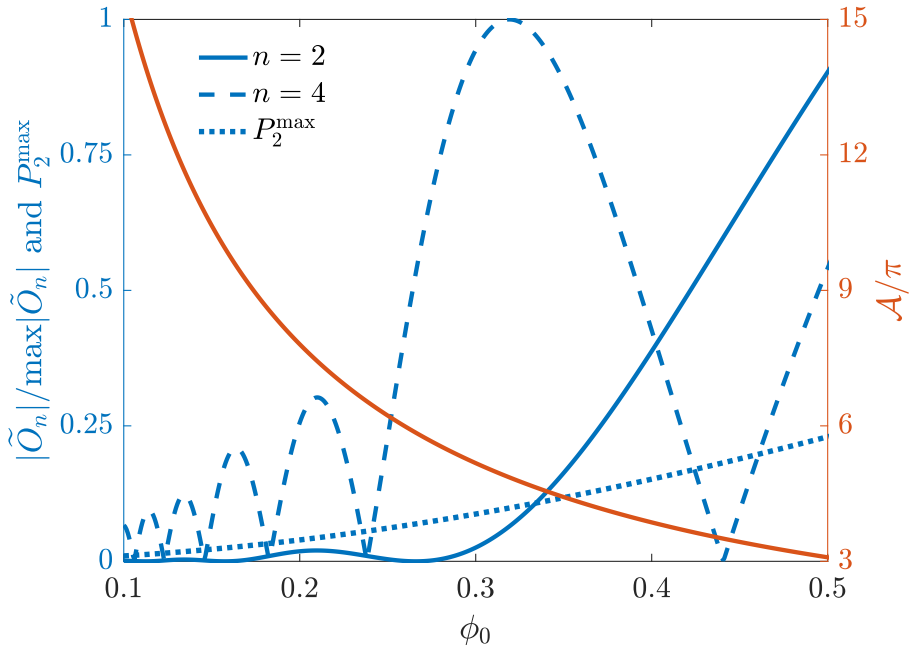

Figure 4.1: Second and fourth orders of infidelity, $\widetilde{O}_2$ and $\widetilde{O}_4$, maximum excited state population $P_2^{\max}$ and the corresponding generalized area $\mathcal{A}$ vs the free parameter ϕ_0.

where the tilde signals functions of θ. These give, with $\dot{\widetilde{\phi}} \equiv \partial\widetilde{\phi}/\partial\theta$,

$$\dot{\widetilde{\theta}}(\theta) = (4/\pi v_0)\theta(\pi/2 - \theta), \tag{4.19a}$$

$$\dot{\widetilde{\phi}}(\theta) = (4\phi_0/\pi)\frac{\pi/4 - \theta}{\sqrt{\theta(\pi/2 - \theta)}}, \tag{4.19b}$$

where $T = t_f - t_i$ is the total duration of the process and v_0 is a parameter setting the speed of the function change (chosen as $v_0 = 0.028T$ to provide a numerical error below 10^{-6} for the normalized field at the boundaries of the process).

The free parameter ϕ_0 allows us to control simultaneously the maximum population on the excited state, parameterized as $P_2^{\max} = \sin^2\phi_0$, and the robustness of the transfer, by means of the nullification or minimization of the first orders of population infidelity $\widetilde{O}_n$'s; the first two non-zero orders are shown in Fig. 4.1.

The relationship between ϕ_0 and the generalized area of the pulses,

$$\mathcal{A} = \int_T \sqrt{\Omega_P^2 + \Omega_S^2}\, dt, \tag{4.20}$$

corresponds to that which is well known from STIRAP: higher the area $\mathcal{A}$ of the pulses, lower the maximum transient population on the excited state $P_2^{\max}$, which can be noted straightforwardly in Fig. 4.1, to where we can also refer to extract the

correspondence between ϕ_0 and $\mathcal{A}$. It can be highlighted that the additional amount of pulse area $\Delta\mathcal{A} = \mathcal{A}\left(P_2^{\max}(\phi_0) + \Delta P_2^{\max}\right) - \mathcal{A}\left(P_2^{\max}(\phi_0)\right)$ that would be required to decrease the maximum intermediate state population by a certain amount $\Delta P_2^{\max}$ rises rapidly when considering ever lower values of ϕ_0, i.e., $\Delta\mathcal{A}/\Delta P_2^{\max} \xrightarrow{\phi_0 \to 0} \infty$, thus exhibiting the asymptotic behavior of the adiabatic condition (the adiabatic limit).

4.3.2 Measurement of robustness

Single-shot shaped pulses

With the purpose of generating simple pulses, we choose to nullify the terms of the perturbative expansion of the infidelity maintaining a single control parameter. Since we only have one free variable, we can't, in general, use it to nullify more than one term; this is visible in Fig. 4.1. However, given the particularity of our control, the absolute value of the perturbations, like the maximum population of the excited state, decreases in average as ϕ_0 is decreased, contrary to the increase of the required pulse areas. We use this feature to restrict our focus to the range of ϕ_0 corresponding to moderate pulse areas, e.g., $\mathcal{A} \leq 15\pi$, and examine the resultant robustness of the fidelity for the desired transfer.

Considering the limited character of a single-parameter parametrization, we opt to not search to nullify individual terms of the perturbative expansion of the fidelity, but to search for particular values of ϕ_0 for which the robustness of the transfer presents local maxima. Figure 4.2 permits to analyze the dependence of the infidelity $\mathcal{I}$ on generalized pulse area and area scaling error ϵ; this figure presents the contours of the regions with very high fidelities (over 99%), showcasing them with the logarithm of the infidelity at the evaluated conditions, where we give special attention to the region of the so called ultra high fidelity (UH-fidelity) for which the infidelity $\mathcal{I} \equiv 1 - P_3(t_f) \leq 10^{-4}$.

The desired robustness can be understood as the non-susceptibility of the fidelity transfer (over a certain limit set to 10^{-4} for UH-fidelity) for different values of ϵ, or how large does ϵ need to be (qualitatively around the unperturbed $\epsilon = 0$ condition) to fall below the UH-fidelity definition. In Fig. 4.2 we can observe how the robustness, in its qualitative sense from the broader UH-fidelity regions, tend to increase when more energy (or generalized pulse area) is invested.

The oscillatory behavior of the robustness is obtained from the oscillations of the infidelity orders $\widetilde{O}_n$'s, shown in Fig. 4.1, and the global increase of robustness with $\mathcal{A}$ from the damping of such oscillations (the asymptotic decrease on the average of the absolute value of the infidelity orders). The asymmetry in Fig. 4.2 arrives

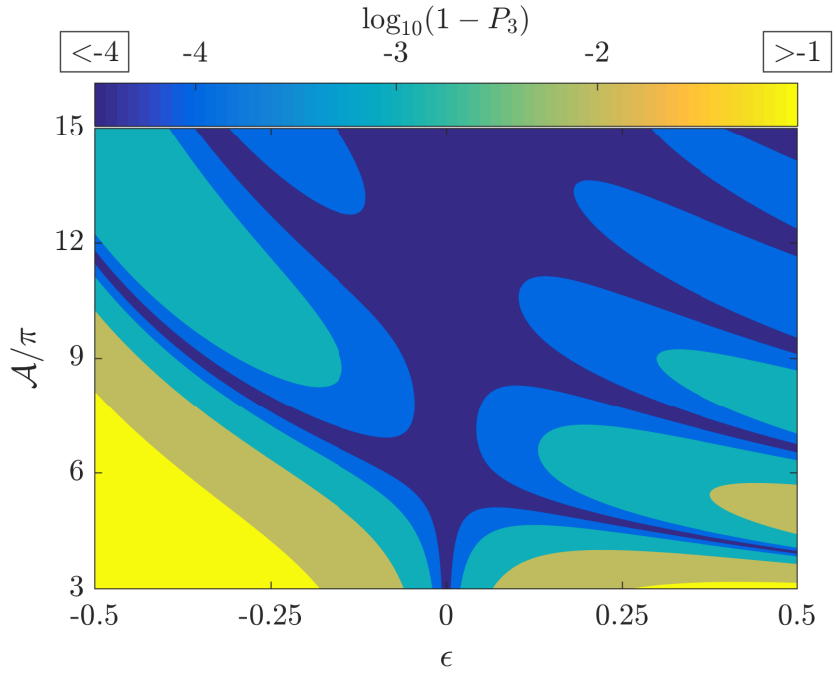

Figure 4.2: Contour plot of infidelity $\mathcal{I}$ (log base 10) vs generalized area $\mathcal{A}$ and area perturbation ϵ.

naturally from the fact that a positive ϵ increases the effective amplitude of the pulses, decreasing the generalized area required to achieve the UH-fidelity transfer, and vice versa.

In order to have a quantitative measure of robustness, appropriate for its exhaustive analysis and for establishing grounds of comparison with other techniques, we extract the maximum absolute area deviation, $\max|\epsilon|$, at which transfers with ultra high fidelity are achieved for $\epsilon < 0$ and $\epsilon > 0$ separately. To the minimum of these two quantities we will refer as UH-fidelity radius and it is shown in Fig. 4.3 in comparison with equal measures for Gaussian pulses and adiabatically-optimized pulses built from hypergaussians [45]. We can remark that the discontinuous character of its definition, the operation of obtaining the minimum between the left and right values $|\epsilon|$ where the infidelity goes over 10^{-4}, produces a UH-fidelity radius function with discontinuous derivatives.

STIRAP with Gaussian pulses

One of the most commonly used pulse shapes, especially for STIRAP, is Gaussian. Gaussian pulses have three free parameters: peak, waist and delay. The pulse areas $\mathcal{A}_P$ and $\mathcal{A}_S$ depend on the first two, and the generalized area $\mathcal{A}$ depends on the three of them. Fixing the waist we can control the area by tuning the peak, but the efficiency of the process will also depend greatly on the delay. Thus, we optimize

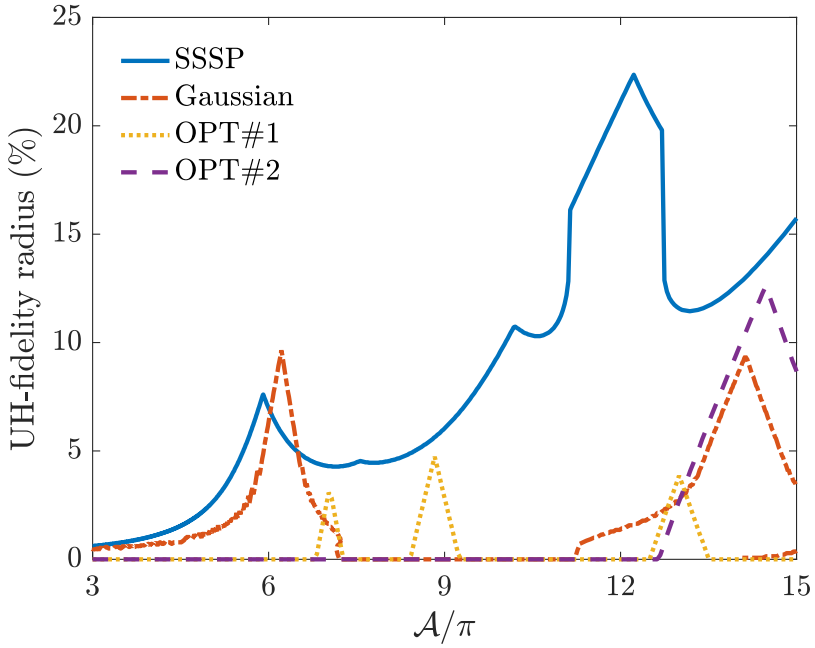

Figure 4.3: UH-fidelity radius vs generalized area $\mathcal{A}$. A comparison between selected techniques.

the delay and show the UH-fidelity radius in terms of $\mathcal{A}$ to serve as a base reference for STIREP in Fig. 4.3.

For the Gaussian pulses, we use

$$\Omega_P^{(G)} = -\Upsilon \exp\left[-(\hat{t} - \tau/2)^2/\sigma^2\right], \quad \Omega_S^{(G)} = \Upsilon \exp\left[-(\hat{t} + \tau/2)^2/\sigma^2\right], \tag{4.21}$$

with $\hat{t} = t - t_i - T/2$. Where Υ, τ and σ are the peak, delay and waist of the gaussian pulses, respectively, which we restrict, while setting $\sigma = 0.04T$, to a set of values that produce moderate area fields with smaller amplitudes (in their absolute values) than $10^{-6} \times \Upsilon$ at the boundaries of the process $[t_i, t_f]$, in order to have a proper numerical implementation with high precision.

Adiabatically-optimized pulses

The conditions for adiabatic optimization of pulse shapes, or designing adiabatically-optimal pulse shapes, are shown in [45] while also proposing a combination of hypergaussian and trigonometric shapes as an example of pulses that fulfill these con-

ditions for UH-fidelity STIRAP. The formulas for these pulses are:

$$\Omega_P^{(O)} = -\Upsilon \exp\left[-\left(\frac{\hat{t}}{m\sigma}\right)^{2n}\right] \sin\left[\frac{\pi/2}{f(\hat{t})}\right], \tag{4.22a}$$

$$\Omega_S^{(O)} = \Upsilon \exp\left[-\left(\frac{\hat{t}}{m\sigma}\right)^{2n}\right] \cos\left[\frac{\pi/2}{f(\hat{t})}\right], \tag{4.22b}$$

with $f = 1 + \exp(-\lambda\hat{t}/\sigma)$. The dependence of the transfer robustness on area for a fixed waist σ, in order to be compared with Gaussian pulses of the same waist, has three remaining free parameters: m (waist factor relative to the Gaussian pulses), n (power of the hypergaussian) and λ (speed of change of the trigonometric function).

These adiabatically-optimized pulses are shown [45] to be superior to Gaussian pulses regarding the pulse area they require to achieve UH-fidelity standards when implemented for STIRAP. Moreover, these pulses are area-wise robuster than Gaussians when sufficiently (for UH-fidelity) high areas are used. The UH-fidelity radius of a pair of adiabatically-optimized pulses, labeled as OPT#1 ($m = 1, n = 1, \lambda = 4$) and OPT#2 ($m = 1, n = 2, \lambda = 5$) for two of the parameter sets (from sets with natural numbers as parameters) performing well at low to moderate pulse areas, is shown in Fig. 4.3 for the purpose of comparison.

4.4 Discussions and conclusions

The UH-fidelity radius for the SSSP pulses developed in this paper, for Gaussian pulses and for adiabatically-optimized pulses is shown as a function of generalized area in Fig. 4.3.

SSSP is shown to be superior, for most areas under $\mathcal{A} \leq 15\pi$ at the very least, to the two other methods considered. The maximum of the UH-fidelity radius of SSSP is about 13% over the Gaussian pulses with the highest performance and almost twice the maximum for the pulses OPT#2, which is the second best performing technique, even though the latter requires over 2π higher pulse areas and is supposed to be, in that regard, more adiabatic than the presented single-parameter SSSP.

Comparing Fig. 4.3 with Fig. 4.1 we can discuss the locations of the maxima of the UH-fidelity radius for SSSP. From the low and insufficient pulse areas to the first maximum at about 6π we are observing the first minimum of the first non-null infidelity order $\widetilde{O}_2$. The second most notable peak (neglecting the almost imperceptible one at 7.5π) is located at about 10π, an intermediate position between the second minimum of $\widetilde{O}_2$ and the fourth of $\widetilde{O}_4$. Finally, the largest, broadest and most relevant maxima to extract from this work is located beyond the third minimum

of $\widetilde{O}_2$ and closer to, presumably, higher infidelity orders $\widetilde{O}_n$'s. This UH-fidelity radius maxima at $\sim 12\pi$ is the consequence of the simultaneous and local minimization of multiple infidelity orders and the best robustness obtained for $\mathcal{A} \leq 15\pi$ and among the comparable implementations of STIRAP shown on this study.

The highest UH-fidelity radius reached by our SSSP, of 22.36% for $\mathcal{A} = 12.23\pi$ or $\phi_0 = 0.12815$, generates the pulse shapes shown in Fig. 4.4 with its corresponding temporal population evolution and state's projection onto the adiabatic eigenvectors, time axis is limited to 40% of the full time interval considered of duration T.

The projection of the state's dynamics onto the adiabatic states shows that the system doesn't follow the dark state along the evolution, it departs from it to populate a superposition of bright states, and, even though it comes back to it towards the end of the process, this differentiates it from the ideal STIRAP. In practice, this result would be similar for all counter-intuitively ordered control fields and differ only in the degree in which the excited state is populated during the dynamics.

The pulses shapes are quite simple and similar to Gaussians but clearly asymmetric. The absolute value of the pump pulse, $|\Omega_P|$, is shown instead of its direct value Ω_P, as it is shown for Ω_S, because observation is simplified this way, providing the figure with the only relevant information about the pulses: their shapes. For the same pulse shapes, pulses with equal or different relative signs will lead to identical results for the population fidelity; only the actual states involved would vary between $|1\rangle \to -|3\rangle$ (or $-|1\rangle \to |3\rangle$) for Ω_P and Ω_S of same sign, and $|1\rangle \to |3\rangle$ (or $-|1\rangle \to -|3\rangle$) for Ω_P and Ω_S of different sign. The population of the excited state finds its maximum in the middle between the pulses, or $t - t_i = T/2$, and it has the reduced maximal value of $P_2 = 0.016$.

The UH-fidelity radius has been defined through the implementation of a Hamiltonian perturbation, shown in (4.15), that can be seen as considering a lack of perfect knowledge over the quantum system while having perfect control over the fields, some practical examples can be readily provided:

- Pump and Stokes beams with equal intensity profiles (like Gaussian profiles with the same waist) interacting with atomic systems of no perfectly known location [64].

- Certain variations on the dipole moment of the transitions, such as on their orientation, can affect both pump and Stokes fields on equal manner.

- All those cases in which both controls are produced by the same source and thus any unexpected deviation affecting field amplitudes would be equal for

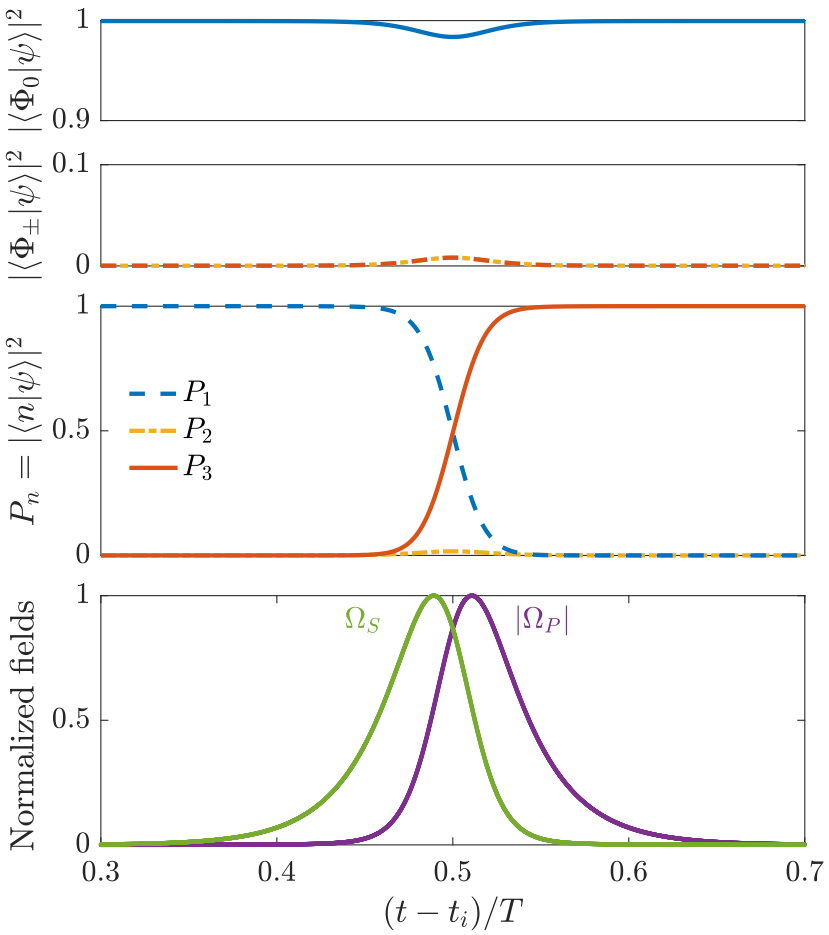

Figure 4.4: Time evolution of populations and the corresponding shaped fields, at best performing conditions, i.e., $\mathcal{A} \approx 12\pi$ (regarding the UH-fidelity radius shown in Fig. 4.3).

the fields [6], such as when the considered transition frequencies are so close to each other that a single field can excite them. Another case would be that of when the addressed transitions involve Zeeman sublevels, where the coupling fields are only required to differ in polarization (right- and left-handed circular polarization for example). Having fields that originate from the same source impose them to have the same temporal shape, or to be mirror images of each other if we can use counter-propagating fields.

In conclusion, we have optimized robustness from an exact solution derived from the Lewis-Riesenfeld method with one mode, which allowed a full shaping of the fields. This strongly contrasts with respect to most of the previous attempts at optimizing STIRAP (fidelity and robustness) which were based on the optimization of a set of natural parameters, e.g., delay, waist, amplitude, among others. We have derived a parametrization achieving high robustness for moderate pulse areas. Additionally, this solution opens further prospects for designing various exact and robust solutions based on STIRAP, or its extensions, such as N-pod STIRAP [65] or other multilevel systems [66–70].

Chapter 5

Optimal Robust STIREP by inverse optimization

5.1 Introduction

Adiabatic passage requires, in principle, infinite pulse areas to perform complete population transfers and to maintain the excited state completely depopulated along the dynamics, as it would be desirable. Alternative protocols with realistic physical conditions have been recently investigated. One can mention acceleration of the transfer by parallel adiabatic passage [31], but still featuring a large transient population in the excited state, shortcut to adiabaticity by counterdiabatic driving [58, 71–74], and, as seen in the preceding chapter, inverse engineering, where the controls are derived from a given dynamics [21, 27, 75, 76]. We have shown that the formulation of the latter allows one to generate infinitely many exact solutions and one can select among them the ones with specific features such as robustness [19–21, 36, 77–79] or stability in the case of non-linear dynamics [44, 80]. Disadvantageously, this method is strongly dependent on the protocol used for the prescription, both in dynamical behavior and in the consequent field characteristics such as pulse area, energy, duration, and robustness.

A method combining inverse engineering and optimization, where the controls are derived from a trajectory that is optimal with respect to a given cost, has been proposed. Robust inverse optimization (RIO) incorporates robustness as additional constraints. It has been demonstrated for a two-level system using a variational procedure based on a geometric representation of the dynamics, producing ultimate solutions that featured exactness, robustness, and absolute optimality (for instance with respect to pulse area, energy, and duration of the controls) [37].

In this work, we apply the RIO technique to derive resonant control pulses in a

Λ system featuring exact, robust, and optimal transfers, taking into account a given admissible total loss. These result from an optimization via the resolution of the Euler-Lagrange equations with the constraints of robustness up to third order (considered in terms of a common scaling inhomogeneity factor for both fields). We find numerically the optimal and robust family of solutions, each of them corresponding to a given loss. These numerical solutions lead to control fields of remarkably simple temporal shapes featuring, when a low loss is considered, a combination of intuitively and counter-intuitively ordered pairs. Their area is only about twice as large as the optimal unconstrained (i.e. non-robust) Λ transfer [23, 81].

A simple guide to the results of this chapter can be pictured as follows: (i) The resonant Λ system, Eq. (5.1), is parametrized in terms of angular variables, Eq. (5.10), and we solve the Euler-Lagrange equations (5.19) for these, with pulse area being the cost function to optimize. (ii) The solutions of the explicit equation (5.22), which depend on a geometrical parameter ($\dot{\widetilde{\phi}}_i$), are systematically derived with their corresponding pulse areas in Fig. 5.1(a) and 5.1(b), and result in the trajectories shown in Figs. 5.2(a) and 5.2(b) for representative values of the parameter $\dot{\widetilde{\phi}}_i$. (iii) The robustness of these trajectories is found in Fig. 5.3 compared with the optimal non-robust solution [23, 81]. (iv) Energy optimization leads to temporal pulse shapes and their respective population dynamics, shown in Figs. 5.5 and 5.6 for selected values of the parameter $\dot{\widetilde{\phi}}_i$. (v) The selected robust and optimal pulse shapes are entirely characterized in Table 5.1.

In section 5.2 we present the model for a resonant three-level system considering a lossy intermediate state; we propose a geometric (angular) parametrization of state, propagator, and loss, while declaring the corresponding boundary conditions appropriate for the Λ transfer. Section 5.3 contains the parametrization of the fields and definition of the cost functions to optimize, pulse area and energy; the fundamentals of robustness and its manipulation are also discussed. Section 5.4 gathers the geometric constraints to be enforced, dealing with both: boundary conditions and robustness, and introduces the corresponding Euler-Lagrange equation for the trajectory. Section 5.5 presents the results on the robust area-optimization, the optimal trajectories and its defining parameters and characteristics, irrespective of any specific time parametrization (thus a geometric trajectory in contrast with a temporal dynamics). Section 5.6 shows the Euler-Lagrange equations for the optimization of the state evolution with respect to the generalized pulse energy, leading to a time parametrization that also minimizes the duration of the transfer. The temporal shape of the coupling fields, the population dynamics, and the corresponding losses are all discussed in Section 5.7, where also the numerical details of the results are gathered. Finally, conclusions are presented.

Appendixes are included with details for the obtainment of the deviation integrals and the numerical resolution of the trajectory equation. Some useful geometrical relations for symmetric trajectories and the time-evolution of the angles are also presented as Appendixes.

5.2 The model

We consider a three-level system driven by two resonant fields of Rabi frequencies $\Omega_P(t)$ and $\Omega_S(t)$ for which the Hamiltonian, on the bare states basis $\{|1\rangle, |2\rangle, |3\rangle\}$ and under the rotating wave approximation, is:

$$H_\Gamma(t) = \frac{\hbar}{2}\begin{bmatrix} 0 & \Omega_P & 0 \\ \Omega_P & -i\Gamma & \Omega_S \\ 0 & \Omega_S & 0 \end{bmatrix}, \tag{5.1}$$

and the state of the system is denoted by $|\psi_\Gamma(t)\rangle$, solution to the time-dependent Schrödinger equation (TDSE) describing the dynamics from the initial to the final times t_i and t_f, accounting for dissipation losses of state $|2\rangle$. We have considered, as it is standard, that the upper state is lossy through the dissipation rate Γ.

As analyzed in Section 3.3.2, when the dissipation rate is much smaller than the peak Rabi frequency (typically at least 10 times smaller), the total loss of the system during the interaction time $T = t_f - t_i$ is well approximated by (3.26):

$$P_{\text{loss}} \approx \Gamma \int_{t_i}^{t_f} dt\, P_2(t), \tag{5.2}$$

where $P_2 = |\langle 2|\psi_{\Gamma=0}\rangle|^2$ is the population in the excited state in absence of dissipation. We will thus consider the dynamics with the lossless Hamiltonian (with $\Gamma = 0$) and the expected loss will be taken into account via (5.2).

Prescribing the desired transfer to be $|\psi(t_i)\rangle \equiv |\psi_i\rangle = |1\rangle \rightarrow |\psi(t_f)\rangle \equiv |\psi_f\rangle = |\psi_T\rangle = \pm|3\rangle$, while hoping to maintain a small excited state population (to minimize the loss), we can parametrize the state of the system, solution of the TDSE for the lossless Hamiltonian, $|\psi_{\Gamma=0}\rangle \equiv |\psi\rangle$, as

$$|\psi(t)\rangle = \begin{bmatrix} \cos\phi\cos\theta \\ i\sin\phi \\ \cos\phi\sin\theta \end{bmatrix}, \tag{5.3}$$

whose time-dependent angular parametrization must satisfy the boundary condi-

tions:

$$\phi_i = 0 \leftarrow \phi(t) \rightarrow \phi_f = 0, \tag{5.4a}$$

$$\theta_i = 0 \leftarrow \theta(t) \rightarrow \theta_f = \theta_f^{\pm} = \pm\pi/2. \tag{5.4b}$$

The arrows to the right and left indicate the limits when $t \rightarrow t_f$ and $t \rightarrow t_i$, respectively. The sign $\pm$ indicates the two possible options for the terminal θ. The phase of the target state $|\psi_T\rangle$ is irrelevant for the transfer of population and can be interpreted, and controlled, as a constant carrier-envelope phase difference between the control fields. Vector (5.3) and

$$|\psi_+(t)\rangle = \begin{bmatrix} i\cos\eta\sin\phi\cos\theta - i\sin\eta\sin\theta \\ \cos\eta\cos\phi \\ i\cos\eta\sin\phi\sin\theta + i\sin\eta\cos\theta \end{bmatrix}, \tag{5.5a}$$

$$|\psi_-(t)\rangle = \begin{bmatrix} -\sin\eta\sin\phi\cos\theta - \cos\eta\sin\theta \\ i\sin\eta\cos\phi \\ -\sin\eta\sin\phi\sin\theta + \cos\eta\cos\theta \end{bmatrix}, \tag{5.5b}$$

form a complete dynamical basis and constitute the propagator of the system, $U(t,t_i) = \begin{bmatrix} |\psi\rangle & |\psi_+\rangle & |\psi_-\rangle \end{bmatrix}$, where $\eta(t_i) \equiv \eta_i = 0$ is required by definition. This parametrization for the propagator can also be obtained from the Lewis-Riesenfeld invariant, as in [21].

The TDSE for the propagator, $H_{\Gamma=0} = i\hbar\dot{U}U^\dagger$, due particularly to the lack of coupling $\langle 1|H_{\Gamma=0}|3\rangle$, imposes the condition

$$\dot{\theta} = -\dot{\eta}\sin\phi \tag{5.6}$$

on the parametrization of the propagator. From (5.3) and (5.5), and by integrating it, we obtain:

$$\int_{t_i}^{t_f} \dot{\eta}\sin\phi\, dt = -\theta_f^{\pm} = \mp\frac{\pi}{2}, \tag{5.7}$$

which translates the terminal condition $\theta(t_f) \equiv \theta_f$, (5.4b), into a constraint on the time-dependence of $\dot{\eta}$ and ϕ.

It can be noted that the transient population of the excited state in this representation is given exactly by

$$P_2 = |\langle 2|\psi\rangle|^2 = \sin^2\phi, \tag{5.8}$$

and the total time-area of the population on the excited state can be written as:

$$A_2 = \int_{t_i}^{t_f} \sin^2\phi \, dt \approx \frac{P_{\text{loss}}}{\Gamma}. \tag{5.9}$$

This area A_2 represents thus the loss of the problem normalized by Γ. We can see that the presence of the dissipation rate $\Gamma \neq 0$ on the upper state induces necessarily a loss to accomplish a Λ transfer. This is true for any pump and Stokes configuration and shaping, since no loss ($A_2 = 0$) would require constant $\phi(t) = 0$ (for $\Gamma \neq 0$), hence constant $\theta(t) = 0$ [$\dot{\theta}(t) = 0$ from (5.6)], and thus no transfer.

As a general strategy to deal with a dissipation rate Γ, leading to a population loss P_{loss}, we will solve for the lossless dynamics while striving for low A_2's.

5.3 Inverse engineering and robustness

The parametrization of the TDSE allows one to define the inverse engineering problem: the controls in the Hamiltonian (5.1), with $\Gamma = 0$, are expressed in terms of the angles, from the parametrization of the propagator defined by (5.3) and (5.5), as

$$\Omega_P/2 = \dot{\eta}\cos\phi\sin\theta - \dot{\phi}\cos\theta, \quad \Omega_S/2 = -\dot{\eta}\cos\phi\cos\theta - \dot{\phi}\sin\theta. \tag{5.10}$$

It can be noticed that the values of the time-derivatives at the initial and final time, $\dot{\eta}_{i,f}$ and $\dot{\phi}_{i,f}$, give the value of the control fields evaluated at the boundaries, i.e., using (5.4),

$$\Omega_P^i = -2\dot{\phi}_i, \quad \Omega_P^f = \pm 2\dot{\eta}_f, \quad \Omega_S^i = -2\dot{\eta}_i, \quad \Omega_S^f = \mp 2\dot{\phi}_f. \tag{5.11}$$

We define the generalized pulse area (referred simply as pulse area from here on) to be

$$\mathcal{A}_t \equiv \int_{t_i}^{t_f} \sqrt{\Omega_P^2 + \Omega_S^2}\, dt = 2\int_{t_i}^{t_f} \sqrt{\dot{\phi}^2 + \dot{\eta}^2\cos^2\phi}\, dt, \tag{5.12a}$$

which can be rewritten as an integral in terms of η if we assume that $\phi(t)$ can be expressed as a function of $\eta(t)$, i.e.,

$$\mathcal{A} = 2\int_{\eta_i}^{\eta_f} \operatorname{sgn}\dot{\eta}\sqrt{\left(\tilde{\dot{\phi}}\right)^2 + \cos^2\tilde{\phi}}\, d\eta, \tag{5.12b}$$

where $\widetilde{\phi}(\eta) \equiv \phi[\eta(t)]$, $\dot{\widetilde{\phi}} \equiv \partial_\eta \widetilde{\phi}$, and ∂_η is the partial derivative operator with respect to η. Once the sign of $\dot{\eta}$ is fixed, Eq. (5.12b) will not depend on time but only on the trajectory $\widetilde{\phi}(\eta)$. Equation (5.7) has a similar property. The dynamic behavior of η can be considered to be monotonic or not, requiring to segment the integral in the latter case and to consider a piecewise function $\widetilde{\phi}(\eta)$.

The issue of robustness can be dealt with by adding perturbation terms to the Hamiltonian, representing errors or imperfections of the practical implementation. We consider an error originated by pulse inhomogeneities, taken as identical for both pulses, modeled by the modified Hamiltonian $H_\epsilon = H_{\Gamma=0} + V = (1+\epsilon)H_{\Gamma=0}$, which translates into a deviation on the desired state dynamics and generalized pulse area. We denote $|\psi_\epsilon(t)\rangle$ as the state of the complete dynamics including the error, solution of the TDSE $i\hbar\partial_t|\psi_\epsilon(t)\rangle = H_\epsilon|\psi_\epsilon(t)\rangle$. The single-shot shaped pulse method [19, 20] allows one to define trajectories, in the dynamical variables space, resistant to errors. It can be formulated by a perturbative expansion of $|\psi_\epsilon(t_f)\rangle$ with respect to ϵ, $\langle\psi_T|\psi_\epsilon(t_f)\rangle = 1 - O_1 - O_2 - O_3 - \cdots$, where O_n denotes the error term of order n: $O_n \equiv O(\epsilon^n)$, and $|\psi_T\rangle$ is the target state.

In practice, we search to attain the optimal solution in terms of certain cost parameter. For instance, we can define the cost to be the required pulse area to reach the target state, and strive to minimize it; or, we can define the cost to be a specific measure of robustness (e.g., the maximum range of ϵ for which the target state is reached with under 10^{-4} deviation), and maximize it. Here, we will consider both, optimization and robustness, which technically corresponds to *searching the optimal solution with respect to a cost (pulse area, energy, or duration) under the constraint of robustness.*

When we consider both optimization and robustness with respect to the generalized pulse area $\mathcal{A}$ (or identically to both pulse amplitudes for a given time of interaction), Eqs. (5.7) and (5.12) show that one can consider the problem in the parameter space formed by the angles $(\eta, \widetilde{\phi})$, without invoking a specific time parametrization; thus providing a purely geometric representation of the problem.

In fact, it is known that, in the absence of robustness constraints, minimizing the pulse area (5.12) is equivalent to minimizing the pulse energy,

$$\mathcal{E} = \hbar \int_{t_i}^{t_f} \left(\Omega_P^2 + \Omega_S^2\right) dt = 4\hbar \int_{t_i}^{t_f} \left(\dot{\phi}^2 + \dot{\eta}^2 \cos^2\phi\right) dt, \tag{5.13}$$

and to minimize the time for a given bound of the pulse amplitudes [23] (equivalently, to minimize the pulse amplitudes for a certain pulse duration). We will show that this property still applies for our constrained problem.

A robust optimal transfer of population corresponds to a special trajectory $\widetilde{\phi}_{\text{opt}}(\eta)$ that, satisfying the boundary conditions (5.4), minimizes the generalized pulse area (5.12b) while attaining robustness up to a certain order. The construction of the actual time-dependent pulses Ω_P and Ω_S from (5.10) necessitates the use of a specific temporal parametrization, $\eta(t)$, which may be chosen at will (it is inconsequential) for the optimization solely with respect to the pulse area. On the other hand, optimization with respect to the pulse energy, corresponding to the minimization of Eq. (5.13), defines a specific temporal parametrization $\eta_{\mathcal{E}}(t)$ for the same optimal trajectory $\widetilde{\phi}_{\text{opt}}(\eta)$, which also minimizes the pulse duration for a fixed maximum of the pulse amplitudes.

5.4 Robust optimal population transfer

For the task of population transfer to a target state $|\psi_T\rangle$, the final global phase is not *a priori* fixed and, since it is irrelevant, its robustness is not cared for. The figure of merit up to the third order of robustness reads

$$\mathcal{F} = |\langle\psi_T|\psi_\epsilon(t_f)\rangle|^2 = 1 - \widetilde{O}_2 - \widetilde{O}_3, \tag{5.14}$$

where the first order is nil (real part of a purely imaginary number which, in this case, is anyway zero), and the second and third orders are

$$\widetilde{O}_2 = \left|\int_{t_i}^{t_f} n\,dt\right|^2 + \left|\int_{t_i}^{t_f} p\,dt\right|^2, \tag{5.15a}$$

$$\widetilde{O}_3 = 2i\left[\int_{t_i}^{t_f} n\,dt \int_{t_i}^{t_f}\int_{t_i}^{t} rp'\,dt'\,dt - \int_{t_i}^{t_f} p\,dt \int_{t_i}^{t_f}\int_{t_i}^{t} rn'\,dt'\,dt\right], \tag{5.15b}$$

with

$$n = \frac{\langle\psi|V|\psi_+\rangle}{\hbar} = -\dot{\eta}\sin\eta\sin\phi\cos\phi - \dot{\phi}\cos\eta, \tag{5.16a}$$

$$p = \frac{\langle\psi|V|\psi_-\rangle}{\hbar} = i(\dot{\eta}\cos\eta\sin\phi\cos\phi - \dot{\phi}\sin\eta), \tag{5.16b}$$

$$r = \frac{\langle\psi_+|V|\psi_-\rangle}{\hbar} = -\dot{\eta}\cos^2\phi. \tag{5.16c}$$

ϵ was used merely to keep track of the orders of the expansion. It has been omitted in the above expressions. We note from (5.15) that the only perturbation we need to be concerned about up to third order is $\widetilde{O}_2$, (5.15a), since (5.15b) shows that the third order deviation is null for any trajectory $\widetilde{\phi}(\eta)$ that nullifies the second order [i.e., the areas under $n(t)$ and $p(t)$]. Some properties used to obtain Eqs. (5.15) are

presented in Appendix 5.A.

5.4.1 Lagrangian formulation of the optimization

The problem of optimal nullification up to the third order can be formulated as a classical optimization problem: finding the trajectory $\widetilde{\phi}(\eta)$ that minimizes the pulse area (5.12b), which is the action (in the language of Lagrangian mechanics) and integral of a Lagrangian $\mathcal{L}$,

$$\mathcal{A} = 2\int_{\eta_i}^{\eta_f} \operatorname{sgn}\dot{\eta}\,\sqrt{\left(\dot{\widetilde{\phi}}\right)^2 + \cos^2\widetilde{\phi}}\,d\eta \equiv \int_{\eta_i}^{\eta_f} \mathcal{L}\left(\dot{\eta}, \widetilde{\phi}, \dot{\widetilde{\phi}}\right) d\eta, \tag{5.17}$$

under the constraints $\theta_f^{\pm} = \pm\pi/2$, from (5.7), and $\widetilde{O}_2 = 0$; rewritten for convenience as

$$\xi_0 = \int_{\eta_i}^{\eta_f} |\operatorname{sgn}\dot{\eta}|\sin\widetilde{\phi}\,d\eta \equiv \int_{\eta_i}^{\eta_f} \varphi_0\big(\widetilde{\phi}\big)\,d\eta = -\theta_f^{\pm} = \mp\frac{\pi}{2}, \tag{5.18a}$$

$$\xi_1 = \int_{\eta_i}^{\eta_f} |\operatorname{sgn}\dot{\eta}|\left(\dot{\widetilde{\phi}}\cos\eta + \sin\eta\sin\widetilde{\phi}\cos\widetilde{\phi}\right) d\eta \equiv \int_{\eta_i}^{\eta_f} \varphi_1\big(\eta, \widetilde{\phi}, \dot{\widetilde{\phi}}\big)\,d\eta = 0, \tag{5.18b}$$

$$\xi_2 = \int_{\eta_i}^{\eta_f} |\operatorname{sgn}\dot{\eta}|\left(\dot{\widetilde{\phi}}\sin\eta - \cos\eta\sin\widetilde{\phi}\cos\widetilde{\phi}\right) d\eta \equiv \int_{\eta_i}^{\eta_f} \varphi_2\big(\eta, \widetilde{\phi}, \dot{\widetilde{\phi}}\big)\,d\eta = 0, \tag{5.18c}$$

while satisfying the boundary conditions, for which the initial state is characterized by the angles $(\theta_i = 0, \phi_i = 0, \eta_i = 0)$ and the target (final) state by $(\theta_f^{\pm} = \pm\pi/2, \phi_f = 0, \eta_f)$. The factor $|\operatorname{sgn}\dot{\eta}|$ was added only as a reminder that we are dealing with a piecewise function $\widetilde{\phi}(\eta)$, where the interval of integration must be split each time $\dot{\eta}$ has a sign change. A way to detect such change of sign can be achieved geometrically during the determination of the trajectory $\widetilde{\phi}(\eta)$ from the initial condition (starting with a given sign of $\dot{\eta}$). The change of sign can occur at a point η_0 only when $|\dot{\widetilde{\phi}}(\eta_0)| \to \infty$. We will see that this does not happen in our problem, and that a monotonic $\eta(t)$ can be considered.

In this representation it is thus relevant to consider the trajectories $\widetilde{\phi}(\eta)$, constrained by the conditions (5.18), in the parameter space $(\eta, \widetilde{\phi})$.

5.4.2 Derivation of the trajectory $\widetilde{\phi}(\eta)$

We consider the representation of the trajectory $\widetilde{\phi}(\eta)$. Robust optimal control can be attained by solving the Euler-Lagrange equations and using the Lagrange multiplier method to account for the constraints. The task of complete population transfer, for the lossless system, is part of the constraints to be imposed, which is equivalent to enforcing the boundary conditions. In this context, complete population transfer

refers to satisfying the boundary conditions (5.4), leaving the loss to be estimated *a posteriori* via (5.2).

The optimal trajectory $\widetilde{\phi}(\eta)$ is a solution of

$$\operatorname{grad}\mathcal{A} + \sum_{j=0}^{2} \lambda_j \operatorname{grad}\xi_j = 0, \tag{5.19}$$

where λ_j $(j = 0, 1, 2)$ is the Lagrangian multiplier associated to each one of the three constraints, and the gradients,

$$\operatorname{grad}\mathcal{A} = \frac{\partial\mathcal{L}}{\partial\widetilde{\phi}} - \frac{d}{d\eta}\left(\frac{\partial\mathcal{L}}{\partial\dot{\widetilde{\phi}}}\right), \quad \operatorname{grad}\xi_j = \frac{\partial\varphi_j}{\partial\widetilde{\phi}} - \frac{d}{d\eta}\left(\frac{\partial\varphi_j}{\partial\dot{\widetilde{\phi}}}\right), \tag{5.20}$$

are defined according to the Euler-Lagrange equations.

We proceed to obtain the differential equation for the trajectory $\widetilde{\phi}(\eta)$ from:

$$\frac{\partial\mathcal{L}}{\partial\widetilde{\phi}} - \frac{d}{d\eta}\left(\frac{\partial\mathcal{L}}{\partial\dot{\widetilde{\phi}}}\right) + \sum_{j=0}^{2} \lambda_j \left[\frac{\partial\varphi_j}{\partial\widetilde{\phi}} - \frac{d}{d\eta}\left(\frac{\partial\varphi_j}{\partial\dot{\widetilde{\phi}}}\right)\right] = 0,$$

which leads, after simplification by $2\cos^2\widetilde{\phi}$, to

$$-\frac{\ddot{\widetilde{\phi}} + \left[2\left(\dot{\widetilde{\phi}}\right)^2 + \cos^2\widetilde{\phi}\right]\tan\widetilde{\phi}}{\operatorname{sgn}\dot{\eta}\left[\left(\dot{\widetilde{\phi}}\right)^2 + \cos^2\widetilde{\phi}\right]^{3/2}} + |\operatorname{sgn}\dot{\eta}|\left(\lambda_0\sec\widetilde{\phi} + \lambda_1\sin\eta - \lambda_2\cos\eta\right) = 0. \tag{5.21}$$

Note that we have redefined $\lambda_0/2$ as λ_0 without loss of generality.

Solving (5.21) means to find a trajectory $\widetilde{\phi}(\eta)$ with the λ_j's as free parameters to be set to satisfy the constraints (5.18). We can solve this numerically assuming a monotonic behavior for $\eta(t)$, i.e.

$$\mp\frac{\ddot{\widetilde{\phi}}^{\pm} + \left[2\left(\dot{\widetilde{\phi}}^{\pm}\right)^2 + \cos^2\widetilde{\phi}^{\pm}\right]\tan\widetilde{\phi}^{\pm}}{\left[\left(\dot{\widetilde{\phi}}^{\pm}\right)^2 + \cos^2\widetilde{\phi}^{\pm}\right]^{3/2}} + \lambda_0\sec\widetilde{\phi}^{\pm} + \lambda_1\sin\eta - \lambda_2\cos\eta = 0, \tag{5.22}$$

where we have used $\widetilde{\phi}^{\pm} \equiv \widetilde{\phi}_{\operatorname{sgn}\dot{\eta}=\pm1}$.

5.5 Robust area-optimal trajectory $\widetilde{\phi}(\eta)$

We determine the solution for the robust area-optimal trajectory via the numerical implementation of (5.22) into an ordinary differential equations solver [see

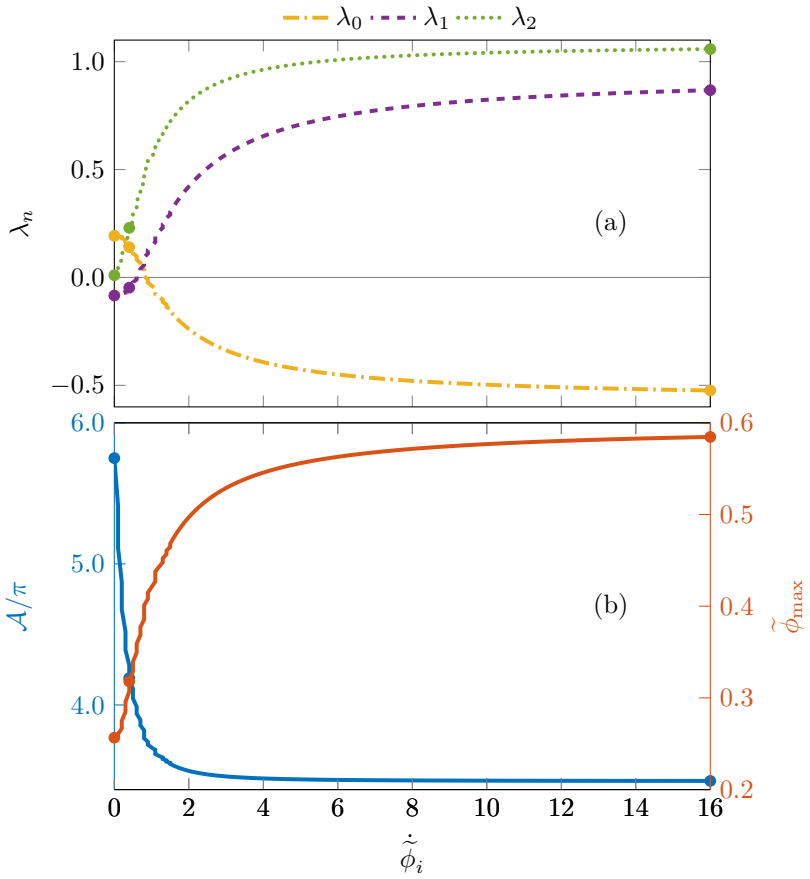

Figure 5.1: Area-optimal solutions vs $\dot{\tilde{\phi}}_i$ regarding (a) the λ_j's and (b) the pulse area and maximum value of $\tilde{\phi}$. The parameters defining the highlighted extrema are summarized in Table 5.1. Thin horizontal gray lines mark a zero.

system (5.44) in Appendix 5.B] and use its solution, in terms of the parameters $\left(\dot{\tilde{\phi}}_i, \lambda_0, \lambda_1, \lambda_2\right)$, for a subsequent nonlinear equations solver that seeks to satisfy the four trajectory constraints by searching in that four-parameter space. It turns out that for each value of $\dot{\tilde{\phi}}_i$ there is a trajectory solution to the Euler-Lagrange equations satisfying the imposed constraints. The parameters solution of this system are presented in Fig. 5.1(a) for values of $0 \leq \dot{\tilde{\phi}}_i \leq 16$.

The corresponding generalized pulse areas and the value of $\tilde{\phi}$ at the summit of the respective trajectories (related to the normalized loss A_2) are shown in Fig. 5.1(b).

The maximum and minimum generalized pulse areas on the plot, Fig. 5.1(b), are, respectively, $\mathcal{A}_{\max} = 5.7498\pi$ and $\mathcal{A}_{\min} = 3.4608\pi$, while the corresponding minimum and maximum values of ϕ (inversely related to the area) are $\phi_{\min} = 0.2566$ and $\phi_{\max} = 0.5893$. If to extend the plot to a large value, much beyond the point were significative change occurs on the trajectory, e.g., $\dot{\tilde{\phi}}_i = 250$, we would obtain

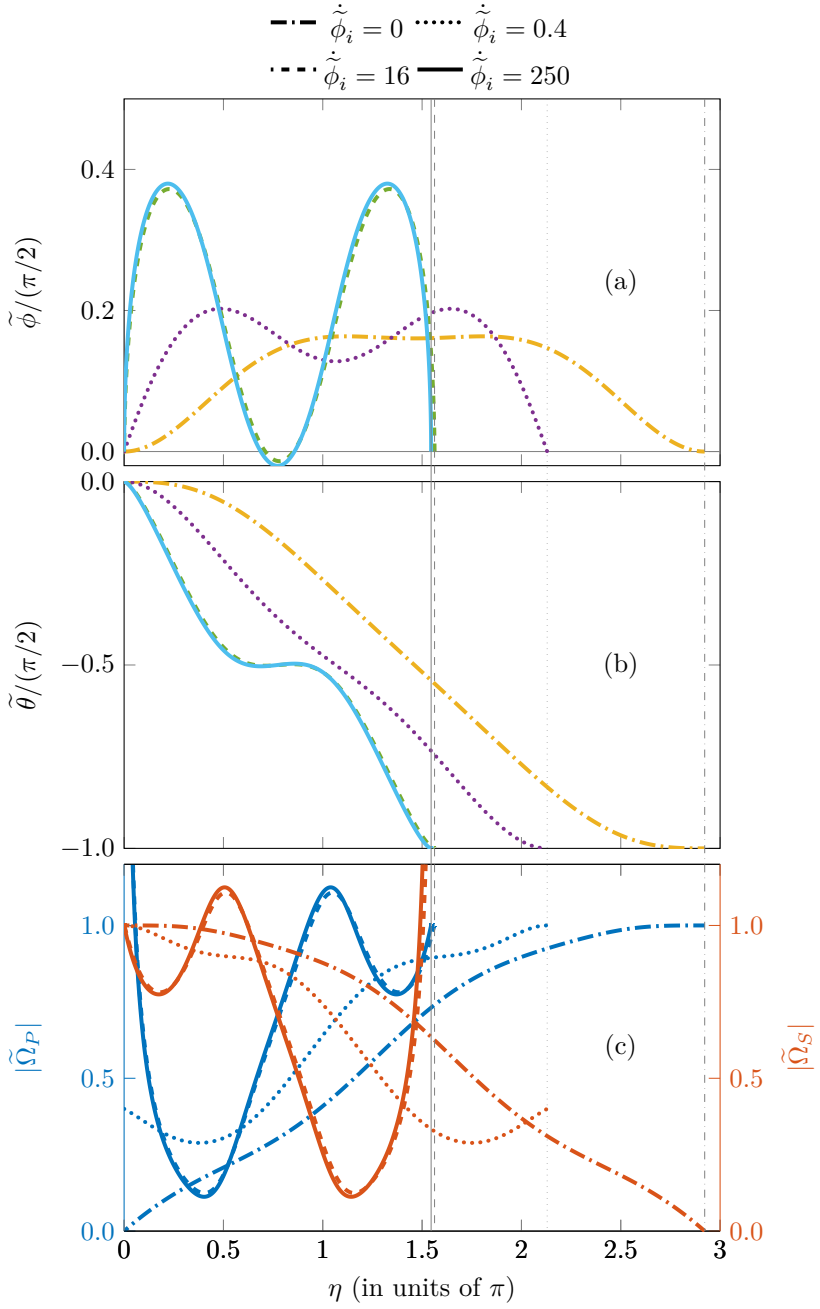

Figure 5.2: Trajectories $\widetilde{\phi}(\eta)$ and $\widetilde{\theta}(\eta)$, for selected extrema of the area minimization problem, are shown in (a) and (b). Respective Pump and Stokes fields, dynamically scaled by $2\dot{\eta}$, are shown in (c) vs η. The parameters defining the corresponding extrema are summarized in Table 5.1. The line style in the legend applies to all plots irrespective of the line color. The thin vertical gray lines are located at the η_f corresponding to each trajectory. Thin horizontal gray lines mark a zero.

$\mathcal{A} = 3.4603\pi$ and $\widetilde{\phi}_{\max} = 0.5975$.

The trajectories represented by each set of points corresponding to a single value of $\dot{\widetilde{\phi}}_i$ are the extrema of the optimization problem, candidates to be an optimal solution. The optimum trajectory is obtained among all these solutions for the one corresponding to the minimum generalized pulse area: $\mathcal{A}_{\min} \approx 3.4603\pi$, associated to $|\dot{\widetilde{\phi}}_i| \to \infty$ and to a normalized loss $A_2 \approx 0.1291$. However, we highlight that all the other extremal solutions, featuring larger pulse areas, represent physical optimal and robust solutions, but with corresponding lower normalized losses.

We notice that these solutions, defined by Fig. 5.1(a) and extensible to $\dot{\widetilde{\phi}}_i \to \infty$, are symmetrically mirrored (with identical pulse areas) for $\dot{\widetilde{\phi}}_i \leq 0$, with a sign change in the λ_j's (and $\phi_{\max}$), thus the sign-changed alternative solution at $\dot{\widetilde{\phi}}_i = 0$ was omitted for clarity. These alternative trajectories, namely with sign-changed $\widetilde{\phi}$ and $\widetilde{\theta}$, produce sign-changed pumps and final states, Ω_P and $|\psi_f\rangle$, and do not differ in any other way; hence, we limit our analysis to $\dot{\widetilde{\phi}}_i \geq 0$.

Although it is far from being actually adiabatic (much lower areas compared to usual adiabatic requirements), the behavior of this family of solutions is reminiscent of adiabatic solutions in terms of correlation between pulse area and normalized loss: higher the invested pulse area, lower the maximum of the transient excited state population and the corresponding normalized loss (see Fig. 5.7).

It is worthy of mention that Eq. (5.22) was solved [i.e. the system (5.44) was integrated] without demanding the symmetry of the trajectory, see Appendix 5.C. Each trajectory was computed from $\eta = 0$ to a large $\eta_{\max}$ (typically $\eta_{\max} = 3\pi$). Then, the solutions were obtained by taking ϕ_f to be a point where the trajectory crossed the $\phi = 0$ line boundary (thus truncating there the trajectory).

Having left the symmetry (or lack of it) of the trajectories to be decided by the solution of the dynamical system and satisfaction of the constraints, we obtained symmetric (of even parity) trajectories with η_f matching (one of) the expected values (5.47) naturally, as it can be seen in Figs. 5.2(a)–5.1(c).

The values of η_f are lower for higher maximum state populations, but the resultant areas are lower; trajectories and pulses are then shorter (in η), leading, presumably, to the optimal time: the fastest way to go from $\eta_i \equiv 0$ to η_f, which would naturally be faster for lower values of η_f.

We notice that all solutions for $\dot{\widetilde{\phi}}_i \leq 5.5$ were obtained by choosing ϕ_f as the first zero-crossing, while for $\dot{\widetilde{\phi}}_i > 5.5$ we had to truncate at the third one.

Other families of solutions, families of extrema of the optimization problem, were found for larger boundaries of the integration ($\eta_{\max} > 3\pi$) and for second- and third-zero–crossings, some of them even displaying asymmetric trajectories. However, all of them presented larger areas to the family in Fig. 5.1 and 5.2, thus they

are irrelevant to the problem of optimization. For example, the asymmetric trajectories corresponding to the second–zero-crossing family of solutions present areas of $5.715\pi \leq \mathcal{A} \leq 5.750\pi$. Meanwhile, the next immediate family of trajectories (third–zero-crossing) exhibit about three times the area and value of η_f, in the vicinity of $\dot{\widetilde{\phi}}_i = 0$, of the optimal family.

The extremum trajectories $\widetilde{\phi}(\eta)$ in Fig. 5.1(a) display a double peak structure, although it is only slight for the the largest-area extremum, $\dot{\widetilde{\phi}}_i = 0$. The well between the persistent positive peaks becomes a negative peak (though of much smaller magnitude) for the optimal trajectory. By comparison between the shown trajectories with the largest $\dot{\widetilde{\phi}}_i$ it is clear that the system geometric evolution is optimal at infinity, but values in the order of the tens already describe it well.

The evolution of the mixing angle $\widetilde{\theta}(\eta)$ behaves as a symmetrical two-step process, two identical consecutive evolutions $0 \to \pi/4 \to \pi/2$; however, it can not be regarded as twice a robust half-transfer, since, although we can take the extrema whose half-point is nil as its endpoint, $\phi_f^{\text{half}} = \phi_m = 0$, this half-transfer is not robust [since it does not satisfy (5.18) for $\eta_f^{\text{half}} = \eta_m$].

Having treated the dynamics as a geometric trajectory $\widetilde{\phi}(\eta)$, we are left only with the dynamically-scaled fields

$$\widetilde{\Omega}_P(\eta) \equiv \Omega_P/(2\dot{\eta}) = \cos\widetilde{\phi}\sin\widetilde{\theta} - \dot{\widetilde{\phi}}\cos\widetilde{\theta}, \tag{5.23a}$$

$$\widetilde{\Omega}_S(\eta) \equiv \Omega_S/(2\dot{\eta}) = -\cos\widetilde{\phi}\cos\widetilde{\theta} - \dot{\widetilde{\phi}}\sin\widetilde{\theta}, \tag{5.23b}$$

to picture the control fields in terms of η. These equations show that the initial and final values of these parametrized ratios are:

$$\widetilde{\Omega}_P^i = -\dot{\widetilde{\phi}}_i, \qquad \widetilde{\Omega}_P^f = \operatorname{sgn}\theta_f, \quad \widetilde{\Omega}_S^i = -1, \qquad \widetilde{\Omega}_S^f = -\operatorname{sgn}\theta_f\,\dot{\widetilde{\phi}}_f. \tag{5.24}$$

The absolute value of the dynamically-scaled control fields $\widetilde{\Omega}_P$ and $\widetilde{\Omega}_S$ is shown in Fig. 5.2(c), evidencing the boundary Eqs. (5.24). Although the actual time-dependent control fields will be described only after a time-parametrization of $\eta(t)$ is decided, we can already note that the couplings present a marked counter-intuitive ordering. This is obvious for the largest-area extrema, but it is still mostly true for the optimum with the exception of the spikes near the boundaries of the trajectory.

The ideal robust optimum solution would demand infinite scaled amplitudes at one of the boundaries for each field, but this does not require the actual pulses to have infinite magnitudes at any point in time. The fields as functions of time may be made indeed finite with a proper choice of the time parametrization, i.e. of $\eta(t)$.

The quantities $\left(\widetilde{\Omega}_P, \widetilde{\Omega}_S\right)$ are sufficient to solve the TDSE parametrized in terms

of η, with $\widetilde{H}_\epsilon(\eta) \equiv H_\epsilon(t)/\dot{\eta}$,

$$i\hbar\partial_\eta|\widetilde{\psi}_\epsilon(\eta)\rangle = \widetilde{H}_\epsilon(\eta)|\widetilde{\psi}_\epsilon(\eta)\rangle, \tag{5.25}$$

which can be reparametrized back to time, to observe populations actual temporal-dynamics, by simply providing the time-dependence of $\eta(t)$.

The non-robust optimal exact Λ transfer has been derived in [23] and their corresponding analytical pulse shapes for pulse-energy optimization were given in [81], producing the coupling fields:

$$\Omega_P = \frac{\sqrt{3}\pi}{T}\cos\Big[\frac{\pi(t-t_i)}{2T}\Big], \quad \Omega_S = \frac{\sqrt{3}\pi}{T}\sin\Big[\frac{\pi(t-t_i)}{2T}\Big], \tag{5.26a}$$

where T is the pulse duration. These coupling fields of generalized area $\sqrt{3}\pi$ are the equivalent of the π-pulse Rabi solution, the diabatic solution by excellence, for the three-level Λ system. It exhibits the minimum area and energy necessary to perform the complete population transfer $|1\rangle \rightarrow |3\rangle$, while the pulse duration fixes the cap on the field amplitudes (equivalently we may fix the pulse amplitudes and extract the minimum time). Hence, it is the ideal benchmark to test the gained robustness of our optimal robust solution; just as the π-pulse would be used to compare with population-inversion schemes in a two-level system [19, 37]. This optimal solution, as it differentiates from our robust optimal results in the fact that it doesn't satisfy the robustness constraints, will be referred to as the unconstrained optimal, or simply optimal, solution. Therefore, another use of this basis for comparison is to use it to understand what is the minimum energy required to gain or acquire a certain order of robustness.

Solving the TDSE taking into account pulse area scaling error up to $\pm 20\%$, we obtain the robustness profile of the population transfer fidelity and base 10 logarithm of the infidelity, presented in Figs. 5.3(a) and 5.3(b), respectively. The profile is slightly broader for larger-area extrema, but all extrema are much more robust than the unconstrained pulse area-optimal solution (5.26). Particularly, the fidelity profile for the optimal extrema is symmetric around the unperturbed condition, while the extrema with larger areas present an advantageous slanted profile towards the positive area-scaling deviations ($\epsilon > 0$).

The symmetry of the optimal solutions is a remarkable feature which is certainly not shared with adiabatic processes (or any other scheme for that matter). For the robustness profile, an increase on energy (equivalently, area) in the adiabatic regime is indeed not equivalent to a decrease. This is shown in ref. [21], where the robustness profile is determined for an exact Λ transfer: the slanting of it is evident for larger

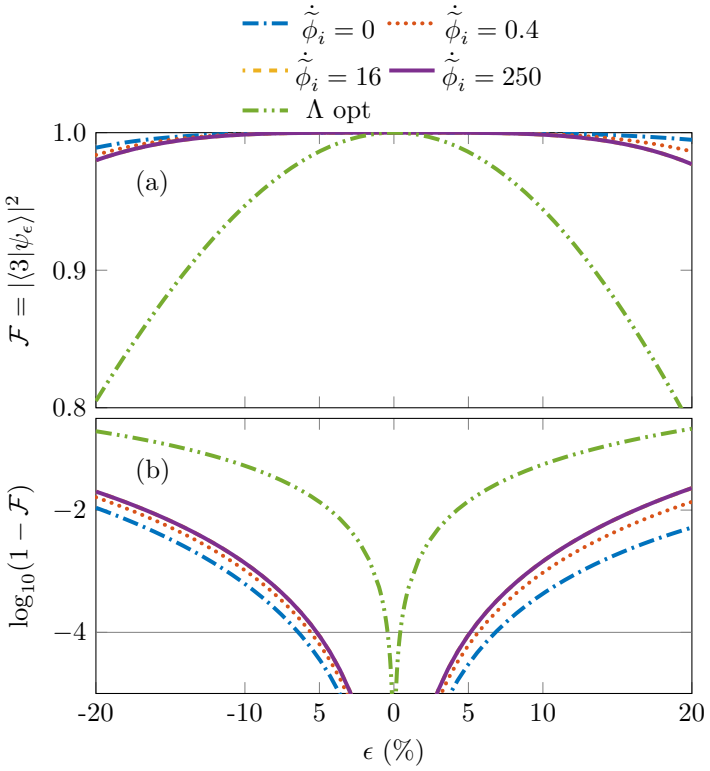

Figure 5.3: Fidelity (a) and logarithm base 10 of the infidelity (b), for the selected optima highlighted in Fig. 5.1 (with trajectories and control fields in Fig. 5.1) with numeric data summarized in Table 5.1, and for the Λ transfer optimized with no constraints of robustness, with respect to the pulse area scaling error ϵ. The thin horizontal gray line denotes the ultrahigh-fidelity benchmark of 10^{-4} infidelity.

areas where adiabaticity starts to prevail. Understanding adiabaticity as the general behavior or tendency of the evolution approaching the dynamics at the adiabatic limit. We can note that the optimal with no constraints of robustness displays a strictly symmetrical robustness profile, which is a shared characteristic with our optimal robust solution.

The effect of investing about one time more the area of the optimal pulse ($\mathcal{A}_{\text{RobOpt}} \approx 2\mathcal{A}_{\text{opt}}$) is remarkable: almost 13 times gain in the width of the robustness between $\epsilon = 0$ and the closest point where infidelity goes above 10^{-4}, i.e. $\Delta\epsilon_{\text{RobOpt}} \approx 0.051$ while $\Delta\epsilon_{\text{opt}} \approx 0.004$. It is worth noting that the unconstrained optimal pulses are intuitively ordered while our robust optimal pulses feature an overall counter-intuitive ordering. As observed in Fig. 5.2(c), the largest-area robust extrema (for $\dot{\tilde{\phi}}_i = 0$) presents the most simple and clearly counter-intuitively–ordered pulse pair. Meanwhile, the actually-minimal–area extrema (global optimum), corresponding to $\dot{\tilde{\phi}}_i \to \infty$, exhibits counter-intuitive behavior at most instances of the "dynamics" (actually, geometric evolution along η), i.e. except near the beginning and the end of the evolution.

5.6 Robust energy-optimal dynamics $\eta(t)$

The time dependence of the area-optimal geometrical trajectory is free to be chosen. However, it is most interesting to consider optimality with respect to the pulse energy, which would also satisfy optimality with respect to time for a certain maximum amplitude, as shown below. We can do this with the Euler-Lagrange equations with constraints, as we have done for the area optimization, but using the energy definition

$$\mathcal{E} = \hbar \int_{t_i}^{t_f} \left(\Omega_P^2 + \Omega_S^2\right) dt = 4\hbar \int_{t_i}^{t_f} \left(\dot{\phi}^2 + \dot{\eta}^2 \cos^2\phi\right) dt \equiv \int_{t_i}^{t_f} \mathcal{L}_{\mathcal{E}}(\phi, \dot{\eta}, \dot{\phi})\, dt, \quad (5.27)$$

as the cost to be minimized. In this case, the time-representation of the constraints (5.18) writes:

$$\xi_{t0} = \int_{t_i}^{t_f} \dot{\eta} \sin\phi\, dt \equiv \int_{t_i}^{t_f} \varphi_{t0}(\phi, \dot{\eta})\, dt = -\theta_f^{\pm} = \mp\frac{\pi}{2}, \quad (5.28a)$$

$$\xi_{t1} = \int_{t_i}^{t_f} (\dot{\phi}\cos\eta + \dot{\eta}\sin\eta\sin\phi\cos\phi)\, dt \equiv \int_{t_i}^{t_f} \varphi_{t1}(\eta, \phi, \dot{\eta}, \dot{\phi})\, dt = 0, \quad (5.28b)$$

$$\xi_{t2} = \int_{t_i}^{t_f} (\dot{\phi}\sin\eta - \dot{\eta}\cos\eta\sin\phi\cos\phi)\, dt \equiv \int_{t_i}^{t_f} \varphi_{t2}(\eta, \phi, \dot{\eta}, \dot{\phi})\, dt = 0, \quad (5.28c)$$

which are satisfied, regardless of the time dependence of η, by the trajectories $\widetilde{\phi}(\eta)$ from (5.21) with their appropriate choices of the λ_j's.

The dynamics $\{\theta(t), \eta(t), \phi(t)\}$ can be formulated as the solution of the optimal problem, as the evolution satisfying the Euler-Lagrange equations

$$\operatorname{grad}\mathcal{E} + \mu_0 \operatorname{grad}\psi_{t0} + \mu_1 \operatorname{grad}\psi_{t1} + \mu_2 \operatorname{grad}\psi_{t2} = 0, \tag{5.29}$$

where the μ_j's ($j = 0, 1, 2$) are the Lagrangian multipliers associated to the constraints, and the gradients are

$$\operatorname{grad}\mathcal{E} = \begin{bmatrix} \frac{\partial \mathcal{L}_\mathcal{E}}{\partial \eta} - \frac{d}{dt}\left(\frac{\partial \mathcal{L}_\mathcal{E}}{\partial \dot{\eta}}\right) \\ \frac{\partial \mathcal{L}_\mathcal{E}}{\partial \phi} - \frac{d}{dt}\left(\frac{\partial \mathcal{L}_\mathcal{E}}{\partial \dot{\phi}}\right) \end{bmatrix}, \quad \operatorname{grad}\xi_{tj} = \begin{bmatrix} \frac{\partial \varphi_{tj}}{\partial \eta} - \frac{d}{dt}\left(\frac{\partial \varphi_{tj}}{\partial \dot{\eta}}\right) \\ \frac{\partial \varphi_{tj}}{\partial \phi} - \frac{d}{dt}\left(\frac{\partial \varphi_{tj}}{\partial \dot{\phi}}\right) \end{bmatrix}. \tag{5.30}$$

The Euler-Lagrange equations lead to

$$0 = -\frac{d}{dt}\left(\frac{\partial \mathcal{L}_\mathcal{E}}{\partial \dot{\eta}}\right) + \sum_{j=0}^{2} \mu_j \left[\frac{\partial \varphi_{tj}}{\partial \eta} - \frac{d}{dt}\left(\frac{\partial \varphi_{tj}}{\partial \dot{\eta}}\right)\right], \tag{5.31a}$$

$$0 = \frac{\partial \mathcal{L}_\mathcal{E}}{\partial \phi} - \frac{d}{dt}\left(\frac{\partial \mathcal{L}_\mathcal{E}}{\partial \dot{\phi}}\right) + \sum_{i=0}^{2} \mu_i \left[\frac{\partial \varphi_{tj}}{\partial \phi} - \frac{d}{dt}\left(\frac{\partial \varphi_{tj}}{\partial \dot{\phi}}\right)\right], \tag{5.31b}$$

which are, for $\cos\phi \neq 0$,

$$\ddot{\eta} = \frac{\dot{\phi}}{4}\left[8\dot{\eta}\tan\phi - \frac{1}{\hbar}\left(\frac{\mu_0}{2}\sec\phi + \mu_1 \sin\eta - \mu_2\cos\eta\right)\right], \tag{5.32a}$$

$$\ddot{\phi} = -\frac{\dot{\eta}}{4}\cos^2\phi\left[4\dot{\eta}\tan\phi - \frac{1}{\hbar}\left(\frac{\mu_0}{2}\sec\phi + \mu_1 \sin\eta - \mu_2\cos\eta\right)\right]. \tag{5.32b}$$

We can combine these, by performing $\dot{\eta}\cos^2\phi$ (5.32a)$+\dot{\phi}$ (5.32b), to obtain a relation not encumbered by the Lagrange multipliers:

$$\frac{d}{dt}\left(\dot{\phi}^2 + \dot{\eta}^2\cos^2\phi\right) = \frac{d}{dt}\left\{\dot{\eta}^2\left[\left(\dot{\widetilde{\phi}}\right)^2 + \cos^2\widetilde{\phi}\right]\right\} = \frac{1}{4\hbar}\frac{d\mathcal{L}_\mathcal{E}}{dt} = 0. \tag{5.33}$$

This relation exhibits a constant of motion, which demonstrates that the energy-optimal dynamics is that whose energy presents a constant argument of integration $\mathcal{L}_\mathcal{E} = \hbar\mathcal{L}^2 = \hbar\Omega^2$, where Ω is a constant Rabi frequency, i.e

$$2|\dot{\eta}|\sqrt{\left(\dot{\widetilde{\phi}}\right)^2 + \cos^2\widetilde{\phi}} = \sqrt{\Omega_P^2 + \Omega_S^2} = \Omega = const, \tag{5.34}$$

thus, the partial pulse area is given by:

$$\widetilde{\mathcal{A}}(t) = \int_{t_i}^{t} dt\, \mathcal{L} = \int_{t_i}^{t} dt\, \Omega = \Omega\,(t - t_i). \tag{5.35}$$

Furthermore, for a given Rabi frequency Ω, the optimal time is then

$$T_{\text{opt}} = \widetilde{\mathcal{A}}(t_f)/\Omega = \mathcal{A}/\Omega. \tag{5.36}$$

Using $\dot{\phi} = \dot{\eta}\dot{\widetilde{\phi}}$, $\ddot{\phi} = \dot{\eta}^2\ddot{\widetilde{\phi}} + \ddot{\eta}\dot{\widetilde{\phi}}$, (5.34), and (5.32a), (5.32b) reads

$$0 = -\frac{\dddot{\widetilde{\phi}} + \left[2(\dot{\widetilde{\phi}})^2 + \cos^2\widetilde{\phi}\right]\tan\widetilde{\phi}}{\operatorname{sgn}\dot{\eta}\left[\left(\dot{\widetilde{\phi}}\right)^2 + \cos^2\widetilde{\phi}\right]^{3/2}} + \frac{1}{2\hbar\Omega}\Big(\mu_0 \sec\widetilde{\phi} + \mu_1 \sin\eta - \mu_2\cos\eta\Big), \tag{5.37}$$

where μ_0 has been redefined as $\mu_0/2 \to \mu_0$. The latter is exactly (5.21) for $\mu_j = 2\lambda_j\hbar\Omega$, i.e., it gives the same trajectory as for the pulse-area optimization.

Equation (5.34) can be rewritten as

$$\widetilde{\mathcal{A}}\big[\eta(t)\big] = 2\int_{\eta_i}^{\eta(t)} \operatorname{sgn}\dot{\eta}\,\sqrt{\left(\dot{\widetilde{\phi}}\right)^2 + \cos^2\widetilde{\phi}}\,d\eta = \Omega\,(t - t_i), \tag{5.38}$$

for a trajectory $\widetilde{\phi}(\eta)$, where the left-hand side is the partial generalized pulse area, see Eq. (5.12b), i.e. $\Omega = \mathcal{A}/(t_f - t_i)$. As a consequence, the energy-optimal dynamics for the trajectory (5.21) is also its time-optimal solution for a given constant Rabi frequency $\Omega = \Omega_0$, i.e $(t_f - t_i)|_{\text{opt}} = \mathcal{A}/\Omega_0$.

Enforcing (5.34) and (5.21) guarantees the resultant dynamics to be globally area-, energy-, and time-optimal.

5.7 Discussion

Fields and populations dynamics are shown in Figs. 5.4–5.6. The double-dot–dashed lines represent the optimal solution for the problem of population transfer without constraints of robustness, the fields are intuitively-ordered cosine-sine pulses (5.26). For the unconstrained optimization the transient population of the excited state is much larger than for the robust extrema. It can be observed that, while the unconstrained solution transfers most of the population from $|1\rangle$ to $|2\rangle$ and $|3\rangle$, with predominance of the excited state, in the first half of the process, the optimal robust solution transfers only about 40% of the population from the initial state to a superposition of the others (with much lower transient population on the excited

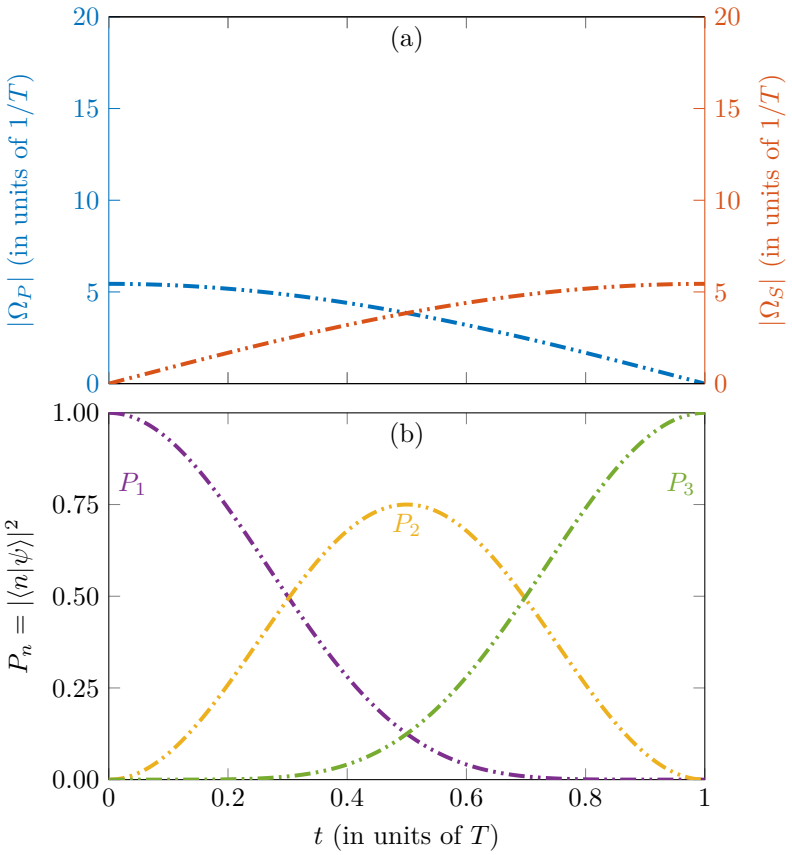

Figure 5.4: Fields and populations vs time for the unconstrained optimum Λ transfer. Numerical parameters details are summarized in Table 5.1.

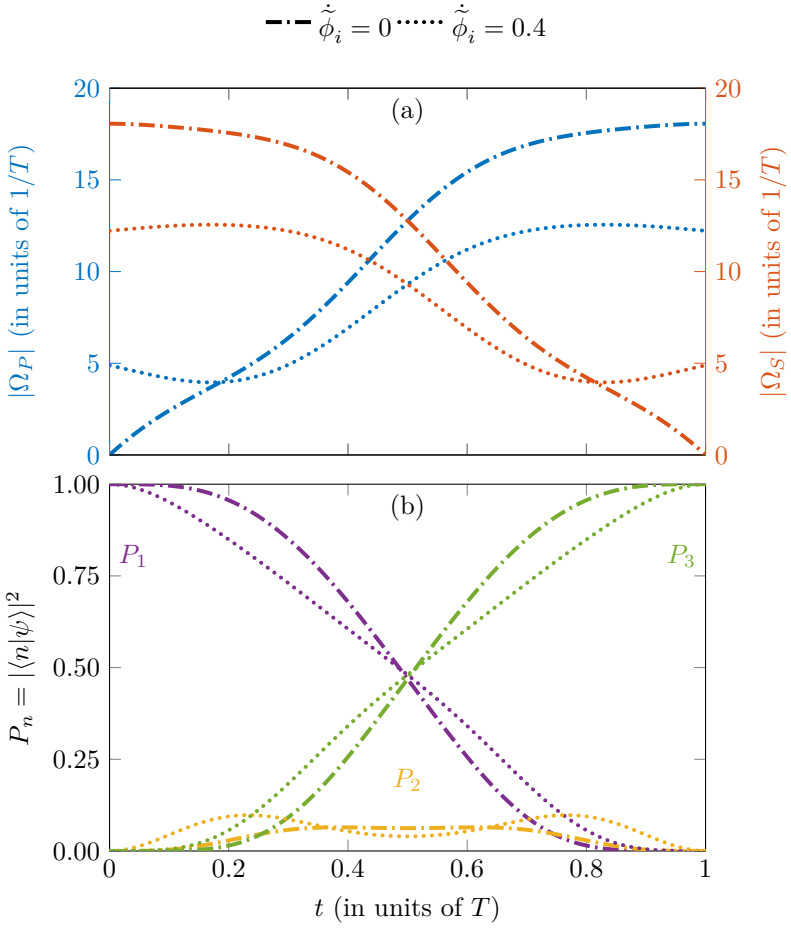

Figure 5.5: Fields and populations vs time for the first two selected robust optima. Numerical parameters details are summarized in Table 5.1. The line style in the legend applies to all plots irrespective of the line color.

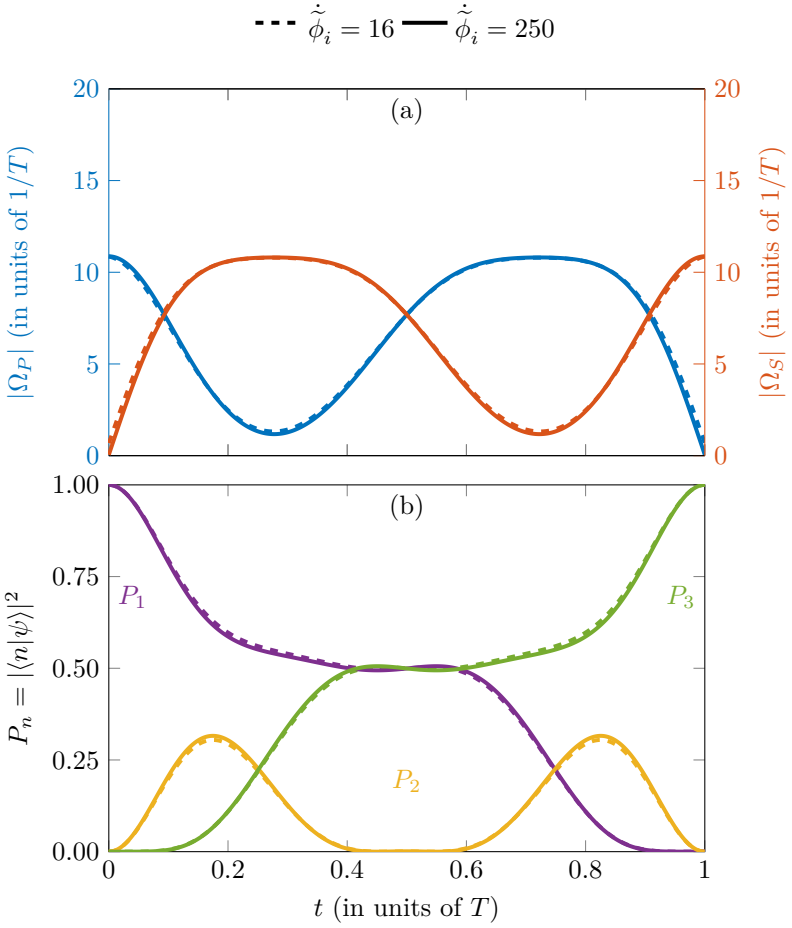

Figure 5.6: Fields and populations vs time for the selected robust optima nearing the asymptotic absolute optimum. Numerical parameters details are summarized in Table 5.1. The line style in the legend applies to all plots irrespective of the line color. The dynamics for $\dot{\tilde{\phi}}_i = 16$ and $\dot{\tilde{\phi}}_i = 250$ are almost indistinguishable at the scale of the figure.

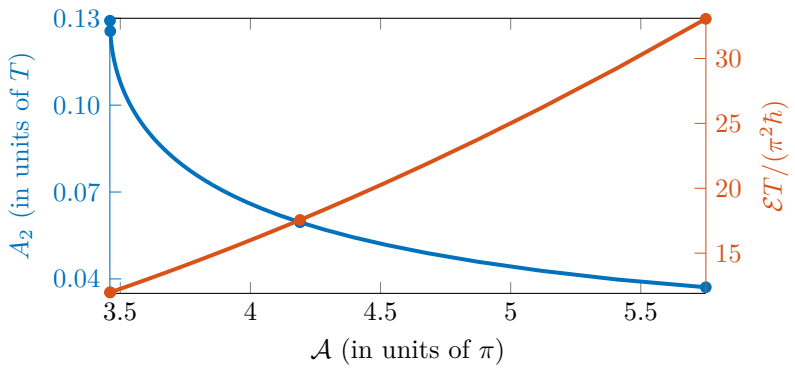

Figure 5.7: Loss-proportional term A_2 vs generalized pulse area for optimal robust family of solutions. To compare with $A_2 = (3/8)T = 0.3750T$ at $\mathcal{A} = \sqrt{3}\pi \approx 1.7321\pi$ and $\mathcal{E} = 3\pi^2\hbar/T$ for the optimal Λ transfer with no constraints of robustness. Numerical details have been gathered in Table 5.1.

state), proceeds to deplete the excited state into the target state, and only then executes the last part of the transfer like the first part. In this manner, while the unconstrained optimal transiently populates the excited state along the transfer, the robust optimal solution only does this in two temporally separated stages of 40% of the process duration and maintains it depopulated 20% of the time. At the middle of the process we obtain maximal superposition of the ground states and no population on the excited state, showing that the robust optimal full transfer appears as a two consecutive unconstrained (non-robust) half transfers (as already noticed in the preceding section).

The pulses corresponding to the extrema of the robust optimization go from a counter-intuitively–ordered pair of fields, to what could be described as a train of nonvanishing pulse pairs with intuitive–counter-intuitive–intuitive orderings. One can remark that composite-pulses STIRAP exhibits precisely the opposite ordering [49]. From the intermediate extremum it can be seen that the optimum is achieved by raising the bounded boundary of the field towards its maximum, Ω, and lowering the other boundary towards 0. All field pairs are complementary to each other and exhibit, as a whole, symmetry around half of the duration.

Now that we have the time-dependence of the angles, we can calculate the loss term A_2, we show its dependence with the generalized pulse area in Fig. 5.7. The minimum energy for the produced losses, calculated elsewhere with no robustness constraints, is between $1.92\pi \lesssim \mathcal{A} \lesssim 2\pi$ or $5.43 \lesssim \mathcal{E}T/(\pi^2\hbar) \lesssim 27$ with mostly overlapping pulses.

The fact that, in addition to the robust optimal solution, we have obtained a family of solutions which perform the desired task robustly and for fairly low areas (compared to adiabatic procedures with $\mathcal{A} > 10\pi$) suggests the following

Table 5.1: Identifying parameters of the highlighted extrema.

Parameter	Λ_{opt}	$\dot{\widetilde{\phi}}_i = 0$	$\dot{\widetilde{\phi}}_i = 0.4$	$\dot{\widetilde{\phi}}_i = 16$	$\dot{\widetilde{\phi}}_i = 250$
A_2/T	0.3750	0.0371	0.0596	0.1256	0.1291
$\mathcal{A}/\pi$	1.7321	5.7498	4.1904	3.4615	3.4603
$\dfrac{\mathcal{E}T}{\pi^2\hbar}$	3	33.0599	17.5597	11.9819	11.9739
$\Delta\epsilon_{\text{uhf}}$	0.4%	6.4%	5.6%	5.1%	5.1%
λ_0		0.1930790914	0.14013	-0.52403	-0.56596
λ_1	0	-0.0838224029	-0.04747	0.86793	0.93853
λ_2	0	0.0102504990	0.22984	1.05836	1.08283
η_f/π		2.9225	2.1297	1.5627	1.5454

practical strategy: These solutions could be used as options that become more or less preferable depending on the constraints of the implementation, e.g., when a $A_2 = 0.1291T$ is an acceptable cost, the actual optimal robust solution may be used; however, when that is too high to be acceptable, a larger-area optimum may be chosen, effectively lowering the associated loss term as low as $A_2 = 0.0371T$. Recalling Fig. 5.3, we can highlight that for roughly the same robustness profile we can choose among the extrema solutions, varying in area and loss parameter, according with the physical limitations of a particular practical implementation and the loss that can be considered acceptable.

The corresponding loss parameters and pulse areas, together with pulse energy and the values of the Lagrange multipliers, for the selected extrema in Figs. 5.5, 5.6, and 5.7 are presented in Table 5.1. Data regarding the nonrobust optimal solution, Fig. 5.4, is also included for comparison. The shown precision of the Lagrange multipliers is the minimum necessary to produce the selected results with their displayed precision (while guaranteeing $\widetilde{O}_2 < 10^{-4}$). It can be noted that the largest area extrema requires the most precision on the multipliers, this is only due to the rapid dependence of the areas for small $\dot{\widetilde{\phi}}_i$'s.

The existence of a continuous family of optima of robust solutions, controlled mathematically by the quantity $\dot{\widetilde{\phi}}_i$, but interpreted physically as the consequent loss, as extracted from Figs. 5.1 and 5.7, is a remarkable result of the applied method of inverse optimization with robustness as constraints. For the chosen family of robust optimal solutions, we have control of the loss parameter A_2 via the pulse area (equivalently, energy) and, like for adiabatic protocols, the relation is inversely proportional: lower loss requires higher energies, although, unlike the adiabatic behavior, there are lower and upper bounds to them.

We can use the relation (5.2) to estimate the upper bound on the time duration or lower bound on the pulse amplitude of the robust optimal pulses (absolute optimum and largest-area extrema) with respect to the dissipation parameter Γ (inverse of relaxation time) considering an admissible loss below the ultrahigh-fidelity benchmark $P_{\text{loss}} \lesssim 10^{-4}$, i.e. $T \lesssim 7.7 \times 10^{-4}\Gamma^{-1}$ and (consequently) $\Omega \gtrsim 1.4 \times 10^{4}\Gamma$, for $\mathcal{A} = 3.4603\pi$, else $T \lesssim 27.0 \times 10^{-4}\Gamma^{-1}$, $\Omega \gtrsim 0.7 \times 10^{4}\Gamma$, for $\mathcal{A} = 5.7498\pi$.

5.8 Conclusions

We have demonstrated a method to obtain robust quantum transfers while optimizing area, energy, and time. We have presented, for the first time, the optimal resonant Λ transfer with robustness up to the third order in terms of field inhomogeneities. The resultant pulse shapes are smooth and very energy economical, far below requirements of STIRAP, while also exhibiting a robust behavior comparable to robust STIREP and STIRAP [21] but with $2\pi \sim 3\pi$ lower areas. Losses remain below the ultrahigh-fidelity benchmark of 10^{-4} for pulse durations in the order of $\Gamma^{-1} \times 10^{-4}$, e.g., for the relaxation time of the excited state $1D_2$ of a praseodymium ion in a Pr^{3+}:Y_2SiO_5 crystal, which is $\Gamma^{-1} = T_1 \approx 164\mu$s [50, 82], the largest pulse duration and smallest amplitude necessary to avoid dissipation losses with the global optimal robust fields are 0.13μs and 85.4MHz, respectively.

The method could be extended to the search of robustness with respect to detuning and for field inhomogeneities unequal between the fields, and to consider higher orders of robustness.

The protocol to produce the pulses can be summarized as follows, focusing on the representative values in Table 5.1:

1. The values of λ_0, λ_1, λ_2, η_f, and the pulse area $\mathcal{A}$ for the chosen representative values of $\dot{\tilde{\phi}}_i$ allow the user to choose between the members of the robust candidates for optimal pulses, for a given admissible loss of the problem.

2. Once $\dot{\tilde{\phi}}_i$ is chosen, taking the other properties summarized in Table 5.1 as deciding factors, the values of the λ_n's, η_f, and pulse area are also taken and $\widetilde{\phi}(\eta)$, $\dot{\widetilde{\phi}}(\eta)$, and $\widetilde{\theta}(\eta)$ are calculated by

   (a) introducing the λ_n's in (5.44), which can then be solved using a standard method for solving ordinary differential equations,

   (b) the system is solved for the chosen $\dot{\tilde{\phi}}_i$, with $\widetilde{\phi}_i = \eta_i = 0$ as additional initial conditions, "integrating" up to η_f.

3. $\dot{\eta}(t)$ is then obtained, in units of $1/T$, from (5.34) choosing the maximum pulse amplitude to be $\Omega = \mathcal{A}/T$.

4. $\widetilde{\phi}(\eta)$, $\dot{\widetilde{\phi}}(\eta)$, $\widetilde{\theta}(\eta)$, and $\dot{\eta}(t)$ are finally introduced in (5.23) to obtain the pump and Stokes pulses, $\Omega_P(t)$ and $\Omega_S(t)$, in units of $1/T$.

Other values than the ones of Table 5.1 can be used with Fig. 5.1(a) and η_f given by (5.47) where $\eta_f \in [0, 2\pi)$ for $\dot{\widetilde{\phi}}_i > 0.5798$ and $\eta_f \in [2\pi, 4\pi)$ for $0 \leq \dot{\widetilde{\phi}}_i \leq 0.5798$.

Appendices

5.A Property of nested integrals

Double nested integrals may be simplified as follows

$$\int_{t_i}^{t_f}\int_{t_i}^{t}[a(t)b(t')+a(t')b(t)]\,dt'\,dt=\int_{t_i}^{t_f}a(t)\,dt\int_{t_i}^{t_f}b(t)\,dt, \tag{5.39}$$

from

$$\int_{t_i}^{t_f}v(t)\,du(t)+\int_{t_i}^{t_f}u(t)\,dv(t)=[u(t)v(t)]_{t_i}^{t_f}, \tag{5.40}$$

where

$$u(t)=\int_{t_i}^{t}a(t')\,dt',\quad du=a(t)\,dt,\quad v(t)=\int_{t_i}^{t}b(t')\,dt',\quad dv=b(t)\,dt. \tag{5.41}$$

For the triple nested integrals, we have

$$\begin{aligned}\int_{t_i}^{t_f}\int_{t_i}^{t}\int_{t_i}^{t'}ab'c''\,dt''\,dt'\,dt&=\int_{t_i}^{t_f}\int_{t_i}^{t}b(t')w(t')\,dt'\,du(t)=\int_{t_i}^{t_f}x(t)\,du(t)\\&=[u(t)x(t)]_{t_i}^{t_f}-\int_{t_i}^{t_f}u(t)\,dx(t)\\&=\int_{t_i}^{t_f}a\,dt\int_{t_i}^{t_f}bw\,dt-\int_{t_i}^{t_f}ubw\,dt,\end{aligned} \tag{5.42}$$

with

$$w(t)=\int_{t_i}^{t}c(t')\,dt',\quad dw=c(t)\,dt,\quad x(t)=\int_{t_i}^{t}b(t')w(t')\,dt',dx=b(t)w(t)\,dt. \tag{5.43}$$

5.B Numerical implementation

For a given set $\left(\dot{\widetilde{\phi}}_i^{\pm},\lambda_0,\lambda_1,\lambda_2\right)$, the differential equation (5.22) is solved numerically from $\eta=\eta_i=0$ to $\eta=3\pi$ (a large enough bound for the low pulse areas we are looking for). A search in this parameter space is then launched in order to find a certain set such that $\widetilde{\phi}=0$ is satisfied at some point $\eta>0$ which we then denote with the coordinate (η_f,ϕ_f), while the constraints (5.18) are also fulfilled.

The implementation for the numerical resolution, via a solver using the Runge-

Kutta method, is then

$$\dot{y}_1 = \dot{\widetilde{\phi}}^{\pm} = y_2, \tag{5.44a}$$

$$\dot{y}_2 = \ddot{\widetilde{\phi}}^{\pm} = -\left(2y_2^2 + \cos^2\widetilde{\phi}^{\pm}\right)\tan\widetilde{\phi}^{\pm} \pm \left(\lambda_0 \sec\widetilde{\phi}^{\pm} + \lambda_1 \sin\eta - \lambda_2\cos\eta\right) \times \left(y_2^2 + \cos^2\widetilde{\phi}^{\pm}\right)^{3/2} = 0. \tag{5.44b}$$

The numerical solutions show that the derived optimal family of trajectories is actually symmetric, implying that the assumptions in Appendix 5.C are valid and that Eqs. (5.47) are satisfied.

5.C Symmetric trajectory

In this Appendix we consider a symmetric solution via the standard forward evolution of (5.22) and its backward counterpart, i.e. we consider the trajectory evolving from $\eta = 0$ to $\eta = \eta_f$ and its reversal starting from the end point of the trajectory and ending at the starting point. The backward-propagating equation is obtained making $\widetilde{\phi}^{\pm}(\eta) \xrightarrow{\eta=\eta_f-u} \widehat{\phi}^{\pm}(u)$, where $\widehat{\phi}^{\pm}(u)$ is the backward-propagating trajectory and u is the counterpart of η (i.e. identical to η but time-reversed). Consequently, $\dot{\widehat{\phi}}^{\pm} = -\dot{\widetilde{\phi}}^{\pm}$ and $\ddot{\widehat{\phi}}^{\pm} = \ddot{\widetilde{\phi}}^{\pm}$. Then,

$$\mp \frac{\ddot{\widehat{\phi}}^{\pm} + \left[2\left(\dot{\widehat{\phi}}^{\pm}\right)^2 + \cos^2\widehat{\phi}^{\pm}\right]\tan\widehat{\phi}^{\pm}}{\left[\left(\dot{\widehat{\phi}}^{\pm}\right)^2 + \cos^2\widehat{\phi}^{\pm}\right]^{3/2}} + \lambda_0\sec\widehat{\phi}^{\pm} + \lambda_1\sin(\eta_f - u) - \lambda_2\cos(\eta_f - u) = 0. \tag{5.45}$$

The symmetric solution is implemented demanding symmetry about the axis $\eta(t = t_i + T/2) = \eta_m = \eta_f/2$, where T is the pulse duration, implying $\widehat{\phi}^{\pm}(u) = \widetilde{\phi}^{\pm}(\eta)$ (i.e. the equality of the counterpropagating trajectories), which leads to:

$$0 = \lambda_1(1 + \cos\eta_f) + \lambda_2\sin\eta_f, \quad 0 = \lambda_1\sin\eta_f + \lambda_2(1 - \cos\eta_f). \tag{5.46}$$

From Eqs. (5.46), we have $\lambda_{1,2} \neq 0$ when the determinant of the right-hand side matrix form is zero, i.e., $(1 + \cos\eta_f)(1 - \cos\eta_f) - \sin^2\eta_f = 0$, which is always satisfied. We can alternatively express the cosine and sine as:

$$\cos\eta_f = \frac{\lambda_2^2 - \lambda_1^2}{\lambda_1^2 + \lambda_2^2}, \quad \sin\eta_f = -\frac{2\lambda_1\lambda_2}{\lambda_1^2 + \lambda_2^2}. \tag{5.47}$$

Equation (5.47) gives η_f with modulus 2π, hence η_f is known once we know in which interval $\eta_{fn} \in \big[2n\pi, 2(n+1)\pi\big)$, with $n = 0, \pm1, \pm2, \ldots$ (where the sign is fixed by the sign of $\dot{\eta}$), it is located. For the obtained cosine and sine in Eq. (5.47), the backward-propagating equation (5.45) becomes identical to the forward-propagating one (5.22) (albeit in terms of u).

We may refer to the controls (5.10) to note that the pulses are mirror images of each other, $\Omega_P(t) = \Omega_S(t_f - t + t_i)$, when we apply the time-reversal symmetry:

$$\theta \to \frac{\pi}{2} - \widehat{\theta}, \quad \phi \to \widehat{\phi}, \quad \dot{\phi} \to -\dot{\widehat{\phi}}, \quad \dot{\eta} \to -\dot{\widehat{\eta}}. \tag{5.48}$$

5.D Dynamics of the angles

The dynamics of the angles and their derivative is presented in Fig. 5.8. The description of the trajectories $\widetilde{\phi}(\eta)$ and $\widetilde{\theta}(\eta)$ can be recalled to discuss their corresponding time-dependent evolutions, although it is worth noting that the process duration T for all solutions was made equal only after proper choice of the generalized pulse amplitude Ω. Unlike for the geometrical trajectory, the time-dependent functions are all finite. The evolution of η is almost a straight line of slope $3/T$ for the maximum-area extrema, however the optimum is obtained when η approaches a slightly oscillating line with zero derivative at the boundaries. All the presented dynamics display a certain parity with respect to $t = T/2$: all functions are mirrored or anti-mirrored (sign-changed) around that point, except θ and η. θ and η are odd functions only when also regarded about their value when evaluated at that point, i.e., the functions $f(t) = \theta(t - T/2) - \theta(T/2)$ and $g(t) = \eta(t - T/2) - \eta(T/2)$ are odd. The only function that is not null-valued at neither of its boundaries is $\dot{\phi}$, giving the pump and Stokes fields their respective nonzero boundary.

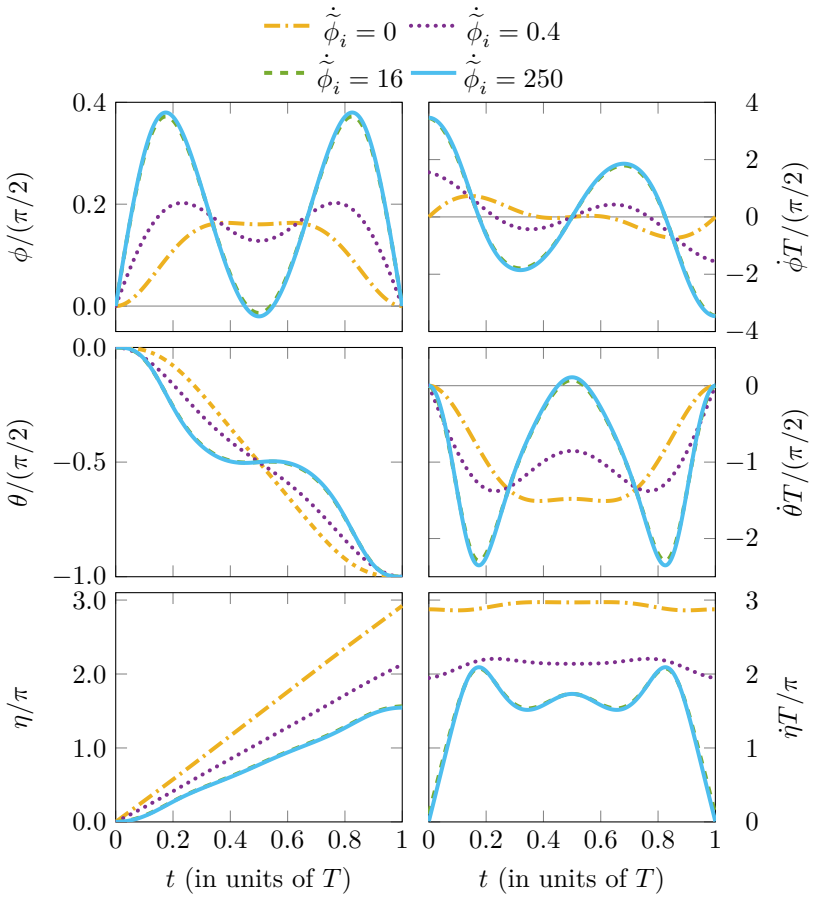

Figure 5.8: Dynamics of the angular parametrization (ϕ, η, θ) for the selected optima from Fig. 5.1 corresponding to the trajectories and fields in Fig. 5.2. Numerical parameters are summarized on Table 5.1. Thin gray lines mark the zero. The process duration T, equal to the pulse duration, is taken to be common among the extrema by letting the pulse amplitudes be given by $\Omega = \mathcal{A}/T$ for each corresponding area.

Conclusions

We have presented the concept of optimal robust control of quantum processes. We have evaluated robustness via a perturbative approach, exposing the distinction between the population transfer and gate corresponding figures of merit (fidelities). The combination of this evaluation of robustness with the inverse-engineering of the controls of the system is exposed as the single-shot shaped-pulses (SSSP). With the addition of optimization of the inverse-engineered controls, we describe the robust inverse optimization (RIO) scheme.

We have demonstrated the application of the RIO method for the control of a two-level system, producing robust and optimal (with respect to area, energy, or pulse duration) arbitrary population transfers and single-qubit quantum gates such as the: NOT, Hadamard, and phase gates. The results of the RIO method are further extended by the analytical forms we have found for the controls for all the aforementioned operations.

We have presented standard methods for the control of a three-level system in Λ configuration. Throughout this document, we have put together a picture of different techniques for quantum control how they relate in terms of the population loss they incur and the robustness of the population transfer, maintaining the ultrahigh-fidelity (UHF) requirement of quantum computation in mind.

The SSSP technique allowed us to put forward a scheme of exact control as an alternative to conventional STIRAP. This technique, that we call STIREP, is more robust for UHF population transfers at low and moderate areas than any of the conventional techniques we compared it with. The control fields designed with this approach displayed simple shapes and other fields may still be obtained following the recipe here described. Although the use of tracking was effective to produce an exact transfer with smooth simple pulses, the results of this protocol are heavily reliant on the tracking functions used; being it likely to produce strongly oscillating controls with widely varying energy requirements depending on the tracking functions.

Based on the classical principle of optimization via the Euler-Lagrange (E-L) equations, the RIO technique exchanges the freedom of the tracking approach in SSSP for an unique pulse shape and dynamics that exhibits both robustness and

the minimal area, energy, or time to achieve the population transfer with said degree of insensitivity to imperfect experimental conditions. We have applied RIO onto the three-level system and obtained relatively simple pulse shapes exhibiting a combination of intuitive and counter-intuitive behavior. These controls produce a transfer robust up to third order (the first nonzero order) and use the minimum area, energy, or time required to perform it.

Perspectives.— We have demonstrated the RIO method for two- and three-level systems subjected to error due to field inhomogeneties (amplitude scaling), equal for pump and Stokes fields in the latter. This method can be used to consider fields subjected to different amplitude scaling errors. Robustness with respect to detuning or transversal noise may also be tackled with the RIO method, though, in those cases, the optimization may not be reduced to a geometrical trajectory and will require the solution of the time-dependent system of E-L equations. We have also provided the required parametrization and recipe to produce robust optimal gates between the ground states of the Λ system. For the two-level system, we have compared our results from the RIO method to those of composite pulses; and we have observed about 20% gain in robustness obtained from allowing a continuous variation of the control fields phase. It remains an interesting study to extend to comparison to various orders of robustness, this to try to answer the question: "at what point does the gain become superfluous and the composite sequence more efficient (if to consider pulse –amplitude and phase– shaping as with a higher difficulty than the constant phases control) ?". This issue will have to be studied in concrete experimental systems such as superconducting qubits [83].

References

[1] M. A. Nielsen and I. L. Chuang, *Quantum computation and quantum information: 10th anniversary edition* (Cambridge University Press, 2010) (cit. on pp. xv, xvi, 2, 5, 37).

[2] D. D'Alessandro, *Introduction to quantum control and dynamics*, Chapman & Hall/CRC Applied Mathematics & Nonlinear Science (CRC Press, 2007) (cit. on pp. xvi, xvii, 2, 3, 22).

[3] D. P. DiVincenzo, "Quantum computation", Science **270**, 255 (1995) (cit. on pp. xvi, 2).

[4] S. Guérin and H. R. Jauslin, "Control of quantum dynamics by laser pulses: adiabatic floquet theory", in *Advances in chemical physics* (John Wiley & Sons, Inc., Feb. 2003), pp. 147–267 (cit. on pp. xvi, 2).

[5] K. Bergmann, N. V. Vitanov, and B. W. Shore, "Perspective: Stimulated Raman adiabatic passage: The status after 25 years", J. Chem. Phys. **142**, 170901 (2015) (cit. on pp. xvi, 2, 82, 85).

[6] N. V. Vitanov, A. A. Rangelov, B. W. Shore, and K. Bergmann, "Stimulated Raman adiabatic passage in physics, chemistry, and beyond", Rev. Mod. Phys. **89**, 015006 (2017) (cit. on pp. xvi, 2, 37, 82, 85, 124).

[7] B. W. Shore, "Picturing stimulated raman adiabatic passage: a STIRAP tutorial", Advances in Optics and Photonics **9**, 563 (2017) (cit. on pp. xvi, 2, 81).

[8] K. Bergmann, H.-C. Nägerl, C. Panda, G. Gabrielse, E. Miloglyadov, M. Quack, G. Seyfang, G. Wichmann, S. Ospelkaus, A. Kuhn, S. Longhi, A. Szameit, P. Pirro, B. Hillebrands, X.-F. Zhu, J. Zhu, M. Drewsen, W. K. Hensinger, S. Weidt, T. Halfmann, H.-L. Wang, G. S. Paraoanu, N. V. Vitanov, J. Mompart, T. Busch, T. J. Barnum, D. D. Grimes, R. W. Field, M. G. Raizen, E. Narevicius, M. Auzinsh, D. Budker, A. Pálffy, and C. H. Keitel, "Roadmap on STIRAP applications", J. Phys. B: At. Mol. Opt. Phys. **52**, 202001 (2019) (cit. on pp. xvi, 2, 85).

[9] M. V. Berry, "Quantum phase corrections from adiabatic iteration", Proceedings of the Royal Society of London. A. Mathematical and Physical Sciences **414**, 31 (1987) (cit. on pp. xvi, 2, 102).

[10] M. V. Berry, "Histories of adiabatic quantum transitions", Proceedings of the Royal Society of London. A. Mathematical and Physical Sciences **429**, 61 (1990) (cit. on pp. xvi, 2, 102).

[11] B. W. Shore, *Manipulating quantum structures using laser pulses* (Cambridge University Press, 2011) (cit. on pp. xvi, 2, 81, 82).

[12] D. Guéry-Odelin, A. Ruschhaupt, A. Kiely, E. Torrontegui, S. Martínez-Garaot, and J. Muga, "Shortcuts to adiabaticity: concepts, methods, and applications", Reviews of Modern Physics **91**, 10.1103/revmodphys.91.045001 (2019) (cit. on pp. xvi, 2, 37).

[13] S. Wimperis, "Broadband, narrowband, and passband composite pulses for use in advanced NMR experiments", Journal of Magnetic Resonance, Series A **109**, 221 (1994) (cit. on pp. xvii, 3, 37, 75).

[14] H. K. Cummins, G. Llewellyn, and J. A. Jones, "Tackling systematic errors in quantum logic gates with composite rotations", Physical Review A **67**, 10.1103/physreva.67.042308 (2003) (cit. on pp. xvii, 3, 37, 60, 61, 75, 77).

[15] J. A. Jones, "Designing short robust not gates for quantum computation", Physical Review A **87**, 10.1103/physreva.87.052317 (2013) (cit. on pp. xvii, 3, 37, 75).

[16] G. T. Genov, D. Schraft, T. Halfmann, and N. V. Vitanov, "Correction of arbitrary field errors in population inversion of quantum systems by universal composite pulses", Phys. Rev. Lett. **113**, 043001 (2014) (cit. on pp. xvii, 3, 37, 75, 109).

[17] B. T. Torosov and N. V. Vitanov, "Arbitrarily accurate variable rotations on the bloch sphere by composite pulse sequences", Physical Review A **99**, 10.1103/physreva.99.013402 (2019) (cit. on pp. xvii, 3, 37, 49, 61, 75).

[18] B. T. Torosov and N. V. Vitanov, "Robust high-fidelity coherent control of two-state systems by detuning pulses", Physical Review A **99**, 10.1103/physreva.99.013424 (2019) (cit. on pp. xvii, 3).

[19] D. Daems, A. Ruschhaupt, D. Sugny, and S. Guérin, "Robust quantum control by a single-shot shaped pulse", Phys. Rev. Lett. **111**, 050404 (2013) (cit. on pp. xvii, 3, 6, 8, 37, 109, 125, 130, 138).

[20] L. Van-Damme, D. Schraft, G. T. Genov, D. Sugny, T. Halfmann, and S. Guérin, "Robust not gate by single-shot-shaped pulses: Demonstration of the efficiency of the pulses in rephasing atomic coherences", Phys. Rev. A **96**, 022309 (2017) (cit. on pp. xvii, 3, 6, 37, 109, 125, 130).

[21] X. Laforgue, X. Chen, and S. Guérin, "Robust stimulated Raman exact passage using shaped pulses", Phys. Rev. A **100**, 023415 (2019) (cit. on pp. xvii, 3, 6, 12, 37, 125, 128, 138, 148).

[22] H. R. Lewis and W. B. Riesenfeld, "An Exact Quantum Theory of the Time-Dependent Harmonic Oscillator and of a Charged Particle in a Time-Dependent Electromagnetic Field", J. Math. Phys. **10**, 1458 (1969) (cit. on pp. xvii, 3, 12, 110, 112).

[23] U. Boscain, G. Charlot, J. P. Gauthier, S. Guérin, and H. R. Jauslin, "Optimal control in laser-induced population transfer for two- and three-level quantum systems", J. Math. Phys. **43**, 2107 (2002) (cit. on pp. xvii, 3, 38, 109, 110, 116, 126, 130, 138).

[24] S. J. Glaser, U. Boscain, T. Calarco, C. P. Koch, W. Köckenberger, R. Kosloff, I. Kuprov, B. Luy, S. Schirmer, T. Schulte-Herbrüggen, D. Sugny, and F. K. Wilhelm, "Training schrödinger's cat: quantum optimal control", The European Physical Journal D **69**, 10.1140/epjd/e2015-60464-1 (2015) (cit. on pp. xvii, 3, 37).

[25] X. Laforgue, G. Dridi, and S. Guérin, "Optimal robust stimulated raman exact passage by inverse optimization", Physical Review A **105**, 10.1103/physreva.105.032807 (2022) (cit. on p. 6).

[26] X. Chen, E. Torrontegui, and J. G. Muga, "Lewis-Riesenfeld invariants and transitionless quantum driving", Phys Rev A **83**, 062116 (2011) (cit. on pp. 12, 109, 110, 112).

[27] X. Chen and J. G. Muga, "Engineering of fast population transfer in three-level systems", Phys. Rev. A **86**, 033405 (2012) (cit. on pp. 12, 109, 110, 112, 116, 125).

[28] T. Tilma and E. C. G. Sudarshan, "Generalized Euler angle parametrization for $SU(N)$", Journal of Physics A: Mathematical and General **35**, 10467 (2002) (cit. on p. 17).

[29] W. Li and Y. Song, "SU(3)-transformation-based inverse engineering for fast population transfer in three-level systems", Journal of Physics B: Atomic, Molecular and Optical Physics, 10.1088/1361-6455/ac6364 (2022) (cit. on p. 19).

[30] B. van Brunt, *The calculus of variations* (Springer New York, 2004) (cit. on pp. 22, 39, 42).

[31] G. Dridi, S. Guérin, V. Hakobyan, H. R. Jauslin, and H. Eleuch, "Ultrafast stimulated Raman parallel adiabatic passage by shaped pulses", Phys. Rev. A **80**, 043408 (2009) (cit. on pp. 37, 109, 125).

[32] B. T. Torosov, S. Guérin, and N. V. Vitanov, "High-fidelity adiabatic passage by composite sequences of chirped pulses", Phys. Rev. Lett. **106**, 233001 (2011) (cit. on pp. 37, 109).

[33] N. Khaneja, T. Reiss, C. Kehlet, T. Schulte-Herbrüggen, and S. J. Glaser, "Optimal control of coupled spin dynamics: design of NMR pulse sequences by gradient ascent algorithms", Journal of Magnetic Resonance **172**, 296 (2005) (cit. on p. 37).

[34] T. Nöbauer, A. Angerer, B. Bartels, M. Trupke, S. Rotter, J. Schmiedmayer, F. Mintert, and J. Majer, "Smooth optimal quantum control for robust solid-state spin magnetometry", Physical Review Letters **115**, 10.1103/physrevlett.115.190801 (2015) (cit. on p. 37).

[35] L. V. Damme, Q. Ansel, S. J. Glaser, and D. Sugny, "Robust optimal control of two-level quantum systems", Physical Review A **95**, 10.1103/physreva.95.063403 (2017) (cit. on pp. 37, 39, 65, 66, 72, 73).

[36] J. Zeng and E. Barnes, "Fastest pulses that implement dynamically corrected single-qubit phase gates", Phys. Rev. A **98**, 10.1103/physreva.98.012301 (2018) (cit. on pp. 37, 125).

[37] G. Dridi, K. Liu, and S. Guérin, "Optimal robust quantum control by inverse geometric optimization", Phys. Rev. Lett. **125**, 250403 (2020) (cit. on pp. 37, 45, 59, 65, 125, 138).

[38] U. Gaubatz, P. Rudecki, S. Schiemann, and K. Bergmann, "Population transfer between molecular vibrational levels by stimulated Raman scattering with partially overlapping laser fields. A new concept and experimental results", J. Chem. Phys. **92**, 5363 (1990) (cit. on pp. 81, 82).

[39] A. Kuhn, M. Hennrich, and G. Rempe, "Deterministic Single-Photon Source for Distributed Quantum Networking", Phys. Rev. Lett. **89**, 067901 (2002) (cit. on pp. 81, 82).

[40] J. L. Sørensen, D. Møller, T. Iversen, J. B. Thomsen, F. Jensen, P. Staanum, D. Voigt, and M. Drewsen, "Efficient coherent internal state transfer in trapped ions using stimulated Raman adiabatic passage", New J. Phys. **8**, 261 (2006) (cit. on pp. 81, 82).

[41] P. Král, I. Thanopulos, and M. Shapiro, "Colloquium: Coherently controlled adiabatic passage", Rev. Mod. Phys. **79**, 53 (2007) (cit. on pp. 81, 82).

[42] J. Preskill, "Reliable quantum computers", Proc. R. Soc. Lond. A **454**, 385 (1998) (cit. on p. 81).

[43] K. Drese and M. Holthaus, "Perturbative and nonperturbative processes in adiabatic population transfer", The European Physical Journal D - Atomic, Molecular and Optical Physics **3**, 73 (1998) (cit. on p. 102).

[44] V. Dorier, M. Gevorgyan, A. Ishkhanyan, C. Leroy, H. R. Jauslin, and S. Guérin, "Nonlinear stimulated Raman exact passage by resonance-locked inverse engineering", Phys. Rev. Lett. **119**, 243902 (2017) (cit. on pp. 109, 110, 116, 125).

[45] G. S. Vasilev, A. Kuhn, and N. V. Vitanov, "Optimum pulse shapes for stimulated Raman adiabatic passage", Phys. Rev. A **80**, 013417 (2009) (cit. on pp. 109, 119–121).

[46] M. H. Levitt, "Composite pulses", Prog. Nucl. Magn. Reson. Spectrosc. **18**, 61 (1986) (cit. on p. 109).

[47] B. T. Torosov and N. V. Vitanov, "Smooth composite pulses for high-fidelity quantum information processing", Phys. Rev. A **83**, 053420 (2011) (cit. on p. 109).

[48] G. T. Genov, B. T. Torosov, and N. V. Vitanov, "Optimized control of multistate quantum systems by composite pulse sequences", Phys. Rev. A **84**, 063413 (2011) (cit. on p. 109).

[49] B. T. Torosov and N. V. Vitanov, "Composite stimulated Raman adiabatic passage", Phys. Rev. A **87**, 043418 (2013) (cit. on pp. 109, 146).

[50] A. Bruns, G. T. Genov, M. Hain, N. V. Vitanov, and T. Halfmann, "Experimental demonstration of composite stimulated Raman adiabatic passage", Phys. Rev. A **98**, 053413 (2018) (cit. on pp. 109, 148).

[51] M. Demirplak and S. A. Rice, "Assisted Adiabatic Passage Revisited", J. Phys. Chem. B **109**, 6838 (2005) (cit. on p. 109).

[52] M. Demirplak and S. A. Rice, "On the consistency, extremal, and global properties of counterdiabatic fields", J. Chem. Phys. **129**, 154111 (2008) (cit. on p. 109).

[53] M. V. Berry, "Transitionless quantum driving", J. Phys. A **42**, 365303 (2009) (cit. on p. 109).

[54] X. Chen, I. Lizuain, A. Ruschhaupt, D. Guéry-Odelin, and J. G. Muga, "Shortcut to adiabatic passage in two- and three-level atoms", Phys. Rev. Lett. **105**, 123003 (2010) (cit. on p. 109).

[55] M. G. Bason, M. Viteau, N. Malossi, P. Huillery, E. Arimondo, D. Ciampini, R. Fazio, V. Giovannetti, R. Mannella, and O. Morsch, "High-fidelity quantum driving", Nat. Phys. **8**, 147 (2012) (cit. on p. 109).

[56] A. Ruschhaupt, X. Chen, D. Alonso, and J. G. Muga, "Optimally robust shortcuts to population inversion in two-level quantum systems", New J. Phys. **14**, 093040 (2012) (cit. on p. 109).

[57] A. Baksic, H. Ribeiro, and A. A. Clerk, "Speeding up Adiabatic Quantum State Transfer by Using Dressed States", Phys. Rev. Lett. **116**, 230503 (2016) (cit. on p. 109).

[58] Y. C. Li and X. Chen, "Shortcut to adiabatic population transfer in quantum three-level systems: Effective two-level problems and feasible counterdiabatic driving", Phys. Rev. A **94**, 063411 (2016) (cit. on pp. 109, 125).

[59] Y. Ban, L. X. Jiang, Y. C. Li, L. J. Wang, and X. Chen, "Fast creation and transfer of coherence in triple quantum dots by using shortcuts to adiabaticity", Opt. Express **26**, 31137 (2018) (cit. on p. 109).

[60] Y. Z. Lai, J. Q. Liang, H. J. W. Müller-Kirsten, and J. G. Zhou, "Time evolution of quantum systems with time-dependent Hamiltonian and the invariant Hermitian operator", J. Phys. A **29**, 1773 (1996) (cit. on p. 112).

[61] Y. Z. Lai, J. Q. Liang, H. J. W. Müller-Kirsten, and J. G. Zhou, "Time-dependent quantum systems and the invariant Hermitian operator", Phys. Rev. A **53**, 3691 (1996) (cit. on p. 112).

[62] M. Gell-Mann, "Symmetries of Baryons and Mesons", Phys. Rev. **125**, 1067 (1962) (cit. on p. 112).

[63] C. E. Carroll and F. T. Hioe, "Three-state systems driven by resonant optical pulses of different shapes", J. Opt. Soc. Am. B **5**, 1335 (1988) (cit. on p. 112).

[64] K. Bergmann, H. Theuer, and B. W. Shore, "Coherent population transfer among quantum states of atoms and molecules", Rev. Mod. Phys. **70**, 1003 (1998) (cit. on p. 122).

[65] B. Rousseaux, S. Guérin, and N. V. Vitanov, "Arbitrary qudit gates by adiabatic passage", Phys. Rev. A **87**, 032328 (2013) (cit. on p. 124).

[66] F. T. Hioe, "Gell-Mann dynamic symmetry for N-level quantum systems", Phys. Rev. A **32**, 2824 (1985) (cit. on p. 124).

[67] F. T. Hioe, "N-level quantum systems with SU(2) dynamic symmetry", J. Opt. Soc. Am. B **4**, 1327 (1987) (cit. on p. 124).

[68] F. T. Hioe, "N-level quantum systems with Gell-Mann dynamic symmetry", J. Opt. Soc. Am. B **5**, 859 (1988) (cit. on p. 124).

[69] U. Güngördü, Y. Wan, M. A. Fasihi, and M. Nakahara, "Dynamical invariants for quantum control of four-level systems", Phys. Rev. A **86**, 062312 (2012) (cit. on p. 124).

[70] B. W. Shore, "Two-state behavior in N-state quantum systems: the Morris–Shore transformation reviewed", J. Mod. Opt **61**, 787 (2014) (cit. on p. 124).

[71] S. Ibáñez, X. Chen, and J. G. Muga, "Improving shortcuts to adiabaticity by iterative interaction pictures", Phys. Rev. A **87**, 043402 (2013) (cit. on p. 125).

[72] X.-K. Song, Q. Ai, J. Qiu, and F.-G. Deng, "Physically feasible three-level transitionless quantum driving with multiple schrödinger dynamics", Phys. Rev. A **93**, 052324 (2016) (cit. on p. 125).

[73] B.-H. Huang, Y.-H. Chen, Q.-C. Wu, J. Song, and Y. Xia, "Fast generating greenberger–horne–zeilinger state via iterative interaction pictures", Laser Phys. Lett. **13**, 105202 (2016) (cit. on p. 125).

[74] Y.-H. Kang, Y.-H. Chen, Q.-C. Wu, B.-H. Huang, J. Song, and Y. Xia, "Fast generation of w states of superconducting qubits with multiple schrödinger dynamics", Sci. Rep. **6**, 36737 (2016) (cit. on p. 125).

[75] B.-J. Liu, X.-K. Song, Z.-Y. Xue, X. Wang, and M.-H. Yung, "Plug-and-play approach to nonadiabatic geometric quantum gates", Physical Review Letters **123**, 10.1103/physrevlett.123.100501 (2019) (cit. on p. 125).

[76] B.-J. Liu and M.-H. Yung, "Coherent control with user-defined passage", Quantum Science and Technology **6**, 025002 (2021) (cit. on p. 125).

[77] J. Zeng, X.-H. Deng, A. Russo, and E. Barnes, "General solution to inhomogeneous dephasing and smooth pulse dynamical decoupling", New J. Phys. **20**, 033011 (2018) (cit. on p. 125).

[78] U. Güngördü and J. P. Kestner, "Analytically parametrized solutions for robust quantum control using smooth pulses", Phys. Rev. A **100**, 10.1103/physreva.100.062310 (2019) (cit. on p. 125).

[79] W. Dong, F. Zhuang, S. E. Economou, and E. Barnes, "Doubly geometric quantum control", PRX Quantum **2**, 10.1103/prxquantum.2.030333 (2021) (cit. on p. 125).

[80] J.-J. Zhu, X. Chen, H.-R. Jauslin, and S. Guérin, "Robust control of unstable nonlinear quantum systems", Phys. Rev. A **102**, 052203 (2020) (cit. on p. 125).

[81] U. Boscain, T. Chambrion, and J.-P. Gauthier, "On the $K + P$ problem for a three-level quantum system: optimality implies resonance", J. Dyn. Control Syst. **8**, 547 (2002) (cit. on pp. 126, 138).

[82] D. Schraft, T. Halfmann, G. T. Genov, and N. V. Vitanov, "Experimental demonstration of composite adiabatic passage", Phys. Rev. A **88**, 063406 (2013) (cit. on p. 148).

[83] B. Pokharel, N. Anand, B. Fortman, and D. A. Lidar, "Demonstration of fidelity improvement using dynamical decoupling with superconducting qubits", Physical Review Letters **121**, 10.1103/physrevlett.121.220502 (2018) (cit. on p. 156).

ECOLE DOCTORALE
CARNOT - PASTEUR

Titre : Contrôle robuste pour les technologies quantiques

Mots clés : Contrôle coherent, optique quantique, technologies quantiques

Résumé : Nous considérons l'optimisation géométrique inverse robuste de transferts de population arbitraires et de portes à un seul qubit dans un système à deux niveaux. La robustesse vis-à-vis des inhomogénéités d'impulsion est démontrée. Nous montrons que pour l'optimisation du temps ou de l'énergie, l'amplitude de l'impulsion est constante, et nous fournissons la forme analytique du désaccord en fréquence comme cosinus elliptique de Jacobi.
Nous traitons la tâche de transfert complet et robuste de population sur un système quantique à 3 niveaux en configuration lambda. Tout d'abord, nous utilisons la méthode de Lewis-Riesenfeld pour dériver une famille de solutions conduisant à un transfert exact. Parmi cette famille, nous identifions une solution de suivi avec un seul paramètre pour contrôler simultanément la fidélité du transfert, la population de l'état excité, et la robustesse. La robustesse de l'ultra-haute fidélité des impulsions formées s'avère supérieure à celle des impulsions gaussiennes et des impulsions optimisées adiabatiquement pour des aires d'impulsion modérées. Deuxièmement, nous appliquons une optimisation inverse robuste pour générer un passage exact Raman stimulé (STIREP) en considérant la perte de l'état supérieur comme un paramètre de caractérisation. Les formes temporelles des champs de contrôle, robustes vis-à-vis des inhomogénéités d'impulsion, qui sont optimales par rapport à l'aire d'impulsion, l'énergie et la durée, forment une séquence simple avec une combinaison de paires d'impulsions intuitive (près du début et de la fin) et contre-intuitive (au centre). D'autres solutions optimales robustes présentant des pertes plus faibles, des aires d'impulsion plus grandes et des séquences d'impulsion totalement contre-intuitives sont dérivées.

Title: Robust control for quantum technologies and quantum information processing

Keywords: Coherent control, quantum optics, quantum technologies

Abstract: We consider the robust inverse geometric optimization of arbitrary population transfers and single-qubit gates in a two-level system. Robustness with respect to pulse inhomogeneities is demonstrated. We show that for time or energy optimization, the pulse amplitude is constant, and we provide the analytic form of the detuning as Jacobi elliptic cosine.
We deal with the task of robust complete population transfer on a 3-level quantum system in lambda configuration. First, we use the Lewis-Riesenfeld method to derive a family of solutions leading to an exact transfer. Among this family, we identify a tracking solution with a single parameter to control simultaneously the fidelity of the transfer, the population of the excited state, and robustness. The ultrahigh-fidelity robustness of the shaped pulses is found superior to that of Gaussian and adiabatically-optimized pulses for moderate pulse areas. Second, we apply robust inverse optimization now to generate a stimulated Raman exact passage (STIREP) considering the loss of the upper state as a characterization parameter. Control fields temporal shapes, robust against pulse inhomogeneities, that are optimal with respect to pulse area, energy, and duration, are found to form a simple sequence with a combination of intuitively (near the beginning and the end) and counter-intuitively ordered pulse pairs. Alternative robust optimal solutions featuring lower losses, larger pulse areas, and fully counter-intuitive pulse sequences are derived.

UBFC
UNIVERSITÉ
BOURGOGNE FRANCHE-COMTÉ

Université Bourgogne Franche-Comté
32, avenue de l'Observatoire
25000 Besançon